



Durham E-Theses

*Synthesis, reactivity and bonding of compounds
containing transition metal-nitrogen multiple bonds
and related studies*

William, David N.

How to cite:

William, David N. (1990) *Synthesis, reactivity and bonding of compounds containing transition metal-nitrogen multiple bonds and related studies*, Durham theses, Durham University. Available at Durham E-Theses Online: <http://etheses.dur.ac.uk/6253/>

Use policy

The full-text may be used and/or reproduced, and given to third parties in any format or medium, without prior permission or charge, for personal research or study, educational, or not-for-profit purposes provided that:

- a full bibliographic reference is made to the original source
- a [link](#) is made to the metadata record in Durham E-Theses
- the full-text is not changed in any way

The full-text must not be sold in any format or medium without the formal permission of the copyright holders.

Please consult the [full Durham E-Theses policy](#) for further details.

**Synthesis, Reactivity and Bonding of Compounds
Containing Transition Metal-Nitrogen Multiple Bonds
and Related Studies.**

by

David N. Williams, B.Sc. (Dunelm)

University of Durham

A thesis submitted in part fulfillment of the requirements for the degree of
Doctor of Philosophy at the University of Durham.

November 1990.

The copyright of this thesis rests with the author.
No quotation from it should be published without
his prior written consent and information derived
from it should be acknowledged.



25 APR 1991

Statement of Copyright

The Copyright of this thesis rests with the author. No quotation from it should be published without his prior written consent and information derived from it should be acknowledged.

Declaration

The work described in this thesis was carried out in the Department of Chemistry at the University of Durham between October 1987 and September 1990. All the work is my own, unless stated to the contrary, and it has not been submitted previously for a degree at this or any other University.

**For my Mother
and Father.**

Acknowledgements

I would like primarily to express my sincere gratitude to Dr. Vernon C. Gibson for his constant support throughout my period of study at Durham, both as a supervisor and a friend. His ability to inspire and stimulate the study of chemistry, has made it a great pleasure to work within his research group.

To my colleagues, past and present, go my heartfelt thanks especially the other members of the group Twinkle, Pete, Ed, Ulrich, Andy, Oliver and Matt for providing an amusing atmosphere in which to work. My thanks also go to Dr. Terence P. Kee for introducing me to organometallic chemistry, and to Dr. Alan Shaw for showing me the lighter aspects of chemical research.

I am especially indebted to Dr. W. Clegg and Mr. D.C.R. Hockless (University of Newcastle-Upon-Tyne) for solving the crystal structures described herein, to Dr. Catherine Housecroft (University of Cambridge) for teaching me the ways of FHMO calculations, and to little Miss Tracey Wells for her project work on bond-stretch isomers and constant support throughout my final year. Furthermore, without the help and co-operation of the Senior Experimental and Technical Staff at the Chemistry Department at Durham, none of this work would have been possible.

I am especially grateful to my brother, Andrew, for unlimited use of his word processor and printer.

Finally, the award of an S.E.R.C. studentship is gratefully acknowledged and I would like to thank all my family for moral support.

Abstract

Synthesis, Reactivity and Bonding of Compounds Containing Transition Metal-Nitrogen Multiple Bonds and Related Studies.

This thesis describes studies directed towards the preparation of new transition metal species containing multiple bonds to nitrogen, with a view to learning more about the structure and reactivity of metal bound nitrogen:

Chapter 1 highlights areas of transition metal nitrido and imido chemistry of relevance to the general theme of the thesis.

Chapter 2 describes the use of silyl amines and amides for convenient solution syntheses of half-sandwich imido complexes of niobium and tantalum of the type $\text{CpM}(\text{NR})\text{Cl}_2$ ($\text{R} = \text{Me}, \text{}^t\text{Bu}, 2\text{-}6\text{-}i\text{Pr}_2\text{C}_6\text{H}_3$). In addition, the preparation and characterisation of alkyl, phenoxide and alkoxide derivatives are presented. The *bis*-neopentyl derivative, $\text{CpNb}(\text{N}^t\text{Bu})(\text{CH}_2\text{CMe}_3)_2$, is found to possess two α -agostic C-H interactions. Finally, attempts to prepare a *bis* imido species of the type $[\text{CpNb}(\text{NR})_2]$ are discussed.

Chapter 3 employs Fenske-Hall quantum chemical MO calculations (FHMO), to learn more about the nature of the imido bonding in $\text{CpNb}(\text{NMe})\text{Cl}_2$, and compares this class of compound with Group 4 metallocenes (Cp_2MX_2) and complexes of the type $\text{Cp}^*\text{Ta}(\eta^2\text{-CHPMe}_2)\text{X}_2$.

Chapter 4 describes a search for metal-nitrogen complexes exhibiting the unusual phenomenon of bond-stretch isomerism. Modified preparations of molybdenum and tungsten nitrido starting materials have been developed and their reactions with tertiary phosphines examined. Attempts to prepare $\text{M}(\text{N})\text{Cl}_3(\text{PMe}_3)_3$ led to the isolation of the phosphiniminato species $[\text{Mo}(\text{NPMe}_3)\text{Cl}_2(\text{PMe}_3)_3]\text{Cl}$, which converts under mild conditions to the binuclear nitrido complex $[(\text{PMe}_3)_2\text{Cl}_3\text{MoNMoCl}_3(\text{PMe}_3)_2][\text{Me}_3\text{PNPMe}_3]$. The X-ray structures, reactivity and bonding of these unusual species are discussed. Other attempts to isolate bond-stretch isomers, from tungsten and rhenium nitride starting materials, resulted in nitrido complexes such as $\text{W}(\text{N})\text{Cl}_3(\text{PR}_3)_2$ ($\text{PR}_3 = \text{PMe}_3, \text{PMe}_2\text{Ph}, \text{PPh}_3$) and $\text{Re}(\text{N})\text{Cl}_2(\text{PR}_3)_n$ ($n = 3, \text{PR}_3 = \text{PMe}_2\text{Ph}; n = 2, \text{PR}_3 = \text{PMePh}_2$).

Chapter 5 presents a detailed analysis of the oxo bonding in the isomers of $\text{Nb}(\text{O})\text{Cl}_3(\text{PMe}_3)_3$ arising by lengthening of the metal-oxygen bond (bond-stretch isomers). The bonding has been analysed over a range of metal-oxygen distances and destabilising anti-bonding interactions found at shorter Nb-O bond lengths. These observations are compared with the results of calculations on the hypothetical nitrido species $\text{Mo}(\text{N})\text{Cl}_3(\text{PMe}_3)_3$.

Chapter 6 gives experimental details for chapter 2-5.

David Neil Williams (November 1990)

Abbreviations

| | |
|------------------|---|
| L | General 2-electron (neutral) donor ligand |
| X | General 1-electron (1-) donor ligand |
| Cp | Cyclopentadienyl (C ₅ H ₅) |
| Cp* | Pentamethylcyclopentadienyl (C ₅ Me ₅) |
| Cp' | Generalised (C ₅ R ₅) ligand |
| THF | Tetrahydrofuran |
| PCy ₃ | Tricyclohexylphosphine |
| Np | Neopentyl (CH ₂ CMe ₃) |
| NMR | Nuclear Magnetic Resonance |
| IR | Infrared |
| HOMO | Highest Occupied Molecular Orbital |
| SHOMO | Second Highest Occupied Molecular Orbital |
| LUMO | Lowest Unoccupied Molecular Orbital |
| SLUMO | Second Lowest Unoccupied Molecular Orbital |
| SOMO | Singly Occupied Molecular Orbital |
| EHMO | Extended Hückel Molecular Orbital (calculations) |
| FHMO | Fenske-Hall Molecular Orbital (calculations) |

CONTENTS

Page

| | |
|---|----------|
| Chapter One - Transition Metal-Nitrogen Multiple Bonds - An Overview of their Synthesis, Structure and Bonding | 1 |
| 1.1 Introduction. | 2 |
| 1.2 Occurrence. | 4 |
| 1.2.1 Nitrido Complexes. | 4 |
| 1.2.2 Imido Complexes. | 5 |
| 1.3. Electronic Structure and Bonding. | 6 |
| 1.3.1 Bonding Modes. | 6 |
| 1.3.1.1 The Nitride ligand. | 6 |
| 1.3.1.2 The Imido ligand. | 11 |
| 1.3.2 Coordination Geometries of Nitrido and Imido Complexes. | 14 |
| 1.3.3 Ligand Field Description. | 16 |
| 1.3.3.1 Octahedral Complexes. | 16 |
| 1.3.3.2 Square Pyramidal Complexes. | 17 |
| 1.3.4 The <i>trans</i> Influence. | 17 |
| 1.4 Spectroscopic Properties. | 18 |
| 1.4.1 Infrared Spectroscopy of Terminal Nitrides. | 18 |
| 1.4.1.1 General Considerations. | 18 |
| 1.4.1.2 Assignment of Terminal M-N Stretching Frequencies. | 19 |
| 1.4.2 Infrared Spectroscopy of Bridging Nitrides. | 20 |
| 1.4.3 Infrared Spectra of Organoimido Complexes. | 22 |
| 1.4.4 Nitrogen NMR of Multiply-Bonded Ligands. | 22 |
| 1.4.5 ¹ H NMR Spectroscopy. | 23 |
| 1.4.6 ¹³ C NMR Spectroscopy. | 24 |
| 1.5 Uses. | 24 |
| 1.5.1 Nitrido Complexes. | 24 |
| 1.5.1.1 New Materials. | 24 |

| | |
|---|-----------|
| 1.5.1.2 Catalytic Properties of Nitride Species. | 26 |
| 1.5.2 Imido Complexes. | 27 |
| 1.5.2.1 Heterogeneous Catalysis. | 27 |
| 1.5.2.2 Organic Synthesis and Homogeneous Catalysis. | 28 |
| 1.6 Summary. | 31 |
| 1.7 References. | 32 |
| Chapter Two - Half-Sandwich Imido Complexes of Niobium and Tantalum. | 39 |
| 2.1 Introduction. | 40 |
| 2.2 A Low Valent Route. | 42 |
| 2.2.1 Reaction of Cp*TaCl ₂ (PMe ₃) ₂ with Me ₃ SiN ₃ : Preparation of Cp*Ta(NSiMe ₃ Cl ₂) (1). | 42 |
| 2.3 A High Valent Route. | 42 |
| 2.4 Preparation of Group 5 Half-Sandwich Imido Species using Bis (Trimethylsilyl) Amines. | 43 |
| 2.4.1 Reaction of CpNbCl ₄ with (Me ₃ Si) ₂ NMe: Preparation of CpNb(NMe)Cl ₂ (2). | 43 |
| 2.4.2 The Reaction of Cp*TaCl ₄ with (Me ₃ Si) ₂ NMe: Preparation of [Cp*TaCl ₃] ₂ [NMe] (3). | 44 |
| 2.4.2.1 Mechanism of Formation of [Cp*TaCl ₃] ₂ [NMe]. | 46 |
| 2.4.3 Reaction of CpTaCl ₄ with (Me ₃ Si) ₂ NCN: Preparation of [CpTa(NCN)Cl ₂ (CH ₃ CN)] _n (6). | 47 |
| 2.5 Preparation of Group 5 Half-Sandwich Imido Species Using Trimethylsilylamine and Amide Reagents. | 48 |
| 2.5.1 Reaction of CpNbCl ₄ with Me ₃ SiNH ^t Bu: Preparation of CpNb(N ^t Bu)Cl ₂ (7). | 49 |
| 2.5.2 Reaction of CpNbCl ₄ with Me ₃ SiNH(2,6- ⁱ Pr ₂ C ₆ H ₃): Preparation of [Cp(N-2,6- ⁱ Pr ₂ C ₆ H ₃)Cl ₃][NH ₂ SiMe ₃ (2,6- ⁱ Pr ₂ C ₆ H ₃)] (8) and CpNb(N-2,6- ⁱ Pr ₂ C ₆ H ₃)Cl ₂ (9). | 50 |
| 2.5.3 Reaction of CpTaCl ₄ with LiN ^t Bu(SiMe ₃): Preparation of CpTa(N ^t Bu)Cl ₂ (10). | 51 |
| 2.5.4 Reaction of CpTaCl ₄ with LiN(2,6- ⁱ Pr ₂ C ₆ H ₃)(SiMe ₃): Preparation of CpTa(N-2,6- ⁱ Pr ₂ C ₆ H ₃)Cl ₂ (11). | 52 |

| | | |
|---------|---|----|
| 2.5.5 | Reaction of Cp*TaCl ₄ with Me ₃ SiNHR Reagents: <i>Preparation of Cp*Ta(NR)Cl₂ (R = ^tBu (12), 2,6-ⁱPr₂C₆H₃ (13)).</i> | 52 |
| 2.6 | The Molecular Structures of Complexes of The Type CpNb(NR)Cl ₂ (R = Me (2), ^t Bu (7), 2,6- ⁱ Pr ₂ C ₆ H ₃ (9)). | 53 |
| 2.7 | Some Derivative Chemistry of CpNb(NMe)Cl ₂ . | 56 |
| 2.7.1 | Reaction of CpNb(NMe)Cl ₂ with Trimethylphosphine: <i>Preparation of CpNb(NMe)Cl₂(PMe₃) (14).</i> | 56 |
| 2.7.1.1 | The Molecular Structure of CpNb(NMe)Cl ₂ (PMe ₃) (14). | 57 |
| 2.7.2 | Reaction of CpNb(NMe)Cl ₂ with LiO-2,6-Me ₂ C ₆ H ₃ : <i>Preparation of CpNb(NMe)(O-2,6-Me₂C₆H₃)Cl₂ (15).</i> | 58 |
| 2.7.3 | Reaction of CpNb(NMe)Cl ₂ with LiO ^t Bu: <i>Preparation of CpNb(NMe)(O^tBu)₂ (16).</i> | 59 |
| 2.7.4 | Reaction of CpNb(NMe)Cl ₂ with RMgX and MeLi (R = Me, CH ₂ CH=CH ₂ ; X = Cl, Br, I) Reagents: <i>Attempted Preparation of CpNb(NMe)RCl and CpNb(NMe)X₂ Species.</i> | 60 |
| 2.8 | Some Derivative Chemistry of CpNb(N ^t Bu)Cl ₂ (7). | 60 |
| 2.8.1 | Reaction of CpNb(N ^t Bu)Cl ₂ with Trimethylphosphine: <i>Preparation of CpNb(N^tBu)Cl₂(PMe₃) (17).</i> | 61 |
| 2.8.2 | Reaction of CpNb(N ^t Bu)Cl ₂ with LiOAr: <i>Preparation of CpNb(N^tBu)(OAr)₂ (Ar = ⁱPr₂C₆H₃ (18), Ph₂C₆H₃ (19)).</i> | 61 |
| 2.8.3 | Reaction of CpNb(N ^t Bu)Cl ₂ with LiO ^t Bu: <i>Preparation of CpNb(N^tBu)(O^tBu)₂ (20).</i> | 62 |
| 2.8.4 | Reaction of CpNb(N ^t Bu)Cl ₂ with Benzaldehyde: <i>Attempted Preparation of CpNb(O)Cl₂.</i> | 63 |
| 2.8.5 | Reaction of CpNb(N ^t Bu)Cl ₂ with MeMgCl: <i>Preparation of CpNb(N^tBu)Cl(Me) (21).</i> | 63 |
| 2.8.5.1 | Molecular Structure of CpNb(N ^t Bu)Cl(Me) (21). | 64 |
| 2.8.5.2 | Reactivity Studies on CpNb(N ^t Bu)Cl(Me): <i>Preparation of CpNb(N^tBu)Cl(Me)(PMe₃) (22).</i> | 65 |
| 2.8.6 | Reaction of CpNb(N ^t Bu)Cl ₂ with Me ₃ CCH ₂ MgCl: <i>Preparation of CpNb(N^tBu)(CH₂CMe₃) (23).</i> | 66 |
| 2.8.6.1 | Evidence of Agostic Interactions in CpNb(N ^t Bu)(CH ₂ CMe ₃) ₂ : <i>Preparation and Spectroscopic Characterisation of CpNb(N^tBu)(CHDCMe₃)₂ (24).</i> | 69 |

| | |
|---|--------|
| 2.9 Other reactions of CpNb(N ^t Bu)Cl ₂ . | 71 |
| 2.10 Attempted Preparation of a Half-Sandwich <i>bis</i> -Imido Species [CpNb(NR) ₂]. | 71 |
| 2.10.1 Synthetic Strategy. | 72 |
| 2.10.2 Reaction of CpNb(N ^t Bu)Cl ₂ with LiNH ^t Bu: <i>Preparation of CpNb(N^tBu)(NH^tBu)Cl (25).</i> | 72 |
| 2.10.3 Reaction of CpNb(N ^t Bu)Cl(Me) with LiNHR: <i>Preparation of CpNb(N^tBu)(NR)(Me)</i> <i>(R = ^tBu (26), 2,6-ⁱPr₂C₆H₃ (27)).</i> | 73 |
| 2.11 ¹³ C NMR Chemical Shifts of Half-Sandwich Imido Species. | 74 |
| 2.12 Summary. | 78 |
| 2.13 References. | 79 |
| Chapter 3 - A Comparative Study of the Bonding in Group 5 Half-Sandwich Imido Complexes & Related Cyclopentadienyl Compounds. | 82 |
| 3.1 Introduction. | 83 |
| 3.2 Fenske-Hall Molecular Orbital Calculations. | 84 |
| 3.3 The Nature of the Imido-Metal Bonding in CpNb(NMe)Cl ₂ . | 86 |
| 3.3.1 The [CpNbCl ₂] ²⁺ Fragment. | 87 |
| 3.3.2 The [NMe] ²⁻ Fragment. | 88 |
| 3.3.3 Interaction [CpNbCl ₂] ²⁺ with [NMe] ²⁻ . | 88 |
| 3.4 The Interaction of Trimethylphosphine with CpNb(NMe)Cl ₂ . | 89 |
| 3.4.1 The [CpNb(NMe)Cl ₂] Fragment. | 90 |
| 3.4.2 The [PMe ₃] Fragment. | 91 |
| 3.4.3 Interaction of [PMe ₃] with [CpNb(NMe)Cl ₂]. | 91 |
| 3.5 A Comparison of the Electronic Structure of CpNb(NMe)Cl ₂ with Complexes of the Type Cp ₂ ZrX ₂ . | 92 |
| 3.5.1 The Frontier Orbital Picture for [Cp ₂ Zr] | 95 |
| 3.5.2 The Frontier Orbitals of the [CpNb(NMe)] ²⁺ Fragment. | 96 |
| 3.5.3 Interaction of [Cp ₂ Zr] ²⁺ with Two Hydride Ligands. | 97 |
| 3.5.4 Interaction of [CpNb(NMe)] ²⁺ with Two Hydride Ligands. | 98 |

| | | |
|--|---|-----|
| 3.5.5 | Interaction of $[\text{Cp}_2\text{Zr}]^{2+}$ with Two Chloride Ligands. | 99 |
| 3.5.6 | Interaction of $[\text{CpNb}(\text{NMe})]^{2+}$ with Two Chloride Ligands. | 100 |
| 3.5.7 | Composition of the Frontier Orbitals of Cp_2ZrCl_2 and $\text{CpNb}(\text{NMe})\text{Cl}_2$. | 102 |
| 3.6 | A Comparison of the Electronic Structure of $\text{Cp}^*\text{Ta}(\eta^2\text{-CHPMe}_2)\text{X}_2$ with Cp_2ZrX_2 and $\text{CpNb}(\text{NR})\text{X}_2$. | 102 |
| 3.6.1 | A Comparison of the Frontier Orbitals of $[\text{CpNb}(\text{NMe})]^{2+}$, $[\text{Cp}_2\text{Zr}]^{2+}$ and $[\text{CpNb}(\eta^2\text{-CHPMe}_2)]^{2+}$ Fragments. | 104 |
| 3.6.2 | Interaction of $[\text{CpNb}(\eta^2\text{-CHPMe}_2)]^{2+}$ with Two Hydride Ligands. | 105 |
| 3.6.3 | The Frontier Orbitals of $\text{CpNb}(\eta^2\text{-CHPMe}_2)\text{Cl}_2$. | 106 |
| 3.7 | Discussion and Summary. | 107 |
| 3.8 | References. | 110 |
| Chapter Four - Multiply-Bonded Nitrogen Ligands to Mo, W and Re Supported by Halide and Trialkylphosphine Ligation - A Search for Bond-Stretch Isomers of Multiply-Bonded Nitrogen Ligands. | | 112 |
| 4.1 | Introduction. | 113 |
| 4.2 | Synthetic Strategy. | 115 |
| 4.3 | Preparation of the Nitrido Starting Materials, $\text{M}(\text{N})\text{Cl}_3$ ($\text{M} = \text{Mo}, \text{W}$). | 115 |
| 4.3.1 | Synthesis of $\text{Mo}(\text{N})\text{Cl}_3$ (1). | 117 |
| 4.3.2 | Synthesis of $\text{W}(\text{N})\text{Cl}_3$ (2). | 117 |
| 4.3.3 | Syntheses of $\text{Mo}(\text{N})\text{Cl}_3\text{L}_2$ ($\text{L} = \text{CH}_3\text{CN}$ (3), THF (4)). | 118 |
| 4.3.4 | Synthesis of $\text{W}(\text{N})\text{Cl}_3(\text{CH}_3\text{CN})_2$ (5). | 119 |
| 4.4 | The Reaction of Molybdenum Nitrido Compounds with Trimethylphosphine: <i>The Preparation, Structure and Reactivity of a Molybdenum Phosphiniminato Complex.</i> | 120 |
| 4.4.1 | The Preparation of $[\text{Mo}(\text{NPMe}_3)\text{Cl}_2(\text{PMe}_3)_3]\text{Cl}\cdot\text{CH}_2\text{Cl}_2$ (6). | 120 |
| 4.4.2 | Molecular Structure of $[\text{Mo}(\text{NPMe}_3)\text{Cl}_2(\text{PMe}_3)_3]\text{Cl}\cdot\text{CH}_2\text{Cl}_2$ (6). | 121 |
| 4.4.3 | A Molecular Orbital Study of NPR_3 in $[\text{Mo}(\text{NPMe}_3)\text{Cl}_2(\text{PMe}_3)_3]^+$. | 124 |
| a). | The $[\text{MoCl}_2(\text{PMe}_3)_3]^{2+}$ Fragment. | 125 |
| b). | The $[\text{NPMe}_3]^-$ Fragment. | 125 |

| | |
|---|-----|
| c). The Interaction of $[\text{MoCl}_2(\text{PMe}_3)_3]^{2+}$ with $[\text{NPMe}_3]^-$. | 126 |
| 4.4.4 The Conversion of (6) into an Anionic Nitrido-Bridged Dimer: <i>Preparation of $\{[\text{MoCl}_3(\text{PMe}_3)_2]_2\text{N}\}[\text{Me}_3\text{PNPMe}_3]$ (7).</i> | 127 |
| 4.4.4.1 The Molecular Structure of $\{[\text{MoCl}_3(\text{PMe}_3)_2]_2\text{N}\}[\text{Me}_3\text{PNPMe}_3]$ (7). | 129 |
| 4.4.4.2 The Metal-Nitrogen Bonding in $\{[\text{MoCl}_3(\text{PMe}_3)_2]_2\text{N}\}[\text{Me}_3\text{PNPMe}_3]$ (7). | 129 |
| 4.4.5 UV/Visible Studies on the Conversion of Complex (6) to (7). | 130 |
| 4.4.6 Further Attempts to Prepare $\text{Mo}(\text{N})\text{Cl}_3(\text{PMe}_3)_3$. | 131 |
| 4.4.6.1 The Reaction of $\text{Mo}(\text{N})\text{Cl}_3$ with Neat PMe_3 . | 131 |
| 4.4.6.2 The Reaction of $\text{Mo}(\text{N})\text{Cl}_3\text{L}_2$ with PMe_3 ($\text{L} = \text{CH}_3\text{CN}, \text{THF}$). | 132 |
| 4.5 The Reaction of $\text{Mo}(\text{N})\text{Cl}_3$ with Other Tertiary Phosphines: <i>Preparation of $\text{Mo}(\text{N})\text{Cl}_3(\text{PR}_3)$ ($\text{R} = \text{Ph}$ (8), Cy (9)).</i> | 132 |
| 4.6 The Reaction of $\text{W}(\text{N})\text{Cl}_3$ with Tertiary Phosphines: <i>Preparation of $\text{W}(\text{N})\text{Cl}_3(\text{PR}_3)$ ($\text{PR}_3 = \text{Me}_3$ (10), PMe_2Ph (11), PPh_3 (12)).</i> | 133 |
| 4.7 The Preparation of $[\text{W}(\text{NPMe}_3)\text{Cl}_2(\text{PMe}_3)_3]^+\text{Cl}^-$ (13). | 135 |
| 4.8. Attempts to Prepare Rhenium Nitrido Bond-Stretch Isomers. | 136 |
| 4.8.1 The Reaction of KReO_4 with $\text{H}_2\text{NNH}_2 \cdot 2\text{HCl}$ and PMe_3 . | 137 |
| 4.8.2 The Reduction of KReO_4 with $\text{H}_2\text{NNH}_2 \cdot 2\text{HCl}$ in the presence of PR_3 ($\text{PR}_3 = \text{PMe}_2\text{Ph}, \text{PPh}_2\text{Me}$): <i>Preparation of $\text{Re}(\text{N})\text{Cl}_2(\text{PMe}_2\text{Ph})_3$ (15) and $\text{Re}(\text{N})\text{Cl}_2(\text{PMePh}_2)_2$ (16).</i> | 138 |
| 4.9 Summary and Conclusions. | 140 |
| 4.10 References. | 141 |
| Chapter Five - A Quantum Chemical Analysis of the Bonding in Seven Coordinate Bond-Stretch Isomers of $\text{Nb}(\text{O})\text{Cl}_3(\text{PMe}_3)_3$ and Closely Related Hypothetical Nitride $\text{Mo}(\text{N})\text{Cl}_3(\text{PMe}_3)_3$. | 145 |
| 5.1 Introduction. | 146 |
| 5.2 Molecular Orbital Calculations on Bond-Stretch Isomer Systems. | 146 |
| 5.2.1 Extended Hückel M.O. Calculations. | 146 |
| 5.2.2 Fenske-Hall M.O. Calculations. | 148 |
| 5.3 Fenske-Hall MO Calculations on α and β - $\text{Nb}(\text{O})\text{Cl}_3(\text{PMe}_3)_3$. | 149 |
| 5.3.1 Two Fragment Analysis. | 150 |

| | |
|--|------------|
| a). The [NbCl ₃ (PMe ₃) ₃] Fragment. | 150 |
| b). Interaction of the [NbCl ₃ (PMe ₃) ₃] Fragment with Oxygen | 151 |
| 5.3.2 Five Fragment Analysis. | 154 |
| a). The [Nb(PMe ₃) ₃] ³⁺ Fragment. | 154 |
| b) β-Nb(O)Cl ₃ (PMe ₃) ₃ Bonding Description. | 155 |
| c). α-Nb(O)Cl ₃ (PMe ₃) ₃ Bonding Description. | 156 |
| d). Mulliken Population Analysis. | 157 |
| 5.3.3 Fenske-Hall Calculations on Nb(O)Cl ₃ (PH ₃) ₃ . | 158 |
| 5.3.4 Variation of the Nb-O Bond Length in Nb(O)Cl ₃ (PMe ₃) ₃ . | 159 |
| a). The MO Energies. | 160 |
| b). The MO Composition. | 161 |
| c). The Mulliken Overlap Population and Final Mulliken Population. | 162 |
| d). Oxygen-Hydrogen Interatomic Distances. | 164 |
| 5.3.5 Overall Bonding Description. | 166 |
| 5.4 Fenske-Hall MO Calculations on Nb(S)Cl ₃ (PMe ₃) ₃ . | 167 |
| 5.5 Fenske-Hall MO Calculations on Mo(N)Cl ₃ (PMe ₃) ₃ . | 168 |
| 5.5.1 Mo-N Bonding in Mo(N)Cl ₃ (PMe ₃) ₃ . | 169 |
| 5.6 Summary and Conclusions. | 171 |
| 5.7 References. | 172 |
| Chapter Six - Experimental Details. | 173 |
| 6.1 General | 174 |
| 6.1.1 Experimental Techniques. | 174 |
| 6.1.2 Solvents and Reagents. | 174 |
| 6.1.3 Computational Methods. | 176 |
| 6.1.4 Basis Functions for FHMO Calculations. | 176 |
| 6.2 Experimental Details to Chapter 2. | 178 |
| 6.2.1 Reaction of Cp*TaCl ₂ (PMe ₃) ₂ with Me ₃ SiN ₃ : <i>Preparation of Cp*Ta(NSiMe₃Cl₂) (1).</i> | 178 |

| | | |
|------------|---|-----|
| 6.2.2 | Reaction of CpNbCl ₄ with (Me ₃ Si) ₂ NMe: <i>Preparation of CpNb(NMe)Cl₂ (2).</i> | 179 |
| 6.2.3 | Reaction of Cp*TaCl ₄ with (Me ₃ Si) ₂ NMe: <i>Preparation of [Cp*TaCl₃]₂[NMe] (3).</i> | 180 |
| 6.2.4 | Reaction of CpTaCl ₄ with (Me ₃ Si) ₂ NCN: <i>Preparation of [CpTa(NCN)Cl₂(CH₃CN)]_n (6).</i> | 180 |
| 6.2.5 | Reaction of CpNbCl ₄ with Me ₃ SiNH ^t Bu: <i>Preparation of CpNb(N^tBu)Cl₂ (7).</i> | 181 |
| 6.2.6 | Reaction of CpNbCl ₄ with Me ₃ SiNH(2,6- ⁱ Pr ₂ C ₆ H ₃): (A) <i>Preparation of [Cp(NAr)Cl₃]⁻[Me₃SiNH₂Ar]⁺</i> (8) <i>Preparation of CpNb(NAr)Cl₂ (9) (Ar = 2,6-ⁱPr₂C₆H₃).</i> | 182 |
| 6.2.7 | Reaction of CpTaCl ₄ with LiN ^t Bu(SiMe ₃): <i>Preparation of CpTa(N^tBu)Cl₂ (10).</i> | 184 |
| 6.2.8 | Reaction of CpTaCl ₄ with LiN(2,6- ⁱ Pr ₂ C ₆ H ₃)(SiMe ₃): <i>Preparation of CpTa(N-2,6-ⁱPr₂C₆H₃)Cl₂ (11).</i> | 185 |
| 6.2.9 | Reaction of Cp*TaCl ₄ with Me ₃ SiNHR Reagents: <i>Preparation of Cp*Ta(N^tBu)Cl₂ (12).</i> | 185 |
| 6.2.10 | Reaction of CpNb(NMe)Cl ₂ with PMe ₃ : <i>Preparation of CpNb(NMe)Cl₂(PMe₃) (14).</i> | 186 |
| 6.2.11 | Reaction of CpNb(NMe)Cl ₂ with LiO-2,6-Me ₂ C ₆ H ₃ : <i>Preparation of CpNb(NMe)(O-2,6-Me₂C₆H₃)Cl₂ (15).</i> | 187 |
| 6.2.12 | Reaction of CpNb(NMe)Cl ₂ with LiO ^t Bu: <i>Preparation of CpNb(NMe)(O^tBu)₂ (16).</i> | 188 |
| 6.2.13 | Reaction of CpNb(N ^t Bu)Cl ₂ with PMe ₃ : <i>Preparation of CpNb(N^tBu)Cl₂(PMe₃) (17).</i> | 189 |
| 6.2.14 a). | Reaction of CpNb(N ^t Bu)Cl ₂ with LiO- ⁱ Pr ₂ C ₆ H ₃ : <i>Preparation of CpNb(N^tBu)(O-ⁱPr₂C₆H₃)₂ (18).</i> | 190 |
| 6.2.14 b). | Reaction of CpNb(N ^t Bu)Cl ₂ with LiO-Ph ₂ C ₆ H ₃ : <i>Preparation of CpNb(N^tBu)(O-Ph₂C₆H₃)₂ (19).</i> | 191 |
| 6.2.15 | Reaction of CpNb(N ^t Bu)Cl ₂ with LiO ^t Bu: <i>Preparation of CpNb(N^tBu)(O^tBu)₂ (20).</i> | 192 |
| 6.2.16 | Reaction of CpNb(N ^t Bu)Cl ₂ with MeMgCl: <i>Preparation of CpNb(N^tBu)Cl(Me) (21).</i> | 193 |
| 6.2.17 | Reaction of CpNb(N ^t Bu)Cl(Me) with PMe ₃ : <i>Preparation of CpNb(N^tBu)Cl(Me)(PMe₃) (22).</i> | 194 |

| | | |
|------------|---|-----|
| 6.2.18 a). | Reaction of $\text{CpNb}(\text{N}^t\text{Bu})\text{Cl}_2$ with $\text{Me}_3\text{CCH}_2\text{MgCl}$: <i>Preparation of $\text{CpNb}(\text{N}^t\text{Bu})(\text{CH}_2\text{CMe}_3)$ (23).</i> | 195 |
| 6.2.18 b). | Reaction of $\text{CpNb}(\text{N}^t\text{Bu})\text{Cl}_2$ with $\text{Me}_3\text{CCH}_2\text{MgBr}$: <i>Preparation of $\text{CpNb}(\text{N}^t\text{Bu})(\text{CHDCMe}_3)$ (24).</i> | 196 |
| 6.2.19 | Reaction of $\text{CpNb}(\text{N}^t\text{Bu})\text{Cl}_2$ with LiNH^tBu : <i>Preparation of $\text{CpNb}(\text{N}^t\text{Bu})(\text{NH}^t\text{Bu})\text{Cl}$ (25).</i> | 197 |
| 6.2.20 a). | Reaction of $\text{CpNb}(\text{N}^t\text{Bu})\text{Cl}(\text{Me})$ with LiNH^tBu : <i>Preparation of $\text{CpNb}(\text{N}^t\text{Bu})(\text{NH}^t\text{Bu})(\text{Me})$ (26).</i> | 198 |
| 6.2.20 b). | Reaction of $\text{CpNb}(\text{N}^t\text{Bu})\text{Cl}(\text{Me})$ with LiNHAr : <i>Preparation of $\text{CpNb}(\text{N}^t\text{Bu})(\text{NHAr})$ ($\text{Ar} = 2,6\text{-}^i\text{Pr}_2\text{C}_6\text{H}_3$ (27)).</i> | 199 |
| 6.3 | Experimental Details to Chapter 3. | 200 |
| 6.3.1 | Geometry and Coordinates for FHMO Calculations. | 200 |
| 6.4 | Experimental Details to Chapter 4. | 201 |
| 6.4.1 | Synthesis of $\text{Mo}(\text{N})\text{Cl}_3$ (1). | 201 |
| 6.4.2 | Synthesis of $\text{W}(\text{N})\text{Cl}_3$ (2). | 201 |
| 6.4.3 | Synthesis of $\text{Mo}(\text{N})\text{Cl}_3(\text{CH}_3\text{CN})_2$ (3). | 202 |
| 6.4.4 | Synthesis of $\text{Mo}(\text{N})\text{Cl}_3(\text{THF})_2$ (4). | 203 |
| 6.4.5 | Synthesis of $\text{W}(\text{N})\text{Cl}_3(\text{CH}_3\text{CN})_2$ (5). | 203 |
| 6.4.6 | Reaction of $\text{Mo}(\text{N})\text{Cl}_3$ with PMe_3 : <i>Preparation of $[\text{Mo}(\text{NPMe}_3)\text{Cl}_2(\text{PMe}_3)_3]^+\text{Cl}^-$ (6). (A) in Dichloromethane. (B) in Neat Trimethylphosphine.</i> | 204 |
| 6.4.7 | Reaction of $\text{Mo}(\text{N})\text{Cl}_3(\text{THF})_2$ with PMe_3 . | 205 |
| 6.4.8 | Conversion of $\text{Mo}(\text{NPMe}_3)\text{Cl}_2(\text{PMe}_3)_3]^+\text{Cl}^-$ (6) to $[(\text{MoCl}_3(\text{PMe}_3)_2)_2\text{N}][\text{Me}_3\text{PNPMe}_3]^+$ (7). | 205 |
| 6.4.9 | Reaction of $\text{Mo}(\text{N})\text{Cl}_3$ with PPh_3 : <i>Preparation of $\text{Mo}(\text{N})\text{Cl}_3(\text{PPh}_3)_2$ (8).</i> | 206 |
| 6.4.10 | Reaction of $\text{Mo}(\text{N})\text{Cl}_3$ with PCy_3 : <i>Preparation of $\text{Mo}(\text{N})\text{Cl}_3(\text{PCy}_3)_2$ (9).</i> | 207 |
| 6.4.11 | Reaction of $\text{W}(\text{N})\text{Cl}_3$ with PMe_3 : <i>(A) Preparation of $\text{W}(\text{N})\text{Cl}_3(\text{PMe}_3)_2$ (10). (A) Preparation of $[\text{W}(\text{NPMe}_3)\text{Cl}_2(\text{PMe}_3)_3]^+\text{Cl}^-$ (13).</i> | 207 |
| 6.4.12 | Reaction of $\text{W}(\text{N})\text{Cl}_3$ with PMe_2Ph : <i>Preparation of $\text{W}(\text{N})\text{Cl}_3(\text{PMe}_2\text{Ph})_2$ (11).</i> | 209 |

| | |
|--|-----|
| 6.4.13 Reaction of $W(N)Cl_3$ with PPh_3 : <i>Preparation of $W(N)Cl_3(PPh_2)_2$ (12).</i> | 210 |
| 6.4.14 The Reaction of $KReO_4$ with $H_2NNH_2 \cdot 2HCl$ and PMe_3 . | 211 |
| 6.4.15 The Reaction of $KReO_4$ with $H_2NNH_2 \cdot 2HCl$ and PMe_2Ph : <i>Preparation of $Re(N)Cl_2(PMe_2Ph)_3$ (15)</i> | 212 |
| 6.4.16 The Reaction of $KReO_4$ with $H_2NNH_2 \cdot 2HCl$ and PMe_2Ph : <i>Preparation of $Re(N)Cl_2(PMe_2Ph)_3$ (16)</i> | 213 |
| 6.4.17 Coordinates Used in FHMO Calculations on $[Mo(NPMe_3)Cl_2(PMe_3)_3]^+$. | 214 |
| 6.5 Experimental Details to Chapter 5. | 214 |
| 6.5.1 Geometry and Coordinates Used in FHMO Calculations. | 214 |
| 6.6 Further Experimental Details. | 215 |
| 6.6.2 Reaction of $W(Ntol)Cl_4$ with $LiO-2,6-Me_2C_6H_3$: <i>Preparation of $W(Ntol)(O-2,6-Me_2C_6H_3)_4$.</i> | 215 |
| 6.6.3 The Synthesis of $Nb(S)Cl_3(CH_3CN)_2$. | 216 |
| 6.7 References. | 217 |
| Appendices. | 219 |
| Appendix 1: | |
| A: Crystal Data for $CpNb(NMe)Cl_2$. | 220 |
| B: Crystal Data for $CpNb(N^tBu)Cl_2$. | 220 |
| C: Crystal Data for $CpNb(N-2,6-^iPr_2C_6H_3)Cl_2$. | 221 |
| D: Crystal Data for $CpNb(NMe)Cl_2(PMe_3)$ | 221 |
| E: Crystal Data for $CpNb(N^tBu)Cl(Me)$. | 222 |
| F: Crystal Data for $[Mo(NPMe_3)Cl_2(PMe_3)_3]Cl \cdot CH_2Cl_2$. | 222 |
| G: Crystal Data for $[(PMe_3)_2Cl_3MoNMoCl_3(PMe_3)_2][Me_3PNPMe_3] \cdot CH_2Cl_2$. | 223 |
| Appendix 2: | 224 |
| First Year Induction Course: October 1987 | 224 |
| Research Colloquia and Lectures Organised by the Department of Chemistry During 1987-1990. | 224 |
| Conferences and Symposia Attended. | 235 |

| | |
|---|-----|
| Publications. | 236 |
| Appendix 3: | |
| Synthesis and Characterisation of $W(Ntol)(O-2,6-Me_2C_6H_3)_4$. | 237 |
| Synthesis and Characterisation of $Nb(S)Cl_3(CH_3CN)_2$. | 238 |
| References. | 239 |

CHAPTER ONE

Transition Metal-Nitrogen Multiple Bonds - An Overview of their Synthesis, Structure, Characterisation and Bonding.

1.1 Introduction.

Transition metal-nitrogen multiply bonded species play a crucial rôle in many chemical processes, acting as homogeneous and heterogeneous catalysts for a variety of important industrial and biochemical reactions. However, as yet relatively little is understood about the nature of the interaction of nitrogen with transition metals. The aim of this thesis is to prepare a range of compounds with metal-bound nitrogen in a number of different but well defined environments, and to gain an understanding of their electronic structure and reactivity.

Recent years have witnessed much renewed interest in the chemistry of cyclopentadienyl metal oxo species. In general, developments in the chemistry of analogous imido systems have lagged behind, primarily due to a lack of suitable synthetic routes to half-sandwich imido species. Thus, in chapter 2, a convenient synthetic entry into a range of half-sandwich imido derivatives of the heavier Group 5 metals is described. Alkyl, alkoxide and phenoxide derivatives have been prepared and characterised, and strategies for the synthesis of half-sandwich '*bis* imido' compounds of the type $[\text{CpM}(\text{NR})_2]$ have been explored.

The bonding of the imido ligand is of central importance to developing an understanding of the chemistry of this multiply bonded unit. These aspects are addressed in chapter 3 using Fenske-Hall quantum chemical MO calculations, which have allowed a comparison between half-sandwich imido compounds, the Group 4 metallocenes and compounds of the type $\text{Cp}^*\text{Ta}(\eta^2\text{-CHPMe}_2)\text{X}_2$ ($\text{X} = \text{H}, \text{Cl}$), containing the unusual phosphino-carbene ligand.

Chapter 4 describes a search for metal-nitrogen compounds exhibiting the intriguing phenomenon of bond-stretch isomerism. A detailed understanding of this phenomenon has been hampered by a lack of systems suitable for study. Following the discovery of a series of perfectly matched bond-stretch isomers for seven coordinate oxo and sulphido complexes of the type $\text{Nb}(\text{E})\text{X}_3(\text{PMe}_3)_3$ ($\text{E} = \text{O}, \text{S}; \text{X} = \text{Cl}, \text{Br}$), it was anticipated that should a compound of the type $\text{M}(\text{N})\text{Cl}_3(\text{PMe}_3)_3$ ($\text{M} = \text{Mo}, \text{W}$) prove accessible, this too might be expected to exhibit a similar effect. Thus, chapter 4 incorporates attempts to prepare such a compound by treatment of molybdenum and tungsten nitrido-halides with tertiary phosphines. An unexpected outcome of these studies was the isolation of a phosphiniminato compound which undergoes a remarkably clean transformation to a binuclear nitrogen-bridged species. Mechanistic aspects of this transformation have been probed. Chapter 4 also includes other attempts to prepare bond-stretch isomers from the tungsten and rhenium nitride starting materials, which led to the isolation of species of the type $\text{W}(\text{N})\text{Cl}_3(\text{PR}_3)_2$ and $\text{Re}(\text{N})\text{Cl}_2(\text{PR}_3)_n$ ($n = 2, 3$).

The potential importance of bond-stretch isomerism to the bonding of main group atoms to metal centres, and a desire to establish some valid criteria for predicting in which systems bond-stretch isomerism will occur, demanded a more detailed analysis of the seven coordinate oxo and thiohalide systems recently established. These bonding studies are described in chapter 5, employing Fenske-Hall quantum chemical MO calculations, firstly on the oxo and sulphido isomers of $\text{Nb}(\text{E})\text{Cl}_3(\text{PMe}_3)_3$ ($\text{E} = \text{O}, \text{S}$) and then on the hypothetical nitrido species $\text{Mo}(\text{N})\text{Cl}_3(\text{PMe}_3)_3$.

The remainder of this chapter is devoted to a review of the occurrence, electronic structure and uses of transition metal nitrido and imido compounds. Since most of the nitrido and imido compounds discussed in this thesis are of low nuclearity, the following review is primarily restricted to mononuclear and binuclear species. Cluster, polymer and interstitial nitrido species are covered in less detail.

1.2 Occurrence.

1.2.1 Nitrido Complexes.

Apart from the carbyne ligand, the nitride ligand is the strongest known π -electron donor. The terminal ligand $M\equiv N:$ is formally described as a triple bond, one σ and two π , the latter from the overlap of the nitrogen $p\pi$ -orbitals with two unoccupied transition metal $d\pi$ -orbitals. High bond order is achieved due to the relatively low electronegativity of the nitrogen atom, and sufficient supply of unoccupied d-orbitals on the transition metal. As a result, monomeric nitrido species are only formed by metals in their higher oxidation states usually with d^0 and d^2 configurations. Most nitrido species are found in second- or third-row transition metal complexes; only recently have first-row vanadium, chromium, manganese and iron species been prepared¹. This trend reflects the very effective high-oxidation-state stabilisation brought about by nitride (N^{3-}), which will favour heavier elements since these are more prone to formation of high oxidation states. For binuclear nitrido complexes the d^4 configuration can be found, as in $[M_2NX_8(H_2O)_2]^{3-}$ (where $M=Ru, Os, X=Cl^-, Br^-, NCS^-$)²⁻⁵. In trinuclear complexes, where there is much reduced capacity on the part of the bridging nitride for π -donation, d^5 and d^6 configurations are found. The distribution of structurally characterised transition metal nitrido compounds is illustrated in Figure 1.1, and clearly shows that the majority of nitrido species are formed by the elements Mo, W, Re and Os.

| Group | 1 | 2 | 3 | 4 | 5 | 6 | 7 | 8 |
|-------|---|----|----|---------|---------|----------|----------|---------|
| | | | | | | | | |
| | K | Ca | Sc | Ti 0 | V 2 | Cr 1 | Mn 2 | Fe 1 |
| | | | | Zr 0 | Nb 1 | Mo 18 | Tc 5 | Ru 4 |
| | | | | Hf 0 | Ta 2 | W 8 | Re 11 | Os 8 |

Figure 1.1, Distribution of structurally characterised metal nitrido compounds in Groups 4-8.

1.2.2 Imido Complexes.

Terminal transition metal imido complexes follow very similar trends to that of nitrido species. This is not surprising, as in most cases the linear imido ligand (NR^{2-}) can be considered to be isoelectronic and isolobal with the nitride ligand (N^{3-}), thus is capable of forming a triple bond. All fully characterised monomeric imido complexes are found with d^0 and d^2 configurations, although d^6 and d^8 fluoro alkylimido complexes have been suggested⁶. The vast majority of imido compounds occur for metals in Groups 5, 6, 7 and 8.

1.3 Electronic Structure and Bonding.

In this section, an outline of modes and simple bonding descriptions of transition metal nitrido and imido complexes is given. More sophisticated views of transition metal nitrogen bonding are discussed in chapters 4 and 5.

1.3.1 Bonding Modes.

1.3.1.1 The Nitride Ligand.

Nitride ligands are found in a number of different environments, as illustrated in Figure 1.2

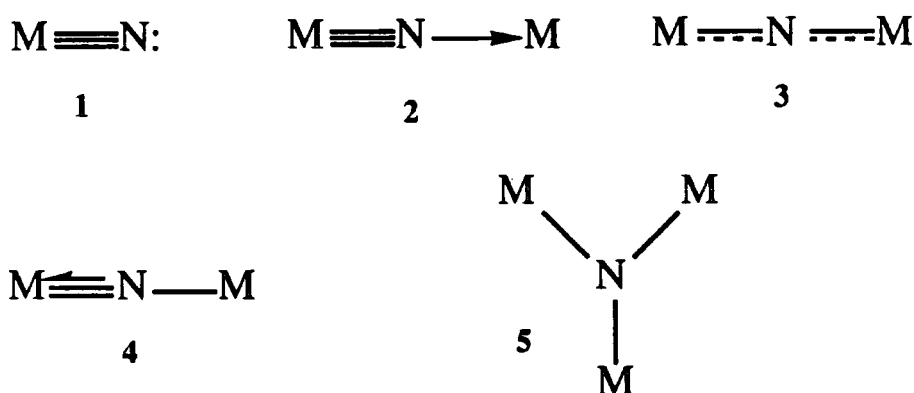


Figure 1.2, *Coordination modes of nitride ligands.*

Most nitrido complexes involve a terminal N^{3-} group (1), the $M \equiv N$ bond being extremely short (1.52-1.79Å) and generally described as a σ -bond and two degenerate π -bonds (Figure 1.3).

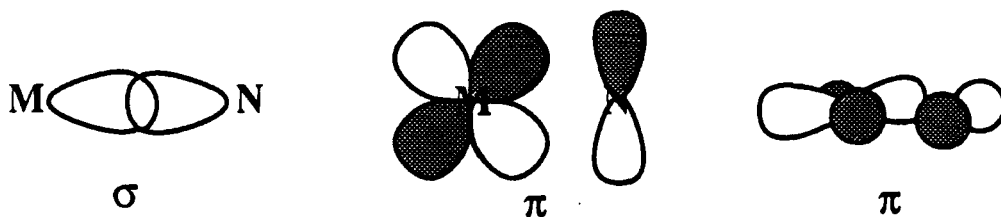


Figure 1.3.

The nitrogen lone pair is thought to have little influence on bonding in terminal nitrido species. Singly bridging nitride ligands may have either linear asymmetric (2), or less commonly linear symmetric bridges (3). In asymmetric bridged species, the free electron pair on the nitride ligand leads to the formation of a second significantly weaker bond to an adjacent metal centre, and the formation of columnar structures, as in $[\text{Re}(\text{N})\text{Cl}_4]_{\infty}^7$, and the recently discovered stable, polymeric $[\text{V}(\mu\text{-N})\text{Cl}_2(\text{py})_2]_{\infty}^8$ (Figure 1.4).

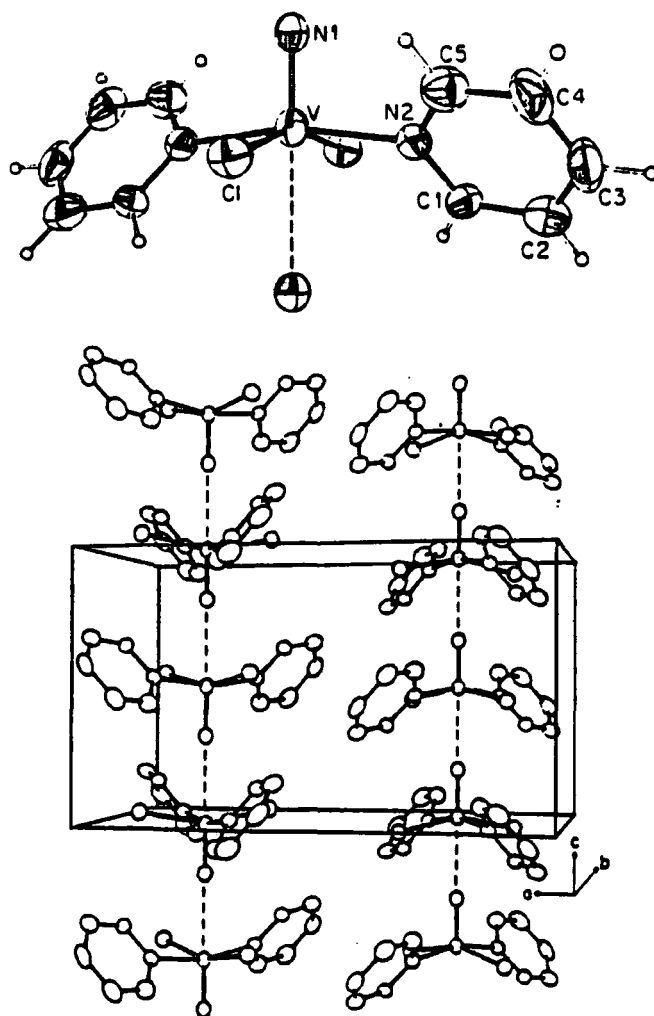


Figure 1.4, ORTEP drawings of $[\text{V}(\mu\text{-N})\text{Cl}_2]_2(\text{py})_2]_{\infty}$.

In these species the short bond can be viewed in the same way as the terminal nitride, the long bond being a σ -dative type bond, in which the occupied nitrogen sp -hybrid lying along the z -axis overlaps with an unoccupied d_{z^2} , p_z hybrid orbital of the metal, as illustrated in Figure 1.5.

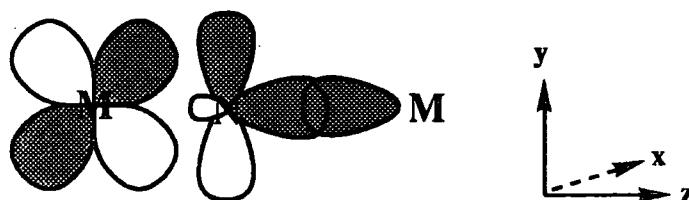


Figure 1.5.

Mixed metal μ_2 -nitride species, such as $(\text{PEt}_2\text{Ph})_3\text{Cl}_2\text{Re}\equiv\text{N}:\rightarrow\text{PtCl}_2(\text{PEt}_3)$ have been reported⁹. More recently, Doherty has shown that by a simple condensation, a roughly linear nitrogen-bridged dimer, $(\text{Me}_3\text{SiO})_3\text{V}\equiv\text{N}-\text{Pt}(\text{PEt}_3)_2(\text{Me})$, possessing robust metal nitrogen bonds can be formed¹⁰. The bonding in this compound has been described as consisting of covalent bonds between the nitride ligand and two different metal centres (4).

More favourable μ_2 -nitride bonding is possible in tetrameric compounds (Figure 1.6), in which a second σ -dative bond is achieved via a metal orbital perpendicular to the z -axis.

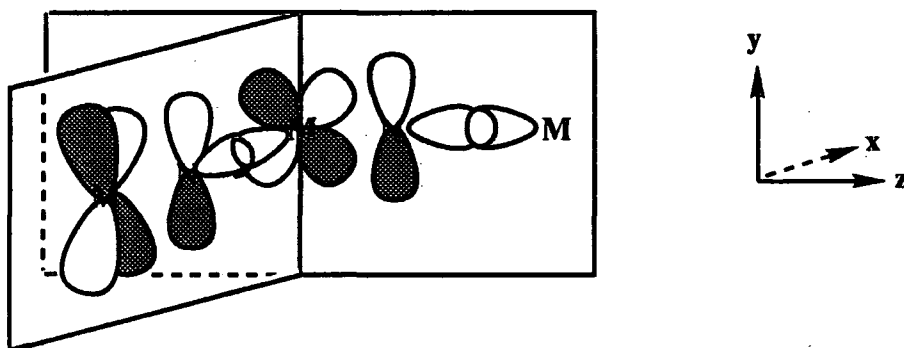


Figure 1.6

Such tetramers occur far more frequently than polymers of the $\text{Re}(\text{N})\text{Cl}_4$ type, for example $[\text{Mo}(\text{N})\text{Cl}_3]_4$ ¹¹ and $[\text{M}(\text{N})\text{Cl}_3\text{POCl}_3]_4$ ($\text{M}=\text{Mo}, \text{W}, \text{Re}$)¹²⁻¹⁴.

Symmetric μ_2 -nitride bridged species are relatively rare, and mainly observed in binuclear complexes. Structurally characterised symmetrically bridged species are shown in Table 1.1.

| Group | Complex | M-N (Å) | ∠ M-N-M (°) | d e ⁻ | Ref. |
|-------|--|------------------------|-------------|------------------|------|
| 5 | $[\text{Nb}_2(\mu\text{-N})\text{Br}_{10}](\text{NH}_4)_3$ | 1.845(2) | 180 | 0 | 16 |
| | $[\text{Ta}_2(\mu\text{-N})\text{Br}_{10}](\text{NH}_4)_3$ | 1.849(2) | 180 | 0 | 15 |
| | $[\text{Ta}_2(\mu\text{-N})\text{I}_{10}](\text{NH}_4)_3$ | 1.847(6) | 180 | 0 | 16 |
| 6 | $[\text{Mo}_2(\mu\text{-N})(\text{S}_2\text{P}(\text{OMe})_2)_2]_2^{\text{a}}$ | 1.867(12) | 174.6(9) | 1 | 17 |
| | $[\text{Mo}_2(\mu\text{-N})\text{Cl}_6(\text{PMe}_3)_4][\text{N}(\text{PMe}_3)_2]$ | 1.873(8), 1.851(8). | 175.3(4) | 2 | 18 |
| | $[\text{W}_2(\mu\text{-N})\text{Cl}_{10}]\text{PPh}_4$ | 1.79, 1.88(2) | 173(1) | 0 | 19 |
| | $[\text{W}_3(\mu\text{-N})_2\text{Cl}_{14}](\text{PPh}_4)_2$ | 1.81, 1.86(1) | 175.6(8) | 0 | 20 |
| 8 | $[\text{Fe}(\text{Ph}_4\text{porphyrin})]_2(\mu\text{-N})$ | 1.6605(7) | 180 | 4.5 | 21 |
| | $[\text{Ru}_2(\mu\text{-N})\text{Cl}_8(\text{H}_2\text{O})_2]\text{K}_3$ | 1.720(4) | 180 | 4 | 4 |
| | $[\text{Ru}_2(\mu\text{-N})\text{Cl}_8(\text{H}_2\text{O})_2](\text{NH}_4)_3$ | 1.725(4) | 180 | 4 | 5 |
| | $[\text{Ru}_2(\mu\text{-N})(\text{en})_5]\text{Cl}_5$ | 1.742(1) | 174.6(4) | 4 | 22 |
| | $[\text{Os}_2(\mu\text{-N})(\text{S}_2\text{CNMe}_2)_5]$ | 1.76(3) | 164.6(18) | 4 | 24 |
| | $[\text{Os}_2(\mu\text{-N})\text{Cl}_{10}]\text{Cs}_4$ | 1.778(2) | 180 | 3.5 | 25 |

^a Average values taken for M-N bond length and MNM angle.

Table 1.1, Structurally characterised symmetrically bridging transition metal nitrido complexes.

The bonding in these species may be interpreted as two M-N double bonds; two σ and two perpendicular occupied π -orbitals form two degenerate $d\pi\text{-}p\pi\text{-}d\pi$ three centred π -molecular orbitals, each being occupied by one electron pair (Figure 1.7). A more detailed analysis of the symmetric μ_2 -nitride nitrogen-metal bond in $\{[\text{MoCl}_3(\text{PMe}_3)_2]_2\text{N}\}^-$ is discussed in chapter 4.



Figure 1.7

μ_3 -nitride bonding (5) has been described in the iridium complex $(\text{NH}_4)_4[\text{Ir}_3\text{N}(\text{SO}_4)_6(\text{H}_2\text{O})_3]^{22}$. In this species the Ir_3N unit is trigonal planar and the Ir-N bond length (1.92\AA) indicates appreciable π -bonding. As shown in Figure 1.8, the bonding can be described as three IrN σ bonds and $p\pi$ - $d\pi$ overlap of the occupied N p_z orbital with each Ir d_{xz} orbital.

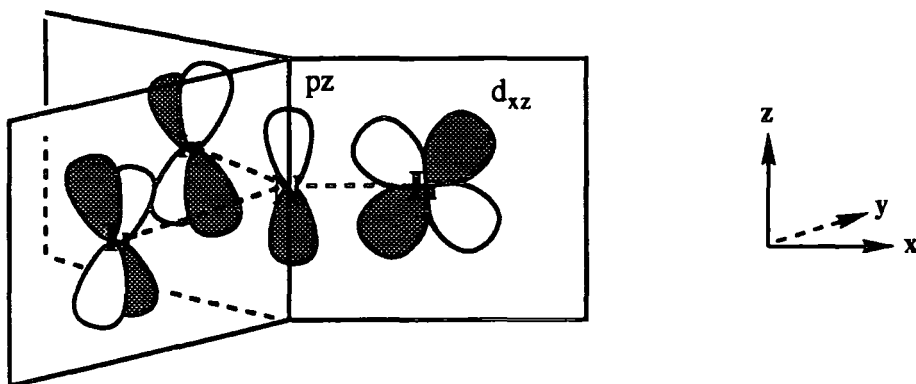


Figure 1.8.

μ_4 , μ_5 and μ_6 are found in a series of later transition metal carbonyl species, such as the homologous series $[\text{Ru}_{4+n}(\mu_{4+n}\text{-N})(\text{CO})_{12+2n}]^-$ (Where $n = 0, 1, 2$)²⁶. μ_6 nitride bonding is also found in Group 8 carbonyl complexes of cobalt and nickel $[\text{M}_6(\text{N})(\text{CO})_{15}]^-$ ($\text{M} = \text{Co}, \text{Ni}$)²⁷.

1.3.1.2 The Imido Ligand.

In the case of imido ligands, five bonding modes have been established²⁸, as illustrated in Figure 1.9.

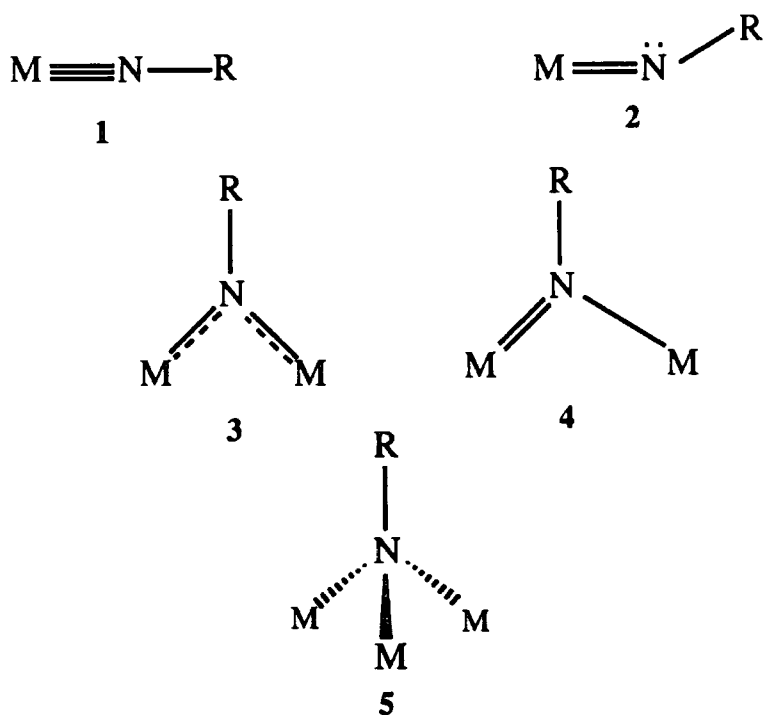


Figure 1.9, *Bonding modes of imido ligands.*

A terminal linear arrangement (1) is by far the most commonly observed. In valence bond terms, this implies that the nitrogen is sp -hybridised and that there is a metal nitrogen triple bond consisting of a σ -bond and two π -bonds, analogous to the nitride (N^{3-}) ligand. The bent terminal imido structure (2) is thought to indicate the presence of a lone pair on the nitrogen and consequently reduced bond order. This is only found when a linear, triply bonded ligand would cause the electron count of the complex to exceed 18 electrons (the effective atomic number rule)²⁹. In orbital terms, a bent imido ligand is observed when there is only one metal orbital of π -symmetry available for bonding to the nitrogen, either because of competition with another π -bonding ligand or because the metal d orbitals are filled. All structurally characterised

monoimido complexes exhibit M-N-R angles $> 155^\circ$, except the bis imido species $\text{Mo}(\text{NPh})_2(\text{S}_2\text{CNEt}_2)_2$ (Figure 1.10) which shows both a bent imido group (Mo-N-C angle of $139.4(4)^\circ$) and a near linear imido group Mo-N-C angle $169.4(4)^\circ$. This molecule is described as having one metal-nitrogen triple bond (Mo-N = 1.754\AA) and one double bond (Mo-N = 1.789\AA), using the three d-orbitals of π -symmetry on the molybdenum centre³⁰.

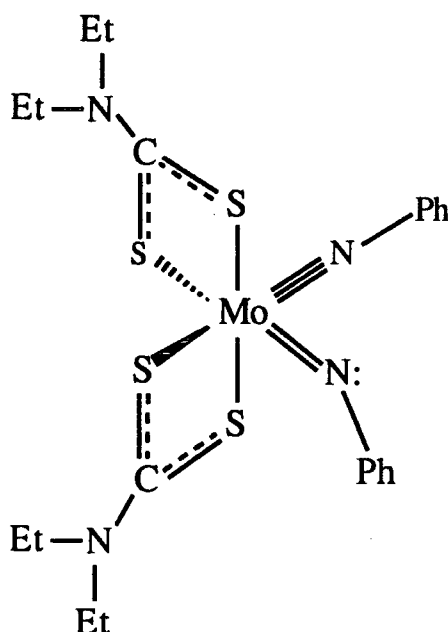


Figure 1.10, Molecular structure of $\text{Mo}(\text{NPh})_2(\text{S}_2\text{CNEt}_2)_2$.

One unusual binuclear linear imido rhenium complex has been prepared by Maatta (Figure 1.11)³¹.

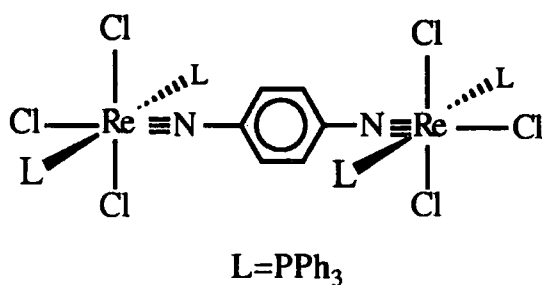


Figure 1.11, Molecular structure of $[\text{Re}_2\text{Cl}_6(\text{PPh}_3)_4\text{N}_2](\text{C}_4\text{H}_6)$.

Recently the novel osmium terminal imido species $\text{Os}(\text{N}-2,6\text{-C}_6\text{H}_3\text{-iPr}_2)_3$ and $\text{Os}(\text{N}-2,6\text{-C}_6\text{H}_3\text{-iPr}_2)_2(\text{PMe}_2\text{Ph})_2$ have been prepared³². These apparently 20 electron species, have been shown to contain linear imido ligands, and so question the validity of the notion that linear or near linear imido species donate the electron pair on the nitrogen to the metal.

The early transition metal imido complexes $[\text{((CH}_3)_2\text{N)}_2\text{M}]_2(\mu\text{-}^t\text{BuN)}_2$ ($\text{M}=\text{Zr}$, Ti)³³⁻³⁵ fall in the symmetrically bridged category (3), but an asymmetric structure (4) has been determined for $[(\text{Me})_2(^t\text{BuN})\text{M}]_2(\mu\text{-}^t\text{BuN)}_2$ ^{30, 36} ($\text{M} = \text{Mo}$, W) (Figure 1.12).

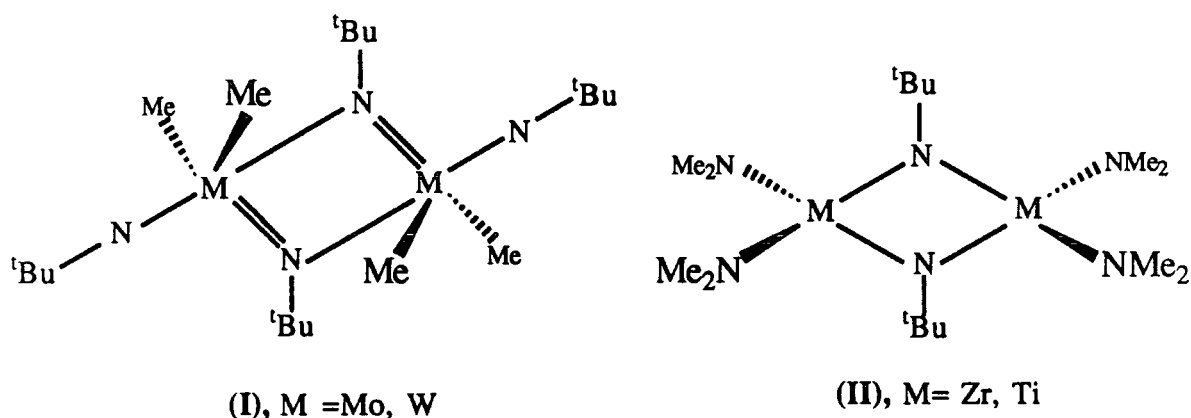


Figure 1.12.

From simple extended Hückel models for the two different imido-bridged metal dimer systems (I) and (II) Nugent et al. have explained the appreciably different structures in terms of a second order Jahn-Teller distortion in compound (I)³⁷.

Triply bridging imido species, type (5), are found in a number of Group 8 transition metal carbonyl complexes³⁸. As in nitrido species there is a greatly diminished capacity for metal-nitrogen π -bonding, and the metal usually possesses a lower formal oxidation state.

1.3.2 Coordination Geometries of Nitrido and Imido Complexes.

Most terminal nitrido and imido complexes have octahedral coordination, with strong axial compression brought about by the shortness of the $M\equiv N$ bond. Octahedral coordination geometry is the most common for compounds of transition metals, due to the excellent overlap possible for both σ and π -bonding. Nitrido species of the type $[M(N)X_4]^{n-}$ ($M = Mo, Re, Ru, Os$; $X = Cl, Br, I, N_3$; $n = 1, 2$) form predominantly square pyramidal complexes with the nitride ligand at the apex³⁹ (Figure 1.13).

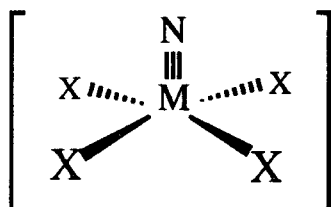


Figure 1.13.

The preference over trigonal bipyramidal coordination can be attributed to better nitrogen-metal bond overlap and due to the large *trans* influence of nitride ligands (section 1.3.4). The compounds $Mo(N)(N_3)_3(py)$ ⁴⁰, $Re(N)(S_2CNEt_2)_2$ ⁴¹ and $Re(N)Cl_2(PPh_3)_2$ ^{18, 42}, also adopt approximately square pyramidal structures, although in these neutral species steric factors govern the geometry.

Seven coordinate complexes tend to exhibit a pentagonal bipyramidal geometry with the multiple bond in the apical position⁴³.

Monoimido species can exhibit pseudotetrahedral geometries, primarily with d^0 configuration, as in the first recorded organoimido complex *t*-butylimidotrioxo osmium(VIII)⁴⁴. Tetrahedral geometry is found in Group 6 compounds^{45, 46} (Figure 1.16), the tungsten derivatives of which find important uses as homogeneous metathesis polymerisation initiators.

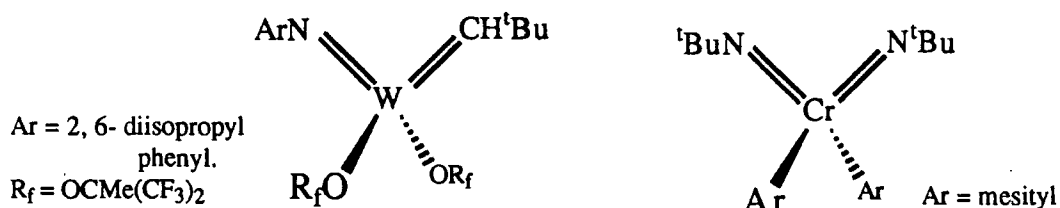


Figure 1.14.

The recently reported compound $\text{Os}(\text{NAr})_2(\text{PMe}_2\text{Ph})_2$ ³², exhibits an unusual square planar geometry, which is believed to be a result of strong π -bonding. To date, only one example of trigonal planar coordination is known, in $\text{Os}(\text{NAr})_3$ ³² (Figure 1.15).

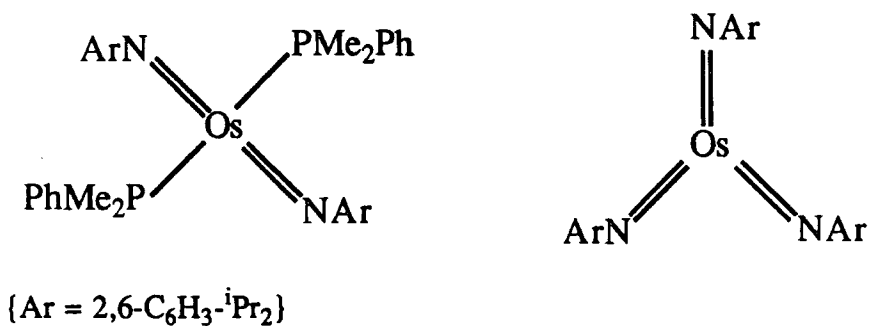


Figure 1.15.

Few generalisations can be made concerning bridging organoimido complexes.

1.3.3 Ligand Field Description.

1.3.3.1 Octahedral Complexes.

The majority of transition metal nitrido and imido complexes are six-coordinate and adopt a geometry best described as octahedral. Octahedral complexes are the easiest structures to analyse in molecular orbital terms because the σ and π orbitals are separate due to the high symmetry. All octahedral complexes have essentially the same σ bonding framework, regardless of π interactions. In a molecule assumed to have full O_h symmetry, the five metal d-orbitals split into a degenerate e_g set ($d_{x^2-y^2}$, d_{z^2}) of σ^* character and a nonbonding t_{2g} set (d_{xy} , d_{xz} , d_{yz}). Introduction of an N^{3-} or NR^{2-} ligand lowers the symmetry to C_{4v} and splits the degeneracy of both the e_g and the t_{2g} orbitals (Figure 1.16).

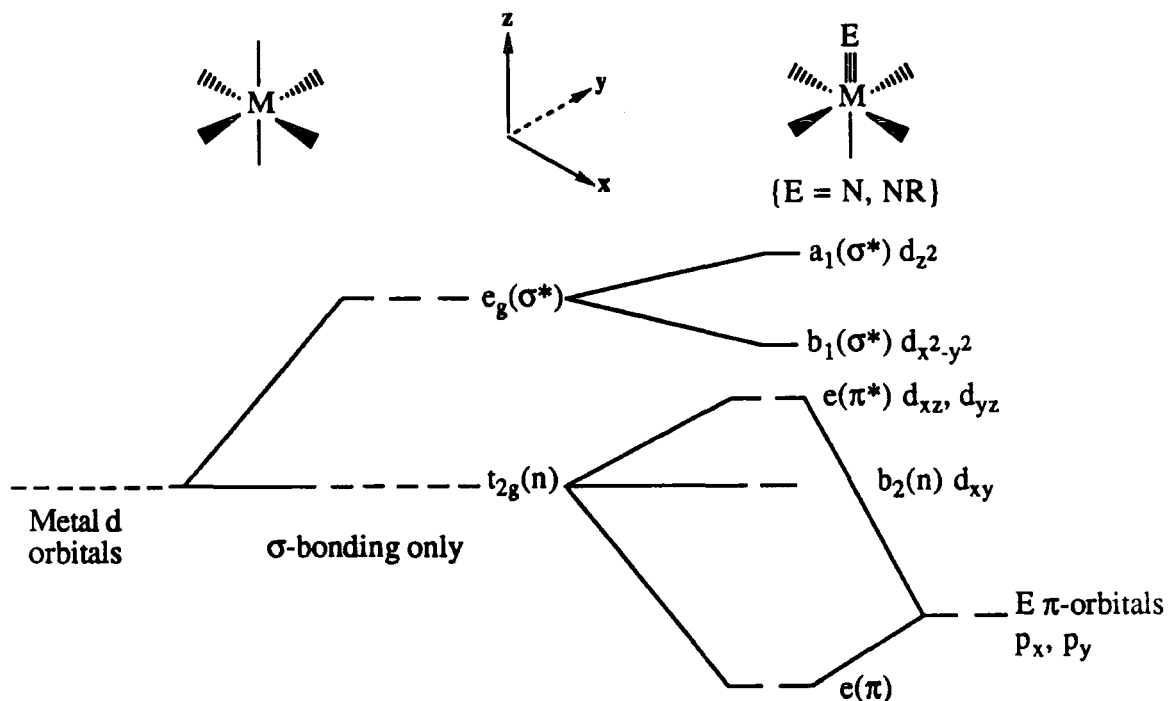


Figure 1.16

Qualitatively the e_g set is unchanged since both orbitals remain σ^* ; the t_{2g} orbitals, however, are substantially split since two of them are now involved in π bonding (d_{xz} and d_{yz} if the z axis is taken as coincident with the metal-ligand bond axis). Thus the ligand field portion of the molecular orbital diagram consists of a non-bonding d_{xy} orbital, a $\pi^* e$ set, and two σ^* levels.

1.3.3.2 Square Pyramidal Complexes.

The molecular orbital scheme for octahedral complexes, shown in Figure 1.16, is also applicable to square pyramidal species. The absence of a sixth ligand in square pyramidal complexes has been suggested to have one significant effect, that of lowering the energy of σ^* component of the metal-ligand multiple bond (a_1 in Figure 1.16). Calculations suggest that in $\text{Os}(\text{N})\text{Cl}_4^-$ a σ^* orbital, composed of roughly equal amounts of osmium d_{z^2} and nitrogen p_z , is close in energy to the π^* orbitals⁴⁷. This orbital was suggested to be involved in the nucleophilic attack of triphenylphosphine at the nitride ligand⁴⁸.

1.3.4 The *trans* Influence.

The *trans* -influence of a ligand is defined as "the extent to which a ligand weakens the bond *trans* to itself"⁴⁹. Not only is the weakening evident in reactions, but is also expressed in the bond lengths between the central atom and *cis* or *trans*-positioned ligands. In the structure of $[\text{Os}(\text{N})\text{Cl}_5]\text{K}_2$, for example, the four Os-Cl bonds *cis* to the nitride ligand are $2.362 \pm 0005 \text{ \AA}$ in length while the *trans* Os-Cl is at $2.605(4)\text{\AA}$ ⁵⁰. Lengthening of the *trans* ligand is invariably accompanied by the bending of *cis* ligands away from the multiple bond. Both steric and electronic explanations have been given for the *trans* influence. In 1969 Bright and Ibers suggested that structures of molecules with multiply-bonded ligands are largely

determined by steric repulsion of neighbouring ligands⁵⁰. That is, that the multiply bonded ligand, which is extremely close to the metal atom, displaces the *cis*-positioned ligands, pushing the *trans* ligand away from the metal. More convincing explanations have been given in terms of electronic effects, based on overlap arguments that the metal orbitals will be more involved with the stronger metal-ligand bond, thus reducing the overlap of the *trans* ligand⁵¹.

The *trans* influence of a particular ligand in a specific complex is hard to quantify, because of difficulty in determining the “unperturbed” bond length of the *trans* ligand. However, if the complex contains the same ligand both *cis* and *trans* to a multiple bond, then the difference in bond length is taken as the *trans* influence. Although the number of useful structures is small, Shustorovich and co-workers have suggested that the nitride ligand has a greater *trans* influence than the imido ligand⁴⁹. Consistent with this order, nitrido species are frequently square pyramidal while imido compounds are usually octahedral (section 1.3.2).

1.4 Spectroscopic Properties.

1.4.1 Infrared Spectroscopy of Terminal Nitrido Complexes.

1.4.1.1 General Considerations.

The terminal nitrido group is an ideal chromophore for I.R. spectroscopy. The large change in bond dipole for this ligand, means that absorbance bands due to $M\equiv N$ stretching modes are generally intense. Moreover, since the stretching vibration in terminal $M\equiv N$ is not coupled significantly to other ligand oscillations, the bands are also often sharp. In addition, force constants derived from such stretching frequencies tend to provide a measure of metal-ligand bond strength. As a diagnostic tool, bending modes have proved much less useful than the stretching modes, as they tend to be broader and weaker.

1.4.1.2 Assignment of Terminal M-N Stretching Frequencies.

In a 1972 review, Griffith⁵² proposed a range of 1020-1150cm⁻¹ for the M-N stretching frequency of terminal nitrides. Although since then much more spectral data has been collected, so far all transition metal terminal nitrido complexes fall within these values. In Table 1.2 the reported values for the IR stretching frequencies of mononuclear nitrido complexes for Groups 5-8 are shown.

| Metal | $\nu(\text{M-N}) \text{ cm}^{-1}$ | Reference ^a |
|-------|-----------------------------------|------------------------|
| V | 970 - 1033 | 53 |
| Nb | _____ | _____ |
| Ta | _____ | _____ |
| Cr | 1012 - 1017 | 52, 54 |
| Mo | 948 - 1109 | 55, 56 |
| W | 980 - 1135 | 57, 58 |
| Mn | 1036 - 1052 | 59, 60 |
| Tc | 1027 - 1089 | 61, 62 |
| Re | 974 - 1099 | 63, 48 |
| Ru | 1023 - 1092 | 64 |
| Os | 1008 - 1125 | 65, 66 |

^a The indicated references are those containing the highest and lowest frequencies stated.

Table 1.2, Range of reported stretching frequencies for mononitrido complexes.

In general, the wavenumbers are seen to increase from left to right along a period, assuming the charge of the species or the d electron count remains constant, and on proceeding down a triad. This is not in accordance with Hooke's law⁶⁷, which implies

that an increase in mass should lead to a decrease in stretching frequency, provided force constants remain unchanged. Clearly, the force constants must change. Calculations confirm that force constants do change, increasing across a period and on descending a group⁶⁸.

1.4.1.3 Infrared Spectroscopy of Bridging Nitrido Complexes.

Chatt and Heaton have shown that on complexation of Lewis acids to the nitrido ligand, in all cases there is an increase in M-N stretching frequency in the range of 80-100cm⁻¹ ⁶⁹. In unsymmetrically bridged transition metal nitrides of the type M≡N-M, the absorption due to the short MN bond is found in roughly the same range as terminal nitrides, though occasionally this band is split. The long MN bond is expected to occur at very low wavenumbers, typically less than 200cm⁻¹ (Table 1.3).

| Complex | $\nu(\text{M}\equiv\text{N}) \text{ cm}^{-1}$ | Ref. |
|---|---|------|
| [Mo(N)Cl ₃] ₄ | 1045 | 8 |
| [Mo(N)Cl ₃ (OPCl ₃) ₄] | 1042, 1049 | 9 |
| [Mo(N)Br ₂] _∞ | 951 | 70 |
| [W(N)Cl ₃] _∞ | 1068, 1084 | 8 |
| [Re(N)Cl ₃] _∞ | 1080 | 71 |
| [Re(N)Cl ₄] _∞ | 944, 995, 1011 | 7 |

Table 1.3, Vibrational modes of unsymmetrically bridging nitrides.

Symmetrically bridging nitrido complexes of the type M=N=M give rise to two stretching vibrations $\nu_{\text{sym}}(\text{M}=\text{N}=\text{M})$ and $\nu_{\text{asy}}(\text{M}=\text{N}=\text{M})$. IR and Raman studies on these species were first carried out by Cleare and Griffith on ruthenium and osmium

complexes³. The symmetric vibration is found at low frequency as the nitrogen is effectively unmoved; reported values range from 465-228cm⁻¹. The asymmetric mode is observed in the IR at higher frequencies; 890-1137cm⁻¹ (Table 1.4).

| Complex | $\nu(\text{asym.}) \text{ cm}^{-1}$ 1 | $\nu(\text{sym.}) \text{ cm}^{-1}$ | Ref. |
|---|--|------------------------------------|------|
| (DTTAA)V(DTTAA) ^a | 890 | — | 72 |
| (NH ₄) ₃ [Br ₅ TaN ₂ TaBr ₅] ^b | 985 | 228 | 12 |
| [PNP][Cl ₃ (PMe ₃) ₂ MoNMo(PMe ₃) ₂ Cl] ^c | 965 | 401 | 18 |
| PPh ₄ [Cl ₅ WNWCl ₅] ^d | 945 | — | 16 |
| (TPP)FeN(TPP) ^e | 910 | 424 ^f | 73 |
| [(TPP)FeN(TPP)]ClO ₄ ^e | 1000 | 465 ^f | 74 |
| (OEP)FeNFe(OEP) ^g | 940 | 439 ^f | 75 |
| (Pc)FeN(Pc) ^h | 915 | — | 76 |
| K ₃ [(H ₂ O)Br ₄ RuNRuBr ₄ (H ₂ O)] | 1050 | 392 | 77 |
| K ₃ [(H ₂ O)Cl ₄ RuNRuCl ₄ (H ₂ O)] | 1080 ⁱ | 402 | 77 |
| [Br(NH ₃) ₄ RuNRu(NH ₄) ₃ Br]Br ₃ | 1039 | 348 | 3 |
| K ₃ [(H ₂ O)Cl ₄ OsNOsCl ₄ (H ₂ O)] | 1137 | 267 | 3 |
| [Br(NH ₃) ₄ OsNOs(NH ₄) ₃ Br]Br ₃ | 1095 ^j | — ^k | 3 |

^a DDTA = dibenzotetramethyltraaza[14]annulene ligand. ^b Band at 375cm⁻¹ was assigned as δ M-N-M.; ^c PNP = Me₃PNPMe₃; ^d Band at 840 cm⁻¹ was assigned as δ M-N-M; ^e TPP = mesotetraphenylporphyrin; ^f Resonance Raman instrument; shifted to higher frequency by ⁵⁴Fe substitution; ^g OEP = octaethylporphyrin ^h Pc = phthalocyanine; ⁱ Shifted to 1047cm⁻¹ by ¹⁵N substitution.; ^j Shifted to 1063cm⁻¹ by ¹⁵N substitution; ^k Reported as 229cm⁻¹ in ref. 78

Table 1.4, Vibrational modes for symmetrically bridging nitrides.

1.4.3 Infrared Spectra of Organoimido Complexes.

The assignment of metal ligand stretching frequencies in organoimido complexes has proven problematic. In these complexes, coupling of M-N with N-R stretching modes and/or vibrations of the R group give rise to significant complications. ^{15}N isotopic labelling studies have been reported for many phenylimido complexes, the majority of these complexes show a band in the $1310\text{-}1360\text{cm}^{-1}$ region, which is shifted to lower frequency on ^{15}N substitution⁷⁹⁻⁸⁴. It is not clear whether this band represents the M-N or the C-N stretching mode or a combination of the two. Dehnicke has suggested that the M-N stretch in organoimido complexes will occur at a considerably higher frequency than the C-N stretch due, in part, to the vibrational coupling³⁹. The essentially opposite viewpoint has been given by Osborn and Trogler⁷⁹. They have noted that the IR spectrum of $\text{Cp}^*_2\text{V}(\text{NPh})$ exhibits two bands that are sensitive to ^{15}N substitution, one band at 1330cm^{-1} and one at 934cm^{-1} , which they assign to $\nu(\text{C-N})$ and $\nu(\text{M-N})$ respectively. Resolution of these conflicting proposals must await labelling studies using both ^{13}C and ^{15}N substitution.

1.4.4 Nitrogen NMR of Multiply Bonded Ligands.

Both ^{14}N and ^{15}N have a magnetic moment, and are capable of giving NMR spectra⁸⁵. ^{14}N is the more abundant, but has a spin of 1 and hence a quadrupole moment. Useful ^{14}N spectra can therefore only be obtained for highly symmetrical molecules. The first complex of this type studied was $[\text{WF}_4(\text{NMe})\text{L}]^n$ ⁸⁶, in which the shielding effect of the nitrogen nucleus was determined on varying the *trans* ligand.

All reported ^{15}N NMR studies on transition metal complexes have used isotopically enriched samples. Chemical shift data, using a nitromethane standard, shows a range from -79ppm in $\text{Ta}(\text{NPh})\text{Cl}(\text{dmpe})_2$ ⁸⁰ to $+190.6\text{ppm}$ in the nitrido complex $\text{Mo}(\text{N})\text{Br}(\text{dppe})_2$ ⁸⁷. In all examples to date, the nitrogen atom is more shielded in imido complexes (-80 to 10ppm), than in nitrido ($+40$ to $+190\text{ppm}$). The

^1H - ^{15}N coupling constant in several NH imido complexes have been shown to have a diagnostic value.

1.4.5 ^1H NMR Spectroscopy

The α -protons in the d^0 alkyl imido complexes are significantly deshielded occurring 1-4 ppm downfield of the α resonance in trialkyl amines, which typically occur in the range 2.2-2.6 ppm⁶⁷. In d^2 imido compounds the situation is more complicated; some α -proton resonances are located upfield of the α -proton in amines; the origin of this effect is not known. The α -proton chemical shifts of some alkylimido species are shown in Table 1.5.

| Complex | d electrons | δ (ppm) | Ref. |
|--|-------------|----------------|------|
| $\text{CpNb}(\text{NMe})\text{Cl}_2$ | 0 | 3.21 | 88 |
| $\text{CpNb}(\text{NMe})(\text{O}-2,6\text{-Me}_2\text{C}_6\text{H}_3)_2$ | 0 | 3.30 | 89 |
| $\text{CpNb}(\text{NMe})(\text{O}^t\text{Bu})_2$ | 0 | 3.43 | 89 |
| $\text{CpNb}(\text{NMe})\text{Cl}_2(\text{PMe}_3)$ | 0 | 3.85 | 88 |
| $\text{Cp}^*\text{Ta}(\text{NMe})\text{Me}_2$ | 0 | 3.97 | 90 |
| $[\text{W}(\text{NMe})\text{F}_5]^-$ | 0 | 5.50 | 86 |
| $\text{W}(\text{NMe})\text{F}_4(\text{MeCN})$ | 0 | 5.53 | 86 |
| $\text{Ta}(\text{NEt})(\text{NEt}_2)_3$ | 0 | 4.04 | 91 |
| $\text{W}(\text{NEt})_2(\text{NEt}_2)_2$ | 0 | 4.22 | 92 |
| $[\text{W}(\text{NEt})\text{F}_5]$ | 0 | 5.80 | 86 |
| $\text{W}(\text{NEt})(\text{O})\text{Cl}(\text{NHEt})$ | 0 | 7.3 | 93 |
| $\text{Re}(\text{NMe})\text{Cl}_3(\text{PEtPh}_2)_2$ | 2 | 0.2 | 94 |
| $\text{Os}(\text{NMe})\text{Me}_4$ | 2 | 0.27 | 95 |
| $\text{Re}(\text{NMe})\text{Cl}_3(\text{AsMe}_2\text{Ph})_2$ | 2 | 0.7 | 94 |
| $\text{Os}(\text{NMe})(\text{CH}_2\text{SiMe}_3)_4$ | 2 | 1.59 | 95 |
| $[\text{Re}(\text{NMe})(\text{dtc})_2(\text{PMe}_2\text{Ph})]\text{BF}_4$ | 2 | 1.77 | 96 |
| $\text{Cp}^*\text{Re}(\text{NMe})\text{Cl}_2$ | 2 | 2.17 | 97 |
| $\text{Re}(\text{NMe})(\text{dtc})_3$ | 2 | 2.20 | 83 |
| $\text{Re}(\text{NMe})(\text{dtc})_2\text{Cl}$ | 2 | 2.21 | 83 |
| $\text{Mo}(\text{NEt})\text{Cl}_2(\text{PhCON}_2\text{Ph})(\text{PMe}_2\text{Ph})$ | 2? | 3.9, 4.6 | 99 |

Table 1.5, α -proton chemical shifts of some mononuclear alkylimido complexes.

1.4.6 ^{13}C NMR Spectroscopy.

^{13}C chemical shift data have been reported for a number of t butylimido complexes of d^0 transition metals^{80, 90, 99}. Nugent et al have shown that decreasing electron density on the imido nitrogen atom causes a downfield shift in the α -carbon resonance and an upfield shift in the β -carbon resonance. The difference between chemical shifts for α and β carbon atoms, Δ , can thus be used as an experimental probe of the electron density on the nitrogen atom⁹⁹. Their ^{13}C studies on a number species; including mono- di- and tri imido compounds, bent and linear terminal imido ligands and symmetrically and unsymmetrically bridging imido ligands, conclude that despite this structural diversity Δ increases (charge on the nitrogen decreases) on proceeding upwards and right on the periodic table. These results have been explained in terms of the relative energies of the imido ligand p-orbital and transition metal d-orbitals. As one proceeds upward and right among the early transition metals, the d-orbitals become less diffuse as indicated by the decreasing radii of the free metal atoms, this results in a shift of a electron density from the ligand to the metal and reduced nucleophilic character of the imido ligand.

1.5 Uses.

1.5.1 Nitrido Complexes.

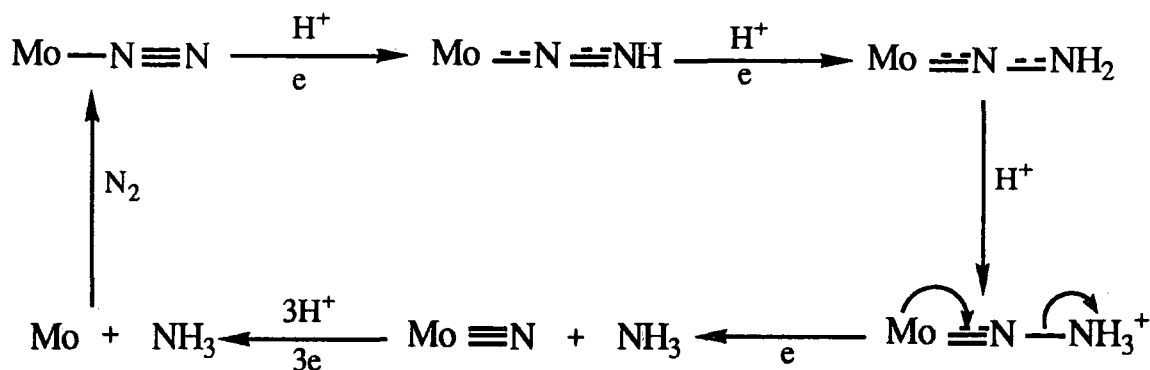
1.5.1.1 New Materials.

The stability of the metal-nitrogen triple bond, reflects many applications of the nitrido ligand. Recently, Belmonte has harnessed this stabilisation to prepare a series of Os derivatives, in order to study the reaction chemistry of high oxidation state Group 8 species⁶⁶ (Figure 1.17).

to new transition metal containing polymers, by controlled formation of metal via bridging ligands, is a critical prerequisite for the study of these new important materials. Doherty and co-workers have prepared the stable bimetallic dimer $(\text{Me}_3\text{SiO})_3\text{V}=\text{N}-\text{Pt}(\text{PEt}_2)_2\text{Me}^{10}$ and polymeric $[\text{V}(\mu\text{-N})\text{Cl}_2(\text{py})_2]_\infty^8$, which represents a first step in this direction.

1.5.1.2 Catalytic Properties of Nitride Species.

Nitrido complexes have been considered as model systems for the study of at least an intermediate step in nitrogen fixation¹⁰⁵. Complexes of Group 6 have been of particular interest as molybdenum is known to play a key rôle in nitrogenase reduction of molecular nitrogen¹⁰⁵. One proposed mechanism for this reduction on a molybdenum atom in nitrogenase is shown in Scheme 1.1.

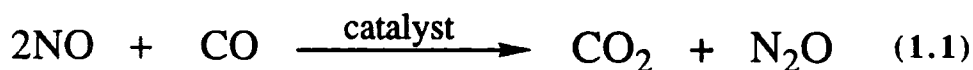


Scheme 1.1, *Proposed mechanism for reduction of molecular nitrogen by molybdenum in nitrogenase.*

Much work has been carried out on nitrogen fixation via nitride formation in the laboratories of Vol'pin and van Tamelen^{106,107}.

Nitrido transition metal clusters are of interest in establishing a relationship between structure and reactivity of surface coordinated nitrogen atoms. These latter species are invoked as intermediates in many catalytic cycles, such as the Haber process¹⁰⁸ and the reduction of NO_x pollutants¹⁰⁹. It has been suggested that the

appearance of isocyanates on the surfaces of metals that catalyse the reduction of nitric oxide (Equation 1.1) is explained by the reaction of metal adsorbed nitrido species with carbon monoxide (Equation 1.2)¹¹⁰.



1.5.2 Imido Complexes

1.5.2.1 Heterogeneous Catalysis

Imido species have been postulated as intermediates in catalytic processes. For example, Grasselli and co-workers at SOHIO have proposed imido species as intermediates in the industrial "ammoxidation" of propylene to acrylonitrile¹¹¹ (Equation 1.3).



The most active and selective catalyst systems for this process are based on mixed oxides of molybdenum and bismuth e.g $\text{Bi}_2\text{Mo}_3\text{O}_{12}$. The SOHIO group have proposed the diimido species (Figure 1.19) for the active sites. C-H cleavage occurs at the adjacent bismuth and the allyl moiety is then trapped by the imido nitrogen.

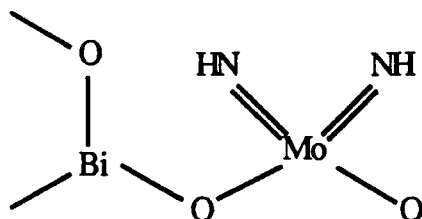
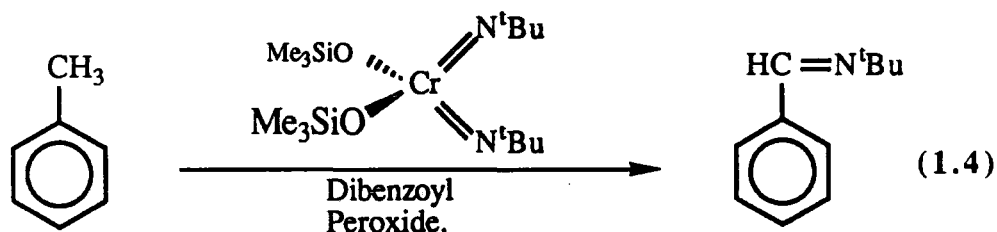


Figure 1.19, *Proposed active sites in propylene ammoxidation.*

To date, no direct evidence for the existence of such species, or their involvement in the ammoxidation has been forthcoming. Nevertheless, studies using organoimido derivatives have succeeded in providing structural models for these putative intermediates¹¹². The C-N bond forming steps from the proposed reaction mechanism have been reproduced using discrete soluble imido species, even under mild conditions¹¹³ (e.g. Equation 1.4).



Imido species are also believed to be involved in such enzymatic pathways as nitrogen fixation and the metabolism of certain hydrazines^{114,115}.

1.5.2.2 Organic Synthesis and Homogeneous Catalysis

The importance of the observation that $\text{Os}(\text{N}^t\text{Bu})\text{O}_3$ reacts with olefins (Equation 1.5) was first recognised by Sharpless¹¹⁶.

Osmium catalysed *cis* vicinal oxyamination can also be achieved with the use of phase transfer catalysts¹¹⁸. Subsequently, the Sharpless group was able to synthesise the di, tri and tetraimido analogs of osmium tetroxide that promote the corresponding vicinal diamination¹¹⁹ (Figure 1.20).

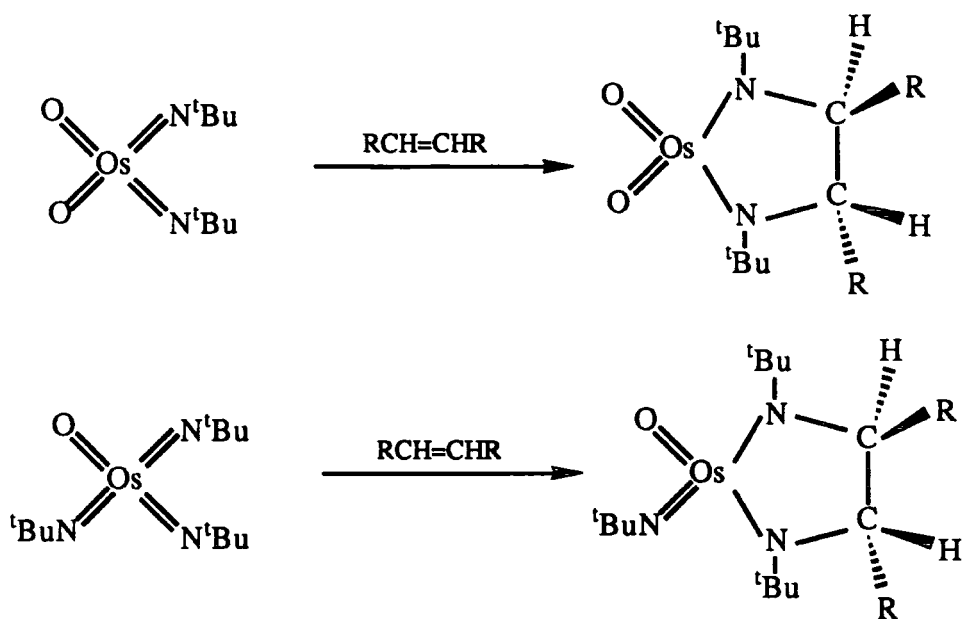
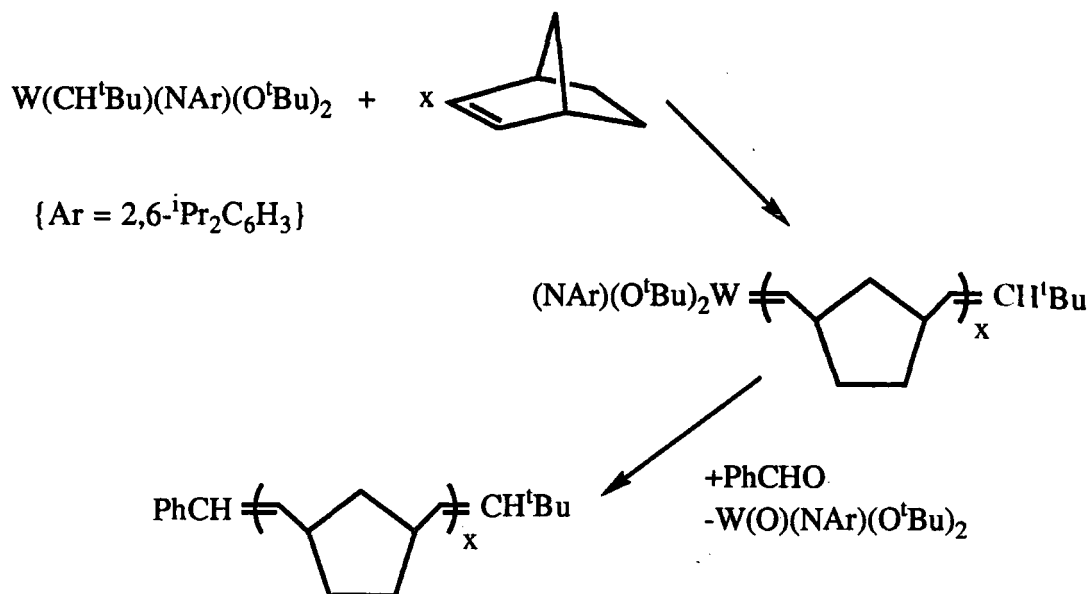


Figure 1.20.

More recently, organoimido groups have shown to play an important role as ancillary ligands in organometallic chemistry and heterogeneous catalysis. Of particular interest is Schrock's use of the alkylimido ligand in the compounds of the type $M(\text{NAr})(\text{CH}^t\text{Bu})(\text{OR})_2$, which are an important new class of metathesis catalyst¹²⁰ (Scheme 1.3).



Scheme 1.3, *The polymerisation of norbornene, using $W(\text{CH}^t\text{Bu})(\text{NAr})(\text{O}^t\text{Bu})_2$.*

1.6 Summary.

This chapter has served to outline the nature of transition metal nitrido and imido complexes. Their occurrence, electronic structure and typical characterising data has been discussed, and finally a number of important industrial and biochemical applications of these species have been described.

The subsequent chapters of this thesis describe the synthesis and characterisation of a variety of new early-transition metal-nitrogen multiply-bonded complexes, and a study of the bonding in transition metal nitrido, imido and related oxo species.

1.7 References.

1. J. Chatt, A.J.L. Pombeiro and R.L. Richards, *J. Chem. Soc. Dalton Trans.*, 1980, 492.
2. M. Mukauda, *Bull. Chem. Soc. Jpn.*, 1970, **43**, 3805.
3. M.J. Cleare and W.P. Griffith, *J. Chem. Soc. (A)*, 1970, 1117.
4. M. Ciechanowicz and A.C. Skapski, *J. Chem. Soc. (A)*, 1971, 1792.
5. R.J.D. Gee and H.M. Powell, *J. Chem. Soc. (A)*, 1971, 1795.
6. M.J. McGlinchey and F.G.A. Stone, *J. Chem. Soc., Chem. Commun.*, 1970, 1265; J. Ashley-Smith, M. Green, N. Mayne and F.G.A. Stone, *J. Chem. Soc., Chem. Commun.*, 1969, 409; J. Ashley-Smith, M. Green and F.G.A. Stone, *J. Chem. Soc. Trans.*, 1972, 1805.
7. W. Liese, K. Dehnicke, I. Walker and J. Strähle, *Z. Naturforsch.*, 1979, **34B**, 693 .
8. N.M. Doherty, S.C. Critchlow, M.E. Lerchen and R.C. Smith, *J. Am. Chem. Soc.*, 1988, **110**, 8071; W. Willing, R. Christopherson, U. Müller and K. Dehnicke, *Z. Anorg. Allg. Chem.*, 1987.
9. J. Chatt and B.T. Heaton, *Chem. Commun.*, 1968, 274.
10. N.M. Doherty and S.C. Critchlow, *J. Am. Chem. Soc.*, 1987, **109**, 7906.
11. J. Strähle, *Z. Anorg. Allg. Chem.*, 1970, **375**, 238; 1971, **380**, 96.
12. J. Strähle, U. Wecher, W. Liebelt and K. Dehnicke, *Z. Naturforsch.*, 1978, **33B**, 1347.
13. W. Musterle, J. Strähle, W. Liebelt and K. Dehnicke, *Z. Naturforsch.*, 1979, **34B**, 942.
14. W. Liese, K. Dehnicke, I. Walker and J. Strähle, *Z. Naturforsch.*, 1980, **35B**, 776.
15. K.P. Frank, J. Strähle and J. Wedlein, *Z. Naturforsch.*, 1980, **35B**, 300.
16. M. Hörner, K.P. Frank and J. Strähle, *Z. Naturforsch.*, 1986, **41B**, 423.

17. M.E. Noble, K. Folting, J.C. Huffman and R.A.D. Wentworth, *Inorg. Chem.*, 1982, **21**, 3772.
18. This thesis, *Chapter 4*.
19. T. Godemeyer, A. Berg, H.D. Gross, U. Müller and K. Dehnicke, *Z. Naturforsch.*, 1985, **40B**, 999.
20. T. Godemeyer, K. Dehnicke and D. Fenske, *Z. Naturforsch.*, 1985, **40B**, 1005.
21. W.R. Scheidt, D.A. Summerville and I.A. Cohen, *J. Am. Chem. Soc.*, 1976, **98**, 6628.
22. W.P. Griffith, N.T. McManus and A.C. Skapski, *J. Chem. Soc., Chem. Commun.*, 1984, 434.
23. K.W. Given and L.H. Piquolet, *Inorg. Chem.*, 1977, **16**, 2982.
24. H.G. von Schnering, *unpublished results*.
25. M. Ciechanowicz, W.P. Griffith, D. Pawson and A.C. Skapski, *Chem. Commun.*, 1971, 876.
26. M.L. Blohm and W.L. Gladfelter, *Organometallics*, 1985, **4**, 45.
27. S. Martinengo, G. Ciani, A. Sironi, B.T. Heaton and J. Mason, *J. Am. Chem. Soc.*, 1979, **101**, 7095.
28. W.A. Nugent and B.L. Haymore, *Coord. Chem. Rev.*, 1980, **31**, 123.
29. W.A. Nugent and J.M. Mayer, *'Metal-Ligand Multiple Bonds'*, Wiley, New York, 1988.
30. B.L. Haymore, E.A. Maatta and R.A.D. Wentworth, *J. Am. Chem. Soc.*, 1979, **101**, 2063.
31. E.A. Maatta and C. Kim, *Inorg. Chem.*, 1989, **28**, 624.
32. J.T. Anhaus, T.P. Kee, M.H. Schofield and R.R. Schrock, *J. Am. Chem. Soc.*, 1990, **112**, 1642.
33. D.L. Thorn, W.A. Nugent and R.L. Harlow, *J. Am. Chem. Soc.*, 1981, **103**, 357.
34. W.A. Nugent and R.L. Harlow, *Inorg. Chem.*, 1979, **18**, 2030.
35. D.C. Bradley and E.G. Torrible, *Can. J. Chem.*, 1963, **41**, 134.

36. W.A. Nugent and R.L. Harlow, *J. Am. Chem. Soc.*, 1980, **102**, 1759.
37. J.K. Burdett, "*Molecular Shapes*", 1980, Wiley, New York.
38. S. Aime, G. Gervasio, L. Malone, R. Rossett and P. Stanghellini, *J. Chem. Soc. Dalton Trans.*, 1978, 534.
39. K. Dehnicke and J. Strähle, *Angew. Chem. Int. Ed. Engl.*, 1981, **20**, 413.
40. E. Schweda and J. Strähle, *Z. Naturforsch.*, 1985, **40B**, 1005.
41. D.A. Summerville and I.A. Cohen, *J. Am. Chem. Soc.*, 1976, **98**, 1747.
42. R.J. Doedens and J.A. Ibers, *Inorg. Chem.*, 1967, **6**, 204.
43. M. Melnik and P. Sharrock, *Coord. Chem. Rev.*, 1985, **65**, 49.
44. A.F. Clifford, C.S. Kobayashi, *Abstracts of, 130th Meeting of the Am. Chem. Soc.*, Atlantic City, NJ.
45. C.J. Schaverien, J.C. Dewan and R.R. Schrock, *J. Am. Chem. Soc.*, 1986, **108**, 2771.
46. M.B. Hursthouse, M. Motevalli, A.C. Sullivan and G. Wilkinson, *J. Chem. Soc., Chem. Commun.*, 1986, 1398.
47. D.L. DuBois and R. Hoffmann, *Nouv. J. Chim.*, 1977, **1**, 479.
48. D. Pawson and W.P. Griffith, *J. Chem. Soc. Dalton Trans.*, 1975, 417.
49. E.M. Shustorovich, H.C. Clark and L.E. Manzer, *Coord. Chem. Rev.*, 1975, **17**, 1.
50. D. Bright and J.A. Ibers, *Inorg. Chem.*, 1969, **8**, 709.
51. A.F. Wells "*Structural Inorganic Chemistry*", 5th edition, Oxford, New York, 1984, pp 18.
52. W.P. Griffith, *Coord. Chem. Rev.*, 1972, **8**, 369.
53. K.D. Scherfise and K. Dehnicke, *Z. Anorg. Allg. Chem.*, 1986, **538**, 119.
54. V.S.I. Arshankow and A.L. Poznjak, *Z. Anorg. Allg. Chem.*, 1981, **481**, 201.
55. J. Chatt and J.R. Dilworth, *J. Chem. Soc., Chem. Commun.*, 1974, 517.
56. L.W. Messerle, P. Jennisch, R.R. Schrock and G. Stucky, *J. Am. Chem. Soc.*, 1980, **102**, 355.

57. P.C. Bevan, J. Chatt, J.R. Dilworth, R.A. Henderson and G.J. Leigh, *J. Chem. Soc. Dalton. Trans.*, 1982, 821.
58. W. Kolitsch and K. Dehnicke, *Z. Naturforsch.*, 1970, **25B**, 1080.
59. O. Bortolini and B. Meunier, *J. Chem. Soc., Chem. Commun.*, 1983, 1364.
60. C. Campochiaro, J.A. Hofmann, Jr. and D.F. Bocian, *Inorg. Chem.*, 1969, **8**, 709.
61. J. Baldas, J. Bonnyman and G.A. Williams, *Inorg. Chem.*, 1986, **25**, 150.
62. U. Abram, H. Spies, W. Görner, R. Kirmse and J. Stach, *Inorg. Chim. Acta*, 1985, **109**, L9.
63. C.J.L. Lock and G. Wilkinson, *J. Chem. Soc. (A)*, 1964, 2281.
64. W. Kafitz, F. Weller and K. Dehnicke, *Z. Anorg. Allg. Chem.*, 1982, **490**, 175.
65. J.W. Butcher, C. Dreher and K.L. Lay, *Z. Naturforsch.*, 1982, **37B**, 1155.
66. P.A. Belmonte and Z.Y. Own, *J. Am. Chem. Soc.*, 1984, **106**, 7493.
67. R.M. Silverstein, C.G. Bassler and T.C. Morrill, '*Spectrometric Identification of Organic Compounds*', 4th Edition, Wiley, New York, 1981.
68. B. Krebs and A. Müller, *J. Inorg. Nucl. Chem.*, 1968, **30**, 463; A. Müller, B. Krebs and W. Hölftje, *Spectrochim. Acta*, 1967, **23A**, 2753; L.A. Woodward, J.A. Creighton and K.A. Taylor, *Trans. Faraday Soc.*, 1960, **56**, 1267.
69. J. Chatt and B.T. Heaton, *J. Chem. Soc. (A)*, 1971, 705.
70. N. Krüger and K. Dehnicke, *Z. Naturforsch.*, 1979, **34B**, 1343.
71. K. Dehnicke, W. Liese and P. Köhler, *Z. Naturforsch.*, 1977, **32B**, 1487.
72. V.L. Goedken and J.A. Ladd, *J. Chem. Soc., Chem. Commun.*, 1981, 910.
73. G.A. Schick and D.F. Bocian, *J. Am. Chem. Soc.*, 1984, **106**, 7493.
74. M.A. Crisanti, T.G. Spiro, D.R. English, D.N. Hendrickson and K.S. Suslick, *Inorg. Chem.*, 1984, **23**, 3897.
75. J.A. Hofmann, Jr. and D.F. Bocian, *J. Phys. Chem.*, 1984, **88**, 1472.
76. V.I. Nefedov, M.A. Porai-Koshits, J.A. Zakharova and M.E. Dyatkina, *Dokl. Akad. Nauk. SSSR*, 1972, **202**, 605.
77. R. Mattes, M. Moumen and I. Pernoll, *Z. Naturforsch.*, 1975, **30B**, 210.

78. D.J. Hewkin and W.P. Griffith, *J. Chem. Soc. (A)*, 1966, 472.
79. J.H. Osborn and W.C. Trogler, *Inorg. Chem.*, 1985, **24**, 3098.
80. S.M. Rocklage and R.R. Schrock, *J. Am. Chem. Soc.*, 1982, **104**, 3077.
81. M.H. Chisholm, K. Folting, J.C. Huffman and A.L. Ratermann, *Inorg. Chem.*, 1982, **104**, 3081.
82. L.S. Tan, G.V. Goeden and B.L. Haymore, *Inorg. Chem.*, 1983, **22**, 1744.
83. G.V. Goeden and B.L. Haymore, *Inorg. Chem.*, 1983, **22**, 157.
84. A.W. Edelblut, R.A.D. Wentworth, *Inorg. Chem.*, 1980, **19**, 1110.
85. J. Mason, *Chem. Rev.*, 1981, **81**, 205.
86. O.R. Chambers, M.E. Harman, D.S. Rycroft, D.W.A. Sharp and J.M. Winfield, *J. Chem. Res.*, 1977, 1849.
87. S. Donovan-Mtunzi, R.L. Richards and J. Mason, *J. Chem. Soc. Dalton Trans.*, 1984, 1329.
88. V.C. Gibson, D.N. Williams, W. Clegg and D.C.R. Hockless, *Polyhedron*, 1989, **8**, 1819.
89. This thesis, *Chapter 5*.
90. J.M. Mayer, C.J. Curtis and J.E. Bercaw, *J. Am. Chem. Soc.*, 1983, **105**, 2651.
91. D.C. Bradley and M.H. Gitlitz, *J. Chem. Soc. (A)*, 1969, 980.
92. D.C. Bradley, M.H. Chisholm, and M.W. Extine, *Inorg. Chem.*, 1977, **22**, 1791.
93. A.A. Kuznetsova, Yu.G. Podzolko and Yu. A. Buslaev, *Russ. J. Inorg. Chem.*, 1969, **14**, 393.
94. J. Chatt, J.R. Dilworth and G.J. Leigh, *J. Chem. Soc. (A)*, 1970, 2239.
95. P.A.B. Shapley, Z.Y. Own and J.C. Huffman, *Organometallics*, 1986, **5**, 1269.
96. M.W. Bishop, J. Chatt, J.R. Dilworth, B.D. Neaves, P. Dahlstrom, J. Hyde and J. Zubieta, *J. Organomet. Chem.*, 1981, **213**, 109.
97. W.A. Herrmann, G. Weichselbaumer, R.A. Paciello, R.A. Fischer, E. Herdtweck, J. Okuda and D.W. Marz, *Organometallics*, 1990, **9**, 489.

98. M.W. Bishop, J. Chatt, J.R. Dilworth, M.B. Hursthouse, S.A.A. Jayaweera and A. Quick, *J. Chem. Soc. Dalton Trans.*, 1979, 914.
99. W.A. Nugent, R.J. McKinney, R.V. Kasowski and F.A. Van-Catledge, *Inorg. Chim. Acta*, 1982, **65**, L91.
100. 'Comprehensive Coordination Chemistry,' ed. G. Wilkinson
Pergamon Press, Oxford, 1987, vol 6, pp. 122-125.
101. J. Baldas, J. Bonnyman, P.M. Pojer, G.A. Williams, and M.F. Mackay, *J. Chem. Soc. Dalton Trans.*, 1981, 1798.
102. L.E. Toth, "Transition Metal Carbides and Nitrides", Academic, New York, 1971.
103. N.V. Troitskaya and Z.G. Pinsker, *Sov. Phys.-Crystallogr.*, 1960, **4**, 33; 1961, **6**, 34; 1964, **8**, 441.
104. R.A. Wheeler, R. Hoffmann and J. Strähle, *J. Am. Chem. Soc.*, 1986, **108**, 5381.
105. J. Chatt, J.R. Dilworth and R.L. Richards. *Chem Rev.*, 1978, **6**, 589.
106. M.E. Vol'pin and V.B. Shur, *Organomet. React.*, 1970, **1**, 55.
107. E.E. van Tamelen, *Acc. Chem. Res.*, 1970, **3**, 361.
108. A. Osaki and K. Aika, *Catal. Sci. Technol.*, 1981, **1**, 87.
109. R. Eisenberg and D.E. Hendriksen, *Adv. Catal.*, 1979, **28**, 79.
110. M.L. Unland, *J. Phys. Chem.*, 1973, **77**, 1952.
111. J.D. Burrington and R.K. Grasselli, *J. Catal.*, 1979, **59**, 79.
112. D.M.-T. Chan, W.A. Nugent, W.C. Fultz, D.C. Roe and T.H. Tulip, *J. Am. Chem. Soc.*, 1985, **107**, 251.
113. D.M.-T. Chan and W.A. Nugent, *Inorg. Chem.*, 1985, **24**, 1422.
114. J. Chatt, L.M. de Camera Pina and R.L. Richards, eds. "New Trends in the Chemistry of Nitrogen Fixation". Academic Press, London, 1980.
115. R.A. Hines and R.A. Prough, *J. Pharm. Exp. Ther.*, 1980, **214**, 80.
116. N.A. Milas and M.I. Iliopoulos, *J. Am. Chem. Soc.*, 1959, **81**, 6089.
117. D.W. Patrick, L.K. Truesdale, S.A. Biller and K.B. Sharpless, *J. Org. Chem.*, 1978, **43**, 2628.

118. E.Herranz and K.B. Sharpless, *J. Org. Chem.*, 1978, **43**, 2628
119. A.O. Chong, K. Oshima and K.B. Sharpless, *J. Am. Chem. Soc.*, 1977, **99**, 3420; S.G. Hentges and K.B. Sharpless, *unpublished results*.
120. R.R. Schrock, *Acc. Chem. Res.*, 1990, **23**, 158.

CHAPTER TWO

Half-Sandwich Imido Complexes of Niobium and Tantalum.

2.1 Introduction.

The ($\eta^5\text{-C}_5\text{R}_5$) ligand ($\text{R} = \text{H}$, alkyl) has been found to be particularly suited to the solubilisation of high oxidation state metal complexes containing hard ligands such as oxygen and nitrogen. The chemistry of half-sandwich oxo transition metal complexes of this type has been the subject of much recent interest¹, but analogous imido systems have remained largely undeveloped. This chapter describes a convenient synthetic route to the niobium and tantalum half-sandwich derivatives of the type shown in Figure 2.1, and initial investigations into the derivative chemistry of these species.

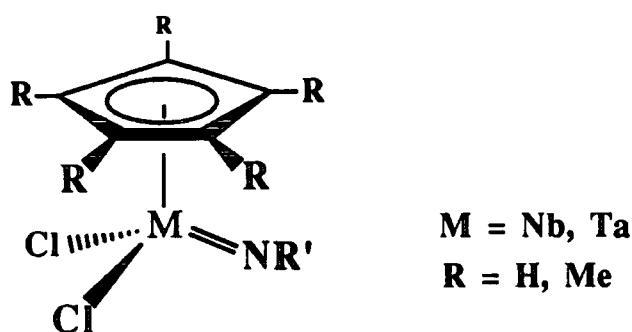
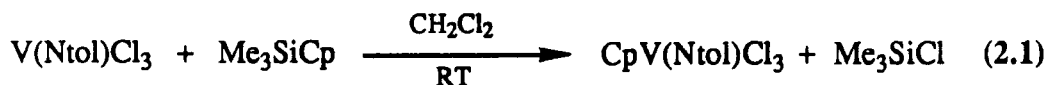
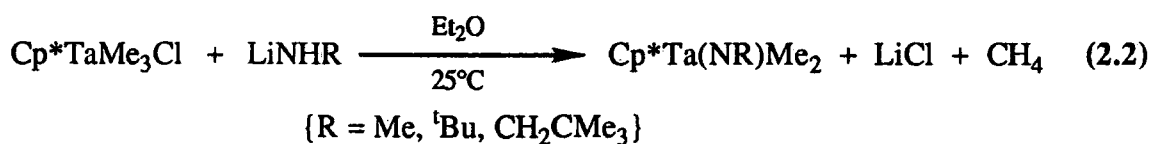


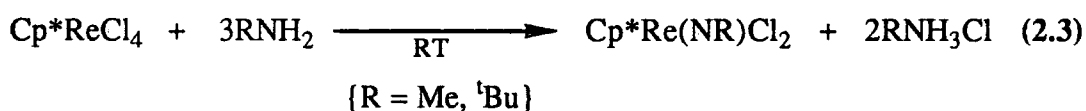
Figure 2.1

Although the vanadium complex $\text{CpV}(\text{Ntol})\text{Cl}_2$ has been prepared by Maatta, by the reaction of $\text{V}(\text{Ntol})\text{Cl}_3$ with Me_3SiCp^2 (Equation 2.1), half-sandwich niobium or tantalum imido halide species have not been prepared. However, a closely related heavy alkyl metal derivative of formula $\text{Cp}^*\text{Ta}(\text{NR})\text{Me}_2$ has been prepared by Bercaw et al., via elimination of methane in the reaction of monoalkylamides (LiNHR) with $\text{Cp}^*\text{TaMe}_3\text{Cl}^3$. (Equation 2.2).





Related to this class of compound is the d² rhenium complex Cp*Re(NR)Cl₂ recently prepared by Hermann⁴ via aminolysis of the tetrachloro precursor compound according to Equation 2.3



Known cyclopentadienyl transition metal imido complexes are collected in Table 2.1.

| Compound | Main Author | Ref. |
|---|-------------------|------|
| Cp ₂ V(NSiR ₃) (R= Me, Ph) | Schubert (1980) | 5 |
| Cp*Ta(NR)Me ₂ (R = Me, ^t Bu, Np) | Bercaw (1983) | 3 |
| Cp* ₂ V(NPh) | Gambarotta (1984) | 6 |
| Cp* ₂ V(NMe ₂ C ₆ H ₃) | Trogler (1985) | 7 |
| CpV(Ntol)Cl ₂ | Maatta (1987) | 2 |
| Cp ₂ Zr(NR) (R = ^t Bu, Ar) | Bergman (1988) | 8 |
| Cp*Ir(N ^t Bu) | Bergman (1989) | 9 |
| Cp*Re(NR)Cl ₂ (R = Me, ^t Bu) | Herrmann (1990) | 3 |

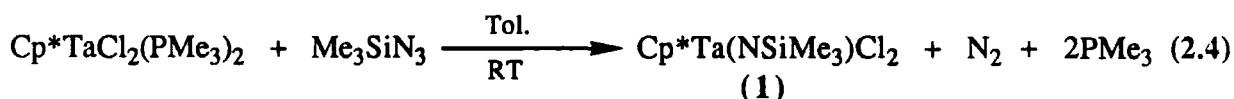
Table 2.1

2.2 A Low Valent Route.

2.2.1 Reaction of Cp*TaCl₂(PMe₃)₂ with Me₃SiN₃:

*Preparation of Cp*Ta(NSiMe₃)Cl₂ (1).*

Initial attempts to prepare Group 5 half-sandwich imido species involved the reaction of the Ta(III) complex Cp*TaCl₂(PMe₃)₂ with trimethylsilyl azide. The reaction in toluene proceeds smoothly over 10h. to afford an orange-yellow solution, from which Cp*Ta(NSiMe₃)Cl₂ (**1**) can be isolated as a yellow solid in low yield (Equation 2.4).



Compound (**1**) was characterised by elemental analysis, infrared, and ¹H NMR spectroscopies and mass spectrometry. The 250MHz ¹H NMR reveals two singlet resonances; attributable to the SiMe₃ group (δ 0.21) and the ring methyl hydrogens (δ 1.97). The infrared spectrum gives very strong bands at 1240cm⁻¹ and 845cm⁻¹, which, although difficult to assign to specific stretching modes (Chapter 1, section 1.4.3), appear to be characteristic of the terminal alkyl imido ligand of the complexes described in this thesis.

Since the low valent starting material is accesible only in the [Cp*Ta] system¹¹, and then only in modest yield, a more convenient, higher yield route was clearly desirable.

2.3 A High Valent Route.

Treatment of metal halides with hexamethyldisiloxane has been shown to provide a convenient route to simple oxyhalide compounds of niobium¹² according to Equation 2.5.

the expected region for the methyl carbon¹⁶. The infrared spectrum reveals bands at 1250 cm⁻¹ and 820 cm⁻¹ attributable to the terminal alkyl imido ligand, while strong bands in the range 400-300 cm⁻¹ are indicative of Nb-Cl stretches¹⁷. The mass spectrum gives an envelope due to the parent ion at m/z 257 (³⁵Cl).

A single crystal, X-ray structure determination on (2) shows that the complex is monomeric and therefore formally a 16 electron species, in which the coordination geometry is best described as a three legged piano stool. A full description of the structure is presented in section 2.6.

The reaction of CpTaCl₄ with (Me₃Si)₂NMe does not afford a terminal imido species analogous to (2), rather a yellow powder can be isolated, which appears to have retained SiMe₃ groups.

2.4.2 The Reaction of Cp*TaCl₄ with (Me₃Si)₂NMe:

*Preparation of [Cp*TaCl₃]₂[NMe] (3).*

The reaction of Cp*TaCl₄ with one equivalent of (Me₃Si)₂NMe was carried out in acetonitrile at room temperature. In this case, the reaction afforded [Cp*TaCl₃]₂[NMe] as an insoluble orange powder in 71% yield. Characterisation was provided by elemental analysis and infra-red spectroscopy. In particular, its elemental analysis was consistent with a stoichiometry of C₂₁H₃₃NCl₆Ta₂:

Found (Required): %C, 28.81 (28.86), %H, 3.61 (3.81), %N, 1.67 (1.60),
%Cl, 23.62 (24.37), %Ta 41.92 (41.40).

Compound (3) is moisture sensitive and insoluble in aromatic and chlorocarbon solvents. Its poor solubility prevented a solution molecular weight determination and solution NMR studies. However, the infrared spectrum shows a band at 670 cm⁻¹, which is assigned to a bridging imido stretch, and absorptions in the range 320-280 cm⁻¹ are indicative of bridging chloride ligands¹⁷. A structure determination on a related

oxo species $[\{\eta^5\text{-C}_5\text{H}_4\text{SiMe}_3\text{NbCl}_3\}_2]_2[\text{O}]$ has been reported by Royo and co-workers¹⁸. These studies revealed a binuclear structure with two bridging chloride ligands and a single oxygen bridge as shown in Figure 2.2. Reactions of CpMCl_4 ($\text{M}=\text{Nb}$, Ta) and Cp^*TaCl_4 with $(\text{Me}_3\text{Si})_2\text{O}$ are also thought to yield this binuclear structure¹⁹.

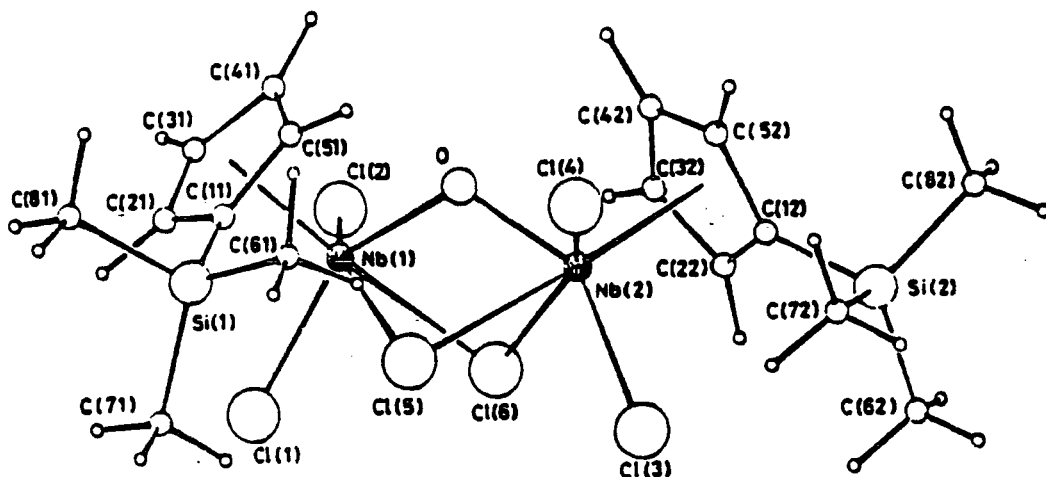


Figure 2.2

(3) is thus formulated as an analogue of these oxo species, such that a more accurate representation is $[\text{Cp}^*\text{TaCl}_2][\mu_2\text{-Cl}]_2[\mu_2\text{-NMe}]$ (Figure 2.3).

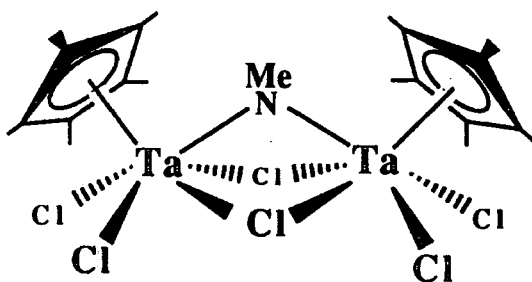


Figure 2.3, Proposed molecular structure of $[\text{Cp}^*\text{TaCl}_3]_2[\mu\text{-NMe}]$.

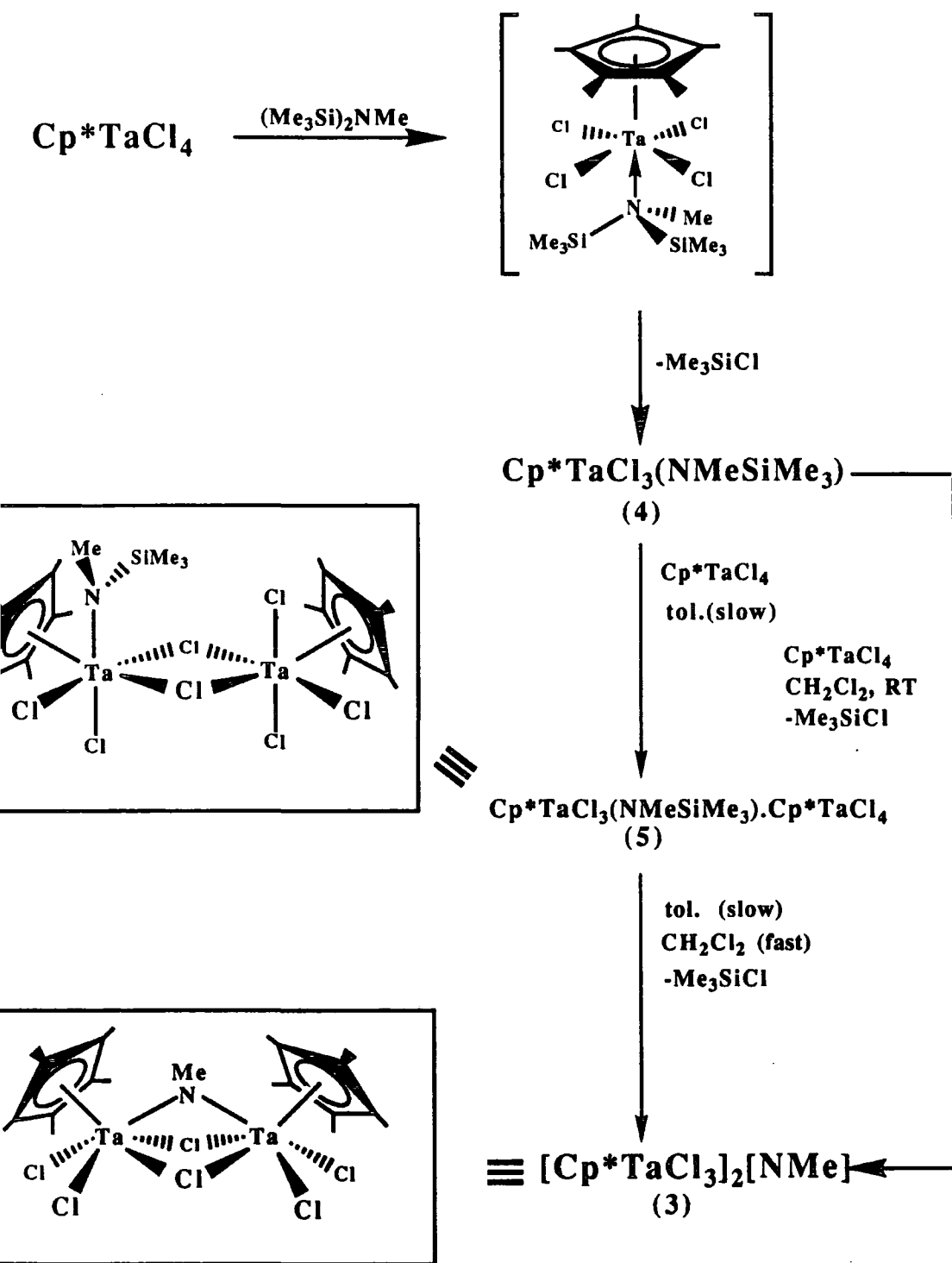
The formation of (3) may be envisaged as shown in Equation 2.8.



The formation of a mono-bridged species, in preference to the desired $\text{Cp}^*\text{Ta}(\text{NMe})\text{Cl}_2$, may suggest an enhanced propensity for intermolecular elimination of the second Me_3SiCl or alternatively may be favoured by binuclear silazane intermediates.

2.4.2.1 Mechanism of Formation of $[\text{Cp}^*\text{TaCl}_3]_2[\text{NMe}]$.

The mechanism for the formation of $[\text{Cp}^*\text{TaCl}_3]_2[\text{NMe}]$ is likely to be closely related to that described for the formation of $[\text{Cp}^*\text{TaCl}_3]_2[\text{O}]$ ¹⁹, obtained upon treatment of Cp^*TaCl_4 with $(\text{Me}_3\text{Si})_2\text{O}$. Here, the intermediates $\text{Cp}^*\text{TaCl}_3(\text{OSiMe}_3)$ and $[\text{Cp}^*\text{TaCl}_4.\text{Cp}^*\text{TaCl}_3(\text{OSiMe}_3)]$ have been isolated. Assuming the amine reaction proceeds in an analogous fashion, rapid condensation of Me_3SiCl with Cp^*TaCl_4 will afford the mono-silylamine $[\text{Cp}^*\text{TaCl}_3(\text{NMeSiMe}_3)]$ (4), from which the simple adduct $[\text{Cp}^*\text{TaCl}_4.\text{Cp}^*\text{TaCl}_3(\text{NMeSiMe}_3)]$ (5) is formed. The formation of (3) is then believed to arise by condensation of Me_3SiCl from the $[\text{Cp}^*\text{TaCl}_4.\text{Cp}^*\text{TaCl}_3(\text{NMeSiMe}_3)]$ intermediate (Scheme 2.1). Some evidence for the proposed intermediates, (4) and (5), was obtained by repeating the reaction of Cp^*TaCl_4 with $(\text{Me}_3\text{Si})_2\text{NMe}$ in toluene. In this solvent the reaction appears to occur more slowly forming a number of intermediate silylamine species, which are evident in the infrared spectrum; bands at 1425 cm^{-1} and 1255 cm^{-1} are indicative of the $\nu_{\text{as}}(\text{CH}_3)$ and $\nu_{\text{s}}(\text{CH}_3)$ vibrations of SiMe_3 respectively. A $\nu(\text{Si-R})$ stretching vibration is observed at 930 cm^{-1} ^{20,21}, and a broad absorption at 845 cm^{-1} is tentatively assigned to the Ta-N stretch. ¹H NMR spectra also indicate the presence of SiMe_3 groups with several resonances occurring in the region δ 0.16-0.18. It has not proved possible to assign these resonances to particular silazane intermediates.



Scheme 2.1, Proposed intermediates and mechanism for the formation of $[\text{Cp}^*\text{TaCl}_3]_2[\text{NMe}]$.

2.4.3 Reaction of CpTaCl₄ with (Me₃Si)₂NCN:

Preparation of [CpTa(NCN)Cl₂(CH₃CN)]_n (6).

Recent interest in the electronic properties of transition metal nitrogen polymers, led us to extend the *bis*(silyl) amine synthetic route from simple heptamethyldisilazane to *bis*(trimethylsilyl) cyanamide, (SiMe₃)₂NCN²². We envisaged that this reaction would lead to the formation of a transition metal carbonitride (Figure 2.4).

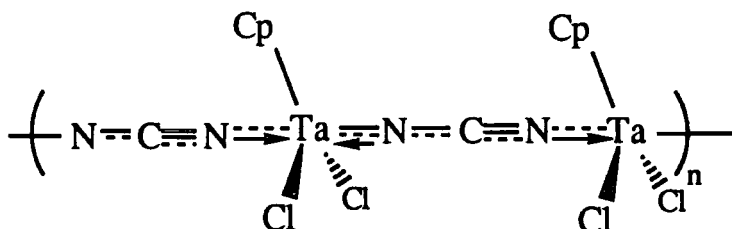


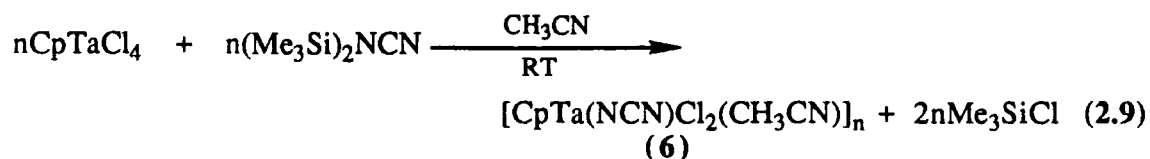
Figure 2.4

The reaction of CpTaCl₄ with (Me₃Si)₂NCN in acetonitrile gives a microcrystalline insoluble red-orange solid for which elemental analysis indicates a stoichiometry of C₈H₈N₃Cl₂Ta:

Found (Required): %C, 24.53 (24.14), %H, 2.24 (2.03), %N, 10.72 (10.56),
%Cl, 17.79 (17.81), %Ta 46.37 (45.46).

The infrared spectrum shows a strong broad band at 2000 cm⁻¹, attributable to the $\nu_{as}(\text{N}=\text{C}=\text{N})$ cyanamide stretching vibration, a band at 851 cm⁻¹ assigned to the $\nu(\text{Ta}-\text{N})$ stretch, and a weak band at 1025 cm⁻¹ indicates the presence coordinated acetonitrile (the C \equiv N stretch presumably being obscured by the broad band at 2000 cm⁻¹). Compound (6) is insoluble in aromatic and chlorocarbon solvents, preventing a solution molecular weight determination and NMR studies. Although the mass spectrum shows no multinuclear fragment ions, the insolubility of (6), combined with

elemental analysis, suggests that it is a polynuclear species of the general formula $[\text{CpTa}(\text{NCN})\text{Cl}_2(\text{CH}_3\text{CN})]_n$ (Equation 2.9).



Attempts to solubilise (6) by replacing the chloride ligands with alkyl substituted phenoxides did not lead to soluble products.

Reactions of CpNbCl_4 and Cp^*TaCl_4 with $(\text{Me}_3\text{Si})\text{NCN}$ yield apparently analogous, although slightly impure, insoluble, red-orange microcrystalline polynuclear cyanamide species. Characterisation of these species is limited to mass spectrometry and infrared data. The bridging cyanamide ligand is evident in the infrared spectra and the mass spectra show fragments corresponding to $[\text{CpM}(\text{NCN})\text{Cl}]^+$.

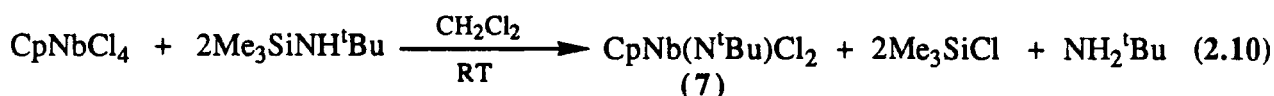
2.5 Preparation of Group 5 Half-Sandwich Imido species using Trimethylsilylamine and Amide Reagents.

Treatment of CpNbCl_4 with $(\text{Me}_3\text{Si})_2\text{N}^t\text{Bu}$ in 1,2-dichloroethane at 80°C leads to the recovery of starting materials, presumably due to the presence of three groups around the nitrogen preventing access of the amine nitrogen to the metal centre. Therefore, in order to access the more sterically demanding imido derivatives, reactions of the half-sandwich halides with amine and amide precursors such as $\text{Me}_3\text{SiNH}^t\text{Bu}$, $\text{Me}_3\text{SiNH}(2,6\text{-}^i\text{Pr}_2\text{C}_6\text{H}_3)$ and $\text{LiN}^t\text{Bu}(\text{SiMe}_3)$ have been investigated.

2.5.1 Reaction of CpNbCl₄ with Me₃SiNH^tBu:

Preparation of CpNb(N^tBu)Cl₂ (7).

The reaction of CpNbCl₄ with two molar equivalents of Me₃SiNH^tBu in methylene chloride yields an orange solution from which CpNb(N^tBu)Cl₂ (7) can be isolated as an orange-yellow crystalline solid in 78% yield. (Equation 2.10).



Compound (7) is soluble in aromatic and chlorocarbon solvents, and has appreciable solubility in pentane. The infrared spectrum shows bands at 1242 cm⁻¹ and 812 cm⁻¹ typical of the terminal imido group, both occurring to lower frequency than in the methylimido species described in section 2.4.1. The 250MHz ¹H NMR spectrum gives a sharp singlet at δ 1.02 due to equivalent methyl groups of the N^tBu ligand, and a singlet at δ 5.88 for the C₅H₅ hydrogens. The mass spectrum shows an envelope for the parent ion at m/z 299 (³⁵Cl), and daughter fragments arising by loss of methyl groups from the ^tbutyl imido ligand. The ¹³C NMR data for this and other ^tbutyl imido species are in discussed in section 2.10.

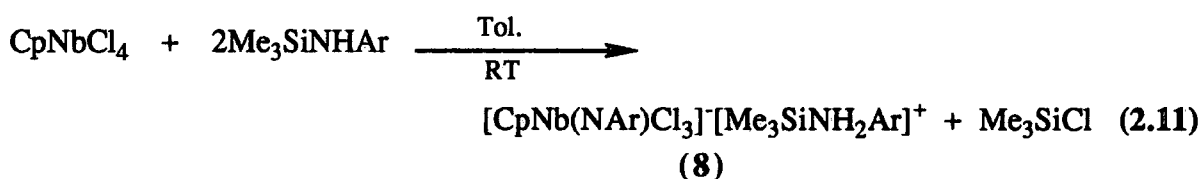
The single crystal X-ray structure determination of (7), is discussed in section 2.6.

2.5.2 Reaction of CpNbCl₄ with Me₃SiNH(2,6-*i*-Pr₂C₆H₃):

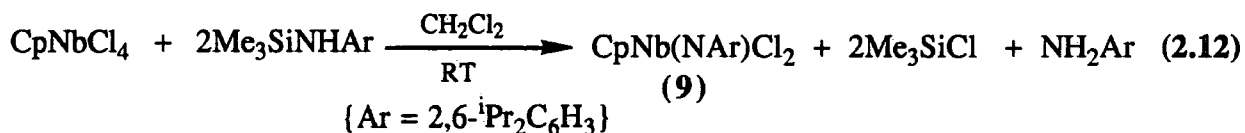
Preparation of



The reaction of one equivalent of Me₃SiNH(2,6-*i*-Pr₂C₆H₃) with CpNbCl₄ in toluene at room temperature yields an insoluble microcrystalline yellow-orange solid in low yield (*ca.* 30 %). Elemental analysis reveals a stoichiometry of C₃₂H₅₀N₂Cl₃Nb and the infrared spectrum shows a band at 3110 cm⁻¹ corresponding to the ν(N-H) stretching vibration. A sharp band at 870 cm⁻¹ and a weak band at 1300 cm⁻¹ are tentatively assigned to vibrations associated with the imido ligand. A peak at *m/z* 263 in the mass spectrum corresponds to the [CpNbCl₃]⁺ fragment. The available evidence, particularly the elemental analysis, suggests that the reaction product is an ion pair, consisting of an arylsilylammonium cation, and a half-sandwich trichloroarylimido anion i.e. [CpNb(NAr)Cl₃]⁻[NH₂SiMe₃Ar]⁺ (Ar = 2,6-*i*-Pr₂C₆H₃) (8). This product can be envisaged to form as shown in Equation 2.11.



If the reaction is carried out with two equivalents of Me₃SiNH(2,6-*i*-Pr₂C₆H₃) in dichloromethane, pink-red CpNb(N-2,6-*i*-Pr₂C₆H₃)Cl₂ (9) may be isolated in 72% yield (Equation 2.12). However, (8) does not convert to (9) on warming to 120°C.

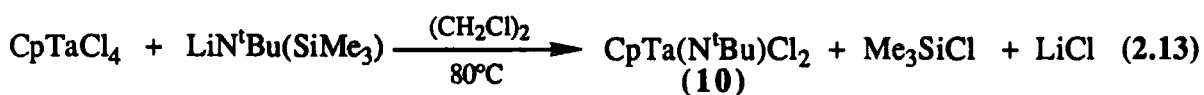


Compound (9) was characterised by elemental analysis, infrared, ^1H and ^{13}C NMR spectroscopies, mass spectrometry and by X-ray structure analysis (section 2.5). The infrared spectrum shows characteristic imido bands at 1285 cm^{-1} and 798 cm^{-1} . The 250 MHz ^1H NMR spectrum (C_6D_6), shows doublet and septet resonances at (δ 1.24 and 3.72) due to isopropyl methyl and methine protons respectively of the N-2,6- $(\text{Me}_2\text{CH})_2\text{C}_6\text{H}_3$ ligand. A signal due to C_5H_5 is observed at δ 5.82, and the expected triplet and doublet resonances of the three aromatic protons are observed at δ 6.88 and δ 6.98. The mass spectrum shows an envelope at m/z 403 (^{35}Cl) corresponding to the parent ion.

2.5.3 Reaction of CpTaCl_4 with $\text{LiNH}^t\text{Bu}(\text{SiMe}_3)$

Preparation of $\text{CpTa}(\text{N}^t\text{Bu})\text{Cl}_2$ (10).

The treatment CpTaCl_4 with $\text{Me}_3\text{SiNH}^t\text{Bu}$ in 1,2-dichloroethane at 80°C leads to the recovery of starting materials but under the same reaction conditions CpTaCl_4 reacts with $\text{LiN}^t\text{Bu}(\text{SiMe}_3)$ to give $\text{CpTa}(\text{N}^t\text{Bu})\text{Cl}_2$ albeit in low yield according to Equation 2.13.



The similar solubility characteristics of (10) to the impurities present in the crude product mixture has contributed to difficulties in its extraction and purification.

As yet, it has only proved possible to obtain enough pure product to collect limited experimental data. The infrared spectrum shows bands 1298 cm^{-1} and 818 cm^{-1} consistent with imido vibrational stretches. The mass spectrum reveals peaks at m/z 387 (^{35}Cl) assignable to the parent ion, and the 250 MHz ^1H NMR spectrum displays two singlet resonances at δ 1.11 and δ 5.81 (ratio 9:5), attributable to the NCMe_3 and C_5H_5 protons respectively.

2.5.4 Reaction of CpTaCl₄ with LiN(2,6-ⁱPr₂C₆H₃)(SiMe₃):

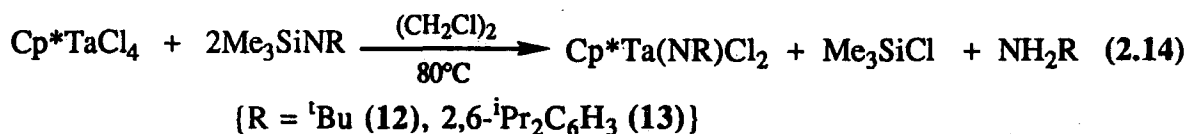
Preparation of CpTa(N-2,6-ⁱPr₂C₆H₃)Cl₂ (11).

In a reaction analogous to that described in the preceding section, CpTa(N-2,6-ⁱPr₂C₆H₃)Cl₂ can be isolated as an impure yellow-orange powder in low yield. The experimental evidence suggests that this species is analogous to its niobium analogue (9). In particular, a similar pattern of ¹H NMR resonances are observed (Chapter 6, section 6.2), and a parent ion is found in the mass spectrum at m/z 491 (³⁵Cl). Improved yields will be required for full characterisation of (11).

2.5.5 Reaction of Cp*TaCl₄ with Me₃SiNHR Reagents

*Preparation of Cp*Ta(NR)Cl₂ (R = ^tBu (12), 2,6-ⁱPr₂C₆H₃)Cl₂ (13)).*

Reactions of Cp*TaCl₄ with two molar equivalents of Me₃SiNHR (R = ^tBu, 2,6-ⁱPr₂C₆H₃) in 1,2-dichloroethane at elevated temperature, afford the yellow-orange compounds Cp*Ta(NR)Cl₂ (R = ^tBu (12), 2,6-ⁱPr₂C₆H₃ (13)), according to Equation 2.14.



The increased solubilising ability of the C₅Me₅ ligand makes isolation of pure (12) and (13) easier than for the analogous C₅H₅ compounds (10) and (11). (13) was first prepared in this laboratory by J.P. Mitchell and orange crystals grown from pentane. A single crystal X-ray structure determination²³ shows the same three-legged piano stool geometry to the niobium analogues (2), (7) and (9), discussed in section 2.6

Characterisation of (12) was limited to elemental analysis and in particular ^1H NMR spectroscopy, which shows two singlet resonances at δ 1.94 and δ 1.23 (ratio 5:3) attributable to C_5Me_5 and CMe_3 protons respectively.

2.6 The Molecular Structures of Complexes of the Type $\text{CpNb}(\text{NR})\text{Cl}_2$. ($\text{R} = \text{Me}$, ^tBu and $2,6\text{-}^i\text{Pr}_2\text{C}_6\text{H}_3$).

Having successfully synthesised a series of compounds of the type $\text{CpNb}(\text{NR})\text{Cl}_2$ ($\text{R} = \text{SiMe}_3$ (1) Me (2), ^tBu (7) and $2,6\text{-}^i\text{Pr}_2\text{C}_6\text{H}_3$ (9)), we were interested in establishing the general structural features of these species as a prelude to the development of their derivative chemistry. We were particularly interested in assessing the influence of imido ligands of differing steric and electronic requirements. With this in mind, crystals of (2), (7) and (9) were grown. For (2), large orange prismatic crystals were obtained by cooling a saturated toluene solution at -20°C . Yellow-orange rhombohedral crystals of (7) and red needle crystals of (9) were obtained by cooling the respective pentane solutions to -20°C . A crystal of suitable dimensions for each compound was selected for an X-ray study and mounted in a Lindemann capillary tube under an inert atmosphere. The data were collected and the structures solved by Dr. W. Clegg and D. C. R. Hockless at the University of Newcastle-upon-Tyne. The molecular structures of (2)¹⁵, (7) and (9) are illustrated in Figures 2.5, 2.6 and 2.7 and selected bond angles and distances are collected in Tables 2.2, 2.3 and 2.4 respectively.

In each case, the molecule possesses a three-legged piano stool geometry. Compound (2) and (9) possess a crystallographic mirror plane which bisects the Cl-Nb-Cl angle and contains the niobium, nitrogen and carbon atom C(1), but this not found in (7), in which there are two discrete molecules within the unit cell (Figure 2.6 (b)). In each case, the metal-nitrogen bond distance lies within the range expected for a niobium-nitrogen triple bond (1.752(3)Å for (2), 1.744(3) and 1.752(3) for the two independent molecules of (7) and 1.761(6) for (9)), c.f. typical values of 1.73-1.79Å

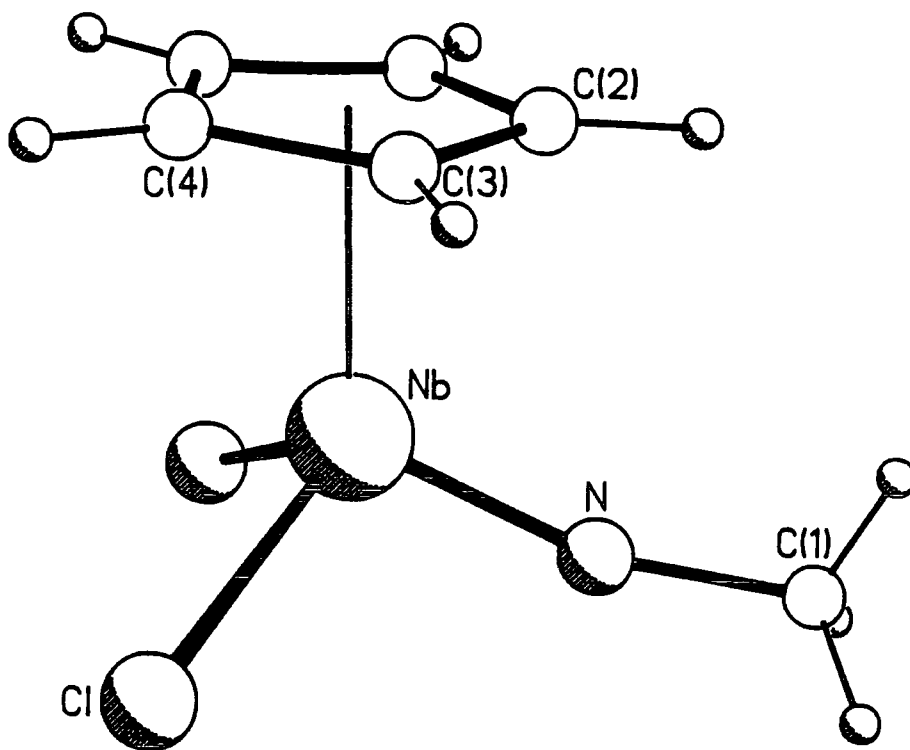


Figure 2.5(a), *The molecular structure of CpNb(NMe)Cl₂ (2).*

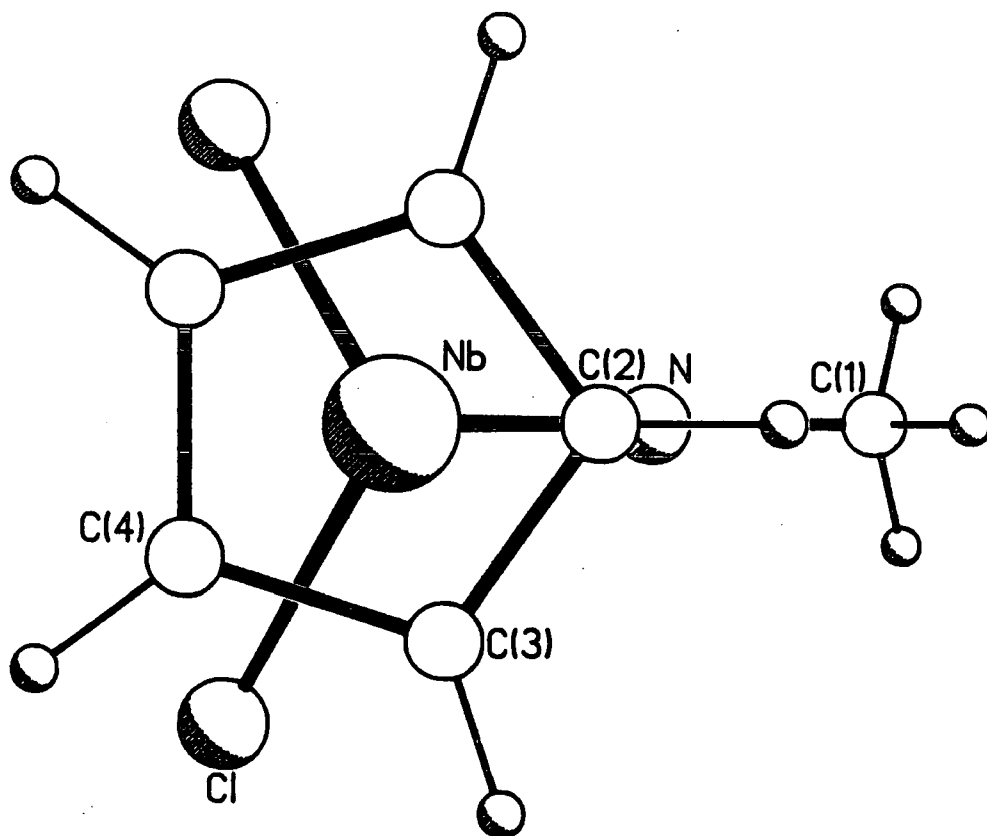


Figure 2.5(b), *View of (2) down the ring centroid-niobium vector.*

| | | | |
|---------------------|----------|--------------------|----------|
| Nb - Cl(1) | 2.355(1) | Nb - N | 1.752(2) |
| Nb - C(2) | 2.380(4) | Nb - C(3) | 2.404(3) |
| Nb - C(4) | 2.500(3) | N - C(1) | 1.432(3) |
| C(2) - C(3) | 1.392(3) | C(3) - C(4) | 1.415(3) |
| C(4) - C(4') | 1.390(6) | | |
| Cl - Nb - N | 103.3(1) | Cl - Nb - C(2) | 125.2(1) |
| N - Nb - C(2) | 87.3(1) | Cl - Nb - C(3) | 92.6(1) |
| N - Nb - C(4) | 105.0(1) | C(2) - Nb - C(3) | 33.8(1) |
| Cl - Nb - C(4) | 87.2(1) | N - Nb - C(4) | 138.2(1) |
| C(2) - Nb - C(4) | 55.3(1) | C(3) - Nb - C(4) | 33.5(1) |
| Cl - Nb - Cl' | 104.7(1) | C(3) - Nb - Cl' | 142.2(1) |
| C(4) - Nb - Cl | 113.0(1) | C(3) - Nb - C(3') | 56.1(1) |
| C(4) - Nb - C(3') | 55.0(1) | C(4) - Nb - C(4') | 32.3(1) |
| Nb - N - C(1) | 163.4(3) | Nb - C(2) - C(3) | 74.0(2) |
| C(3) - C(2) - C(3') | 108.5(2) | Nb - C(3) - C(2) | 72.2(2) |
| Nb - C(3) - C(4) | 77.0(2) | C(2) - C(3) - C(4) | 107.8(2) |
| Nb - C(4) - C(3) | 69.5(2) | Nb - C(4) - C(4') | 73.9(1) |
| C(3) - C(4) - C(4') | 107.9(2) | | |

Table 2.2, Bond distances (Å) and angles (°) for CpNb(NMe)Cl₂ (2).

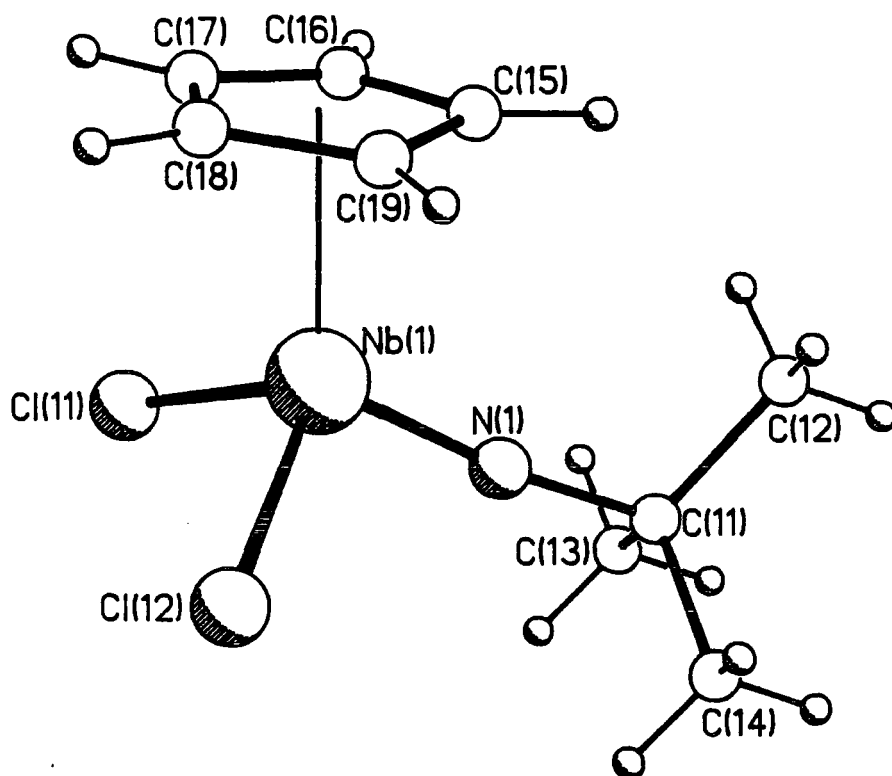


Figure 2.6(a), *The molecular structure of CpNb(N^tBu)Cl₂ (7).*

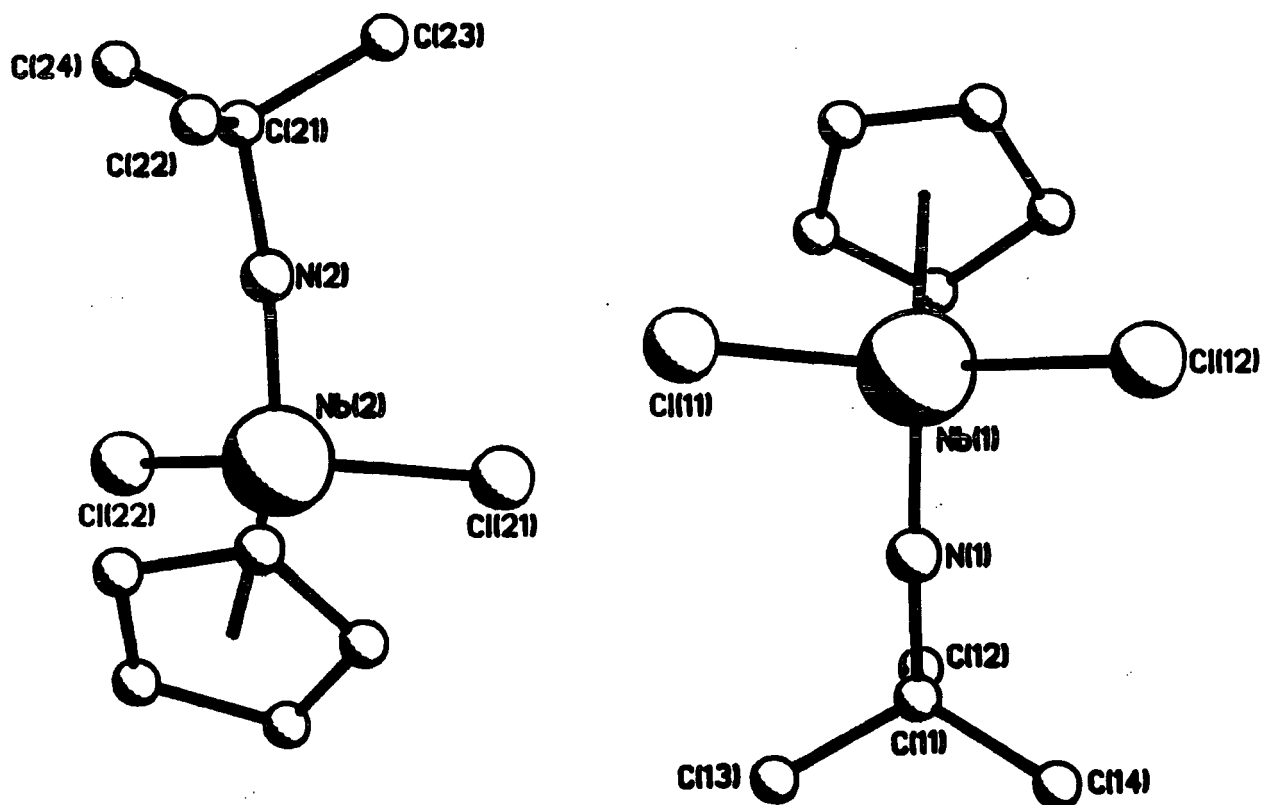


Figure 2.6(b), *The two independent molecules within the unit cell of CpNb(N^tBu)Cl₂ (7).*

| | | | |
|----------------|-----------|----------------|-----------|
| Nb(1) - Cl(11) | 2.354(1) | Nb(1) - Cl(12) | 2.358(2) |
| Nb(1) - N(1) | 1.744(3) | Nb(1) - C(15) | 2.345(10) |
| Nb(1) - C(16) | 2.372(14) | Nb(1) - C(17) | 2.474(9) |
| Nb(1) - C(18) | 2.489(7) | Nb(1) - C(19) | 2.395(8) |
| N(1) - C(11) | 1.444(5) | C(11) - C(12) | 1.508(10) |
| C(11) - C(13) | 1.515(8) | C(11) - C(14) | 1.488(13) |
| C(15) - C(16) | 1.339(17) | C(15) - C(19) | 1.437(18) |
| C(16) - C(17) | 1.269(14) | C(17) - C(18) | 1.264(13) |
| C(18) - C(19) | 1.338(13) | Nb(2) - Cl(21) | 2.348(1) |
| Nb(2) - Cl(22) | 2.357(2) | Nb(2) - N(2) | 1.752(3) |
| Nb(2) - C(25) | 2.379(7) | Nb(2) - C(26) | 2.437(8) |
| Nb(2) - C(27) | 2.513(7) | Nb(2) - C(28) | 2.471(7) |
| Nb(2) - C(29) | 2.373(5) | N(2) - C(21) | 1.447(5) |
| C(21) - C(22) | 1.517(7) | C(21) - C(23) | 1.525(6) |
| C(21) - C(24) | 1.520(9) | C(25) - C(26) | 1.339(8) |
| C(25) - C(29) | 1.344(10) | C(26) - C(27) | 1.382(11) |
| C(27) - C(28) | 1.392(12) | C(28) - C(29) | 1.375(11) |

| | | | |
|-------------------------|-----------|------------------------|----------|
| Cl(11) - Nb(1) - Cl(12) | 106.4(1) | Cl(11) - Nb(1) - N(1) | 103.1(1) |
| Cl(12) - Nb(1) - N(1) | 102.1(1) | Cl(11) - Nb(1) - C(15) | 125.2(4) |
| Cl(12) - Nb(1) - C(15) | 121.4(4) | N(1) - Nb(1) - C(15) | 92.2(2) |
| Cl(11) - Nb(1) - C(16) | 92.8(2) | Cl(12) - Nb(1) - C(16) | 139.6(3) |
| N(1) - Nb(1) - C(16) | 107.8(3) | C(15) - Nb(1) - C(16) | 33.0(5) |
| Cl(11) - Nb(1) - C(17) | 85.1(1) | Cl(12) - Nb(1) - C(17) | 115.1(2) |
| N(1) - Nb(1) - C(17) | 138.1(2) | C(15) - Nb(1) - C(17) | 52.4(3) |
| C(16) - Nb(1) - C(17) | 30.3(3) | Cl(11) - Nb(1) - C(18) | 106.2(2) |
| Cl(12) - Nb(1) - C(18) | 89.0(3) | N(1) - Nb(1) - C(18) | 144.3(2) |
| C(15) - Nb(1) - C(18) | 53.9(3) | C(16) - Nb(1) - C(18) | 51.1(4) |
| C(17) - Nb(1) - C(18) | 29.5(3) | C(11) - Nb(1) - C(19) | 136.3(2) |
| Cl(12) - Nb(1) - C(19) | 88.7(2) | N(1) - Nb(1) - C(19) | 113.8(3) |
| C(15) - Nb(1) - C(19) | 35.3(4) | C(16) - Nb(1) - C(19) | 54.7(3) |
| C(17) - Nb(1) - C(19) | 51.8(3) | C(18) - Nb(1) - C(19) | 31.7(3) |
| Nb(1) - N(1) - C(11) | 172.5(3) | N(1) - C(11) - C(12) | 109.5(4) |
| N(1) - C(11) - C(13) | 107.5(4) | C(12) - C(11) - C(13) | 109.3(6) |
| N(1) - C(11) - C(14) | 108.2(5) | C(12) - C(11) - C(14) | 111.7(6) |
| C(13) - C(11) - C(14) | 110.6(6) | Nb(1) - C(15) - C(16) | 74.6(7) |
| Nb(1) - C(15) - C(19) | 74.3(6) | C(16) - C(15) - C(19) | 104.1(8) |
| Nb(1) - C(16) - C(15) | 72.4(8) | Nb(1) - C(16) - C(17) | 79.3(8) |
| C(15) - C(16) - C(17) | 109.7(11) | Nb(1) - C(17) - C(16) | 70.4(7) |
| Nb(1) - C(17) - C(18) | 75.9(6) | C(16) - C(17) - C(18) | 112.0(8) |
| Nb(1) - C(18) - C(17) | 74.6(5) | Nb(1) - C(18) - C(19) | 70.2(5) |
| C(17) - C(18) - C(19) | 109.6(8) | Nb(1) - C(19) - C(15) | 70.5(5) |
| Nb(1) - C(19) - C(18) | 78.1(4) | C(15) - C(19) - C(18) | 104.6(8) |
| Cl(21) - Nb(2) - Cl(22) | 105.4(1) | Cl(21) - Nb(2) - N(2) | 103.6(1) |
| Cl(22) - Nb(2) - N(2) | 100.7(1) | Cl(21) - Nb(2) - C(25) | 115.1(2) |
| Cl(22) - Nb(2) - C(25) | 133.1(2) | N(2) - Nb(2) - C(25) | 92.2(2) |
| Cl(21) - Nb(2) - C(26) | 88.0(1) | Cl(22) - Nb(2) - C(26) | 136.1(2) |
| N(2) - Nb(2) - C(26) | 116.7(2) | C(25) - Nb(2) - C(26) | 32.2(2) |
| Cl(21) - Nb(2) - C(27) | 92.0(2) | Cl(22) - Nb(2) - C(27) | 104.3(2) |
| N(2) - Nb(2) - C(27) | 145.7(2) | C(25) - Nb(2) - C(27) | 53.5(2) |
| C(26) - Nb(2) - C(27) | 32.4(3) | Cl(21) - Nb(2) - C(28) | 122.5(2) |
| Cl(22) - Nb(2) - C(28) | 84.8(2) | N(2) - Nb(2) - C(28) | 130.4(2) |
| C(25) - Nb(2) - C(28) | 54.1(3) | C(26) - Nb(2) - C(28) | 54.0(3) |
| C(27) - Nb(2) - C(28) | 32.4(3) | C(21) - Nb(2) - C(29) | 141.8(2) |
| Cl(22) - Nb(2) - C(29) | 100.3(2) | N(2) - Nb(2) - C(29) | 98.8(2) |

| | | | |
|-----------------------|----------|-----------------------|----------|
| C(25) - Nb(2) - C(29) | 32.9(2) | C(26) - Nb(2) - C(29) | 54.2(2) |
| C(27) - Nb(2) - C(29) | 54.0(2) | C(28) - Nb(2) - C(29) | 32.9(3) |
| Nb(2) - N(2) - C(21) | 170.0(3) | N(2) - C(21) - C(22) | 110.1(4) |
| N(2) - C(21) - C(23) | 107.7(3) | C(22) - C(21) - C(23) | 110.5(4) |
| N(2) - C(21) - C(24) | 107.1(4) | C(22) - C(21) - C(24) | 111.3(4) |
| C(23) - C(21) - C(24) | 110.1(4) | Nb(2) - C(25) - C(26) | 76.2(4) |
| Nb(2) - C(25) - C(29) | 73.3(4) | C(26) - C(25) - C(29) | 109.5(6) |
| Nb(2) - C(26) - C(25) | 71.5(4) | Nb(2) - C(26) - C(27) | 76.8(5) |
| C(25) - C(26) - C(27) | 108.3(6) | Nb(2) - C(27) - C(26) | 70.8(4) |
| Nb(2) - C(27) - C(28) | 72.1(5) | C(26) - C(27) - C(28) | 106.8(6) |
| Nb(2) - C(28) - C(27) | 75.4(4) | Nb(2) - C(28) - C(29) | 69.6(4) |
| C(27) - C(28) - C(29) | 106.9(7) | Nb(2) - C(29) - C(25) | 73.8(3) |
| Nb(2) - C(29) - C(28) | 77.5(4) | C(25) - C(29) - C(28) | 108.5(6) |

Table 2.3, Bond distances (Å) and angles (°) for CpNb(NⁱBu)Cl₂ (7).

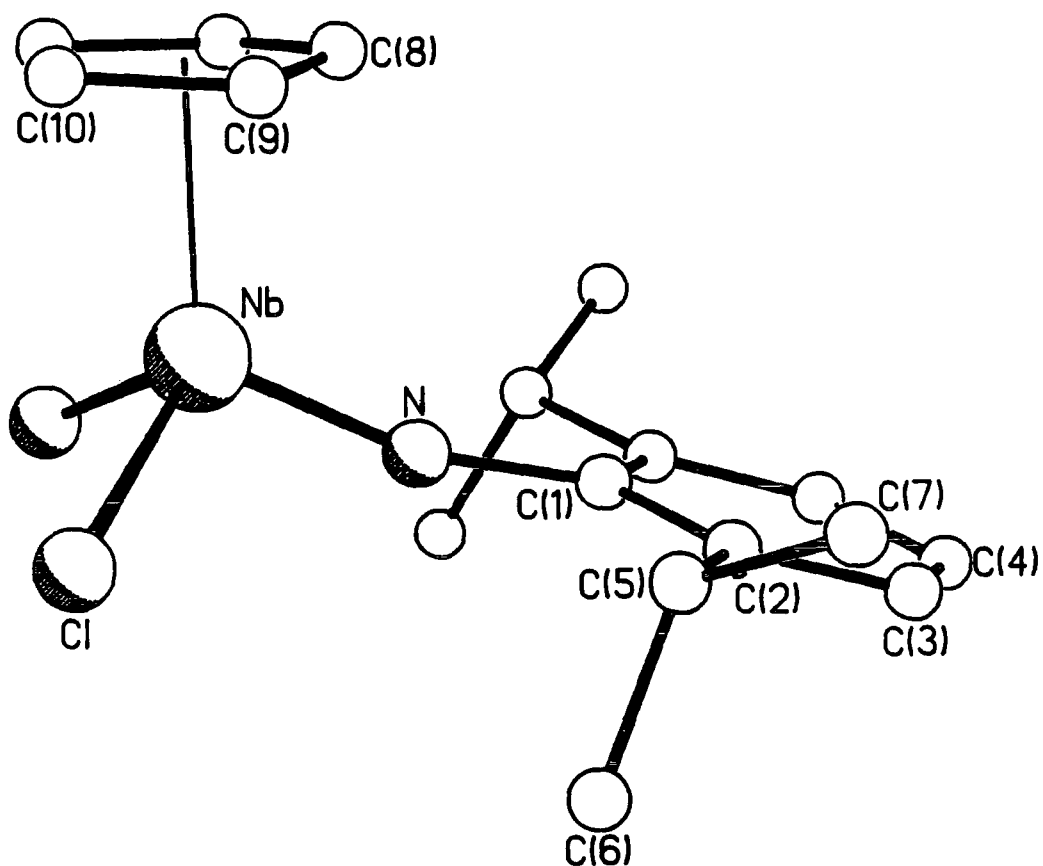


Figure 2.7(a), The molecular structure of $\text{CpNb}(\text{N}-2,6\text{-}i\text{Pr}_2\text{C}_6\text{H}_3)\text{Cl}_2$ (9).

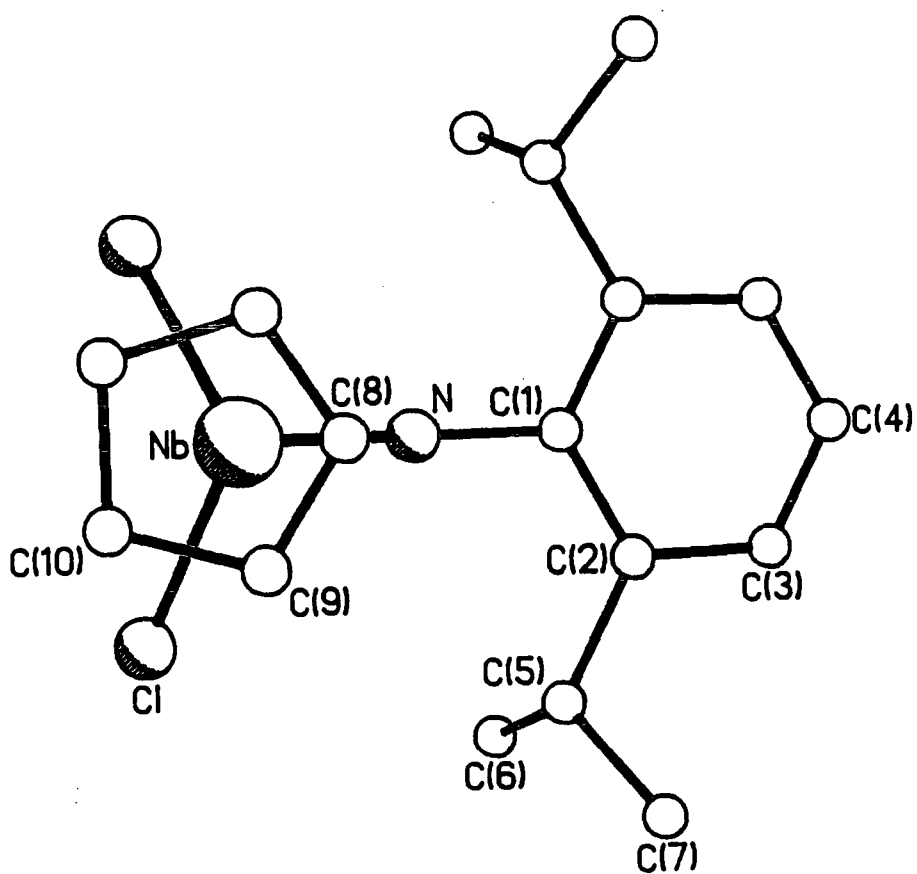


Figure 2.7(b), View of (9) down the ring centroid-niobium vector.

| | | | |
|----------------------|-----------|---------------------|-----------|
| Nb - Cl | 2.338(2) | Nb - N | 1.761(6) |
| Nb - C(8) | 2.396(11) | Nb - C(9) | 2.362(14) |
| Nb - C(10) | 2.442(10) | N - C(1) | 1.408(9) |
| C(1) - C(2) | 1.401(6) | C(2) - C(3) | 1.411(12) |
| C(2) - C(5) | 1.524(8) | C(3) - C(4) | 1.378(10) |
| C(5) - C(6) | 1.507(10) | C(5) - C(7) | 1.487(10) |
| C(8) - C(9) | 1.285(13) | C(9) - C(10) | 1.360(21) |
| Cl - Nb - N | 102.4(1) | Cl - Nb - C(8) | 123.0(1) |
| N - Nb - C(8) | 90.7(3) | Cl - Nb - C(9) | 141.2(3) |
| N - Nb - C(9) | 105.1(4) | C(8) - Nb - C(9) | 31.3(3) |
| Cl - Nb - C(10) | 114.0(3) | N - Nb - C(10) | 137.8(4) |
| C(8) - Nb - C(10) | 52.0(4) | C(9) - Nb - C(10) | 32.8(5) |
| Cl - Nb - Cl' | 108.0(1) | C(9) - Nb - Cl' | 92.4(3) |
| C(10) - Nb - Cl' | 86.6(3) | C(9) - Nb - C(9') | 54.2(5) |
| C(10) - Nb - C(9') | 54.7(4) | C(10) - Nb - C(10') | 33.4(6) |
| Nb - N - C(1) | 165.6(5) | N - C(1) - C(2) | 118.7(3) |
| C(2) - C(1') - C(2') | 122.6(7) | C(1) - C(2) - C(3) | 117.6(5) |
| C(1) - C(2) - C(5) | 122.1(5) | C(3) - C(2) - C(5) | 120.4(5) |
| C(2) - C(3) - C(4) | 120.5(8) | C(3) - C(4) - C(3') | 121.2(11) |
| H(4) - C(4) - C(3') | 119.4(6) | C(2) - C(5) - C(6) | 109.5(5) |
| C(2) - C(5) - C(7) | 113.5(5) | C(6) - C(5) - C(7) | 112.8(6) |
| Nb - C(8) - C(9) | 72.9(8) | H(8) - C(8) - C(9') | 123.1(8) |
| C(9) - C(8) - C(9') | 113.8(15) | Nb - C(9) - C(8) | 75.8(7) |
| Nb - C(9) - C(10) | 76.8(8) | C(8) - C(9) - C(10) | 106.7(10) |
| Nb - C(10) - C(9) | 70.3(7) | Nb - C(10) - C(10') | 73.3(3) |

Table 2.4. Bond distances (Å) and angles (°) for *CpNb(N-2,6-ⁱPr₂C₆H₃)Cl₂ (9)*.

for terminal niobium imido compounds²⁴⁻²⁶, arising from the donation of the nitrogen to the metal centre. The Nb-N-C bond angles of these molecules lie in the range (161-180°) typically observed for a terminal imido containing sp-hybridised nitrogen¹⁶. For (2) this angle is 163.4(3)°, for (9) 165.6(5)°, and 172.5(3)° and 170.0(3)° for the two independent molecules of (7). The slight deviations from linearity arise from a bending of the imido substituent towards the cyclopentadienyl ring. This suggests that the interaction of the nitrogen lone pair containing p-orbitals is with a vacant metal d-orbital *trans* to the cyclopentadienyl ring (see Chapter 3, section 3.5). The steric congestion around the metal centre in (7) appears to favour a more linear Nb-N-C arrangement. Clearly (2), (7) and (9) can be considered as sixteen electron complexes, with the 'linear' imido ligand donating four electrons to the niobium metal centre. The niobium-chlorine distances, varying from 2.338-2.357Å, are at the low end of the range expected for Nb(V)-Cl bond lengths²⁷, presumably as a result of significant Cl→Nb pπ-dπ interaction, not an unusual feature for electron deficient transition metal centres²⁸.

In these three crystallographically characterised complexes, the cyclopentadienyl moiety is not coordinated in the ideal η^5 fashion; instead, a trend towards η^2/η^3 (allylene) coordination is observed leading to three short and two long Nb-Cp ring carbon distances and to a distortion of the cyclopentadienyl ring, the extent of which can be evaluated by considering the three parameters ΔM , ΔR , and ΔD (Figure 2.8).

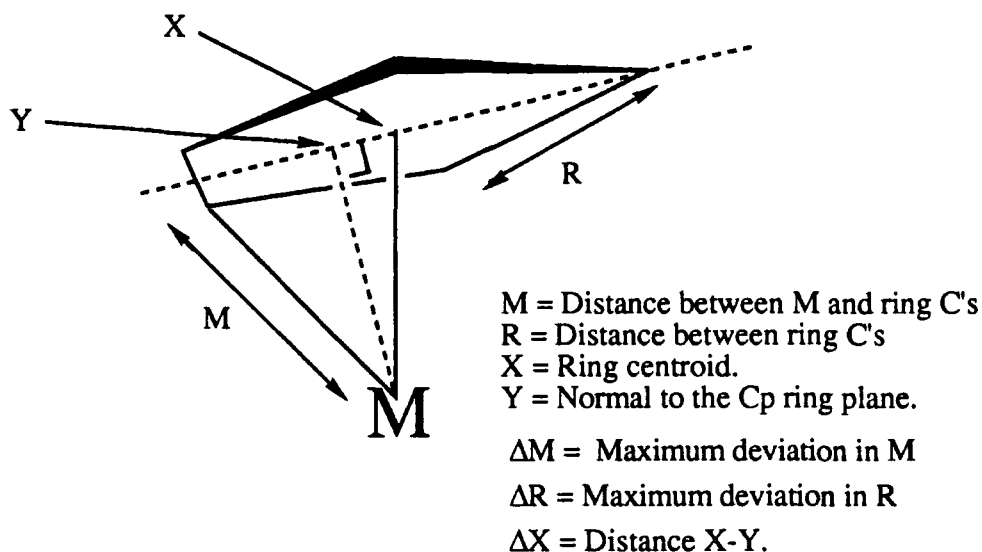


Figure 2.8, Ring parameters used to evaluate ring slippage.

Maximum deviations of the Nb-C_{ring} (ΔM) and inter-ring carbon distances (ΔR), are shown in Table 2.5, together with the distance between the Cp ring centroid and the point where the Nb-Cp ring normal meets the plane of the Cp ring (ΔX), giving an indication of ring slippage. α is the M-N-C angle.

| Complex | ΔM (Å) | ΔR (Å) | ΔX (Å) | α (°) |
|---|----------------|----------------|----------------|--------------|
| CpNb(NMe)Cl ₂ (2) | 0.120 | 0.025 | 0.115 | 16.6 |
| CpNb(N ^t Bu)Cl ₂ ^a | 0.144 | 0.183 | 0.143 | 7.5 |
| (7) | 0.140 | 0.060 | 0.083 | 10.0 |
| CpNb(NAr)Cl ₂ ^b (9) | 0.080 | 0.044 | 0.048 | 14.4 |

^a Two independent molecules within the unit cell.

^b Ar = 2,6-*i*Pr₂C₆H₃.

Table 2.5

Clearly, the most distorted of the structurally characterised species are the two molecules of (7). The cyclopentadienyl rings of (2) and (9) are orientated in an eclipsed fashion with respect to the the imido ligand; the two molecules of (7), however show a staggered conformation. These pronounced differences in structure

are likely to be due to a steric rather than an electronic effect, arising from the bulky ^tBu group. Related, but smaller distortions are seen in the bulky pentamethylcyclopentadienyl tantalum species Cp*Ta(N-2,6-ⁱPr₂C₆H₃)Cl₂ (13) ²³.

Symmetrical species (2) and (9) adopt an alkyl-alkene type structure similar to that found in Cp*Re(N^tBu)Cl₂ described recently by Herrmann et al⁴. The essential features of this structure type are:

(1) the Cp C-C bond *trans* to the imido ligand is the shortest bond in the cyclopentadienyl unit.

(2) the bonds between the metal and the two *trans* Cp carbon atoms are considerably longer than the other three Nb-C distances.

However, the quite markedly differing parameters found for the two independent molecules of (7) suggest that crystal packing forces may have an important influence on these distortions.

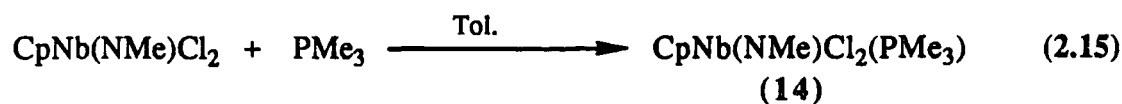
2.7 Some Derivative Chemistry of CpNb(NMe)Cl₂ (2).

Having established a satisfactory route to CpNb(NMe)Cl₂ (2), attention turned to the development of its derivative chemistry.

2.7.1 Reaction CpNb(NMe)Cl₂ with Trimethylphosphine:

Preparation of CpNb(NMe)Cl₂(PMe₃) (14).

The reaction of (2) with PMe₃ in toluene yields CpNb(NMe)Cl₂(PMe₃) as an off-white solid in high yield (85%). This simple adduct is envisaged to form according to Equation 2.15.



Compound (14), is soluble in chlorocarbon solvents, but has limited solubility in aromatic solvents. Elemental analysis confirmed a stoichiometry of $C_9H_{17}NCl_2PNb$ while its infrared spectrum indicates the presence of coordinated PMe_3 with characteristic bands at 1278 cm^{-1} , 960 cm^{-1} and 734 cm^{-1} , attributable to $\sigma(CH_3)$, $\rho(CH_3)$ and $\nu_{as}(C-P)$ respectively²⁹. Characteristic absorptions due to the imido ligand are found at 1240 cm^{-1} and 814 cm^{-1} , close in frequency to the vibrations observed in the starting complex (2). The 250MHz 1H NMR spectrum ($CDCl_3$) reveals a doublet at δ 1.58, corresponding to coordinated PMe_3 . The methyl and C_5H_5 protons, at δ 3.85 and δ 6.16 respectively, show a slight downfield shift compared with (2).

2.7.1.1 The Molecular Structure of $CpNb(NMe)Cl_2(PMe_3)$ (14).

Pale orange needles of (14) were obtained by slow cooling of a saturated hot toluene solution. A crystal of dimensions $0.52 \times 0.20 \times 0.18$ mm was chosen for a crystallographic study and mounted in a Lindemann capillary. The data were collected and analysed by Dr W. Clegg and D.C.R. Hockless of the University of Newcastle-upon-Tyne (Appendix 1D) and the results are described below¹⁵. The molecular structure is illustrated in Figure 2.10 and Figure 2.11 and selected bond distances and angles given in Table 2.6

The geometry of (14), is best described as a four-legged piano stool, with the trimethylphosphine ligand lying *trans* to one chloro group and *cis* to the methylimido and remaining chloro ligand. A comparison of selected bond angles and distances of the PMe_3 adduct and the 16 electron precursor is presented in Table 2.7

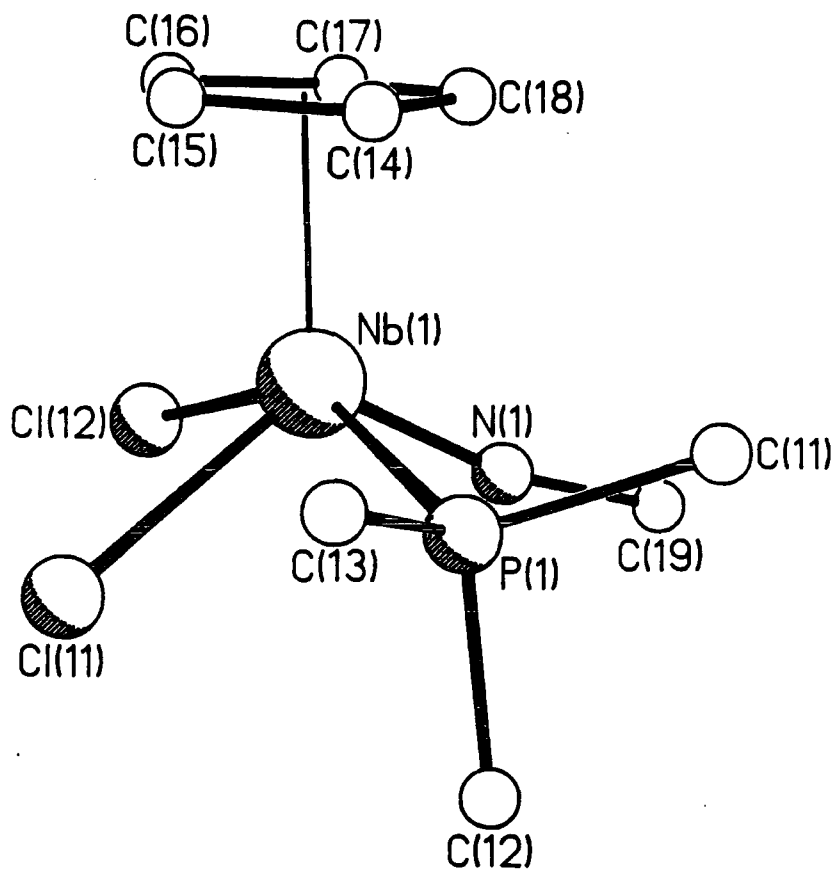


Figure 2.10, The molecular structure of $CpNb(NMe)Cl_2(PMe_3)$ (14).

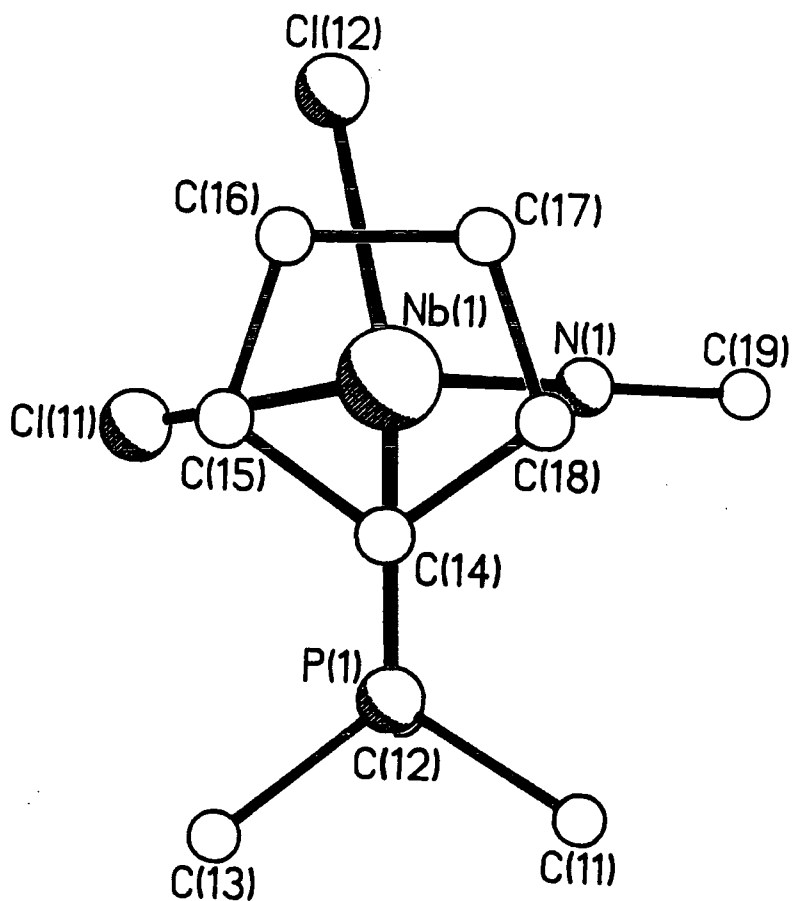


Figure 2.11, View of (14) down the ring centroid-niobium vector.

| | | | |
|---------------|-----------|----------------|----------|
| Nb(1) - Cl(1) | 2.499(2) | Nb(1) - Cl(12) | 2.494(2) |
| Nb(1) - P(1) | 2.604(2) | Nb(1) - C(14) | 2.440(5) |
| Nb(1) - C(15) | 2.504(4) | Nb(1) - C(16) | 2.472(4) |
| Nb(1) - C(17) | 2.399(5) | Nb(1) - C(18) | 2.397(5) |
| Nb(1) - N(1) | 1.772(4) | P(1) - C(11) | 1.814(7) |
| P(1) - C(12) | 1.804(5) | P(1) - C(13) | 1.803(6) |
| C(14) - C(15) | 1.403(8) | C(14) - C(18) | 1.380(8) |
| C(15) - C(16) | 1.358(8) | C(16) - C(17) | 1.403(8) |
| C(17) - C(18) | 1.381(10) | N(1) - C(19) | 1.404(7) |

| | | | |
|-------------------------|----------|------------------------|----------|
| Cl(11) - Nb(1) - Cl(12) | 80.1(1) | Cl(11) - Nb(1) - P(1) | 75.6(1) |
| Cl(12) - Nb(1) - P(1) | 149.0(1) | Cl(11) - Nb(1) - C(14) | 112.2(1) |
| Cl(12) - Nb(1) - C(14) | 134.6(1) | P(1) - Nb(1) - C(14) | 73.6(1) |
| Cl(11) - Nb(1) - C(15) | 92.7(1) | Cl(12) - Nb(1) - C(15) | 107.2(1) |
| P(1) - Nb(1) - C(15) | 93.1(1) | C(14) - Nb(1) - C(15) | 32.9(2) |
| Cl(11) - Nb(1) - C(16) | 105.1(2) | Cl(12) - Nb(1) - C(16) | 80.6(1) |
| P(1) - Nb(1) - C(16) | 124.1(1) | C(14) - Nb(1) - C(16) | 54.0(2) |
| C(15) - Nb(1) - C(16) | 31.7(2) | Cl(11) - Nb(1) - C(17) | 138.3(1) |
| Cl(12) - Nb(1) - C(17) | 86.0(2) | P(1) - Nb(1) - C(17) | 125.0(2) |
| C(14) - Nb(1) - C(17) | 55.0(2) | C(15) - Nb(1) - C(17) | 54.3(2) |
| C(16) - Nb(1) - C(17) | 33.4(2) | Cl(11) - Nb(1) - C(18) | 144.9(1) |
| Cl(12) - Nb(1) - C(18) | 118.7(2) | P(1) - Nb(1) - C(18) | 92.2(2) |
| C(14) - Nb(1) - C(18) | 33.1(2) | C(15) - Nb(1) - C(18) | 54.6(2) |
| C(16) - Nb(1) - C(18) | 54.9(2) | C(17) - Nb(1) - C(18) | 33.5(2) |
| Cl(11) - Nb(1) - N(1) | 119.3(1) | Cl(12) - Nb(1) - N(1) | 92.8(2) |
| P(1) - Nb(1) - N(1) | 82.7(1) | C(14) - Nb(1) - N(1) | 114.5(2) |
| C(15) - Nb(1) - N(1) | 145.0(2) | C(16) - Nb(1) - N(1) | 133.3(2) |
| C(17) - Nb(1) - N(1) | 100.4(2) | C(18) - Nb(1) - N(1) | 90.7(2) |
| Nb(1) - P(1) - C(11) | 114.4(2) | Nb(1) - P(1) - C(12) | 110.8(2) |
| C(11) - P(1) - C(12) | 103.0(3) | Nb(1) - P(1) - C(13) | 119.3(2) |
| C(11) - P(1) - C(13) | 103.6(3) | C(12) - P(1) - C(13) | 103.9(3) |
| Nb(1) - C(14) - C(15) | 76.1(3) | Nb(1) - C(14) - C(18) | 71.7(3) |
| C(15) - C(14) - C(18) | 108.0(5) | Nb(1) - C(15) - C(14) | 71.0(2) |
| Nb(1) - C(15) - C(16) | 72.9(3) | C(14) - C(15) - C(16) | 107.9(5) |
| Nb(1) - C(16) - C(15) | 75.5(3) | Nb(1) - C(16) - C(17) | 70.4(3) |
| C(15) - C(16) - C(17) | 108.5(5) | Nb(1) - C(17) - C(16) | 76.2(3) |
| Nb(1) - C(17) - C(18) | 73.2(3) | C(16) - C(17) - C(18) | 107.6(5) |
| Nb(1) - C(18) - C(14) | 75.1(3) | Nb(1) - C(18) - C(17) | 73.3(3) |
| C(14) - C(18) - C(17) | 108.0(5) | Nb(1) - N(1) - C(19) | 167.9(4) |

Table 2.6. Bond distances (Å) and angles (°) for *CpNb(NMe)Cl₂(PMe₃) (14)*.

| | CpNb(NMe)Cl₂ (2) | CpNb(NMe)Cl₂(PMe₃) (14) |
|------------------|------------------------------------|--|
| Nb-N | 1.752(2)Å | 1.772(4)Å |
| Nb-Cl | 2.335(1)Å | 2.499(7)Å, 2.494(2)Å ^a |
| N-C(1) | 1.432(3)Å | 1.404(7)Å |
| Nb-N-C(1) | 163.4(3)° | 167.9(4)° |
| Cl-Nb-Cl' | 104.7(1)° | 80.1(1)° |

^a values for *trans* and *cis* to the imido ligand respectively.

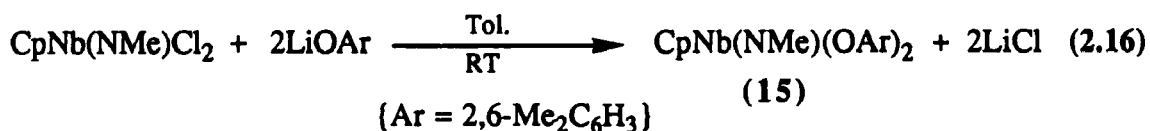
Table 2.7

There appears to be very little change in coordination of the methylimido ligand upon binding PMe₃ to the metal centre, remaining essentially a 4 electron donor. The Nb-N bond distance of 1.772(4)Å still lies within the range expected for a niobium-nitrogen triple bond, although slightly longer than that found in the base free complex. The Nb-N-C angle of 170.1° is typical of terminal sp-hybridised nitrogen¹⁶. A larger difference is seen in Nb-Cl bond lengths indicative of reduced Cl ππ-dπ metal bonding in (14).

2.7.2 Reaction of CpNb(NMe)Cl₂ with LiO-2,6-Me₂C₆H₃:

Preparation of CpNb(NMe)(O-2,6-Me₂C₆H₃)₂ (15).

Reaction of (2) with two molar equivalents of LiO-2,6-Me₂C₆H₃ in ether or toluene yields CpNb(NMe)(O-2,6-Me₂C₆H₃)₂ (15) in good yield (74%) according to Equation 2.16.



Pale yellow crystals of (15) can be grown from cold pentane. Compound (15) gives bands in the infrared spectrum characteristic of the terminal imido ligand at

1276 cm⁻¹ and 819 cm⁻¹, while absorptions at 890 cm⁻¹ and 1215 cm⁻¹ are indicative of $\nu(\text{Nb-O})$ and $\nu(\text{C-O})$ stretching vibrations respectively^{17, 30}. In the mass spectrum, the ion of highest mass (at m/z 429) corresponds to $[\text{CpNb}(\text{NMe})(\text{DMP})_2]^+$. The ¹H NMR spectrum indicates the presence of coordinated aryloxo ligands, which are equivalent at room temperature, and shows methylimido and C₅H₅ proton resonances at δ 3.30 and δ 6.16 respectively. The ¹³C NMR spectrum reveals a quartet resonance at δ 53.5 corresponding to the methylimido carbon, and the expected aryl carbon signals in the region δ 123-163. The data are therefore indicative of a monomeric terminal imido species, with a structure related to that established for compound (2), in which the chloride ligands are exchanged for OAr groups.

2.7.3 Reaction of CpNb(NMe)Cl₂ with LiO^tBu:

Preparation of CpNb(NMe)(O^tBu)₂ (16).

CpNb(NMe)Cl₂ reacts readily with two equivalents of LiO^tBu in diethylether solvent at -78°C leading to formation of a pale yellow solution. Removal of solvent affords an oil, which ¹H NMR shows to be *ca* 97% pure CpNb(NMe)(O^tBu)₂ (16) (Equation 2.17). Colourless, moisture sensitive crystals of (16) were isolated in low yield by sublimation.



Compound (16), is very soluble in aromatic hydrocarbon solvents and petroleum ether, presumably due to the presence of the highly solubilising ^tbutyl groups. Elemental analysis confirms a stoichiometry of C₁₄H₂₆NO₂Nb, and the data obtained from mass spectrometry, and infrared and NMR spectroscopies, indicate that compound (16) is a monomeric terminal imido species with a structure analogous to that of compound (15).

2.7.4 Reaction of $\text{CpNb}(\text{NMe})\text{Cl}_2$ with RMgX and MeLi ($\text{R} = \text{Me}$, $\text{CH}_2\text{CH}=\text{CH}_2$; $\text{X} = \text{Cl}, \text{Br}, \text{I}$) Reagents.

Attempted Preparation of $\text{CpNb}(\text{NMe})\text{RCl}$ and $\text{CpNb}(\text{NMe})\text{R}_2$ Species.

Reactions of (2) with alkyl Grignard reagents were investigated in an attempt to prepare coordinatively unsaturated alkyl derivatives for use as precursors to other half-sandwich imido complexes.

We envisaged that a reaction of $\text{CpNb}(\text{NMe})\text{Cl}_2$ with one or two equivalents of Grignard reagent, RMgX , would afford $\text{CpNb}(\text{NMe})\text{RCl}$ and $\text{CpNb}(\text{NMe})\text{R}_2$ species respectively. However, these reactions did not yield the expected niobium imido alkyl species, but in all cases insoluble pale brown or grey powders. Elemental analysis on these complexes, indicated the presence of a substantial percentage of magnesium, in addition to niobium halide. It is therefore believed that these products are complex niobium-magnesium adducts, presumably with halides bridging the niobium and magnesium atoms. The formation of such species would not be inconsistent with the highly electron deficient, and sterically accessible metal centre. No attempts were made to isolate these mixed metal species.

Reactions of MeLi with compound (2) also afford analytically impure insoluble pale powders, presumably for the same reasons as mentioned above.

2.8 Some Derivative Chemistry of $\text{CpNb}(\text{N}^t\text{Bu})\text{Cl}_2$ (7).

A similar series of experiments to those described in the preceding sections have been carried out on the more sterically demanding ^tbutylimido analogue (7). In particular, it was hoped that the increased steric congestion around the metal centre might prevent the formation of halide bridges to magnesium and thus allow access to alkyl derivatives.

2.8.1 The Reaction of CpNb(N^tBu)Cl₂ with Trimethylphosphine:

Preparation of CpNb(N^tBu)Cl₂(PMe₃) (17).

In a reaction analogous to that described in section 2.6.1, (7) reacted with trimethylphosphine to yield a yellow solution from which a moisture sensitive pale yellow crystalline compound (17) was extracted in high yield (89%) (Equation 2.18).

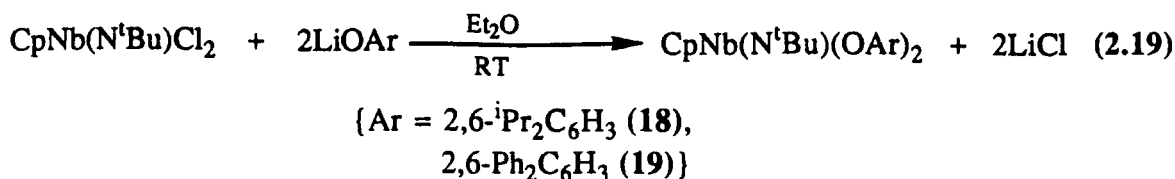


Compound (17) is soluble in aromatic and chlorocarbon solvents. The infrared spectrum reveals bands at 1238 cm⁻¹ and 805 cm⁻¹, corresponding to terminal imido stretches, slightly lower in frequency than the corresponding methylimido species (14) and the ^tbutylimido starting material. The ¹H NMR spectrum shows a resonance at δ 1.26, typical for ^tbutylimido protons^{3, 4, 31}, and a doublet at δ 1.63 attributable to PMe₃ protons coupled to the ³¹P nucleus (²J_{PH} = 9 Hz). The resonances found in the ¹³C NMR spectrum are in the usual region for ^tbutylimido species (section 2.10). (17) is thus likely to be a monomeric terminal imido 18 electron species, with a four-legged piano stool geometry, analogous to the structurally characterised methylimido species (14).

2.8.2 Reaction of CpNb(N^tBu)Cl₂ with LiOAr:

Preparation of CpNb(N^tBu)(OAr)₂ (Ar = 2,6-ⁱPr₂C₆H₃ (18), 2,6-Ph₂C₆H₃ (19)).

The reaction of CpNb(N^tBu)Cl₂ with two molar equivalents of LiOAr, in cold diethylether affords yellow solutions, from which CpNb(N^tBu)(OAr)₂ can be isolated in high yield, according to Equation 2.19.



CpNb(N^tBu)(O-2,6-ⁱPr₂C₆H₃)₂ (**18**) and CpNb(N^tBu)(O-Ph₂C₆H₃)₂ (**19**) are readily recrystallised from cold pentane. These yellow moisture sensitive crystals are soluble in aromatic and chlorocarbon solvents, although compound (**18**) shows considerably greater solubility in pentane. Both compounds have been fully characterised by elemental analysis, infrared and NMR spectroscopies and mass spectrometry. In particular, the mass spectrum of (**18**) shows a parent ion peak at *m/z* 583. The infrared spectra are complex, but show bands in the expected terminal imido region (see chapter 6, section 6.2). ¹H NMR spectra reveal resonances attributable to ^tbutyl groups at δ 0.87 and 0.64 respectively, and signals corresponding to the respective aryl groups.

2.8.3 Reaction of CpNb(N^tBu)Cl₂ with LiO^tBu:

Preparation of CpNb(N^tBu)(O^tBu)₂ (20).

Compound (**7**) reacts with LiO^tBu in an analogous manner to CpNb(NMe)Cl₂, but in this case we were unable to isolate a solid product. The brown oil, however, appears remarkably pure (>95% by ¹H NMR). Comparison of the 400 MHz ¹H and 100 MHz ¹³C data, with those of compound (**20**) suggest a related monomeric terminal imido structure.

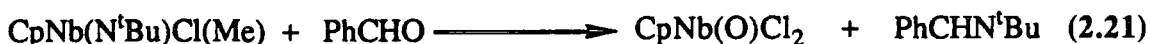
2.8.4 Reaction of CpNb(N^tBu)Cl₂ with Benzaldehyde :

Attempted Preparation of CpNb(O)Cl₂.

In many cases, early transition metal imido species have been shown to react with aldehydes and ketones to form the metal oxo species and corresponding unsaturated imine (Equation 2.20)³²⁻³⁴.



We envisaged that the reaction between CpNb(N^tBu)Cl₂ and benzaldehyde may provide a convenient route to the particularly elusive half-sandwich oxohalide CpNb(O)Cl₂ (Equation 2.21).



However, the reaction of CpNb(N^tBu)Cl₂ with benzaldehyde in toluene or methylene chloride yields insoluble yellow powders of apparently differing composition depending on the reaction conditions. The insolubility of these products suggests that they are polynuclear species, possibly obtained after further reaction or decomposition of the initially formed oxo product. Previously, it has been shown that Cp*Ta(O)Cl₂³⁵ is unstable at room temperature in chlorocarbons decomposing to afford a polynuclear complex²⁰.

2.8.5 Reaction of CpNb(N^tBu)Cl₂ with MeMgCl:

Preparation of CpNb(N^tBu)Cl(Me) (21).

Although (7) reacts in a similar way to CpNb(NMe)Cl₂ with MeMgI, that is to form insoluble niobium-magnesium products, the same is not true for its reaction with MeMgCl. The addition of one molar equivalent of MeMgCl to CpNb(N^tBu)Cl₂ in

diethylether at -78°C , affords an orange solution of $\text{CpNb}(\text{N}^t\text{Bu})\text{Cl}(\text{Me})$ and MgCl_2 precipitate. (Equation 2.22)



Compound (21) can be isolated as large orange cubes upon prolonged cooling to -20°C of a pentane solution. These moisture sensitive crystals are soluble in aromatic and chlorocarbon solvents, and have a melting point of $54\text{-}55^{\circ}\text{C}$. Elemental analysis confirms a stoichiometry consistent with the monomethyl complex. Terminal imido bands are found at 1248cm^{-1} and 828cm^{-1} in the infrared spectrum and only a weak band is seen for $\nu(\text{Nb}-\text{Cl})$ at 303cm^{-1} . The $250\text{ MHz } ^1\text{H NMR}$ spectrum (C_6D_6) reveals the expected three singlet resonances at $\delta 1.13$, $\delta 1.15$ and $\delta 5.69$, corresponding to t butyl, methyl and cyclopentadienyl protons respectively. $^{13}\text{C NMR}$ spectra reveal expected singlet for the t butyl groups, but the methyl carbon is seen only as a broadened singlet at $\delta 66.7$ ($\Delta^{1/2}$ *ca.* 20Hz) This broadening can be attributed to coupling to the ^{93}Nb nucleus ($I = 9/2$, 100% , natural abundance), combined with partial 'decoupling' of the ^{93}Nb nucleus due to quadrupolar relaxation, an effect observed on carbons attached to niobium species such as $\text{Cp}_2\text{NbH}(\text{C}_2\text{H}_4)^{36}$. The mass spectrum reveals an envelope at $m/z 279$ (^{35}Cl) corresponding to the parent ion.

$\text{CpNb}(\text{N}^t\text{Bu})\text{Cl}_2$ reacts with two equivalents of MeMgCl , to give an intractable oil, analysis of which was inconsistent with $\text{CpNb}(\text{N}^t\text{Bu})\text{Me}_2$. Thus, to date, the dimethyl derivative has not proved accessible for the t butyl imido species.

2.8.5.1 The Molecular Structure of $\text{CpNb}(\text{N}^t\text{Bu})\text{Cl}(\text{Me})$ (21).

A saturated pentane solution of (21) was cooled at -20°C over several days to afford orange crystals. A crystal of suitable size was sealed in a Lindemann capillary and the X-ray crystal structure determination carried out by Dr W. Clegg at the

University of Newcastle-upon-Tyne. The structural parameters are collected in Appendix 1. The molecular structure is illustrated in Figure 2.12. Selected bond angles and lengths are collected in Table 2.8. The structure shows the species to be a monomeric, three-legged piano stool molecule with only minor changes in the ring, imido and chloride ligand parameters compared with the ^tbutyl starting material (7). Selected bond lengths and angles, along with the ring parameters of (21) and dichloride starting material are compared in Table 2.9.

| | CpNb(N^tBu)Cl(Me) (21) | CpNb(N^tBu)Cl₂^a (7) |
|----------|---|--|
| d(Nb-N) | 1.740(4)Å | 1.744(3)Å, 1.752(3)Å |
| d(Nb-Cl) | 2.365(2)Å | 2.354Å(2) (average) |
| ∠ Nb-N-C | 169.2(3)° | 172.5(3)° |
| ΔM | 0.113Å | 0.144Å, 0.140Å |
| ΔR | 0.125Å | 0.123Å, 0.060Å |
| ΔX | 0.082Å | 0.143Å, 0.083Å |

^a Two independent molecules within the unit cell

Table 2.9

Interestingly, the Nb-Cl bond length in (21) is slightly longer than the average found in (7). The opposite might be expected, since stabilisation of the electron deficient Nb metal centre through the pπ-dπ interaction is only possible through one chloride in the monomethyl complex.

2.8.5.2 Reactivity Studies on CpNb(N^tBu)Cl(Me):

Preparation of CpNb(N^tBu)Cl(Me)PMe₃ (22):

A series of reactions of CpNb(N^tBu)Cl(Me), were carried out on a small scale. Treatment of (21) with (1) C₂H₄, (2) PhC≡CPh and (3) CO, somewhat surprisingly, failed to afford adducts or insertion products even at elevated temperature.

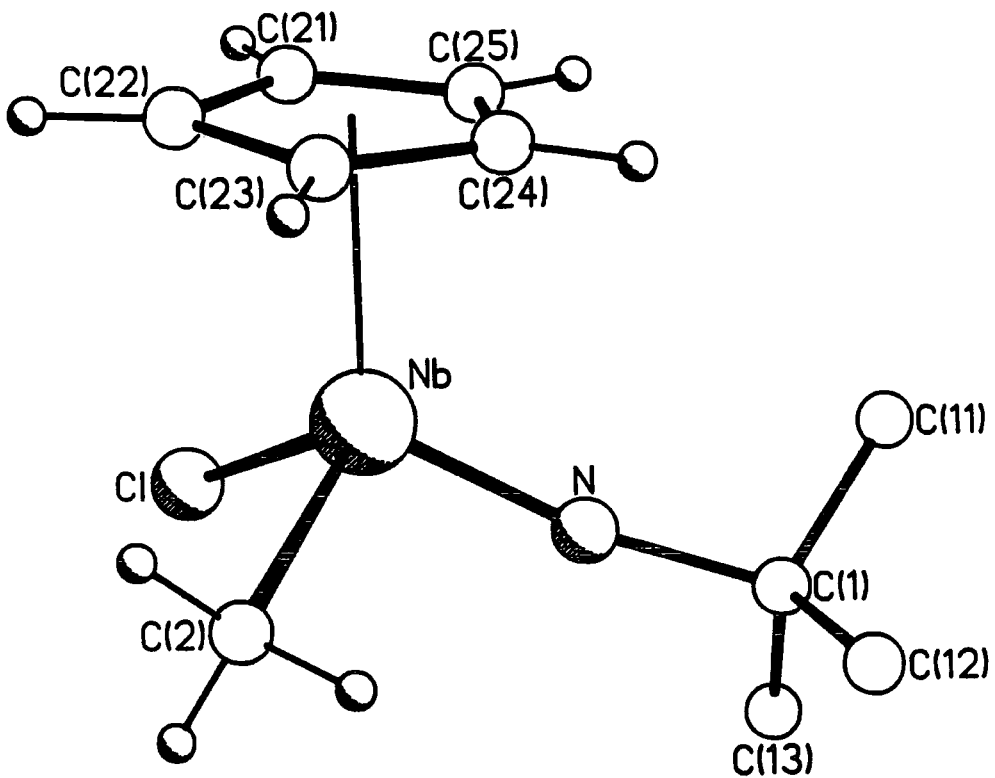
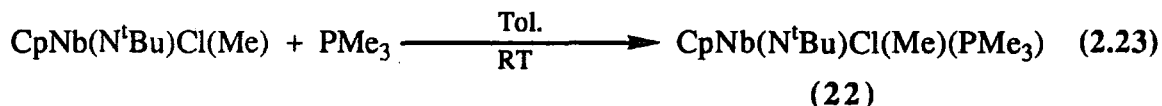


Figure 2.12, The molecular structure of $\text{CpNb}(\text{N}^t\text{Bu})\text{Cl}(\text{Me})$ (21).

| | | | |
|-----------------------|-----------|-----------------------|-----------|
| Nb - Cl | 2.365(2) | Nb - N | 1.740(4) |
| Nb - C(2) | 2.193(5) | Nb - C(21) | 2.473(6) |
| Nb - C(22) | 2.497(11) | Nb - C(23) | 2.444(9) |
| Nb - C(24) | 2.384(6) | Nb - C(25) | 2.386(6) |
| N - C(1) | 1.456(6) | C(1) - C(11) | 1.508(14) |
| C(1) - C(12) | 1.454(22) | C(1) - C(13) | 1.448(25) |
| C(21) - C(22) | 1.380(15) | C(22) - C(23) | 1.444(12) |
| C(21) - C(25) | 1.334(9) | C(23) - C(24) | 1.319(10) |
| C(24) - C(25) | 1.326(9) | | |
| Cl - Nb - N | 107.1(1) | Cl - Nb - C(2) | 104.3(2) |
| N - Nb - C(2) | 98.1(2) | Cl - Nb - C(21) | 89.7(2) |
| N - Nb - C(21) | 127.1(2) | C(2) - Nb - C(21) | 126.4(3) |
| Cl - Nb - C(22) | 99.1(2) | N - Nb - C(22) | 147.2(2) |
| C(2) - Nb - C(22) | 94.2(3) | C(21) - Nb - C(22) | 32.3(3) |
| Cl - Nb - C(23) | 132.5(2) | N - Nb - C(23) | 119.3(2) |
| C(2) - Nb - C(23) | 80.2(2) | C(21) - Nb - C(23) | 54.7(3) |
| C(22) - Nb - C(23) | 34.0(3) | Cl - Nb - C(24) | 142.4(1) |
| N - Nb - C(24) | 94.2(2) | C(2) - Nb - C(24) | 102.8(2) |
| C(21) - Nb - C(24) | 53.1(2) | C(22) - Nb - C(24) | 53.4(2) |
| C(23) - Nb - C(24) | 31.7(2) | Cl - Nb - C(25) | 112.4(2) |
| N - Nb - C(25) | 97.7(2) | C(2) - Nb - C(25) | 133.3(2) |
| C(21) - Nb - C(25) | 31.8(2) | C(22) - Nb - C(25) | 53.2(2) |
| C(23) - Nb - C(25) | 53.9(2) | C(24) - Nb - C(25) | 32.3(2) |
| Nb - N - C(1) | 169.2(3) | N - C(1) - C(11) | 108.6(7) |
| N - C(1) - C(12) | 107.4(11) | C(11) - C(1) - C(12) | 109.8(14) |
| N - C(1) - C(13) | 107.2(8) | C(11) - C(1) - C(13) | 107.5(11) |
| C(12) - C(1) - C(13) | 116.2(14) | Nb - C(21) - C(22) | 74.8(5) |
| Nb - C(21) - C(25) | 70.5(4) | C(22) - C(21) - C(25) | 107.5(7) |
| Nb - C(22) - C(21) | 72.9(6) | Nb - C(22) - C(23) | 71.0(5) |
| C(21) - C(22) - C(23) | 106.3(7) | Nb - C(23) - C(22) | 75.0(6) |
| Nb - C(23) - C(24) | 71.6(5) | C(22) - C(23) - C(24) | 105.0(7) |
| Nb - C(24) - C(23) | 76.7(4) | Nb - C(24) - C(25) | 73.9(4) |
| C(23) - C(24) - C(25) | 111.7(6) | Nb - C(25) - C(21) | 77.7(4) |
| Nb - C(25) - C(24) | 73.8(4) | C(21) - C(25) - C(24) | 109.6(6) |

Table 2.8, Bond distances (\AA) and angles ($^\circ$) for $\text{CpNb}(\text{N}^i\text{Bu})\text{Cl}(\text{Me})$ (21).

However the reaction of $\text{CpNb}(\text{N}^t\text{Bu})\text{Cl}(\text{Me})$ with trimethylphosphine yields a yellow solution, from which $\text{CpNb}(\text{N}^t\text{Bu})\text{Cl}(\text{Me})\text{PMe}_3$ can be isolated (Equation 2.23).



Compound (22) is soluble in chlorocarbon solvents and has limited solubility in aromatic hydrocarbon solvents. Characterisation of (22) was provided by elemental analysis, and infrared and NMR spectroscopies. In the ^1H NMR spectrum the methyl proton resonance is found at δ 0.67, considerably upfield from the base free starting material. A doublet at δ 1.42 ($^2J_{\text{PH}} = 13.4\text{Hz}$) indicates the presence of strongly bound PMe_3 , which is confirmed by a doublet resonance observed in the ^{13}C $\{^1\text{H}\}$ NMR spectrum at δ 16.23 ($J_{\text{CP}} = 26\text{Hz}$).

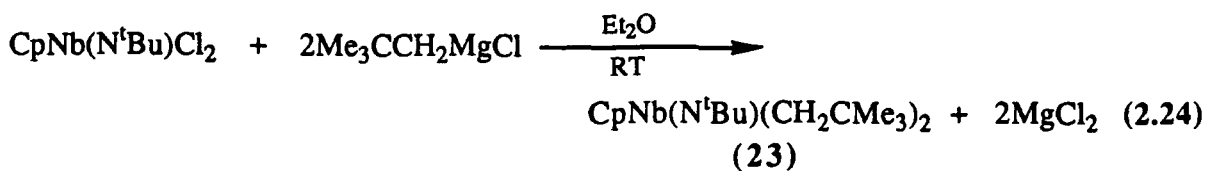
(22) is most likely to possess a four-legged piano stool geometry analogous to that found in structurally characterised $\text{CpNb}(\text{NMe})\text{Cl}_2(\text{PMe}_3)$ (14).

2.8.6 Reaction of $\text{CpNb}(\text{N}^t\text{Bu})\text{Cl}_2$ with $\text{Me}_3\text{CCH}_2\text{MgCl}$:

Preparation of $\text{CpNb}(\text{N}^t\text{Bu})(\text{CH}_2\text{CMe}_3)_2$ (23).

The reaction of $\text{CpNb}(\text{N}^t\text{Bu})\text{Cl}_2$ with one molar equivalent of $\text{Me}_3\text{CCH}_2\text{MgCl}$ in diethylether, yields a pale brown oil. Although this oil is impure (by ^1H NMR) there is evidence for the coordination of at least one alkyl ligand.

A much cleaner reaction takes place with two equivalents of $\text{Me}_3\text{CCH}_2\text{MgCl}$, affording an orange solution from which pale yellow crystals of $\text{CpNb}(\text{N}^t\text{Bu})(\text{CH}_2\text{CMe}_3)_2$ (23) can be isolated. This reaction is envisaged to occur according to Equation 2.24



Compound (23), is soluble in aromatic, chlorocarbon and pentane solvents. Characterisation is provided by elemental analysis and mass spectrometry, and infrared and NMR spectroscopies. In particular, the 400Hz ^1H NMR spectrum reveals a singlet resonance at δ 1.22, and a singlet at δ 1.32, which can be attributed to equivalent methyl groups of the neopentyl ligands and t butyl hydrogens respectively, and doublets at δ -0.20 and δ 2.31 (ratio 1:1, $^3J_{\text{HH}} = 11$ Hz) indicating the presence of diastereotopic α -CH₂ protons. The infrared spectrum reveals bands at 1242cm⁻¹ and 810 cm⁻¹ typical of the terminal imido ligand.

There is strong spectroscopic evidence for the presence of α -agostic interactions in (23). The infrared spectrum recorded on a thin film of (23), shows a broad weak band at 2750cm⁻¹ possibly attributable to a weakened $\nu(\text{C-H})$ vibration³⁷. The quite different chemical shifts of the doublets associated with the methylene protons are believed to arise due to averaged H_{up} (towards the Cp ring) and H_{down} (away from the Cp ring) α environments, although it has not yet proved possible to establish which is which. The ^{13}C NMR spectrum gives a broadened signal at δ 81.2 ($\Delta^{1/2}$ *ca.* 28Hz) due to the equivalent methylene carbons of the neopentyl groups; the resonance is broadened due to the quadrupolar ^{93}Nb nucleus³⁶. Consequently, the $^1J_{\text{CH}}$ coupling constant of 112Hz could only be obtained from the natural abundance of ^{13}C satellites in the ^1H NMR spectrum. This value is reasonable for an average of a terminal C-H bond (typically $^1J_{\text{CH}} = 120\text{-}130\text{Hz}$)³⁸ and a bridging agostic interaction (typically $^1J_{\text{CH}} = 70\text{-}100\text{Hz}$)^{37,38}. Low temperature ^1H NMR studies (CDCl₃, 0 to -50°C) on compound (23), failed to "freeze out" the agostic structure, but the methylene proton resonances shifted upfield (*ca.* 0.1ppm), relative to the Cp and t butylimido signals, providing further support for agostic interactions³⁷. Further spectroscopic evidence has been obtained by NMR analysis of the deuterated species (see following section).

Confirmation of these unusual interactions, via a crystal structure determination, has proved difficult due to its low melting point (31-32°C). However, the X-ray structure of closely related $\text{CpNb}(\text{N}-2,6\text{-}i\text{Pr}_2\text{C}_6\text{H}_3)(\text{CH}_2\text{CMe}_3)_2$ ³⁹ shows Nb-C-H angles in both neopentyl ligands to be only 89.4° and short Nb-H distances at 2.31 and 2.41 Å, consistent with two α -agostic C-H interactions (Figure 2.13).

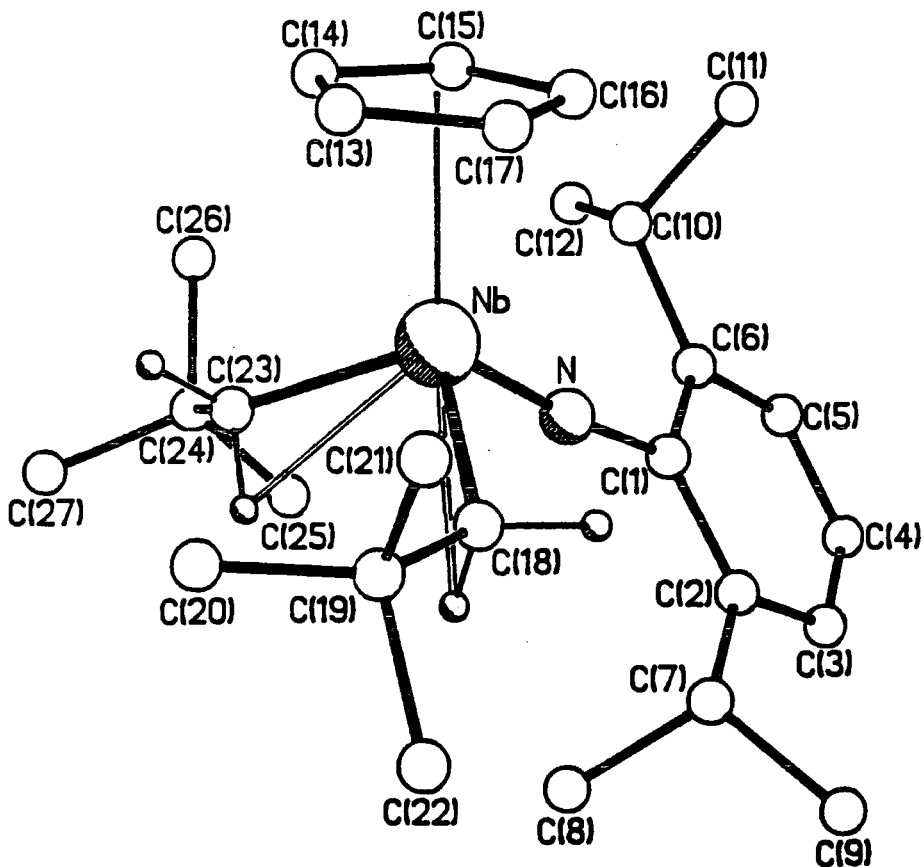


Figure 2.13, The molecular structure of $\text{CpNb}(\text{N}-2,6\text{-}i\text{Pr}_2\text{C}_6\text{H}_3)(\text{CH}_2\text{CMe}_3)_2$.

On standing, $\text{CpNb}(\text{N}^t\text{Bu})(\text{CH}_2\text{CMe}_3)_2$ decomposes to give neopentane (^1H NMR δ 0.90), and an unidentified paramagnetic niobium species, which is an intense brown-black colour, in solution. This decomposition is accelerated upon heating.

The liberation of neopentane suggests that decomposition may occur via a neopentylidene species, although none could be observed by NMR. Schrock et al. have found that niobium alkylidenes in general are unstable⁴⁰, and this may account for further decomposition and the presence of additional resonances in the ^1H NMR spectrum. The relatively facile decomposition may also be aided by the presence of the agostic interactions.

2.8.6.1 Evidence for α -Agostic Interactions in

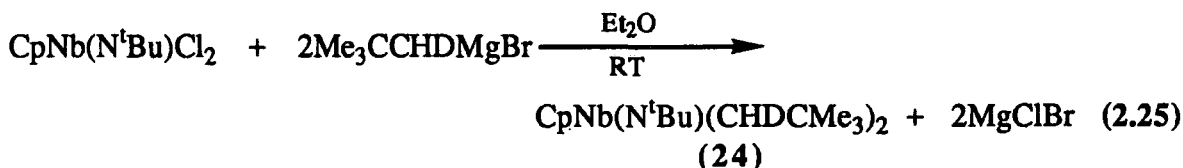


Preparation and Spectroscopic Characterisation of



A useful NMR method for identifying agostic C-H systems is that of "isotopic perturbation of resonance" first used by Shapley⁴¹. For the osmium methyl compound $\text{Os}_3(\text{CO})_{10}(\text{Me})\text{H}$, he noted that the ^1H chemical shift and J_{CH} values decrease in the order $\delta \text{CH}_3 > \delta \text{CH}_2\text{D} > \delta \text{CHD}_2$. This phenomenon arises because of the thermodynamic preference for deuterium rather than hydrogen to occupy a terminal position. The reason for this preference is the smaller zero point energy difference between H and D in C-H-M and C-D-M bonds relative to the differences in "terminal" C-H and C-D bonds.

In order to verify the presence of α -agostic interactions in solutions of $\text{CpNb}(\text{N}^t\text{Bu})(\text{CH}_2\text{CMe}_3)_2$, its preparation was repeated using deuterated Grignard $\text{Me}_3\text{CCHDMgBr}$ provided by Mr A.D. Poole. This reaction yielded pale yellow crystals of $\text{CpNb}(\text{N}^t\text{Bu})(\text{CHDCMe}_3)_2$ (24) according to Equation 2.25.



The ^1H NMR of (24) reveals signals identical in chemical shift to those found in (23) for the C_5H_5 , CMe_3 , and CHDCMe_3 groups. For the methylene protons, however, four singlet broadened resonances of equal intensity, each integrating for *ca.*0.5 protons, are found at δ -0.30, δ -0.25, δ 2.21 and δ 2.25. These resonances are shifted upfield by 0.1-0.5 ppm relative to the protons of the per-protio complex. This is much greater than would be expected for non-agostic alkyls which would be

expected to result in shifts of only *ca.* 0.01 ppm on deuteration⁴². ¹H NMR spectra of (23) and (24) are shown in Figure 2.14 for comparison.

A rationalisation for the appearance of four deuterated species is provided by considering the possible isomers of CpNb(N^tBu)(CHDCMe₃)₂. Having introduced two deuterium atoms at the α carbon, two chiral centres have been generated. Four isomeric species are now possible; RR, SS, RS and SR. (Figure 2.15).

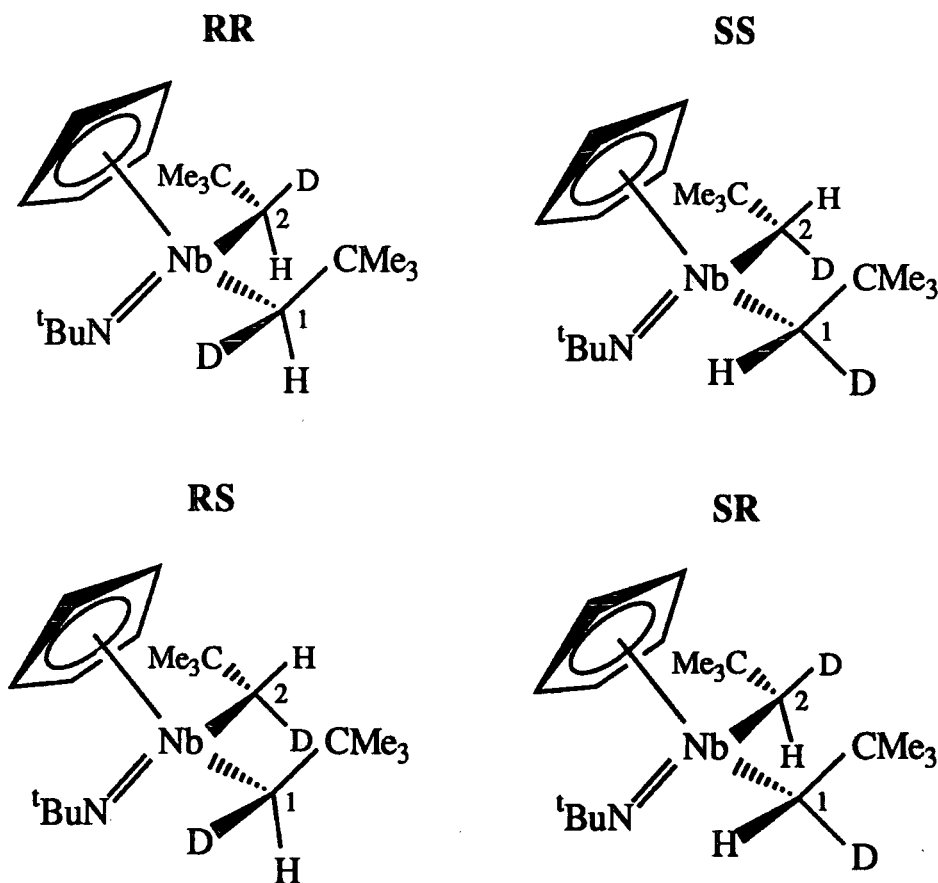


Figure 2.15, *The four isomeric forms of CpNb(N^tBu)(CHDCMe₃)₂ (24).*

RR and SS are indistinguishable by NMR but give rise to two singlet resonances, due to the H_{up} and H_{down} environments. Similarly RS and SR are indistinguishable by NMR, again giving rise to an H_{up} and an H_{down} singlet resonance. From the crystal structure of CpNb(N-2,6-ⁱPr₂C₆H₃)Np₂, the ground state structure appears to be equivalent to the SS isomer of compound (24)³⁷.

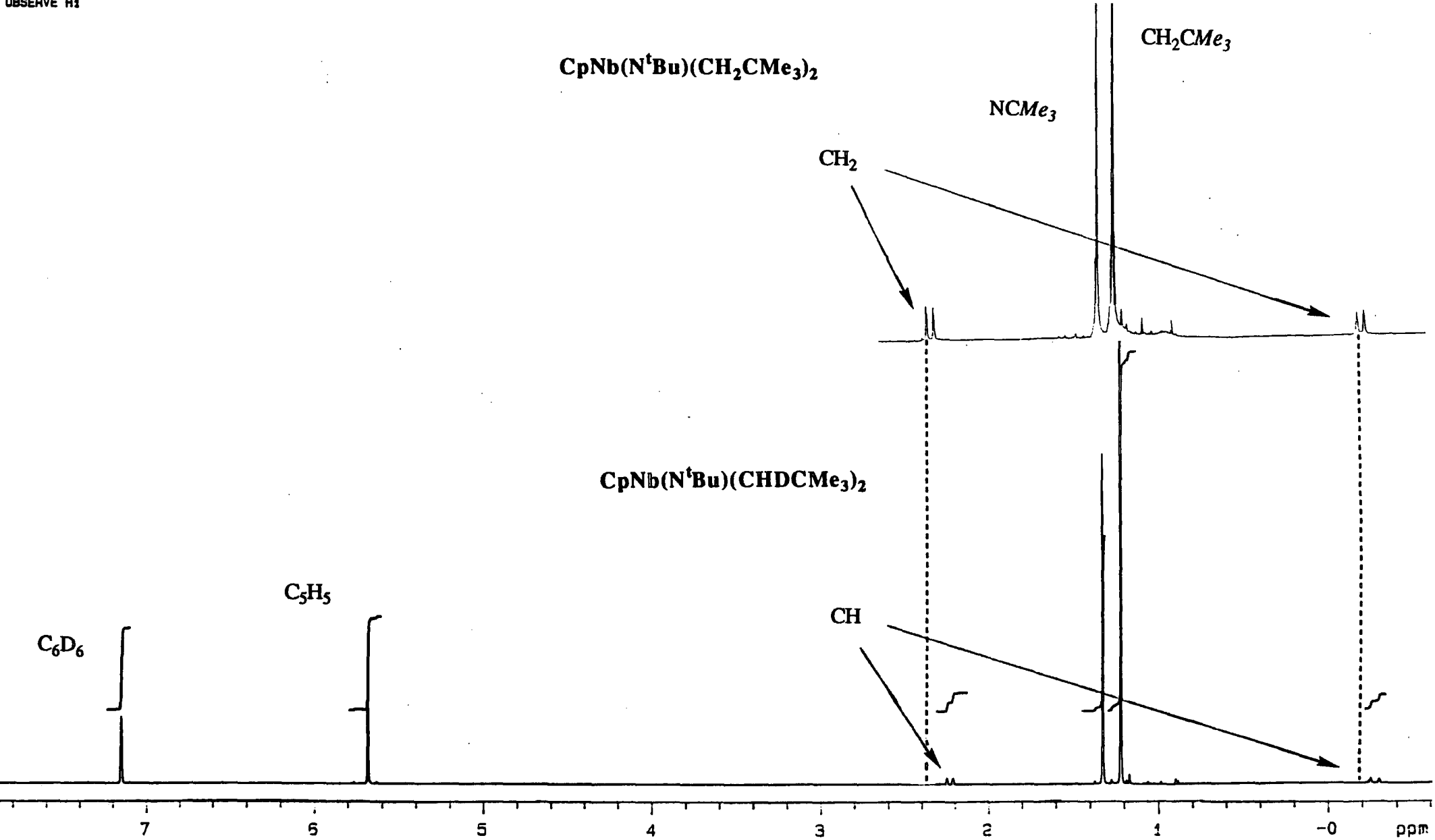


Figure 2.14, A comparison of the ^1H NMR spectra of $\text{CpNb}(\text{N}^t\text{Bu})(\text{CH}_2\text{CMe}_3)_2$ (23) and $\text{CpNb}(\text{N}^t\text{Bu})(\text{CHDCMe}_3)_2$ (24).

The infrared spectrum of (24), shows three weak bands at 2695cm^{-1} , 2585cm^{-1} and 2495cm^{-1} . One or more of these bands may be attributable to $\nu(\text{C-D})$ stretches of the agostic complex. However, infrared, in general, is not the most reliable diagnostic technique for establishing the presence of agostic interactions.

2.9. Other Reactions of $\text{CpNb}(\text{N}^t\text{Bu})\text{Cl}_2$ (7).

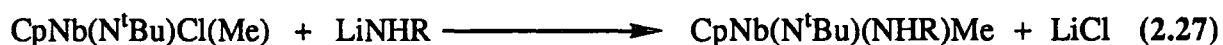
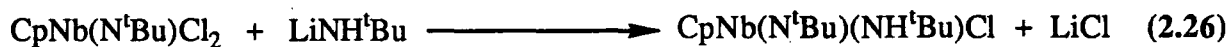
Further investigations into the reactivity of $\text{CpNb}(\text{N}^t\text{Bu})\text{Cl}_2$ (7) were performed on an NMR scale. Treatment of (7) with (1) C_2H_4 , (2) $\text{PhC}\equiv\text{CPh}$ and (3) CO , failed to afford adducts or insertion products even after prologed heating at temperatures up to 160°C . This is less surprising for (7) compared with the mono-alkyl species (21), since (7) is a d^0 compound with ligands that are relatively inert and therefore would not be expected to bind or undergo substitution with π -acidic ligands. Of more interest is the apparent inert nature of the alkylimido group in this coordinatively unsaturated complex.

2.10 Attempted preparation of a Half-sandwich *bis*-Imido species of Formula $(\text{CpNb}(\text{NR})_2)$

Half-sandwich dioxides and diimides of the Group 5 metals still remain to be prepared. Due to the propensity for oxo ligands to bridge early transition metal centres, the diimido species was envisaged to be a more viable target, and if accessible would allow the reactivity of *cis*-multiply bonded imido units to be explored in half-sandwich systems.

2.10.1 Synthetic Strategy

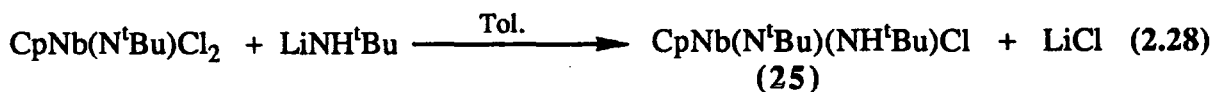
Monoalkylamides (LiNHR) have been shown to react with half-sandwich tantalum alkyl halide species to form corresponding imido complexes by elimination of methane (Equation 2.2)². We envisaged that the reaction of LiNHR with CpNb(N^tBu)Cl₂ (2), or CpNb(N^tBu)Cl(Me) (21), might produce a precursor (Equation 2.26 and 2.27) which subsequently could eliminate HCl or methane respectively, to give the 'bis-imido' species.



2.10.2 Reaction of CpNb(N^tBu)Cl₂ with LiNH^tBu:

Preparation of CpNb(N^tBu)(NH^tBu)Cl (25).

The reaction CpNb(N^tBu)Cl₂ with LiNH^tBu proceeds rapidly in methylene chloride to yield an orange solution. The product isolated from this solution is the amidoimide complex CpNb(N^tBu)(NH^tBu)Cl (25) (Equation 2.28)



Compound (25), can be isolated in low yield, as a pale brown powder, soluble in chlorocarbons, aromatic hydrocarbons and pentane solvents. Elemental analysis confirms the stoichiometry of C₁₃H₂₄N₂ClNb. The infrared spectrum has notable bands at 3292cm⁻¹ corresponding to the ν(N-H) stretch, and at 805cm⁻¹ and 1250cm⁻¹ due to the terminal ^tbutyl imido ligand. The 400MHz ¹H NMR spectrum confirms the presence of an imido and amido ligand ^tBu groups with singlet resonances at δ 1.25 and δ 1.18, and a broadened signal at δ 7.6 due to the NH proton.

Clearly, elimination of HCl from (25) would lead to the formation of the required *bis-imido* species. However, heating a sample of CpNb(N^tBu)(NH^tBu)Cl in C₆D₆ failed to eliminate HCl even at temperatures of up to 160°C, only affording slight decomposition with the formation of several new Cp signals. Addition of base, in the form of Et₃N or 2,6-lutidine, failed to catalyse this elimination, with similar decomposition again occurring at high temperature.

2.10.3 Reaction of CpNb(N^tBu)Cl(Me) with LiNHR:

Preparation of CpNb(N^tBu)(NHR)Me

(R = ^tBu, (26) 2,6-ⁱPr₂C₆H₃ (27)).

Having failed to obtain CpNb(N^tBu)₂ by elimination of HCl, CpNb(N^tBu)Cl(Me) was reacted with LiNH^tBu, in the hope of forming CpNb(N^tBu)₂ via the elimination of methane.

The reaction of CpNb(N^tBu)Cl(Me) with LiNH^tBu in toluene gave the intermediate species CpNb(N^tBu)(NH^tBu)Me (26). This compound can be isolated as pale yellow crystals from cold pentane, but isolation in high yield is difficult due to its low melting point, 21-22°C. These difficulties led us to repeat the reaction with the less solubilising monoarylamide, LiNH(-2,6-ⁱPr₂C₆H₃). Indeed, the reaction yields a yellow product which can be isolated in crystalline form in high yield, and possesses a higher melting point of 154-155°C. These reactions are envisaged to occur according to Equation 2.29



{R = ^tBu (26), 2,6-ⁱPr₂C₆H₃ (27)}

Compounds (26) and (27) have been fully characterised by elemental analysis, mass spectrometry and infrared and NMR spectroscopies.

Infrared spectra show $\nu(\text{N-H})$ vibrations at 3300 cm^{-1} and 3288 cm^{-1} respectively. In the ^1H NMR spectra the methyl protons are located at δ 0.58 and δ 0.75 respectively, slightly downfield from the related $\text{Cp}^*\text{Ta}(\text{NR})\text{Me}_2$ species (δ 0.13-0.19)³, but upfield from the monomethyl starting material (δ 1.15). The NH proton is seen in compound (26) as a broad singlet at δ 6.72 due to coupling with ^{15}N (spin 1). This proton resonance has not been located in (27), and is probably obscured by aromatic proton resonances in the region δ 6.96-7.10.

Heating chloroform or benzene solutions of (26) and (27) failed to eliminate methane, even up to a temperature of 160°C . Prolonged heating led to decomposition, and a number of unidentified products. Addition of base, triethylamine or 2,6-lutidine, again failed to catalyse the elimination of methane, even at elevated temperatures. The stability of (24) and (25) to elimination methane seems surprising. One possible explanation is the absence of a suitable empty metal orbital to facilitate transfer of the hydrogen from the nitrogen to the methyl carbon.

2.11 NMR ^{13}C Chemical Shifts of Half-Sandwich Imido Species.

It has been suggested that the difference between chemical shifts for the α and β carbon atoms in t butylimido species, $\Delta\delta$, may be a suitable probe of the electronic nature of the imido ligand. A series of structurally diverse d^0 t butylimido α - and β -carbon shifts have been examined by Nugent et al. leading to the conclusion that decreasing electron density on the imido nitrogen atoms results in a downfield shift of the α -carbon resonance and an upfield shift in β -carbon resonance⁴³. The $\Delta\delta$ values have some predictive value for the reaction chemistry of imido complexes. For example, imido ligands where $\Delta\delta < 50\text{ppm}$ react metathetically with benzaldehyde to afford the corresponding oxo complex; imido ligands where $\Delta\delta > 50$ do not undergo this reaction⁴⁴.

The availability of a range of d^0 niobium cyclopentadienyl ^tbutylimido species prepared in our studies (Scheme 2.2, section 2.11) presented an opportunity to see if there is any correlation between ¹³C chemical shifts for changes in ligands on the same metal centre.

The α - and β -carbon shifts of cyclopentadienyl ^tbutylimido species are collected in Table 2.10.

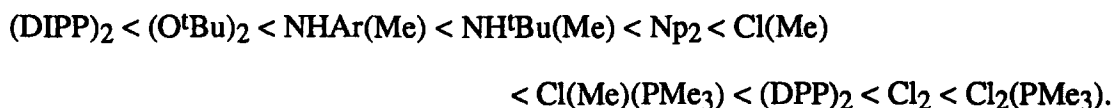
| Complex ^a | δ , C(α) ppm | δ , C(β) ppm | $\Delta\delta$ |
|--|------------------------------|-----------------------------|----------------|
| CpNb(N ^t Bu)(DIPP) ₂ (18) ^b | 60.0 | 31.2 | 28.8 |
| CpNb(N ^t Bu)(O ^t Bu) ₂ (20) | 64.5 | 32.6 | 31.9 |
| CpNb(N ^t Bu)(NHAr)Me (27) ^c | 65.3 | 33.4 | 32.0 |
| CpNb(N ^t Bu)(NH ^t Bu)Me (26) | 65.5 | 32.9 | 32.6 |
| CpNb(N ^t Bu)(Np) ₂ (23) ^d | 65.6 | 32.8 | 32.8 |
| CpNb(N ^t Bu)Cl(Me) (21) | 65.1 | 31.3 | 33.8 |
| CpNb(N ^t Bu)(NH ^t Bu)Cl (25) | 67.4 | 33.5 | 33.9 |
| CpNb(N ^t Bu)Cl(Me)(PMe ₃) (22) ^f | 66.0 | 31.0 | 35.0 |
| CpNb(N ^t Bu)(DPP) ₂ (19) ^e | 67.9 | 31.3 | 36.6 |
| CpNb(N ^t Bu)Cl ₂ (7) | 70.0 | 30.4 | 39.6 |
| CpNb(N ^t Bu)Cl ₂ (PMe ₃) (17) | 71.4 | 30.8 | 40.6 |

^a NMR spectra recorded in C₆D₆, at 100 MHz unless stated otherwise. ^b DIPP = 2,6-Diisopropylphenoxide. ^c Ar = 2,6-ⁱPr₂C₆H₃. ^d Np = Neopentyl (CH₂CMe₃). ^e DPP = 2,6-Diphenylphenoxide. ^f Spectrum taken in CDCl₃.

Table 2.10

The $\Delta\delta$ values lie between 28 and 41, which is within the range previously recorded for imido species, (55 in (Me₃SiO)₂CrO(NR) to 25 in [(Me₂N)Hf(μ -NR)]₂^{34, 45}), with the dichloro derivatives (7) and (17) lying at the high end of this range and alkoxide and phenoxide derivatives lying at the low end. The $\Delta\delta$ values are also typical of the other recorded niobium imido species, e.g 35 in (Me₃N)₃Nb(NR) and 36 in (dmc)₃Nb(NR) (dmc = dimethylcarbamate)⁴⁶.

The magnitude of $\Delta\delta$ is found to increase in the order:



Although a detailed comparison of the effects on chemical shift of such a diverse array of ancillary ligands is probably not too meaningful, some general features are worth noting. For example, the ordering: $(\text{DIPP})_2 < (\text{DPP})_2 < \text{Cl}_2$, is consistent with greater electronegativity of Cl versus the phenoxide ligand and reflects the reduced π -donor capacity of the ancillary ligand.

Interestingly, the α - ^{13}C shift for the PMe_3 adduct (17) suggests an imido nitrogen of similar electronic nature to that of the PMe_3 -free species (7). This is consistent with the findings of the X-ray structure determination which shows that PMe_3 coordination has a minimal effect on the imido Nb-N bond length and Nb-N-C bond angle. This also appears to be true for the monomethyl derivatives (21) and (22). Since $\Delta\delta$ appears to be much more sensitive to a change in transition metal centre than to a change in the ancillary ligand environment, it is unlikely to have much diagnostic value for assessing the reactivity of imido groups on identical metal centres.

It appears that the α -carbon chemical shifts in t butylimido species (17)-(27) are more sensitive to the change in ancillary ligand, varying over the range δ 71.4-60.0, compared with a variation of less than 3ppm for the β -carbon shifts. This observation led us to compare the α -methylcarbon chemical shift of compounds (2) and (14)-(16), and those of the two other known half-sandwich methylimido species. (Table 2.11).

| Compound | δ , C(α) ppm ^a |
|--|---|
| CpNb(NMe)Cl ₂ (2) | 54.3 q, ¹ J _{CH} = 119 Hz |
| CpNb(NMe)Cl ₂ (PMe ₃) (12) ^b | 54.9 q, ¹ J _{CH} = 137 Hz |
| CpNb(NMe)(DMP) ₂ (13) ^c | 54.5 ^d |
| CpNb(NMe)(O ^t Bu) ₂ (16) | 50.8 ^d |
| Cp*Ta(NMe)Me ₂ ^e | 46.4 q, ¹ J _{CH} = 133 Hz |
| Cp*Re(NMe)Cl ₂ ^f | 56.2 q |

^a ¹³C NMR spectra were recorded at 100 MHz in C₆D₆ solvent at 293°C unless otherwise noted.

Chemical shifts in δ from internal Me₄Si. ^b Sample recorded in CDCl₃.

^c DMP = 2,6-dimethylphenoxide. ^d Broad signal, coupling constant could not be determined. ^e See reference 3, spectra recorded at 34°C. ^f See reference 4.

Table 2.11

As observed for the ^tbutyl species, the α -carbon chemical shifts show a similar sensitivity to the identity of the metal in the complex, and values reflect the decrease in electron density on the imido ligand on proceeding right and upwards on the periodic table.

The values of the *ipso*-carbon chemical shifts of closely related half-sandwich dichloro arylimido species are shown in Table 2.12.

| Complex ^a | δ , C(i) ppm ^b |
|---|----------------------------------|
| CpNb(NAr)Cl ₂ (9) | 152.01 |
| Cp*Nb(NAr)Cl ₂ ^c | 148.90 |
| Cp*Ta(NAr)Cl ₂ ^d (13) | 148.26 |

^a Ar = 2,6-ⁱPr₂C₆H₃ ^b C(i) = *ipso*-carbon ^c Reference 47 ^d Reference 23

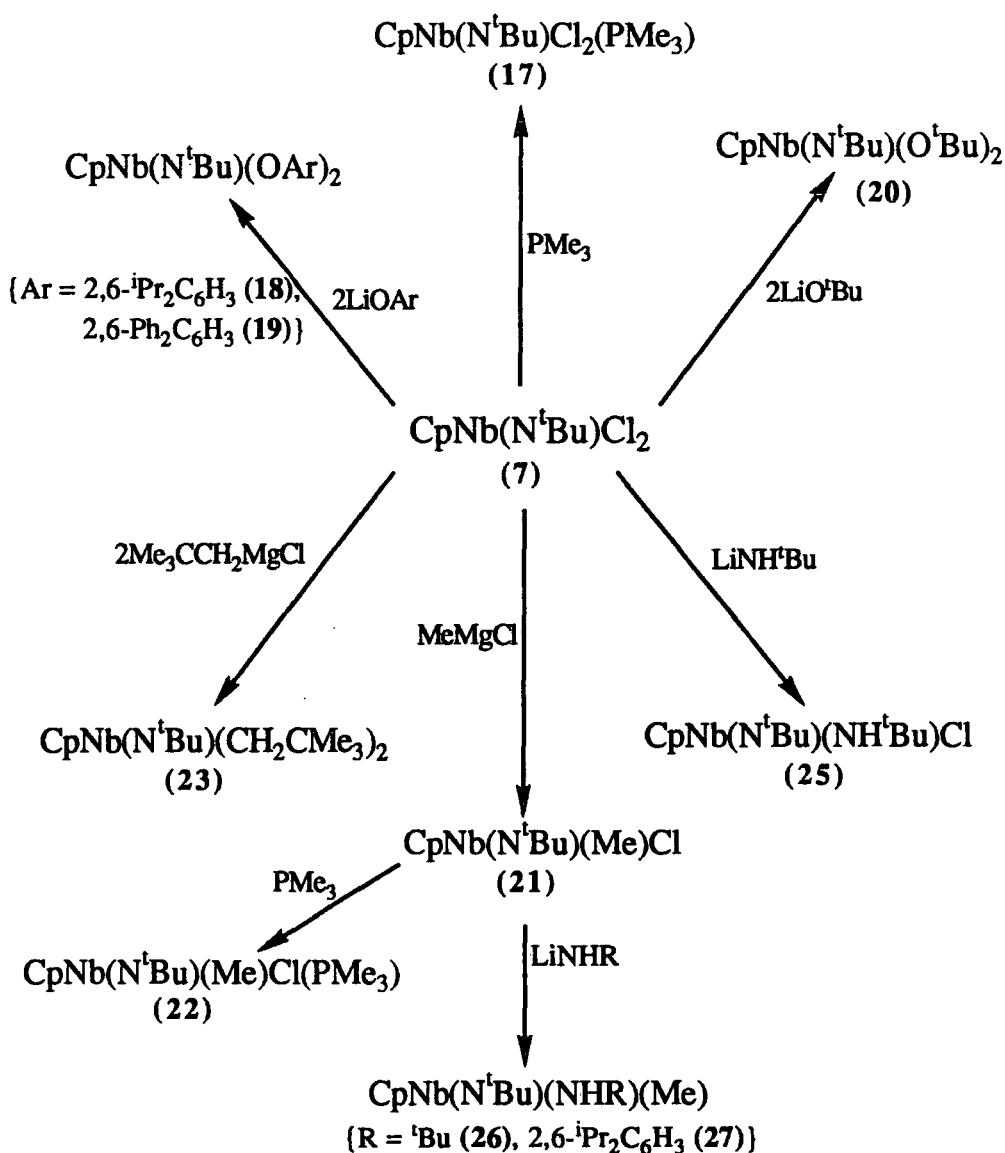
Table 2.12.

Here, from the limited data available, the *ipso* carbon chemical shift appears to change little on exchanging niobium for tantalum. However, more data on arylimido

arylimido derivatives of other metals would be required before any meaningful conclusion could be drawn.

2.12 Summary.

Convenient preparations of half-sandwich imido complexes, particularly for niobium, have been established, employing the use of silyl amine and amide reagents. A number of derivatives have been prepared and characterised (Scheme 2.2) which suggest that a rich and diverse chemistry may be anticipated for these systems



Scheme 2.2.

2.13 References

1. W.A. Herrmann, E. Herdtweck, M. Flöel, J. Kulpe, U. Küsthardt and J. Okuda, *Polyhedron*, 1987, **9**, 1165 and references therein.
2. D.D. Devore, J.D. Lichtenhan, F. Takusagawa and E.A. Maatta, *J. Am. Chem. Soc.*, 1978, **109**, 7408.
3. J.M. Mayer, C.J. Curtis and J.E. Bercaw, *J. Am. Chem. Soc.*, 1983, **105**, 2651.
4. W.A. Herrmann, G. Weichselbaumer, R.A. Paciello, R.A. Fischer, E. Herdtweck, J. Okuda and D.W. Marz, *Organometallics*, 1990, **9**, 489.
5. N. Wiberg, H.W. Häring and U. Schubert, *Z. Naturforsch*, 1980, **35B**, 599.
6. S. Gambarotta, A. Chiesi-Villa and G. Guastini, *J. Organomet. Chem.*, 1984, **C49**, 270.
7. J.H. Osborne, A.L. Rheingold and W.C. Trogler, *J. Am. Chem. Soc.*, 1985, **107**, 7945.
8. P.J. Walsh, F.J. Hollander and R.G. Bergman, *J. Am. Chem. Soc.*, 1988, **110**, 8729.
9. D.S. Glueck, F.J. Hollander and R.G. Bergman, *J. Am. Chem. Soc.*, 1989, **111**, 2719.
10. W.A. Nugent and B.L. Haymore, *Coord. Chem. Rev.*, 1980, **31**, 123.
11. T.P. Kee, V.C. Gibson, W. Clegg, *J. Organomet. Chem.*, 1987, **325**, C14.
12. V.C. Gibson, T.P. Kee and A. Shaw, *Polyhedron*, 1988, **7**, 2217.
13. M.J. Bunker, A. De Cain, M.L.H. Green, J.J. Moreau and N. Siganporia, *J. Chem. Soc. Dalton Trans.*, 1980, 2155.
14. V.C. Gibson, J.E. Bercaw, W.J. Burton Jr. and R.D. Sanner, *Organometallics*, 1986, **5**, 976.
15. V.C. Gibson, D.N. Williams, W. Clegg and D.C.R. Hockless, *Polyhedron*, 1989, **8**, 1819
16. W.A. Nugent and J.M. Mayer, *'Metal-Ligand Multiple Bonds'*, John Wiley, New York, 1988.

17. D.M. Adams, '*Metal -Ligand and Related Vibrations*', Edward Arnold, London, 1967.
18. A. Andreu, F.A. Jalon, A. Oro and P. Royo, *J. Chem. Soc. Dalton Trans.*, 1987, 953.
19. A. Shaw, *Thesis*, Durham University, 1989, Chapter 5.
20. R.R. Schrock, S.F. Pederson, M.R. Churchill and J.W. Ziller, *Organometallics*, 1984, 3, 1574.
21. C. Eaborn, '*Organosilicon Compounds*', Butterworth Scientific Publications, 1960.
22. A.J. Banister, W.Clegg, I.B. Gorrell, Z.V.Hauptman, and R.W.H. Small, *J. Chem. Soc., Chem. Commun.*, 1987, 1611.
23. V.C. Gibson , J.P. Mitchell, W. Clegg and D.C.R. Hockless, *Unpublished results*, 1990.
24. F.A. Cotton, S.A. Duraj and W.J. Roth, *J. Am. Chem. Soc.*, 1984, 106, 4749.
25. P.A. Finn, M.S. King, P.A. Kitty and R.E. McCarley, *J. Am. Chem. Soc.*, 1975, 97, 220.
26. L.S. Tan, G.V. Goeden and B.L. Haymore, *Inorg. Chem.*, 1983, 22, 1744.
27. A.G Orpen L. Brammer, F.H. Allen, O. Kennard, D.G. Watson and R. Taylor, *J. Chem. Soc., Dalton Trans.*, 1989, 12, S1.
28. T.P.Kee, *Thesis*, 1988, Durham University, Chapter 2.
29. J. Nieman, J.H. Huffman and K.G.Caulton, *J. Organomet. Chem.*, 1983, 255, 193.
- 30 R.M. Silverstein, C.G. Bassler and T.C. Morrill, '*Spectrometric Identification of Organic Compounds*', 4th Edition, Wiley, New York, 1981.
31. S.M. Rocklage and R.R. Schrock, *J. Am. Chem. Soc.*, 1982, 104, 3077.
32. F.A. Cotton and W.T. Hall, *J. Am. Chem. Soc.*, 1979, 101, 5094.
33. S.M. Rocklage and R.R. Schrock, *J. Am. Chem. Soc.*, 1980, 102, 7808.
34. W.A. Nugent and R.L. Harlow, *Inorg. Chem.*, 1980, 19, 777.
35. V.C. Gibson and T.P. Kee, *J. Chem. Soc. Chem. Commun.*, 1989, 656.

36. R.F. Jordan, 'Symposium on Catalysis and Organometallic Chemistry', New Orleans, 1987, Vol. 65, 4, 285.
37. M. Brookhart and M.L.H. Green, *J. Organomet. Chem.*, 1983, 250, 395.
38. M. Brookhart, T.H. Whitesides and Crockett, *Inorg. Chem.*, 1976, 15, 1550.
39. V.C. Gibson, A.D. Poole, W. Clegg and D.C.R. Hockless, *Unpublished results*, 1990.
40. R.R. Schrock and J.D. Fellman, *J. Am. Chem. Soc.*, 1978, 100, 3359.
41. R.B. Calvert and J.R. Shapley, *J. Am. Chem. Soc.*, 1978, 100, 7726.
42. J.B. Lambert and L.G. Greifenstein, *J. Am. Chem. Soc.*, 1974, 96, 5120.
43. W.A. Nugent, R.J. McKinney R.V. Kasowski and F.A. Van-catledge, *Inorg. Chim. Acta*, 1982, 65, L91.
44. B.R. Ashcroft, G.R. Clark, A.J. Nielson and C.E.F. Rickard, *Polyhedron*, 1986, 5, 2081.
45. W.A. Nugent and R.L. Harlow, *Inorg. Chem.*, 1979, 18, 2030.
46. W.A. Nugent and R.L. Harlow, *J. Chem. Soc., Chem. Commun.*, 1978, 579
47. U. Siemeling, *Unpublished Results*, Durham University, 1990.

CHAPTER THREE

A Comparative Study of the Bonding in Group 5 Half-Sandwich Imido Complexes & Related Cyclopentadienyl Compounds.

3.1 Introduction.

Following the synthetic entry established into half-sandwich Group 5 imido complexes, it became desirable to gain further insight into the metal-nitrogen bonding in these complexes before embarking upon further development of their derivative chemistry. Thus, Fenske-Hall quantum mechanical calculations¹ have been carried out on the structurally characterised complex $\text{CpNb}(\text{NMe})\text{Cl}_2$ ², and also its 18 electron PMe_3 adduct $\text{CpNb}(\text{NMe})\text{Cl}_2(\text{PMe}_3)$ ², firstly to understand more about the bonding between niobium and the alkylimido ligand, and then with a view to understanding why the PMe_3 ligand should bind preferentially to a lateral position rather than a central site between the two chloride ligands. It was during the course of these calculations that a more general relationship to bent metallocene complexes of the Group 4 metals became apparent. Therefore, the scope of the calculations were extended to include a comparison of (2) with the zirconocene complex (1) and also the phosphino-carbene complex (3) (Figure 3.1). A close similarity between the steric and electronic constraints present in (3) and Group 4 metallocene derivatives has already been suggested to account for the stability of their alkyl derivatives³.

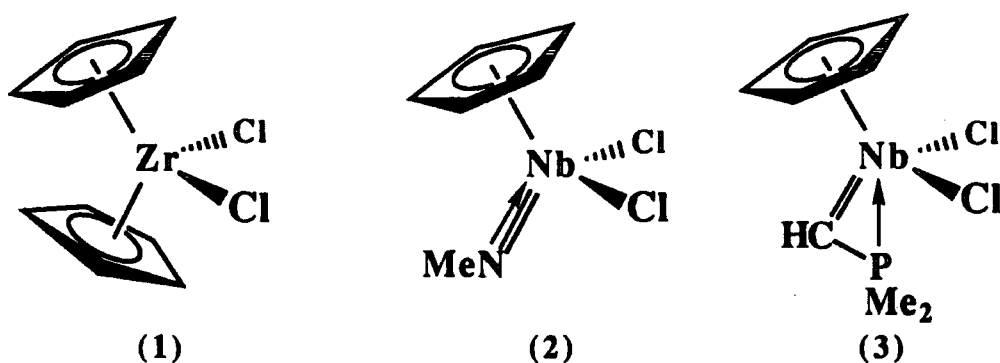


Figure 3.1

3.2 Fenske-Hall Molecular Orbital Calculations.

The basis of most molecular orbital (MO) calculations involves consideration of the one electron energies of the closed-shell system in terms of a Linear Combination of Atomic Orbitals-Self Consistent Field (LCAO-SCF) calculation. A rigorous, complete, one-electron calculation for systems of transition metal complexes is not feasible at the present time; the choice of approach depends on the degree of compromise between rigor and simplicity of calculation.

The Fenske-Hall Molecular Orbital (FHMO) calculations¹ used in this and subsequent chapters involves the application of various well known approximations to the Hartree-Fock-Roothaan operator (HFR)⁴. The HFR operator is a one-electron operator, whose application yields the energy of an electron moving in the average field of the other electrons and nuclei. We can write a model one-electron operator, F , as a kinetic energy operator plus a potential energy operator for each centre in the system (Equation 3.1).

$$F = -\frac{1}{2} \nabla^2 + \sum_C V_C \quad (3.1)$$

Equation 3.1 assumes that we can assign the electron density to the appropriate centre; this is achieved through the use of Mulliken population analysis⁵. The approximate operator is used to generate matrix elements between atomic basis functions, and the final wavefunction is obtained by solving, self-consistently, the Hartree-Fock-Roothaan equation with appropriate matrix elements.

The diagonal matrix element for a function χ_a is given by the final equation:

$$F_{aa} = \epsilon_a + \sum_{C \neq A,B} (-q_C)(1/R_{AC}) \quad (3.2)$$

The first term ϵ_a , the atomic orbital energy; consisting of a term for kinetic energy and nuclear attraction energy, the Mulliken population of orbital χ_a and Slater's average configuration, electrostatic repulsion integral, can be calculated using Slater's average configuration approach⁶. The second term in Equation 3.2 describes the influence of each of the other centres (nuclei and electrons) on the diagonal matrix element. q_C , the point charge on centre C, can be calculated via Mulliken populations⁵, and $1/R_{AC}$ is the potential energy of two unit charges at a distance R_{AC} from each other.

After approximations^{4c,7}, the expression for the off-diagonal matrix element between two different centres becomes:

$$F_{ab} = (\chi_a | \chi_b)(\epsilon_a + \epsilon_b) - (\chi_a | -\frac{1}{2} \nabla^2 | \chi_b) - \frac{1}{2}(\chi_a | \chi_b) \sum_{C \neq A,B} (q_C/R_{AC} + q_C/R_{BC}) \quad (3.3)$$

where $(\chi_a | \chi_b)$ and $(\chi_a | -\frac{1}{2} \nabla^2 | \chi_b)$, the overlap and kinetic energy integrals, are evaluated exactly. The other terms are calculated by employing the Mulliken point charge approximations^{5,8}.

The formulae for the matrix elements, given in Equations 3.2 and 3.3, are used to calculate the approximate HFR matrix. The complete HFR equation⁹ is then solved:

$$FC = SC\epsilon \quad (3.4)$$

where S is the overlap matrix, C is the eigenvector matrix and ϵ is the diagonal eigenvalue matrix. The general procedure for solving the equation is one of trial and error. One assumes a set of eigenvectors (the basis functions), calculates F , solves the equation for the n lowest eigenvalues ϵ_i and compares the resulting eigenvectors, c_i 's, with the assumed one; a new set of c_i 's are chosen and the procedure repeated until the assumed and the calculated c_i 's agree.

Initially $S^{-1/2} 10$ is used as the transformation matrix, for each subsequent cycle it is advantageous to use the vectors from the previous cycle. For each iteration new Mulliken populations must be calculated to generate the new F matrix. In order to improve the rate of convergence to a self-consistent solution damping each new input population, and a modification of Aitkins δ^2 extrapolation method are used¹¹.

There are several points about the Fenske-Hall method which should be mentioned:

- (1) Fenske-Hall does not involve the use of any adjustable or empirical parameters; this differs from many MO calculations, including EHMO, which obtain orbital energies from experimental values of the valence state ionisation energies. This approximation has the undesirable feature that variations in the choice of basis functions have no effect on orbital energies, as should be the case. In Fenske-Hall calculations the orbital energies, are determined as indicated earlier, by the evaluation of kinetic energy, nuclear attraction and one-centre electrostatic integrals, hence the final results depend only on the choice of basis function and the internuclear distance, both which are chosen in a consistent non-arbitrary fashion.
- (2) The Fenske-Hall method includes effects of all neighbouring atoms in determining the energetic placement of the levels.
- (3) Fenske-Hall is invariant to a rotation of the local coordinate system on each atom.

The subsequent sections of this chapter describe the use of the FHMO method for a series of cyclopentadienyl complexes. Where appropriate comparisons with results obtained by other computational methods are included.

3.3 The Nature of the Imido-Metal Bonding in $CpNb(NMe)Cl_2$.

In order to gain insight into the nature of the methylimido-niobium multiple bonding in $CpNb(NMe)Cl_2$, interactions of the $[CpNbCl_2]^{2+}$ and $[NMe]^{2-}$ fragments were considered. The frontier orbitals of the fragments were constructed and then the

interaction of these molecular orbitals used to create a bonding picture. For ease of calculation the x-axis was taken along the Nb-N bond, as shown in Figure 3.2.

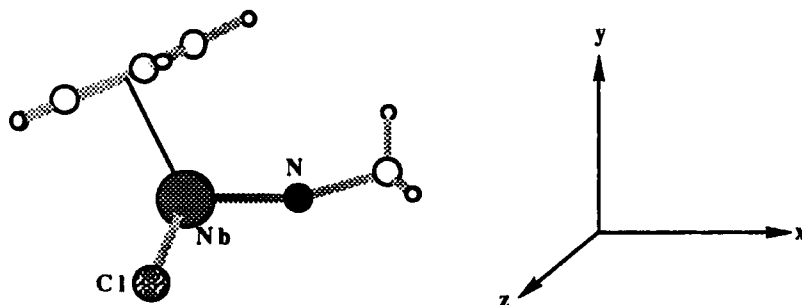


Figure 3.2, Axial framework for FHMO calculation on $CpNb(NMe)Cl_2$.

3.3.1 The $[CpNbCl_2]^{2+}$ Fragment.

The frontier orbitals of the $[CpNbCl_2]^{2+}$ fragment are represented schematically on the left-hand side of Figure 3.3. The composition of the fragment frontier molecular orbitals are important in assessing their bonding capability, and Table 3.1 shows the composition of these frontier orbitals (21-26).

| Orbital | Composition, % | |
|----------|----------------|---|
| | Ligands Cp, Cl | Metal |
| 21(HOMO) | 95 | 3 d_{yz} , 2 p_z |
| 22(LUMO) | 22 | 30 d_{xy} , 26 $d_{x^2-y^2}$, 15 d_{z^2} , 7 s |
| 23 | 25 | 65 d_{xz} , 10 p_z |
| 24 | 23 | 48 d_{z^2} , 11 p_y , 10 d_{xy} , 8 $d_{x^2-y^2}$ |
| 25 | 28 | 26 d_{xy} , 23 $d_{x^2-y^2}$, 12 s, 11 p_x |
| 26 | 42 | 47 d_{yz} , 11 p_z |

Table 3.1

The filled metal fragment frontier orbital 21 contains mainly Cl 3p orbital character, with little metal character involved. The LUMO(22) and fragment MO 25

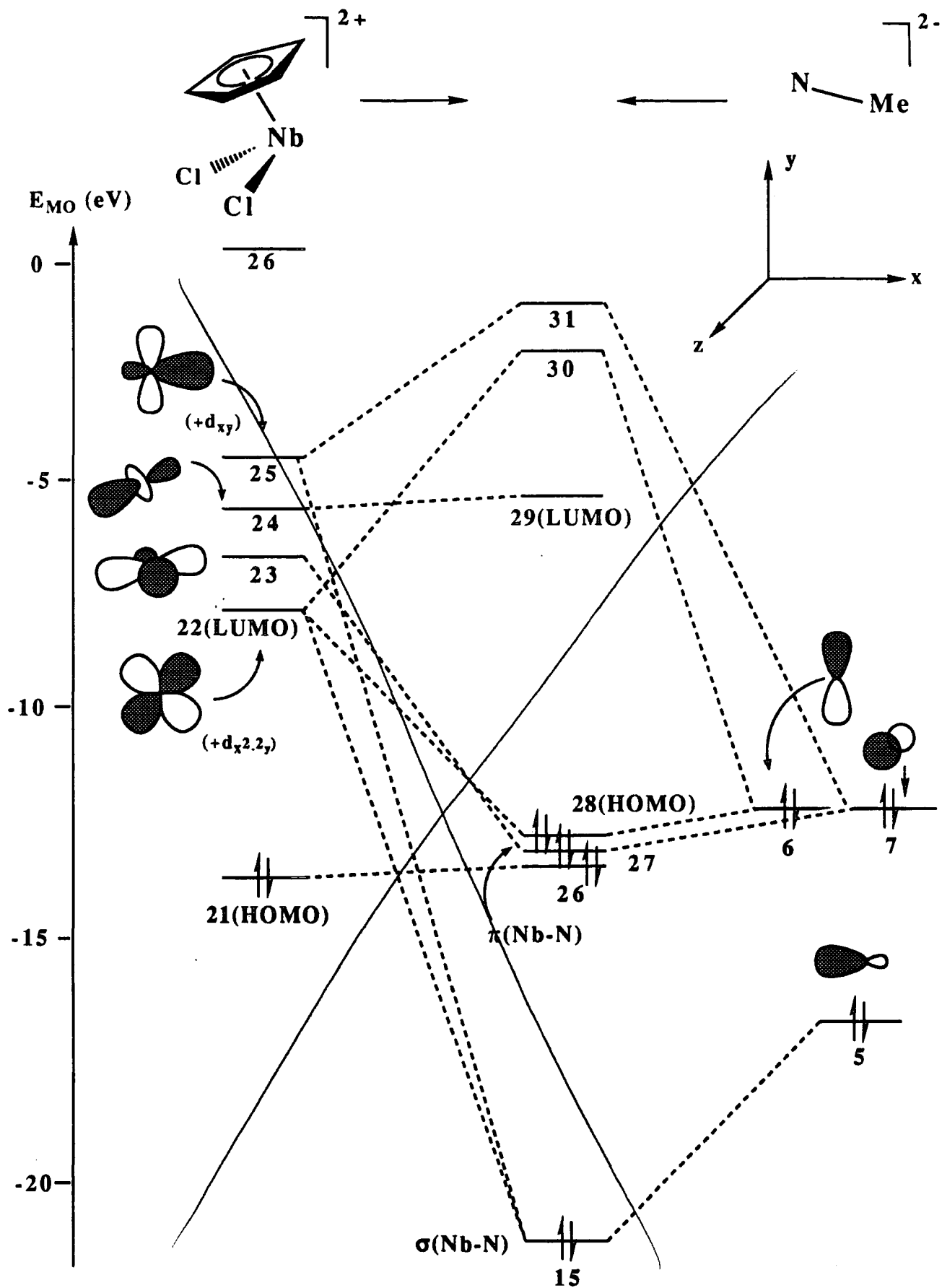


Figure 3.3, Molecular orbital correlation diagram, showing interaction of the fragments $[CpNbCl_2]^{2+}$ and $[NMe]^{2-}$. Representations of the fragment MO's show the most important orbital contributions only.

contain a large σ and π -component in the xy plane, while MO 23 is chiefly d_{xz} in character.

3.3.2 The $[\text{NMe}]^{2-}$ Fragment.

The frontier orbitals of $[\text{NMe}]^{2-}$ are shown schematically on the right-hand side of Figure 3.3. The compositions of these orbitals (Table 3.2) indicate that filled MO 5 is essentially sp in character, directed along the x-axis, MO 6 and 7(HOMO) are nearly pure p_y and p_z orbitals respectively.

| Orbital | Composition, % Nitrogen |
|---------|-------------------------|
| 5 | 59 p_x , 28 s |
| 6 | 91 p_y |
| 7 | 99 p_z |
| 8 | 29 s, 29 p_x |

Table 3.2 *Composition of $[\text{NMe}]^{2-}$ -fragment frontier MO's.*

3.3.3. Interaction of the $[\text{CpNbCl}_2]^{2+}$ with $[\text{NMe}]^{2-}$.

The formation of $\text{CpNb}(\text{NMe})\text{Cl}_2$ shown in the correlation diagram (Figure 3.3), arises from the interaction of $[\text{CpNbCl}_2]^{2+}$ and $[\text{NMe}]^{2-}$. The most important interactions, in terms of Mulliken inter-fragment overlap population are collected in Table 3.3.

| Metal fragment MO | Ligand fragment MO | Mull. Ov. Population |
|-------------------|--------------------|----------------------|
| 22(LUMO) | 5(HOMO) | 0.086 |
| 22(LUMO) | 6 | 0.108 |
| 23 | 7 | 0.176 |
| 25 | 5(HOMO) | 0.154 |

Table 3.3

The interaction of MO 5 with metal fragment MO's 22 and 25, essentially the sp-orbital on nitrogen with the empty $d_{x^2-y^2}$ orbital on the metal, leads to the formation a σ -bond found in complex MO 15. The Mulliken overlap populations suggest that fragment MO 25 is primarily responsible for the σ -interaction. π -bonds are found in complex MO's 27 and 28(HOMO) arising through the interaction of the essentially degenerate MO's 6 (p_y) and 7 (p_z) of $[\text{NMe}]^{2-}$ with metal fragment MO's 22 and 23 respectively. Empty metal fragment MO 24 remains essentially non-bonding, forming complex LUMO (29).

From the final mulliken population, it is found that approximately 1.6 electrons are transferred from the nitrogen atom of the $[\text{NMe}]^{2-}$ ligand to metal fragment MO's 22-25.

3.4 The Interaction of Trimethylphosphine with $\text{CpNb}(\text{NMe})\text{Cl}_2$.

The reaction of trimethylphosphine with $\text{CpNb}(\text{NMe})\text{Cl}_2$ yields the 18 electron adduct $\text{CpNb}(\text{NMe})\text{Cl}_2(\text{PMe}_3)$, as described in chapter 2. Calculations were carried out on this species, using the crystallographically determined coordinates for the adduct, in order to assess the principal interactions of the empty metal orbitals with the PMe_3 lone pair in forming this four legged piano-stool complex.

The coordinate axes chosen here are the same as those adopted in the previous calculation to allow a direct comparison (Figure 3.4). The frontier orbitals of $[\text{CpNb}(\text{NMe})\text{Cl}_2]$ and $[\text{PMe}_3]$, arising from fragmentation of the adduct, were then interacted in order to give the complex MO bonding picture.

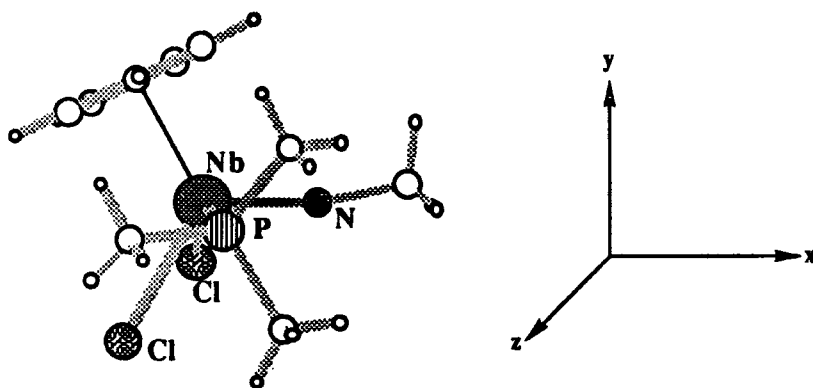


Figure 3.4, Axial framework for FHMO calculation on $\text{CpNb}(\text{NMe})\text{Cl}_2(\text{PMe}_3)$.

3.4.1 The $[\text{CpNb}(\text{NMe})\text{Cl}_2]$ Fragment.

The frontier orbitals of the $[\text{CpNb}(\text{NMe})\text{Cl}_2]$ fragment are illustrated in Figure 3.5. Since the geometry of the $[\text{CpNb}(\text{NMe})\text{Cl}_2]$ fragment in $\text{CpNb}(\text{NMe})\text{Cl}_2(\text{PMe}_3)$ is not substantially different to that found in structurally characterised $\text{CpNb}(\text{NMe})\text{Cl}_2$, the frontier orbitals of the metal fragment are very similar to those of the complex MO's found in $\text{CpNb}(\text{NMe})\text{Cl}_2$ described in Section 3.3.3. The empty niobium fragment frontier orbitals are clearly the most important in understanding the interaction with a donor ligand such as PMe_3 . The composition of MO's 29(LUMO) to 33 are shown in Table 3.4.

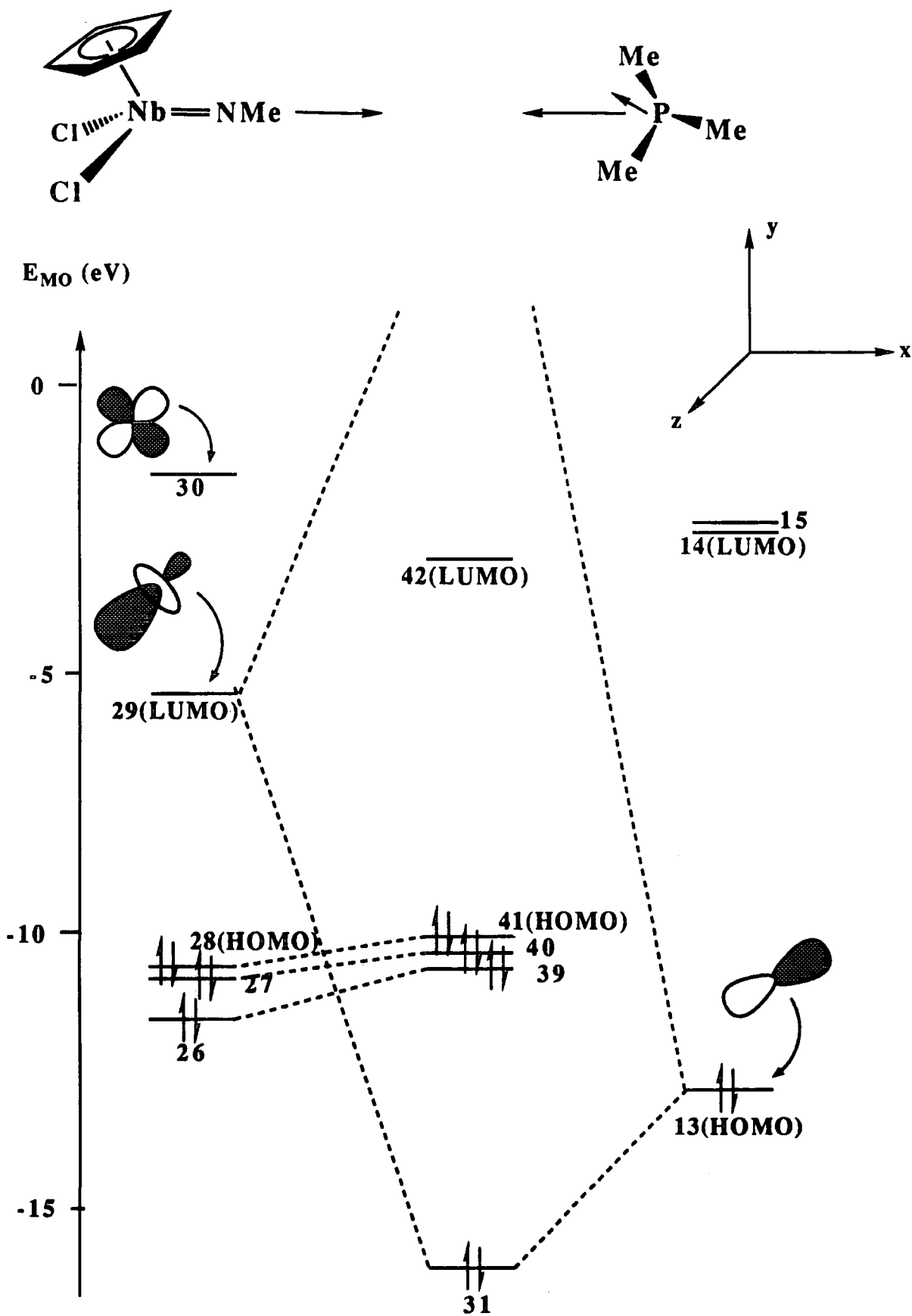


Figure 3.5, Molecular orbital correlation diagram, showing interaction of the fragments $[\text{CpNb}(\text{NMe})\text{Cl}_2]$ and $[\text{PMe}_3]$. Representations of the fragment MO's show the most important orbital contributions only.

| Orbital | Composition, % | |
|----------|----------------|--|
| | Ligands | Metal |
| 29(LUMO) | 24 | 37 d _{z2} , 22 d _{yz} , 6 d _{xz} , 5 p _z , 4 s, 2 d _{x2-y2} |
| 30 | 35 | 26 d _{xz} , 12 d _{xy} , 11 d _{z2} , 8 d _{x2-y2} , 4 d _{yz} , 2 p _x , 2p _z |
| 31 | 33 | 20 d _{xy} , 20 d _{xz} , 13 d _{x2-y2} , 6 p _x , 3 d _{yz} , 3 s, 2 p _y |
| 32 | 37 | 38 d _{yz} , 7 d _{z2} , 7 d _{xz} , 5 p _z , 4 d _{xy} , 2 s |
| 33 | 32 | 28 d _{x2-y2} , 23 d _{xy} , 17 p _x |

Table 3.4

3.4.2. The [PMe₃] Fragment.

The frontier orbitals of [PMe₃] are illustrated on the right-hand side Figure 3.5. The orbital of greatest importance is the HOMO(13), which consists mainly of phosphorus s and p_z character (13: P, 9% s, 3% p_x, 3% p_y and 71% p_z).

3.4.3 Interaction of PMe₃ with CpNb(NMe)Cl₂.

The formation of CpNb(NMe)Cl₂(PMe₃) from [CpNb(NMe)Cl₂] and [PMe₃] fragments, is illustrated in the correlation diagram, Figure 3.5. The inter-fragment Mulliken overlap population shows one major interaction (0.172) between phosphine HOMO(13) and metal fragment LUMO(29). This interaction is essentially between phosphorus 3p_z and niobium d_{z2} and d_{yz} and leads to the formation of a σ-dative covalent bond, found in metal complex MO 31. Final Mulliken population shows the transfer of 0.55 electrons from the neutral phosphine HOMO to the metal fragment MO 29.

3.5 A Comparison of the Electronic Structure of CpNb(NMe)Cl₂ with Complexes of the Type Cp₂ZrX₂.

During the course of constructing the MO interaction diagrams for the half-sandwich imido species described in the previous section, similarities between the frontier orbitals of CpNb(NMe)Cl₂ and complexes of the type Cp₂ZrX₂ became apparent. It was realised that these similarities reflected the symmetry properties of the frontier orbitals of the imido fragment, NR²⁻, and those of the cyclopentadienyl ligand, η⁵-C₅H₅. Both the ligands contain an orbital of a₁ symmetry and a set of degenerate e₁ orbitals. In bonding to a transition metal, the Cp group in Cp₂ZrX₂ complexes engages in strong π-type interactions between metal d_{xz} and d_{yz} (e) and Cp e₁ orbitals, and a σ-type bonding interaction between metal s and p_z orbitals and the Cp a₁ orbital. The remaining three d-orbitals of the metal, the d_{z²}, d_{x²-y²} and d_{xy}, remain essentially non-bonding. One might have thought that the d_{z²} would also interact with the the cyclopentadienyl a₁ orbital, but the π-orbital lobes probe the region of the d_{z²} nodal surface. As we have just seen, the bonding of an imido ligand to a transition metal is very similar, although in this case a considerable metal d_{z²}-imido nitrogen sp (a₁) interaction is seen; this is essentially the only significant difference between the the metal-ligand bonding for the Cp and NR groups.

These similarities imply that d⁰ species of the type Cp₂ZrCl₂¹², and CpNb(NR)Cl₂² and therefore even non-cyclopentadienyl species such as M(NR)₂Cl₂ (M = W, Mo)¹³ (Figure 3.6) may have closely related electronic and chemical properties.

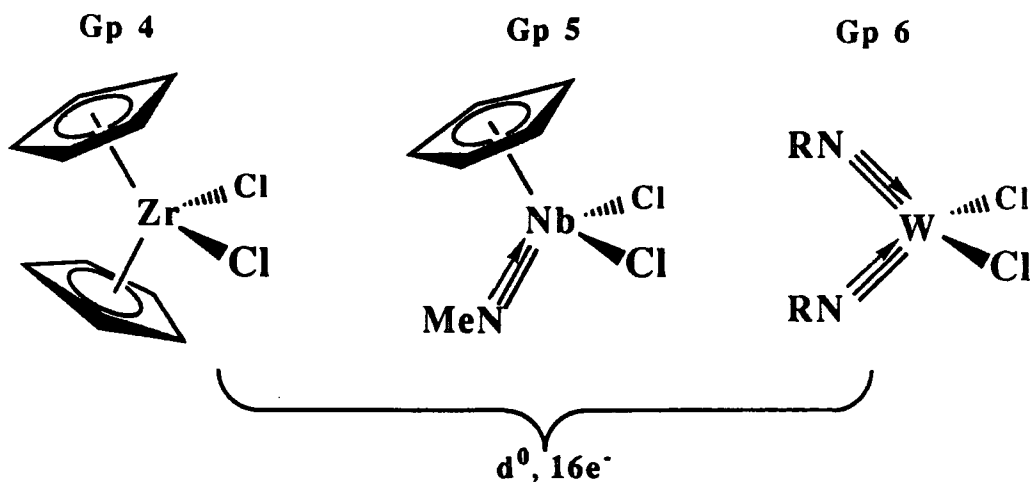


Figure 3.6

The nature of the bonding in Cp_2MX_2 complexes has been the subject of much interest. In 1961 Ballhausen and Dahl¹⁴ formulated a qualitative description to represent the bonding in Cp_2MH_2 ($M = Mo$ and W). A hybridisation scheme was postulated with nine orthogonal hybrid orbitals in three sets of three. Two of these sets interact with the bis- π -cyclopentadienyl ligands and the third is in the plane at right-angles to that containing the normals to the cyclopentadienyl ring at the metal atom (Figure 3.7(a)). It is this third set which is said to be available for bonding to further ligands. A later model proposed by Alcock¹⁵ places the non-bonding orbital in Cp_2MX_2 outside ligands X, Figure (3.7(b)).

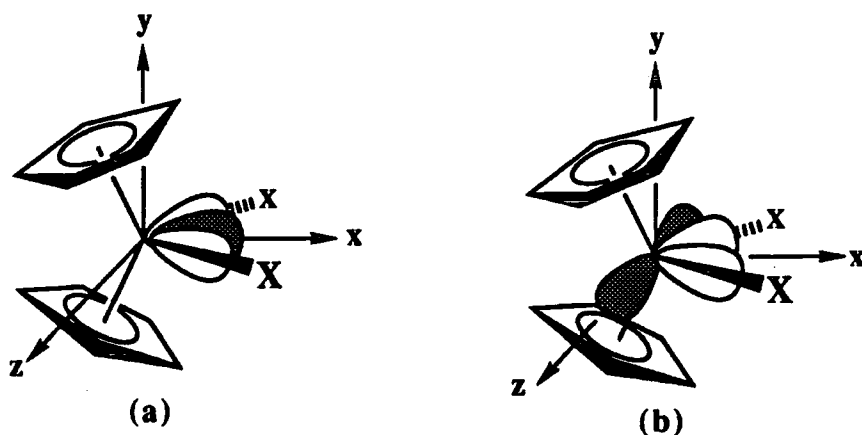


Figure 3.7, Bent bis- π -cyclopentadienyl -metal systems: metal hybrid orbitals available for bonding to mono-dentate ligands according to (a) Ballhausen and Dahl (1961) and (b) Alcock (1967).

Since then many more complex models have been described for the bonding in Cp_2MX_2 complexes employing a variety of quantum mechanical techniques¹⁶⁻²¹. Fenske-Hall-type molecular orbital calculations were carried out by Dahl et al on several d^0 , d^1 and d^2 M(IV) Cp_2MX_2 complexes¹⁸, and more recently by Zhu and Kostic on Cp_2ZrCl_2 ²¹. Lauher and Hoffmann have used Extended Hückel Molecular Orbital Calculations (EHMO) to construct the frontier orbitals of the bent *bis*(η^5 -cyclopentadienyl)M fragment, Cp_2M and from this starting point they give an extensive account of the electronic structure of Cp_2MX_n molecules ($n = 1-3$)²¹. As a test of the Fenske-Hall approach, we have repeated these calculations for the $[\text{Cp}_2\text{Zr}]^{2+}$ fragment (geometry taken from crystal structure of Cp_2ZrCl_2 ¹²), and thus also allowing a direct comparison with the electronic structure of the $[\text{CpNb}(\text{NMe})]^{2+}$ fragment. For comparison purposes, the coordinate axes chosen are the same as those used in the Lauher and Hoffmann calculations (see Figure 3.8).

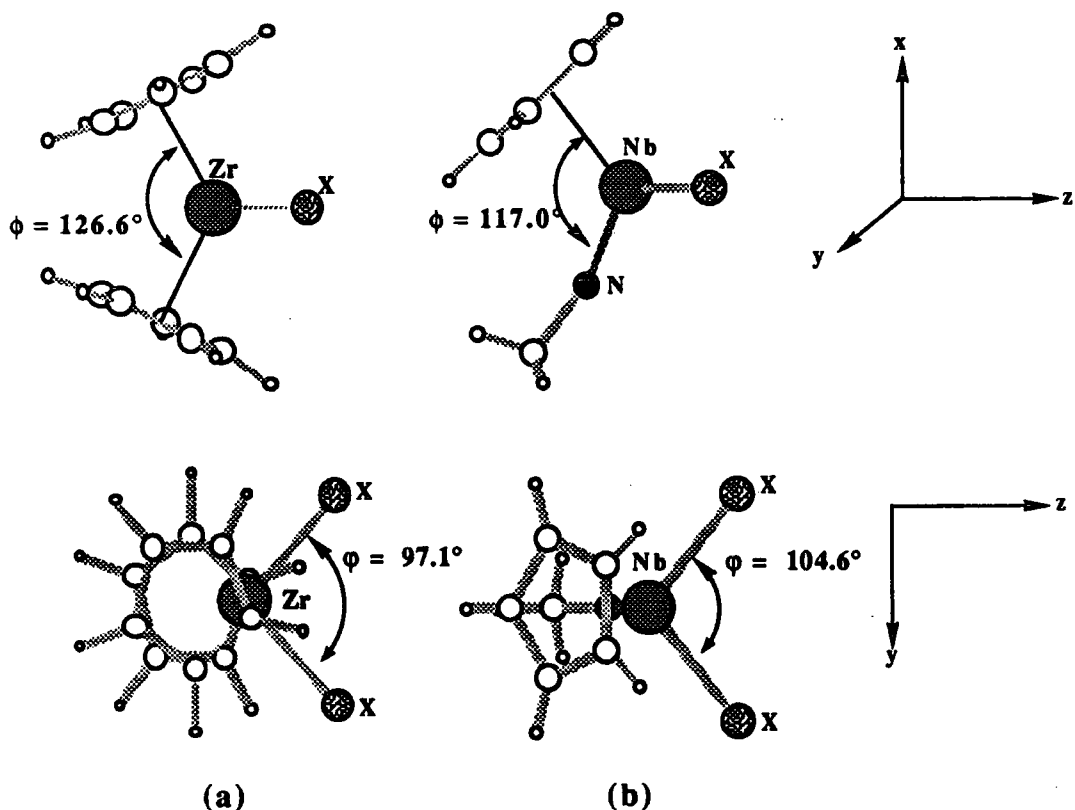


Figure 3.8, Axial framework for FHMO calculations on; (a) Cp_2ZrX_2 and (b) $\text{CpNb}(\text{NMe})\text{X}_2$ ($\text{X} = \text{H}, \text{Cl}$).

3.5.1 The Frontier Orbital Picture for [Cp₂Zr].

The composition of the unoccupied frontier orbitals generated by our calculations and those generated by Lauher and Hoffmann for [Cp₂Ti] using Extended Hückel calculations are summarised in Table 3.5.

| Fenske-Hall Calcs. for [Cp ₂ Zr] ^a | | | Extended Hückel Calcs for [Cp ₂ Ti] ^b | | |
|--|---------------|---|---|---------------|---|
| | % Composition | | | % Composition | |
| Orbital | Ligands | Metal ^c | Orbital | Ligands | Metal ^c |
| 27(1a ₁) | 16 | 84 d _{y2} , 5 s | 1a ₁ | 18 | 51 d _{x2-y2} , 30 d _{z2} , 1 s |
| 28(b ₂) | 27 | 66 d _{yz} , 7 p _y | b ₂ | 34 | 64 d _{yz} , 2 p _y |
| 29(2a ₁) | 14 | 36 d _{z2-x2} , 33 s, 17 p _z | 2a ₁ | 21 | 33 d _{z2} , 27 d _{x2-y2} , 11 s, 8 p _z |
| 30(b ₁) | 40 | 60 d _{xz} , 7 p _y | b ₁ | 57 | 43 d _{xz} |
| 31(a ₂) | 40 | 60 d _{xy} | a ₂ | 69 | 31 d _{xy} |

^a Taken from calculations on Cp₂ZrCl₂ x-ray structure, $\phi = 126.6^\circ$ ref. 21

^b Taken from Lauher and Hoffmann results, $\phi = 136^\circ$ ref. 20

^c Metal orbitals are defined with respect to the coordinate system in Figure 3.8

Table 3.5

On initial inspection there appear to be some significant differences, particularly for complex MO's 27 and 29, but on closer inspection, the orbital contributions described by Lauher and Hoffmann lead to complex MO's with shapes and directions similar to 27 and 29. For example, Lauher and Hoffmann note that the 1a₁ orbital comprising 51% d_{x2-y2} and d_{z2} has a significant component in the y-direction and may be described as being similar to a d_{y2} orbital, c.f. MO 27 which contains mainly d_{y2} character. MO 28 is chiefly d_{yz} in character while MO 29 is hybridised along the z-axis away from the C₅H₅⁻ ligands, and is closely related to the 2a₁ orbital found in Hoffmann's calculations. These frontier orbitals are illustrated in Figure 3.9. In previous studies these orbitals have been described as the 1a₁, b₂ and 2a₁ respectively.

The next highest unoccupied orbitals, the b_1 and a_2 , show mainly d_{xz} and d_{xy} character respectively.

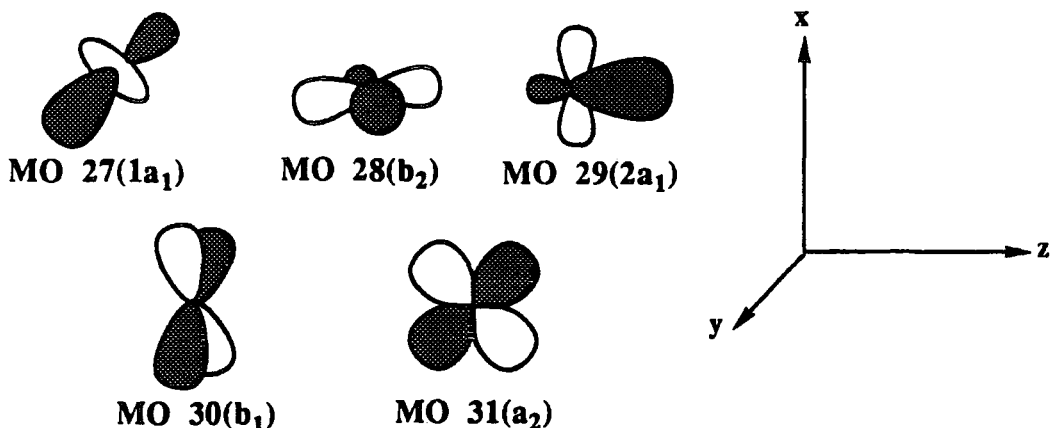


Figure 3.9, Frontier MO's of the $[Cp_2Zr]$ fragment (most important contributions only).

3.5.2. The Frontier Orbitals of the $[CpNb(NMe)]^{2+}$ Fragment.

Fenske-Hall molecular orbital calculations were carried out on the $[CpNb(NMe)]^{2+}$ fragment, with the geometry found in the $CpNb(NMe)Cl_2$ x-ray structure. The axial framework for this calculation is illustrated in Figure 3.8. The orbital composition of the $[CpNb(NMe)]^{2+}$ fragment, Table 3.6, reveal striking similarities between the frontier orbitals of this fragment with those of the $[Cp_2Zr]^{2+}$ fragment just described, Table 3.5.

| Orbital ^a | Composition, % | |
|----------------------|----------------|---|
| | Ligands | Metal |
| 21($1a_1$) | 12 | 79 d_{yz} , 9 s |
| 22(b_2) | 41 | 57 d_{yz} , 2 d_{xy} |
| 23($2a_1$) | 24 | 23 $d_{z^2-x^2}$, 19 d_{xz} , 18 s, 14 p_z , 2 p_x |
| 24(b_1) | 21 | 35 d_{xz} , 17 s, 14 p_x , 7 $d_{z^2-x^2}$, 6 p_z |
| 25(a_2) | 53 | 55 d_{xy} , 3 p_x , 2 d_{yz} |

^aThe symmetry labels, although not applicable to the $[CpNb(NMe)]^{2+}$ fragment are included to allow direct comparison with $[Cp_2Zr]$.

Table 3.6

The only significant difference appears to be in the composition of the 23(2a₁) orbital, which for the latter appears to contain a significant contribution (19%) from the niobium d_{xz} orbital. This lies out of the normal "equatorial" ligand binding plane of a [Cp₂M] fragment, and therefore may be where differences in the chemistries of [Cp₂M] and [CpM(NR)] could occur.

In order to probe how the frontier orbitals of [Cp₂Zr] and [CpNb(NR)] interact with additional ligands, calculations have been carried out for dihydride and dihalide derivatives. These are described in the following sections.

3.5.3 Interaction of [Cp₂Zr]²⁺ with Two Hydride Ligands.

The interaction of a transition metal fragment of the type [Cp₂M] with two hydride ligands, has been studied by a number of groups^{20,21}, mostly by EHMO calculations. In order to allow a meaningful comparison with the FHMO calculations on the imido system, we have used the Fenske-Hall orbital picture for [Cp₂Zr] just described. Very similar interactions are found.

The interaction diagram for the bonding of two hydride ligands to [Cp₂M]²⁺ is shown in Figure 3.10. Two σ-type bonds are formed between the H 1s orbitals and the transition metal 2a₁ and b₂ orbitals, the 1a₁ remaining virtually non-bonding.

The percentage mulliken overlap population of frontier metal MO's with hydride AO's obtained by our calculations are shown in Table 3.7.

| Metal fragment MO | % Total Mull. Ov. Pop. |
|----------------------------|------------------------|
| 27(LUMO)(1a ₁) | 15.2 |
| 28(b ₂) | 53.8 |
| 29(2a ₁) | 31.0 |
| 30(b ₁) | 0 |
| 31(a ₂) | 0 |

Table 3.7

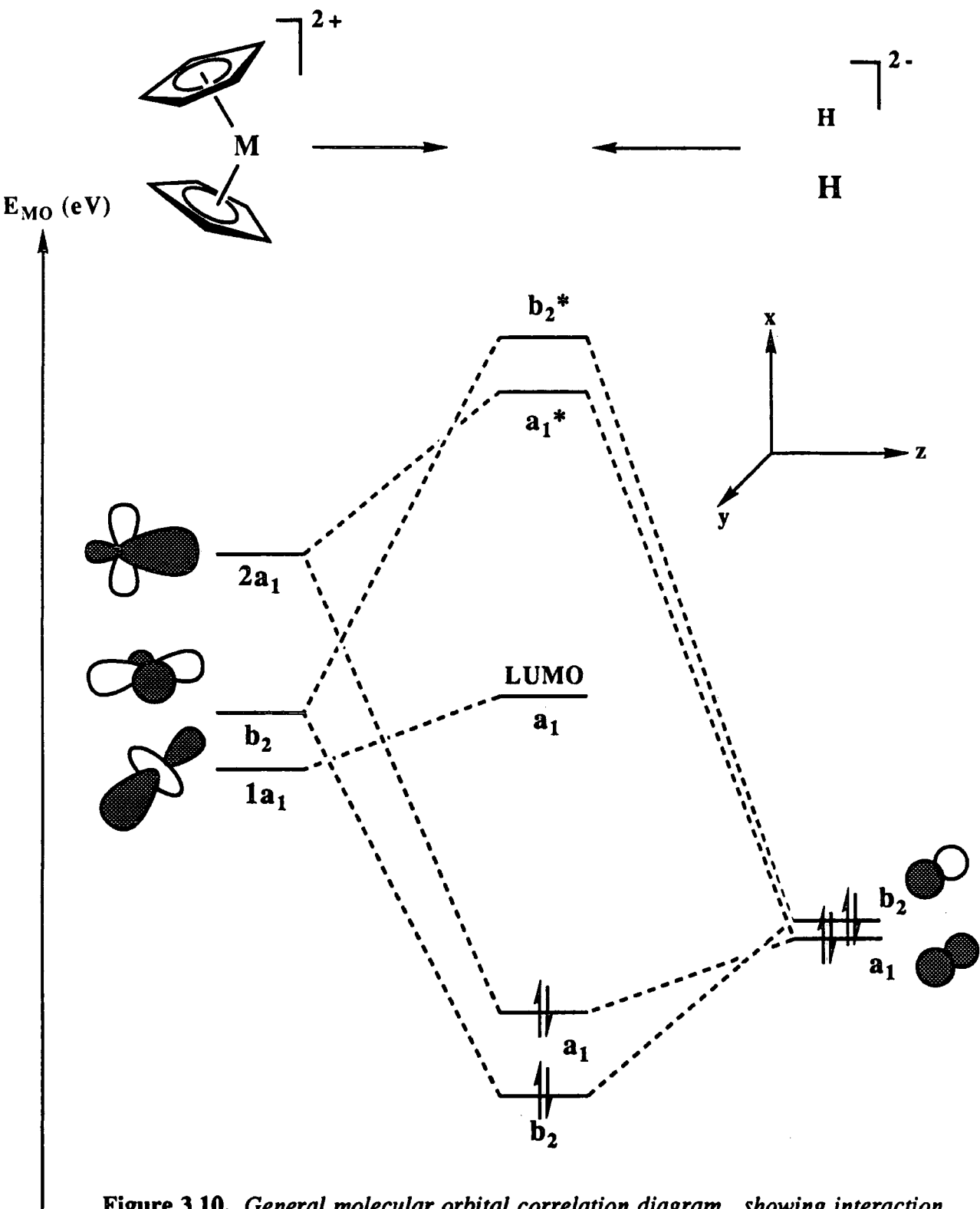


Figure 3.10, General molecular orbital correlation diagram, showing interaction of the fragments $[CpM]^{2+}$ and $2H$. ($M =$ Transition metal).

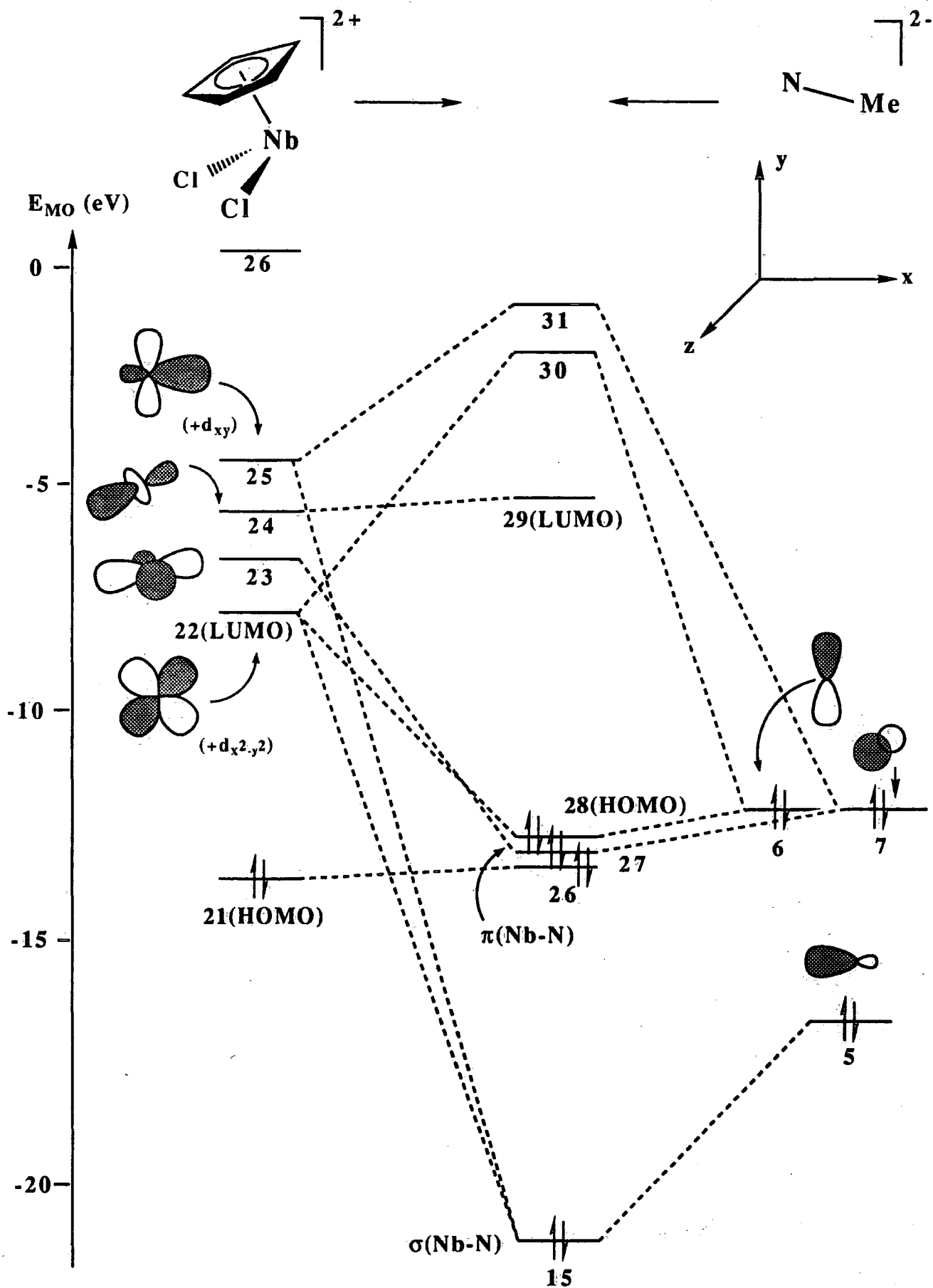


Figure 3.3, Molecular orbital correlation diagram, showing interaction of the fragments $[CpNbCl_2]^{2+}$ and $[NMe]^{2-}$. Representations of the fragment MO's show the most important orbital contributions only.

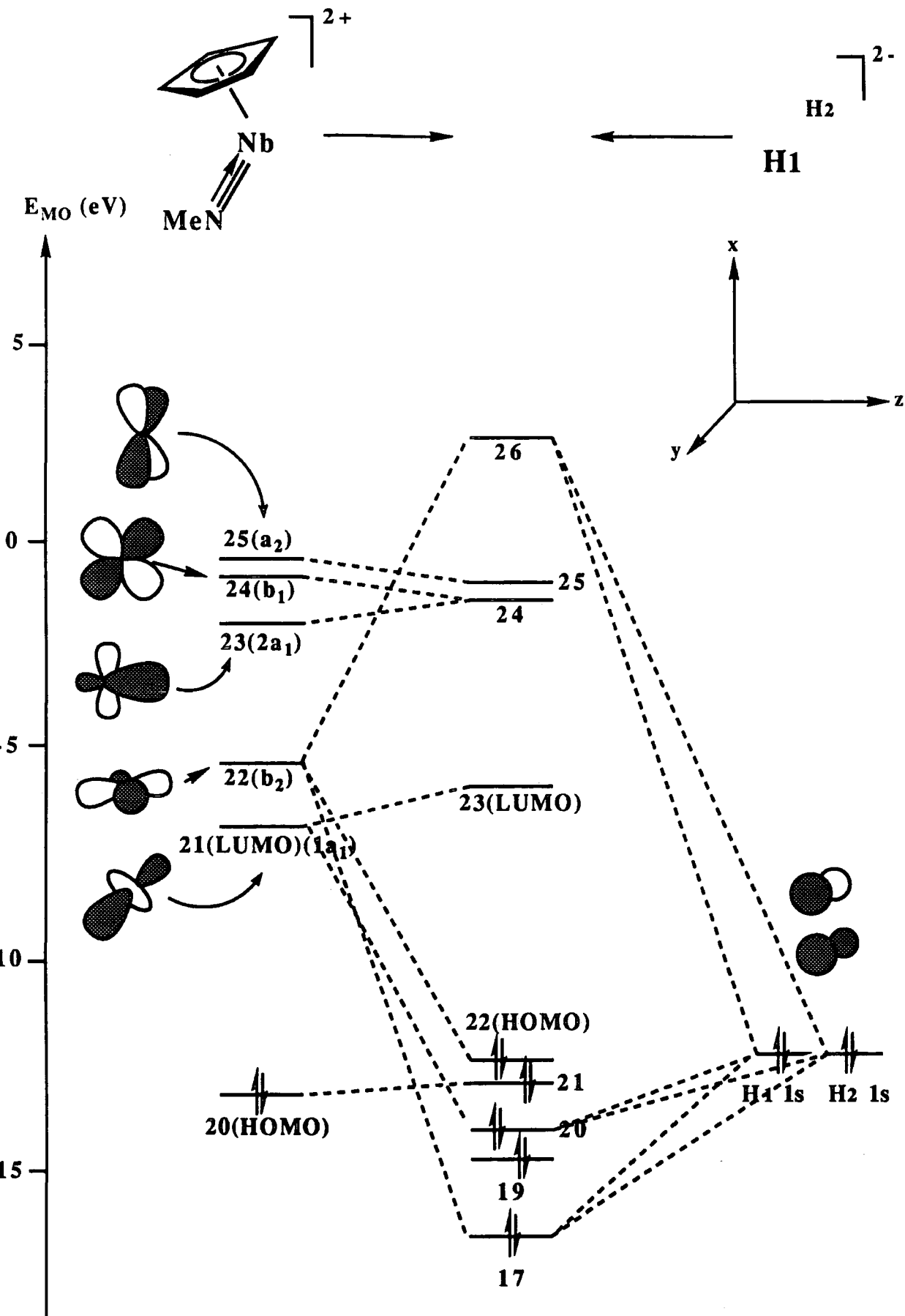


Figure 3.11, *Molecular orbital correlation diagram, showing the interactions of the fragments $[CpNb(NMe)]^{2+}$ and $2H^-$. Representations of the fragment MO's show the most important orbital contributions only.*

This picture is essentially the same as that generated by others using EHMO calculations.

3.5.4 Interaction of $[\text{CpNb}(\text{NMe})]^{2+}$ with Two Hydride Ligands.

The correlation diagram for the interaction of the $[\text{CpNb}(\text{NMe})]^{2+}$ fragment with two hydride ligands is shown in Figure 3.11. Compared with the interaction of $[\text{Cp}_2\text{Zr}]^{2+}$ with 2H^- , there is appreciably greater interaction of the metal fragment LUMO($1a_1$) with the hydride $1s$ AO's (24% c.f. 15% Cp_2ZrH_2), at the expense of overlap with the MO of ' $2a_1$ ' symmetry whose % total Mulliken overlap population is halved. The overlap between the ' b_2 '-orbital is not substantially different (Table 3.8).

| Metal Fragment MO ^a | % of Total Overlap |
|--------------------------------|--------------------|
| 21(LUMO)($1a_1$) | 24.3 |
| 22(b_2) | 50.0 |
| 23($2a_1$) | 15.7 |
| 24(b_1) | 7.7 |
| 25(a_2) | 2.3 |

^aThe symmetry labels, although not applicable to the $[\text{CpNb}(\text{NMe})]^{2+}$ fragment, are included to allow direct comparison with $[\text{Cp}_2\text{Zr}]$.

Table 3.8

The increased overlap with the $[\text{CpNb}(\text{NR})]$ fragment MO 21($1a_1$), which is essentially d_{y^2} in character, and the decreased overlap with 23('2a₁') can be rationalised due to the greater $\angle \text{H-Nb-H}$ bond angle in $\text{CpNb}(\text{NR})\text{H}_2$ (104.6° c.f. 97.1° in Cp_2ZrH_2).

The final Mulliken populations of $\text{CpNb}(\text{NMe})\text{H}_2$, are comparable with those of Cp_2ZrH_2 , with the total electron transfer from hydride ligands to the metal fragment of 1.10 electrons (c.f. 1.05 electrons in Cp_2ZrH_2).

3.5.5 Interaction of $[\text{Cp}_2\text{Zr}]^{2+}$ with Two Chloride Ligands.

The interaction of two chloride ligands with the bent $[\text{Cp}_2\text{Zr}]^{2+}$ fragment, show a somewhat different picture to the hydride interaction, due to the presence of lone pairs on the chloride ligands. The correlation diagram is shown in Figure 3.12. The bonding to the chloride ligands consists mainly of interactions between Cl 3s, 3p_z and 3p_y with all three of the low lying zirconium unfilled orbitals. Table 3.9, shows the inter-fragment Mulliken overlap population in terms of % of total chloride (s,3p) overlap.

| Metal Fragment MO | % of Total Overlap |
|----------------------------|--------------------|
| 27(LUMO)(1a ₁) | 24.2 |
| 28(b ₂) | 36.3 |
| 29(2a ₁) | 30.2 |
| 30(b ₁) | 5.0 |
| 31(a ₂) | 4.2 |

Table 3.9

The strongest bonding interaction, in terms of inter-fragment Mulliken overlap population, is with metal fragment MO 28(b₂), leading to formation of σ -type bonding complex MO 25. Metal fragment MO's 27(1a₁) and 29(2a₁) interact with Cl 3p_z AO's, leading to metal complex MO 28. Small bonding interactions are also found in complex MO's 29-32. Complex SHOMO(33) and HOMO(34) consist of mainly Cl 3p_x and Cl 3p_y character (71% and 51% respectively). From the Mulliken population (Table 3.10) the total charge transfer from the Cl⁻ to the zirconium fragment is 0.61 electrons per chloride, mainly into Metal fragment MO 28(b₂), from Cl 3p_z and 3p_y.

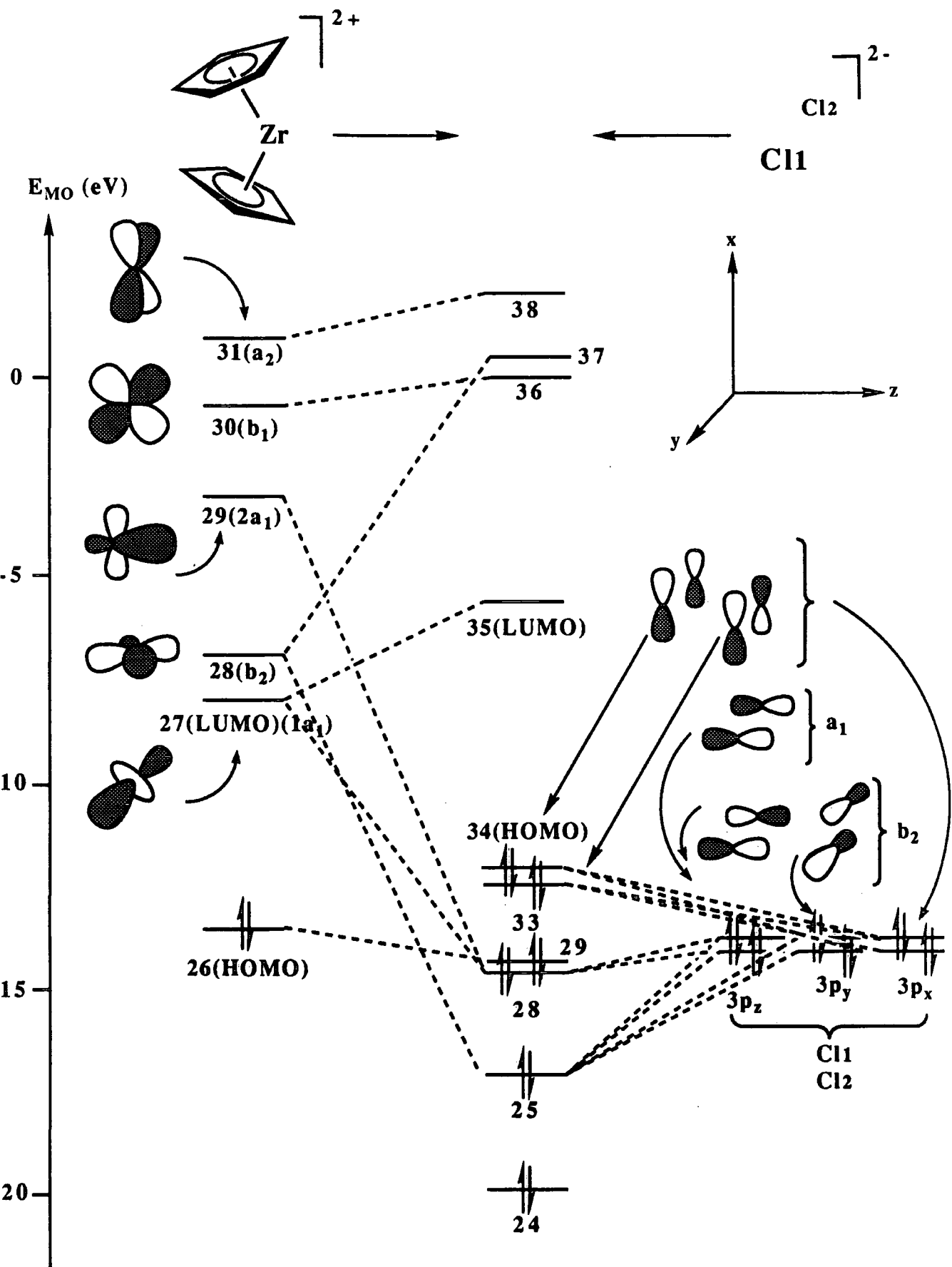


Figure 3.12, Molecular orbital correlation diagram, showing the the fragments $[Cp_2Zr]^{2+}$ and $2Cl^-$. Representations of the fragment MO's show the most important orbital contributions only.

| Fragment Orbital | Mull. Pop ⁿ · Before Inter. | Mull. Pop ⁿ · After Inter. |
|-------------------------------|--|---------------------------------------|
| Cl 3s | 2 | 1.95 |
| Cl 3p _x | 2 | 1.95 |
| Cl 3p _y | 2 | 1.76 |
| Cl 3p _z | 2 | 1.73 |
| Zr 26(HOMO) | 2 | 1.98 |
| Zr 27(LUMO)(1a ₁) | 0 | 0.37 |
| Zr 28(b ₂) | 0 | 0.53 |
| Zr 29(2a ₁) | 0 | 0.30 |

Table 3.10

These results are in agreement with the bonding descriptions obtained by Zhu and Kostic²¹.

3.5.6 Interaction of [CpNb(NMe)]²⁺ with Two Chloride Ligands.

The interaction of the [CpNb(NMe)]²⁺ fragment with two chloride ligands, produces a closely related, but more complex, correlation diagram to that of Cp₂ZrCl₂ (Figure 3.13). The most important interactions are again those between chloride AO's, 3p_z and 3p_y, but there is considerably more overlap between the higher unfilled fragment MO's 24(b₁) and 25(a₂), and Cl⁻ 3p_z and 3p_x, at the expense of overlap with MO 23(2a₁) This possibly reflects the greater steric accessibility of these orbitals, which are out of the equatorial plane, for [CpNb(NMe)]²⁺

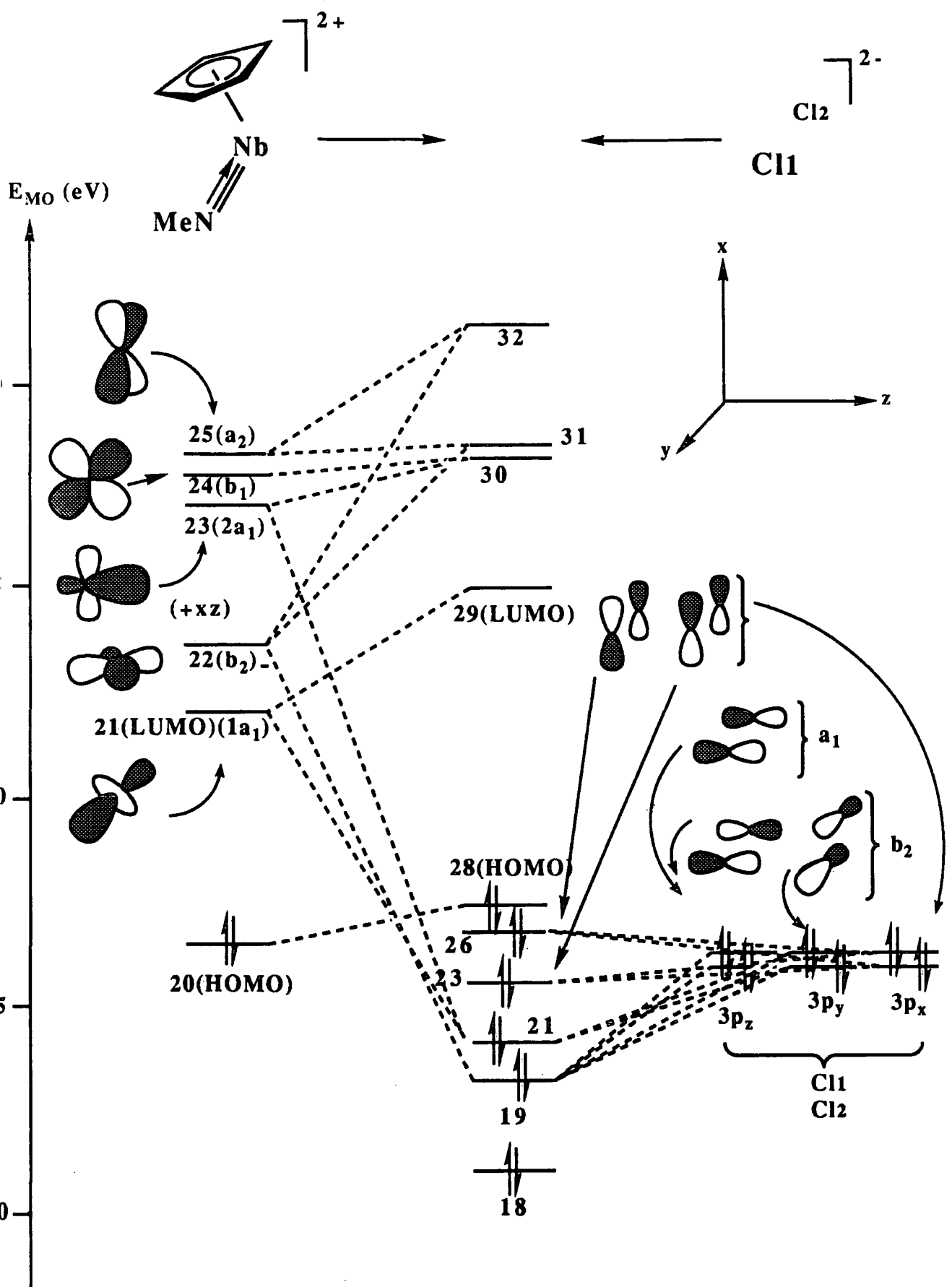


Figure 3.13, Molecular orbital correlation diagram, showing the interactions of the fragments $[\text{CpNb(NMe)}_2]^+$ and 2Cl^- . Representations of the fragment MO's show the most important orbital contributions only.

| Metal Fragment Orbital ^a | % of Total Overlap |
|-------------------------------------|--------------------|
| 21(LUMO)(1a ₁) | 25.6 |
| 22(b ₂) | 33.2 |
| 23(2a ₁) | 20.2 |
| 24(b ₂) | 13.8 |
| 25(a ₂) | 7.2 |

^aThe symmetry labels, although not directly valid for the [CpNb(NMe)]²⁺ are included to allow direct comparison with [Cp₂Zr].

Table 3.11

The total Mulliken population suggests stronger bonding between the chloride ligand AO's and metal fragment MO's 24(b₁) and 25(a₂), as well as stronger overall chloride bonding than found for Cp₂ZrCl₂. The total charge transfer from chloride to metal fragment is 0.65 electrons (Table 3.12). These results are supported by the observation of shorter (and hence stronger) M-Cl bonds for CpNb(NMe)Cl₂, (Nb-Cl = 2.35Å) than for Cp₂ZrCl₂ (Zr-Cl = 2.44Å).

| Fragment Orbital | Mull. Pop ⁿ . Before Inter. | Mull. Pop ⁿ . After Inter. |
|-------------------------------|--|---------------------------------------|
| Cl 3s | 2 | 1.95 |
| Cl 3p _x | 2 | 1.93 |
| Cl 3p _y | 2 | 1.74 |
| Cl 3p _z | 2 | 1.73 |
| Nb 20(HOMO) | 2 | 1.98 |
| Nb 21(LUMO)(1a ₁) | 0 | 0.42 |
| Nb 22(b ₂) | 0 | 0.55 |
| Nb 23(2a ₁) | 0 | 0.21 |
| Nb 24(b ₁) | 0 | 0.15 |
| Nb 25(a ₂) | 0 | 0.11 |

Table 3.12



3.5.7 Composition of the Frontier Orbitals of Cp_2ZrCl_2 and $\text{CpNb}(\text{NMe})\text{Cl}_2$.

The compositions of the frontier orbitals of the complex MO's of Cp_2ZrCl_2 and $\text{CpNb}(\text{NMe})\text{Cl}_2$ are collected for comparison purposes in Table 3.13.

| $\text{CpNb}(\text{NMe})\text{Cl}_2$: Composition, % | | | Cp_2ZrCl_2 : Composition, % | | |
|---|---------|---|---|--------|--|
| Orbital | Ligands | Metal | Orbital | Ligand | Metal |
| 8(HOMO) | 95 | 5 d_{xz} | 34(HOMO) | 97 | 3 d_{xz} |
| 9(LUMO) | 25 | 58 d_{y^2} , 9 $d_{z^2-x^2}$, 8 p_z | 35(LUMO) | 28 | 61 d_{y^2} , 7 $d_{z^2-x^2}$, 4 p_z |
| 10 | 31 | 57 d_{xz} , 10 p_x , 2 $d_{z^2-x^2}$ | 36 | 30 | 64 d_{xz} , 6 p_x |
| 11 | 43 | 43 d_{xy} , 11 d_{yz} , 3 p_y | 37 | 53 | 37 d_{yz} , 13 p_y |
| 12 | 36 | 34 d_{yz} , 21 d_{xy} , 9 p_y | 38 | 36 | 64 d_{xy} |
| 13 | 22 | 46 $d_{z^2-x^2}$, 20 p_x , 7 p_z , 5 d_{y^2} | 39 | 27 | 58 $d_{z^2-x^2}$, 7 d_{y^2} , 8 p_z |

Table 3.13

It can be seen that the LUMO's of $\text{CpNb}(\text{NMe})\text{Cl}_2$ and Cp_2ZrCl_2 are very similar in terms of composition; this, of course, is particularly relevant to the binding of donor ligands. Differences between the complexes only become noticeable in the higher unoccupied MO's.

3.6 A Comparison of the Electronic Structure of $\text{Cp}^*\text{Ta}(\eta^2\text{-CHPMe}_2)\text{X}_2$ with Cp_2ZrX_2 and $\text{CpNb}(\text{NR})\text{X}_2$.

In order to further probe the isolobal analogy between half-sandwich Group 5 complexes and metallocenes of the Group 4 metals, we decided to examine the frontier orbitals of the $[\text{Cp}^*\text{Ta}(\eta^2\text{-CHPMe}_2)]$ fragment to see if similarities exist with $[\text{CpNb}(\text{NR})]$ and $[\text{Cp}_2\text{M}]$.

The bond lengths found in the Ta(η^2 -CHPMe₂) metallacycle are consistent with contributions from canonical forms (I) and (II) (Figure 3.14)²², with calculations suggesting that (I) is the most appropriate representation of the bonding²³. Here, (I) may be regarded as a 4 electron phosphino-carbene and bears close similarity to an imido group, the lone pair now effectively located on the remote phosphorus atom.

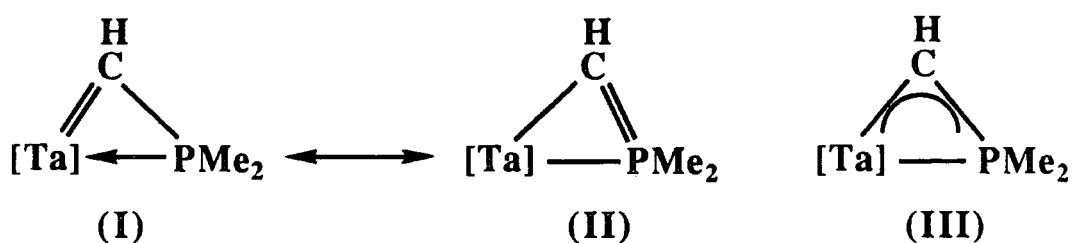


Figure 3.14, *Canonical forms of metal-(η^2 -CHPMe₂) ligand bonding.*

Previously, Fenske-Hall-type molecular orbital calculations have been used to study Nb(η^2 -CHPMe₂) bonding using Cp*Nb(η^2 -CHPMe₂)Cl₂ as a model complex²³. The most important bonding interactions of this calculation are shown schematically in Figure 3.15.

The interactions are complex because of the asymmetric nature of the η^2 -CHPMe₂ ligand, but similarities can be seen between the imido and CHPMe₂ ligand; the principal d-orbitals used in binding both ligands are the same ($d_{x^2-y^2}$, d_{xy} and d_{xz}) (Figure 3.16), and the net transfer of charge from the metal to ligand species (if considered neutral) is 0.27 electrons in the phosphine species c.f. 0.35 in the imido species.

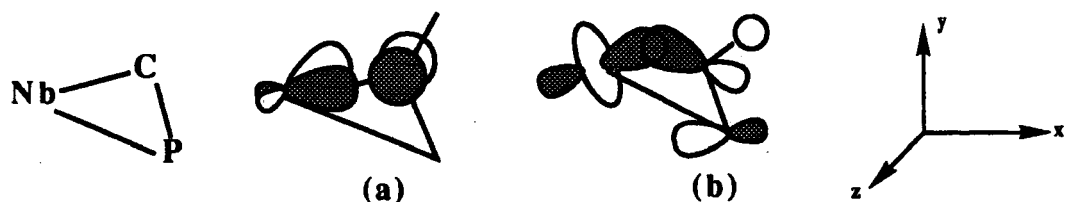


Figure 3.16, *Schematic representations between (a) MO's 37-13, and (b) MO's 38 -12 of [Cp*NbCl₂] and [CHPMe₂] fragments respectively.*

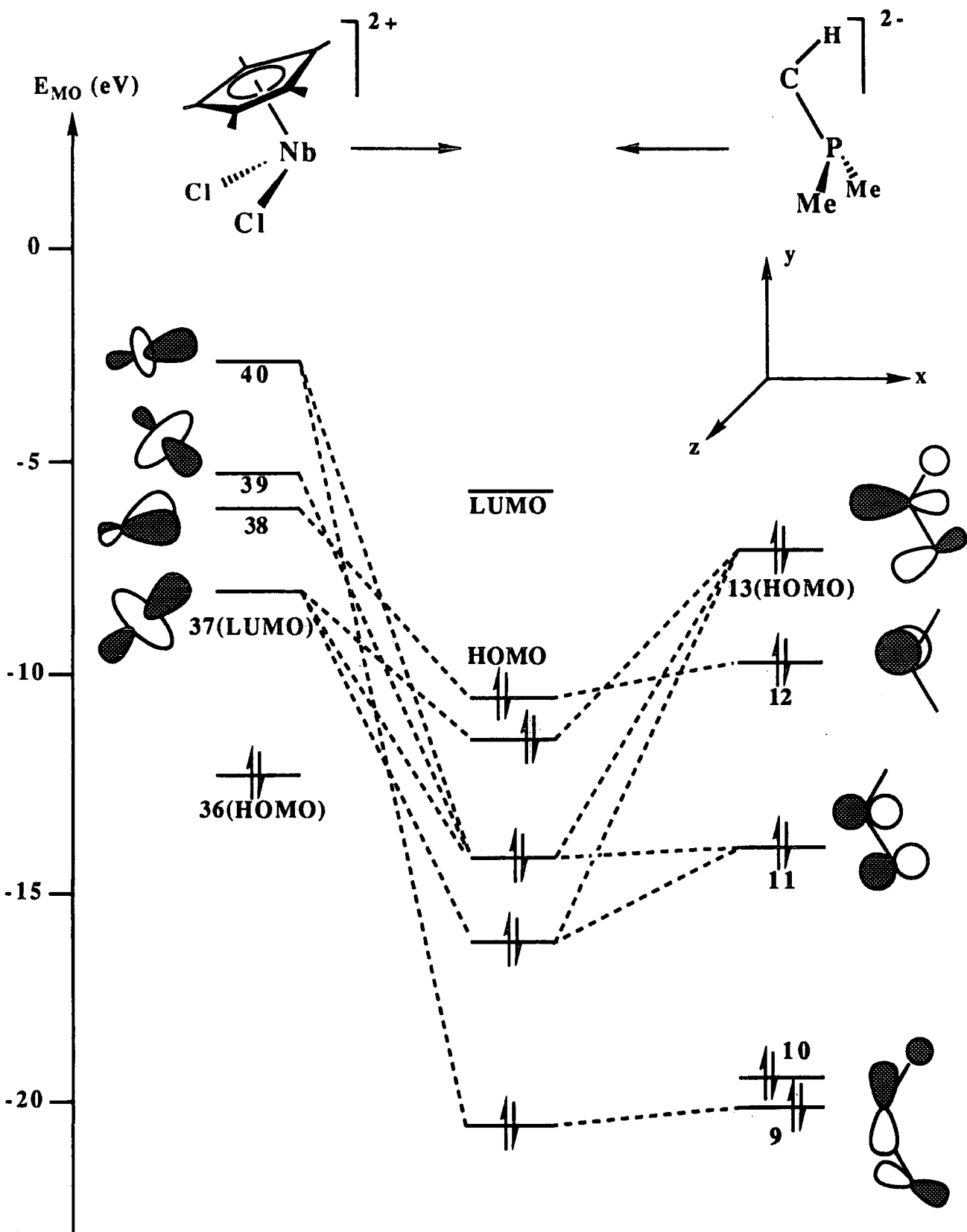


Figure 3.15, Molecular orbital correlation diagram, showing interaction of the fragments $[Cp^*NbCl_2]^{2+}$ and $[\eta^2-CHPMe_2]^{2-}$.

A series of calculations on the model complexes $\text{CpNb}(\eta^2\text{-CHPMe}_2)\text{X}_2$ ($\text{X} = \text{H,Cl}$) are discussed below. The axes used for these calculations are illustrated in Figure 3.17, chosen for clarity to allow a direct comparison with the $\text{CpNb}(\text{NR})\text{X}_2$ and Cp_2ZrX_2 complexes discussed previously.

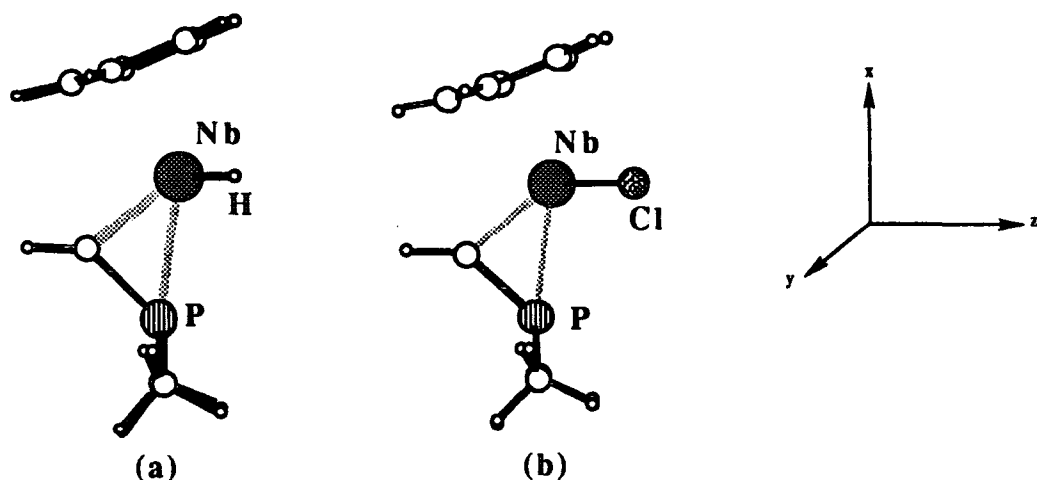


Figure 3.17, Axial framework for FHMO calculations on model complexes;
 (a) $\text{CpNb}(\eta^2\text{-CHPMe}_2)\text{H}_2$ and (b) $\text{CpNb}(\eta^2\text{-CHPMe}_2)\text{Cl}_2$.

3.6.1 A Comparison of the Frontier Orbitals of the $[\text{CpNb}(\text{NMe})]^{2+}$, $[\text{Cp}_2\text{Zr}]^{2+}$ and $[\text{CpNb}(\eta^2\text{-CHPMe}_2)]^{2+}$ Fragments.

The frontier orbitals of $[\text{CpNb}(\text{NMe})]^{2+}$, $[\text{Cp}_2\text{Zr}]^{2+}$ and $[\text{CpNb}(\eta^2\text{-CHPMe}_2)]^{2+}$, in terms of % AO composition, are compared in Table 3.14. It can be seen that $[\text{CpNb}(\eta^2\text{-CHPMe}_2)]^{2+}$ possesses very similar contributions to the frontier orbitals with the main exception being MO 31, which apparently has a much reduced metal orbital contribution. Since this is a relatively high lying empty orbital, it is not expected to have a strong influence on the bonding of the metal fragment to ligands.

| [Cp ₂ Zr] ²⁺ : Composition, % | | | [CpNb(NMe)] ²⁺ : Composition, % | | | [CpNb(η ² -CHPMe ₂)] ²⁺ : Composition, % | | |
|---|---------|---|--|---------|---|--|---------|---|
| Orbital | Ligands | Metal | Orbital ^a | Ligands | Metal | Orbital ^a | Ligands | Metal |
| 27(1a ₁) | 16 | 84 d _{y2} , 5 s | 21(1a ₁) | 12 | 79 d _{y2} , 9 s | 27(1a ₁) | 16 | 70 d _{y2} , 12 s, 2 d _{z²-x²} |
| 28(b ₂) | 27 | 66 d _{yz} , 7 p _y | 22(b ₂) | 41 | 57 d _{yz} , 2 d _{xy} | 28(b ₂) | 38 | 59 d _{yz} , 3 p _y |
| 29(2a ₁) | 14 | 36 d _{z²-x²} , 33 s, 17 p _z | 23(2a ₁) | 24 | 23 d _{z²-x²} , 19 d _{xz} , 18 s, 14 p _z , 2 p _x | 29(2a ₁) | 25 | 36 d _{z²-x²} , 18 s, 15 p _z , 6 d _{xz} |
| 30(b ₁) | 40 | 60 d _{xz} , 7 p _y | 24(b ₁) | 21 | 35 d _{xz} , 17 s, 14 p _x , 7 d _{z²-x²} , 6 p _z | 30(a ₂) | 36 | 55 d _{xy} , 9 p _y |
| 31(a ₂) | 40 | 60 d _{xy} | 25(a ₂) | 53 | 55 d _{xy} , 3 p _x , 2 d _{yz} | 31(b ₁) | 76 | 14 d _{xz} , 5 s, 5 p _x |

^a The symmetry labels, although not applicable to a fragment of this symmetry, are included to allow direct comparison with [Cp₂Zr]²⁺.

Table 3.14, Composition of the frontier orbitals of metal fragments [Cp₂Zr]²⁺, [CpNb(NMe)]²⁺ and [CpNb(η²-CHPMe₂)]²⁺.

3.6.2 Interaction of $[\text{CpNb}(\eta^2\text{-CHPMe}_2)]^{2+}$ with Two Hydride Ligands.

The interaction of metal fragment $[\text{CpNb}(\eta^2\text{-CHPMe}_2)]^{2+}$ with two hydride ligands is illustrated in correlation diagram shown in Figure 3.18. The overall picture of hydride bonding is very similar to that seen in $\text{CpNb}(\text{NMe})\text{H}_2$ (Figure 3.11). The strongest interaction, in terms of Mulliken overlap population, is found between hydride 1s orbitals and metal fragment MO 28, an orbital mainly consisting of d_{xy} character (Table 3.14). A substantial overlap is also found between hydride 1s AO's and MO 27 and 28. These interactions are found in low lying complex MO's 10, 7 and 9 respectively. Table 3.15, illustrates the % of total overlap of metal complex empty frontier MO's with hydride 1s AO's.

| Metal Fragment MO ^a | % of Total Overlap |
|--------------------------------|--------------------|
| 27(LUMO)(1a ₁) | 23.9 |
| 28(b ₂) | 52.5 |
| 29(2a ₁) | 22.9 |
| 30(b ₁) | 0.7 |
| 31(a ₂) | 0 |

^aThe symmetry labels, although not applicable to the $[\text{CpNb}(\eta^2\text{-CHPMe}_2)]^{2+}$ fragment, are included to allow direct comparison with $[\text{Cp}_2\text{Zr}]$.

Table 3.15

The $\text{CpNb}(\eta^2\text{-CHPMe}_2)\text{H}_2$ complex HOMO and LUMO are similar to those seen in both Cp_2ZrH_2 and $\text{CpNb}(\text{NMe})\text{H}_2$, the LUMO consisting mainly of d_{y^2} character, of a₁ symmetry. A comparison of the % composition of the frontier orbitals of all three species is presented in Table 3.16.

Interestingly, although the composition of the LUMO in all three complexes are similar, mostly d_{y^2} in character, the higher unoccupied MO's of $\text{CpNb}(\eta^2\text{-CHPMe}_2)\text{H}_2$ differ considerably.

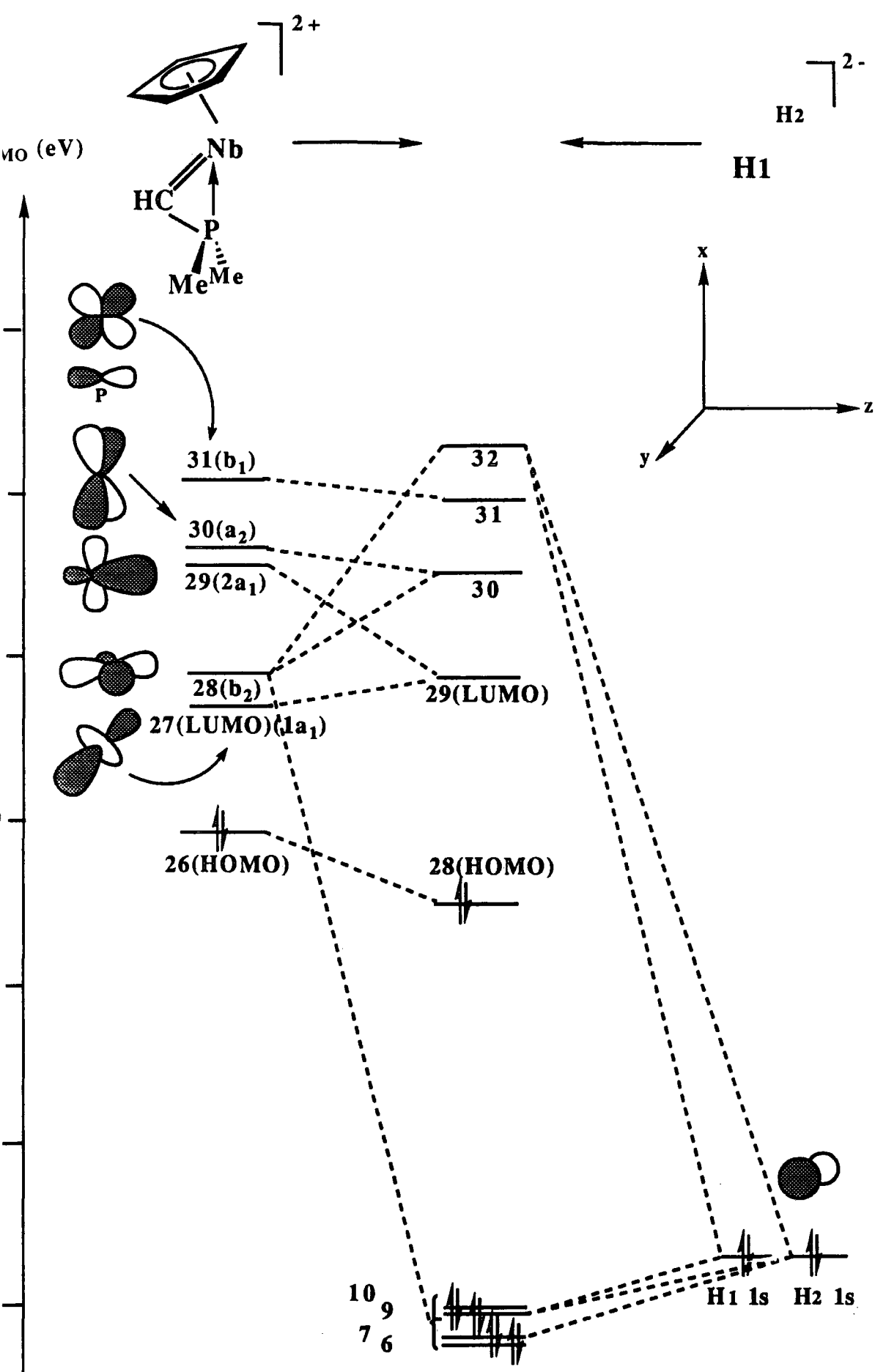


Figure 3.18, *Molecular orbital correlation diagram, showing the interactions of the fragments $[\text{CpNb}(\eta^2\text{-CHPMe}_2)]^{2+}$ and 2H^+ . Representations of the fragment MO's show the most important orbital contributions only.*

| Cp₂ZrH₂: Composition, % | | | CpNb(NMe)H₂: Composition, % | | | CpNb(η^2-CHPMe₂)H₂: Composition, % | | |
|--|----------------|---|---|----------------|--|---|----------------|---|
| Orbital | Ligands | Metal | Orbital | Ligands | Metal | Orbital | Ligands | Metal |
| 28(HOMO) | 89 | 8 d _{y2} , 3 s | 22(HOMO) | 94 | 4 p _y , 2 d _{xy} | 28(HOMO) | 97 | 3 d _{xz} |
| 29(LUMO) | 18 | 66 d _{y2} , 11 d _{z2-x2} , 5 p _z | 23(LUMO) | 18 | 58 d _{y2} , 14 d _{z2-x2} , 10 p _z | 29(LUMO) | 19 | 53 d _{y2} , 14 d _{z2-x2} , 10p _z |
| 30 | 28 | 66 d _{xz} , 6 p _x | 24 | 28 | 59 d _{xz} , 12 p _x | 30 | 37 | 46 d _{xy} , 10 d _{yz} , 7 p _y |
| 31 | 41 | 55 d _{xy} , 3 d _{yz} , 1 p _y | 25 | 40 | 54 d _{xy} , 4 d _{yz} , 2 p _y | 31 | 87 | 7 d _{z2-x2} , 3 d _{y2} , 3 d _{xz} |
| 32 | 58 | 23 d _{yz} , 11 p _y , 8 d _{xy} | 26 | 46 | 27 d _{yz} , 14 p _y , 13 d _{xy} | 32 | 61 | 24 d _{yz} , 8 p _y , 7 d _{xy} |
| 33 | 31 | 54 d _{z2-x2} , 9 p _z , 6 d _{y2} | 27 | 22 | 45 d _{z2-x2} , 19 p _x , 9 p _z , 5 d _{y2} | 33 | 62 | 19 d _{xz} , 13 d _{z2-x2} , 6 p _z |

Table 3.16, Composition of the frontier orbitals of Cp₂ZrH₂, CpNb(NMe)H₂ and CpNb(η^2 -CHPMe₂)H₂.

Weaker hydride bonding in $\text{CpNb}(\eta^2\text{-CHPMe}_2)\text{H}_2$ compared to $\text{CpNb}(\text{NMe})\text{H}_2$ and Cp_2ZrH_2 , is evident from comparison of total Mulliken overlap population and final Mulliken population. The electron transfer from the hydride ligands (2H^-) to metal fragment MO's of these model species is collected in Table 3.17. However, it should be noted that, whereas Cp_2ZrH_2 is a stable species, $\text{CpNb}(\text{NMe})\text{H}_2$ and $\text{CpNb}(\eta^2\text{-CHPMe}_2)\text{H}_2$ are likely to require an additional L donor ligand to stabilise the complex, as observed for $\text{Cp}^*\text{Ta}(\text{NR})\text{H}_2(\text{PMe}_3)^{24}$ ($\text{R} = \text{tBu, Np}$) and $\text{Cp}^*\text{Ta}(\eta^2\text{-CHPMe}_2)\text{H}_2(\text{PMe}_3)^{22, 28}$.

| Complex | Tot. e ⁻ Transfer | Transfer to met. Frag. MO | | |
|---|------------------------------|---------------------------|----------------|-----------------|
| | | 1a ₁ | b ₂ | 2a ₁ |
| Cp_2ZrH_2 | 1.05 | 0.22 | 0.69 | 0.26 |
| $\text{CpNb}(\text{NMe})\text{H}_2^{\text{a}}$ | 1.11 | 0.36 | 0.70 | 0.13 |
| $\text{CpNb}(\eta^2\text{-CHPMe}_2)\text{H}_2^{\text{a}}$ | 0.57 | 0.20 | 0.47 | 0.13 |

^aThe symmetry labels, although not applicable to a model species of this symmetry, are included to allow direct comparison with Cp_2ZrH_2 .

Table 3.17

3.6.3 The Frontier Orbitals of $\text{CpNb}(\eta^2\text{-CHPMe}_2)\text{Cl}_2$

The composition of the frontier MO's of $\text{CpNb}(\eta^2\text{-CHPMe}_2)\text{Cl}_2$, are shown in Table 3.18.

| Orbital | Composition, % | |
|----------|----------------|--|
| | Ligands | Metal |
| 34(HOMO) | 84 | 6 $d_{z^2-x^2}$, 7 d_{xz} , 3 p_x |
| 35(LUMO) | 25 | 52 d_{y^2} , 11 $d_{z^2-x^2}$, 4 d_{xz} , 8 p_z |
| 36 | 39 | 35 d_{xz} , 20 d_{yz} , 6 p_y |
| 37 | 72 | 14 $d_{z^2-x^2}$, 4 d_{y^2} |
| 38 | 53 | 27 d_{yz} , 20 d_{xy} |
| 39 | 49 | 23 d_{xz} , 15 $d_{z^2-x^2}$, 5 s , 4 d_{y^2} , 4 p_x |

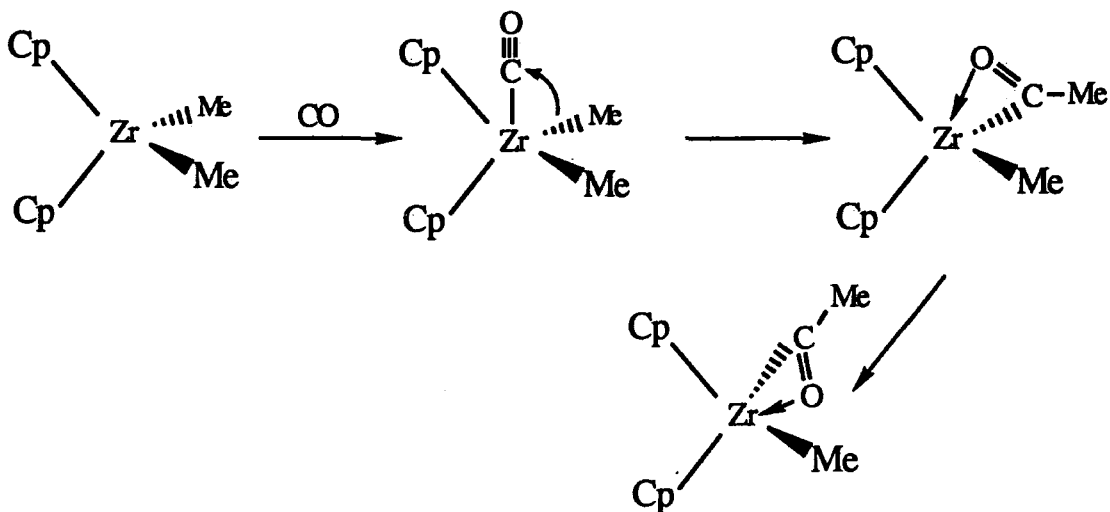
Table 3.18

Overall, their compositions are similar to those of Cp_2ZrCl_2 and $CpNb(NMe)Cl_2$ (for comparison see Table 3.13, section 3.4.7). In particular, the LUMO is mainly d_{y^2} in character.

3.7 Discussion and Summary

The calculations presented in this chapter have revealed close similarities between the electronic structure of complexes of the type Cp_2ZrX_2 , $CpNb(NR)X_2$ and $CpNb(\eta^2-CHPMe_2)X_2$, and therefore suggest that $CpNb(NR)X_2$ and $CpNb(\eta^2-CHPMe_2)X_2$ complexes are likely to mirror, in a broad sense, the type of reactivity observed for Cp_2ZrX_2 .

A much debated topic has been the site of attack by $2e^-$ donor ligands on Cp_2ZrX_2 species. It has been shown that attack of carbon monoxide on Cp_2ZrMe_2 occurs at the lateral site, although the subsequent rearrangement of the resultant η^2 -acyl product to the thermodynamically preferred form, apparently arising from central attack, led, for sometime, to conflicting opinions²⁵ (Scheme 3.1).



Scheme 3.1, *The reaction of Cp_2ZrMe_2 with carbon monoxide.*

The dichotomy arose due to the close energies of the LUMO and SLUMO coupled with the steric accessibility of these vacant orbitals. Proponents of 'central attack' argued that this site represented the pathway of least steric hindrance.

Zhu and Kostic have since shown that the site of attack will depend markedly on the X-M-X inter ligand angle ϕ ²¹. As ϕ increases, the LUMO d_z^2 character (i.e. vacant lateral orbital) decreases, whereas the $d_{x^2-y^2}$ character (i.e. vacant central orbital) increases making central attack more favourable (Figure 3.19).

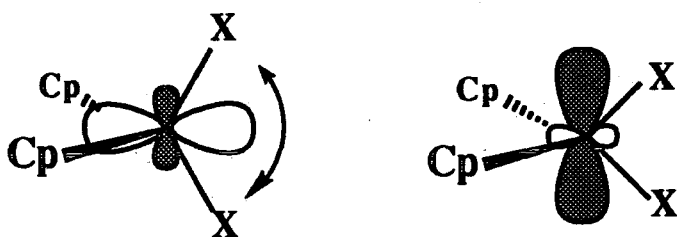


Figure 3.19, *Changing character of the LUMO of Cp_2MX_2 species on widening of X-M-X angle ϕ .*

For $CpNb(NR)Cl_2$, attack clearly occurs at the lateral site as shown by the crystal structure of $CpNb(NMe)Cl_2(PMe_3)$. In all structurally characterised species of the type $CpM(NR)X_2$ ($M = Nb, Ta$; $R = Me, ^tBu, 2,6\text{-}^iPr_2C_6H_3$; $X = Me, Cl$) the X-M-X angle lies in the range $104\text{-}108^\circ$, a little larger than that found in complexes of the type

Cp_2ZrX_2 ($\text{X} = \text{F}, \text{Cl}, \text{I}$) (94-96°). Unfortunately, phosphine adducts of Cp_2ZrCl_2 are not accessible²⁶. Carbonylation of the dichloride also does not occur which is perhaps less surprising for such a d^0 species. Zhu and Kostic have offered the explanation that repulsive interactions between the carbon lone pair and the filled chloride p-orbitals account for this lack of reactivity. A similar steric explanation may also account for the lack of reactivity between Cp_2ZrCl_2 and tertiary phosphines, although the larger size of these ligands may lead to additional steric repulsions with the chloride and C_5H_5 ligands (Figure 3.20).

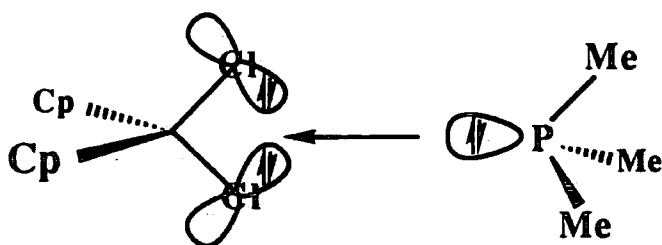


Figure 3.20

The alkylimido ligand is therefore presumed to be sufficiently small to allow PMe_3 to bind, although it is noticeable that the phosphine binds less strongly to the *t*-butyl imido complex and only weakly to the 2,6-diisopropylphenyl imido derivative²⁷.

The results of the calculations on $\text{Cp}^*\text{Ta}(\eta^2\text{-CHPMe}_2)\text{X}_2$ also suggest that lateral attack should dominate the reaction pathway with donor ligands. However, $\text{Cp}^*\text{Ta}(\eta^2\text{-CHPMe}_2)\text{H}_2(\text{PMe}_3)$ exists with the PMe_3 ligand occupying the central site; to date it has not proved possible to determine whether this is the kinetic or thermodynamic product²⁸. $\text{Cp}^*\text{Ta}(\eta^2\text{-CHPMe}_2)\text{X}_2$ also interacts, albeit weakly, with PMe_3 ²². Again it has not proved possible to determine whether the PMe_3 occupies a lateral or central site.

In general, the relationships established here are likely to be of considerable use in further development of the derivative chemistry of $\text{CpM}(\text{NR})\text{X}_2$ and $\text{Cp}^*\text{Ta}(\eta^2\text{-CHPMe}_2)\text{H}_2(\text{PMe}_3)$.

3.8 References.

1. R.F. Fenske and M.B. Hall, *Inorg Chem.*, 1972, **11**, 768.
2. V.C. Gibson and D.N. Williams, *Polyhedron*, 1989, **8**, 1819; this thesis, *Chapter 2*.
3. V.C. Gibson, T.P. Kee and W. Clegg, *J. Chem. Soc., Chem. Commun.*, 1990, 313.
4. (a) R.F. Fenske, K.G. Caulton, D.D. Radtke and C.C. Sweeny, *Inorg. Chem.*, 1966, **5**, 951.
(b) R.F. Fenske and D.D. Radtke, *Inorg. Chem.*, 1968, **7**, 479.
(c) K.G. Caulton and R.F. Fenske, *Inorg. Chem.*, 1968, **7**, 1273.
5. R.S. Mulliken, *J. Chem. Phys.*, 1955, **23**, 1841.
6. J.C. Slater, '*Quantum Theory of Atomic Structure*', Vol I, McGraw, New York, N.Y., 1960, p322.
7. H. Basch and H.B. Gray, *Inorg. Chem.*, 1967, **6**, 639.
8. I.H. Hillier, *J. Chem. Soc. (A)*, 1969, 878.
9. C.C.J. Roothaan, *Rev., Mod. Phys.*, 1951, **23**, 69.
10. P.O. Lowdin, *J. Chem. Phys.*, 1950, **18**, 365.
11. A. Ralston, '*A First Course in Numerical Analysis*', McGraw-Hill, New-York, N.Y., 1965, p348.
12. K. Prout, T.S. Cameron, R.A. Forder, S.R. Critchley, B. Denton and G.V. Rees, *Acta Crystallor.*, 1974, **B30**, 2290.
13. (a) W.A. Nugent, *Inorg Chem.*, 1983, **22**, 965.
(b) G.Schoettel, J. Kress and J.A. Osborn, *J. Chem. Soc., Chem. Commun.*, 1989, 1062.
(c) R.R. Schrock, J.S. Murdzek, G.C. Bazan, J. Robbins, M. DiMare and M.B. O'Regan, *J. Am. Chem. Soc.*, 1990, **112**, 3875.
14. C.J. Ballhausen and J.P. Dahl, *Acta Chem. Scand.*, 1961, **15**, 1333.
15. N.W. Alcock, *J. Chem. Soc. (A)*, 1967, 2001.

16. H.H. Brintzinger and L.S. Bartell, *J. Am. Chem. Soc.*, 1970, **92**, 1105; H.H. Brintzinger L.L. Lohr Jr. and K.L.T. Wong, *J. Am. Chem. Soc.*, 1975, **97**, 5146.
17. J.C. Green, M.L.H. Green and C.J. Prout, *Chem. Commun.*, 1972, 421; M.L.H. Green, *Pure Appl. Chem.*, 1972, **30**, 373.
18. J.L. Petersen and L.F. Dahl, *J. Am. Chem. Soc.*, 1974, **96**, 2248; *Ibid*, 1975, **97**, 6416; J.L. Petersen, D.L. Lichtenberger, R.F. Fenske and L.F. Dahl, *J. Am. Chem. Soc.*, 1975, **97**, 6433.
19. J.C. Green, S.E. Jackson and B. Higgenson, *J. Am. Chem. Soc. Dalton Trans.*, 1975, 403.
20. J.W. Lauher and R. Hoffmann, *J. Am. Chem. Soc.*, 1976, **98**, 1729.
21. L. Zhu and N.M. Kostic, *J. Organomet. Chem.*, 1987, **335**, 395.
22. T.P. Kee, *Thesis*, Durham University, 1988, Chapter 4.
23. V.C. Gibson, H.M. Anstice, H.H. Fielding and C.E. Housecroft, *Unpublished Results*, 1988.
24. J. Mayer, C.J. Calvin and J.E. Bercaw, *J. Am. Chem. Soc.*, 1983, **105**, 2651.
25. G. Erker, *Acc. Chem. Res.*, 1984, **17**, 103.
26. J.A. Marsella, C.J. Curtis, J.E. Bercaw and K.G. Caulton, *J. Am. Chem. Soc.*, 1980, **102**, 7244.
27. V.C. Gibson and A.D. Poole, *Unpublished Results*, 1990.
28. T.P. Kee, V.C. Gibson and W. Clegg, *J. Organomet. Chem.*, 1987, **325**, C14.

CHAPTER FOUR

Multiply-Bonded Nitrogen Ligands to Mo, W and Re
Supported by Halide and Trialkylphosphine Ligation-
A Search for Bond-Stretch Isomers of Multiply-Bonded
Nitrogen Ligands.

4.1 Introduction.

The term "distortional isomerism" was first used by Chatt, Manojlovic-Muir and Muir in 1971 to describe two structures of *cis*-meridional $\text{Mo}(\text{O})\text{Cl}_2(\text{PR}_2\text{Ph})_3$ which differ in the length of the molybdenum-oxygen bond and molybdenum-chlorine bond *trans* to the oxo ligand¹. Hoffmann described this phenomenon as bond-stretch isomerism, and defined bond-stretch isomers as molecules which differ only in the length of one (or more) bonds and which are capable of existing not only in the solid state but also in solution².

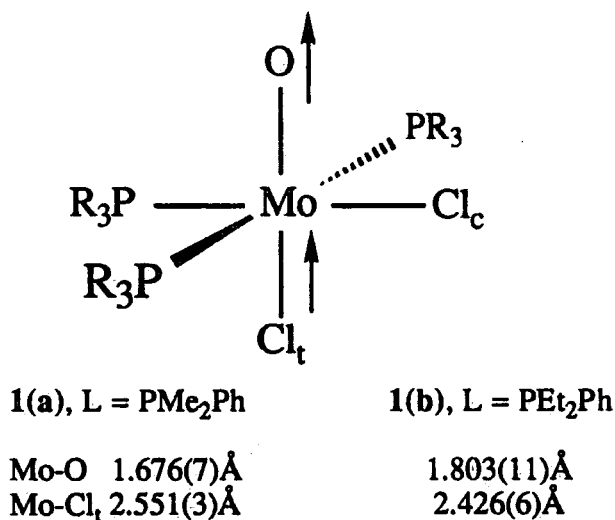


Figure 4.1, *The molecular structures of $\text{Mo}(\text{O})\text{Cl}_2\text{L}_3$ compounds.*

Compounds of the type 1a and 1b are not unique, a number of other structures have been reported with metal-ligand multiple bond distances differing by more than 0.1Å longer (Table 4.1), although differing ancillary ligands, and in some cases rather large e.s.d's accompanying the bond lengths, have hindered the development and understanding of this phenomenon. To date, only three systems with identical ligand sets have proved amenable to detailed examination. In addition to Chatt's molybdenum system, Wieghardt and co-workers have characterised, in both solid state and solution, two stable isomers of $[\text{LWOCl}_2]^+$ (L=N,N',N'' trimethyl-1,4,7-triazacyclononane)³,

| Complex | Form | M-L (Å) | d ⁰ | Ref |
|--|---------------------|-----------|----------------|-----|
| Mo(O)Cl ₂ (PMe ₂ Ph) ₃ | Blue | 1.676(7) | 2 | 4 |
| Mo(O)Cl ₂ (PMe ₂ Ph) ₃ | Green | 1.80(2) | | 5 |
| Mo(O)Cl ₂ (PEt ₂ Ph) ₃ | Green | 1.801(9) | | 6 |
| [Mo(O)(CN) ₄ (H ₂ O)](PPh ₄) ₂ | Green | 1.72(2) | 2 | 7 |
| [Mo(O)(CN) ₄ (H ₂ O)](AsPh ₄) ₂ | Blue | 1.60(2) | | 7 |
| [Mo(O)Cl(HBpz ₃) ₂](μ-O) | C ₁ form | 1.779(6) | 1 | 8 |
| [Mo(O)Cl(HBpz ₃) ₂](μ-O) | C ₂ form | 1.671(4) | | 8 |
| [Mo(O)(OH)(dppe) ₂] ⁺ BF ₄ ⁻ | | 1.883(5) | 2 | 9 |
| [Mo(O)Cl(dppe) ₂] ⁺ | | 1.708(12) | | 10 |
| [Mo(O)Br ₄]PPh ₄ | | 1.726(14) | 1 | 11 |
| [Mo(O)Cl ₄]AsPh ₄ | | 1.610(10) | | 12 |
| Mo(O) ₂ (ONCH ₂ CH ₂ CH ₂ CH ₂ CH ₂) ₂ | | 1.879(5), | 2 | 13 |
| Mo(O) ₂ (ONEt ₂) ₂ | | 1.701(5) | | 14 |
| | | 1.714(2), | | |
| | | 1.713(2) | | |
| [W(O)Cl ₂ (NMeCH ₂ CH ₂) ₃]PF ₆ | Blue | 1.719(18) | 1 | 3 |
| W(O)Cl ₂ (NMeCH ₂ CH ₂) ₃]PF ₆ | Green | 1.893(20) | | 3 |
| [Ru(O)Cl-C-(NMe) ₄ C ₁₀ H ₂₀]ClO ₄ | | 1.765(7) | 4 | 15 |
| [Ru(O)Cl(Py) ₄]ClO ₄ | | 1.862(8) | | 16 |
| [Nb(O)Cl ₅](AsPh ₄) ₂ | | 1.976(6) | 0 | 17 |
| [Nb(O)F ₅] ²⁻ | | 1.75(2) | | 18 |
| [Nb(O)Cl ₃ (PMe ₃) ₃] | Green | 1.929(6) | 0 | 19 |
| [Nb(O)Cl ₃ (PMe ₃) ₃] | Yellow | 1.781(6) | | 20 |
| Re(N)Cl ₂ (PEt ₂ Ph) ₃ | Yellow | 1.788(11) | 2 | 21 |
| Re(N)Cl ₂ (PMe ₂ Ph) ₃ | Yellow | 1.660(8) | | 22 |
| [Nb(S)Cl ₃ (PMe ₃) ₃] | Green | 2.296(1) | 0 | 19 |
| [Nb(S)Cl ₃ (PMe ₃) ₃] | Yellow | 2.194(2) | | 19 |

Table 4.1, Bond-stretch isomers and related species.

which at the time provided the best evidence that bond-stretch isomerism is not purely a crystal packing or disorder effect.

More recently, yellow and green isomers of $\text{Nb}(\text{O})\text{Cl}_3(\text{PMe}_3)_3$ ^{19,20} has been isolated. These seven coordinate d^0 species show the characteristic metal-oxygen and metal-chlorine bond length changes (Figure 4.2).

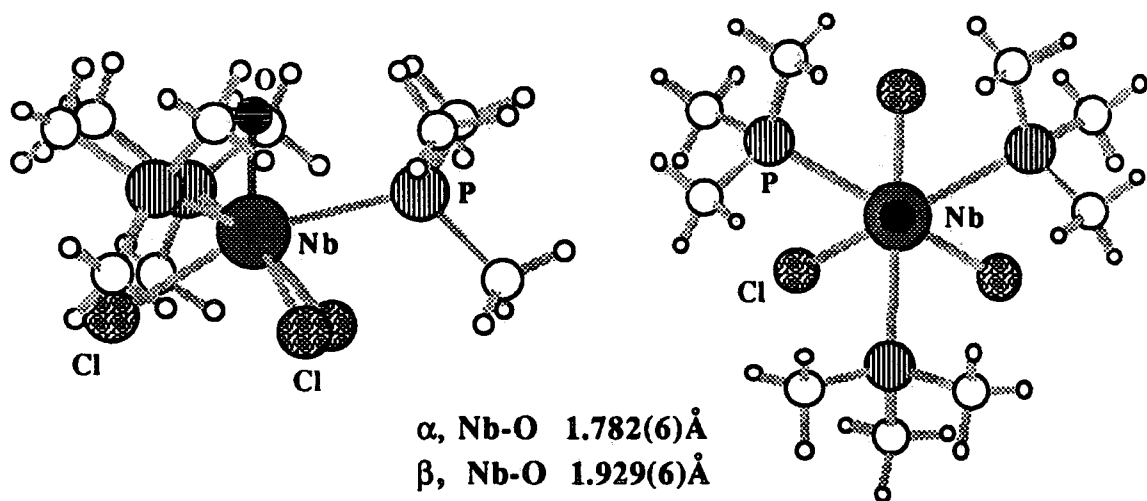
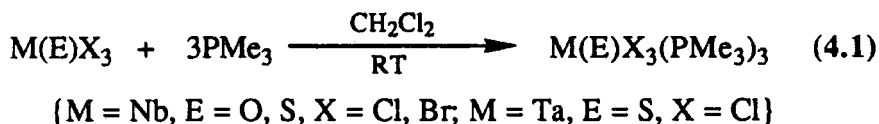


Figure 4.2, The molecular structure of α and β - $\text{Nb}(\text{O})\text{Cl}_3(\text{PMe}_3)_3$.

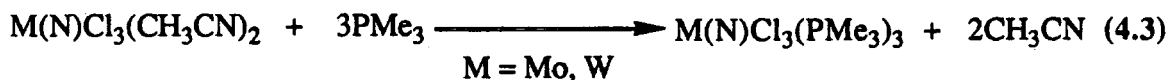
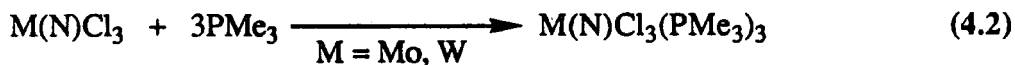
The isomers have been termed "alpha" and "beta", corresponding to the shorter, and longer niobium-oxygen distance respectively. Further examples, including tantalum and bromide derivatives have since been prepared and characterised by A.Shaw in this laboratory¹⁹. Following the discovery of this series of perfectly matched bond-stretch isomers, it was decided to attempt to prepare a nitrido analogue, since bond-stretch isomerism has been suggested to explain differing metal-nitrogen distances in isomers of the type $\text{Re}(\text{N})\text{Cl}_2(\text{PR}_3)_3$ ($\text{PR}_3 = \text{PMe}_2\text{Ph}, \text{PEt}_2\text{Ph}$)^{21,22}. Some further investigations of this rhenium system are presented. However, the principal objective of this chapter was to prepare nitrido compounds of molybdenum and tungsten of the type $\text{M}(\text{N})\text{Cl}_3(\text{PMe}_3)_3$ as direct analogues of the oxo and sulphido compounds mentioned previously.

4.2 Synthetic Strategy.

Previous work has shown that bond-stretch isomers of the general formula $M(E)X_3(PMe_3)_3$ ($M = Nb$; $E = O, S$; $X = Cl, Br$ and $M = Ta$; $E = S$; $X = Cl$) are most readily prepared via the reaction of $M(E)X_3$ or $M(E)X_3(CH_3CN)_2$ with trimethylphosphine^{19, 20} (Equation 4.1).

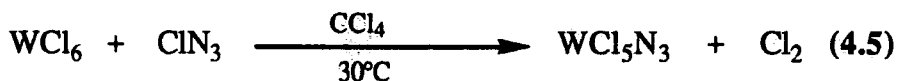


Thus, it was envisaged that the analogous nitrido compounds $M(N)Cl_3(PMe_3)_3$ ($M = Mo, W$) might prove accessible by treatment of $M(N)Cl_3$ or $M(N)Cl_3(CH_3CN)_2$ with trimethylphosphine (Equation 4.2 and 4.3).

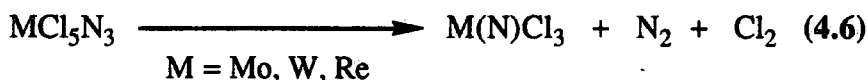


4.3 Preparation of the Nitrido Starting Materials, $M(N)Cl_3$ ($M = Mo, W$).

Transition metal nitrido species have been prepared by a number of methods²³. For example, metal halides react with chlorine azide to form the metal azide species²⁴⁻²⁶ shown in Equations 4.4 and 4.5.

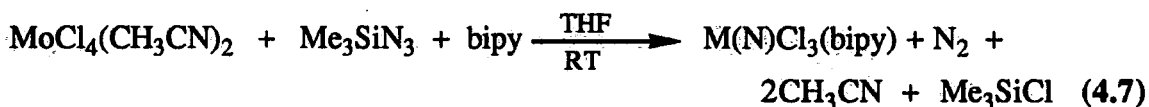


These metal azides of molybdenum, tungsten and rhenium, while potentially explosive in the solid state, undergo smooth decomposition in solution to form the corresponding nitrido species (Equation 4.6).



Other preparations involve the use of IN_3 ²⁷ and PhN_3 ²⁸, and more recently Seyferth and Taube have used NaN_3 to form base coordinated molybdenum nitrido species²⁹.

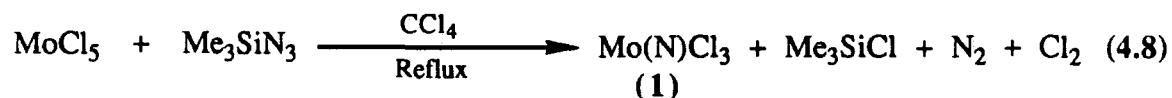
Chatt and Dilworth have reported that nitrido compounds of molybdenum can be obtained by reaction of trimethylsilylazide with the pentachloride dissolved in acetonitrile in the presence of donor molecules (e.g. Equation 4.7)³⁰.



We decided to employ trimethylsilylazide to prepare appropriate nitrido starting materials, primarily due to the potential hazards associated with some of the other starting materials, and the ease of purification of products, the Me_3SiCl side product being volatile and hence readily removed.

4.3.1 Synthesis of Mo(N)Cl₃ (1).

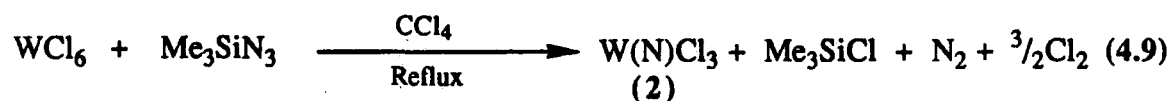
The reaction of MoCl₅ with one equivalent of trimethylsilylazide in refluxing carbon tetrachloride proceeds as suggested by Chatt and Dilworth³⁰ to yield Mo(N)Cl₃ as a red-brown solid (Equation 4.8).



Its infrared spectrum shows a strong absorption at 1045 cm⁻¹, attributable to the ν(Mo-N) stretch²⁴, and Mo-Cl vibrations in the range 412-317 cm⁻¹. (1) is air and moisture sensitive, decomposing in air to give 'molybdenum blues' (oxo-bridged species are suggested by strong bands in the region 600-900 cm⁻¹ in the infrared spectrum³¹). (1) is insoluble in aromatic solvents and only slightly soluble in chlorocarbon solvents. A single crystal X-ray structure carried out by Strähle has shown it to be tetrameric in the solid state with asymmetric Mo-N-Mo bridges³².

4.3.2 Synthesis of W(N)Cl₃ (2).

Orange moisture sensitive W(N)Cl₃ is obtained upon the reaction of WCl₆ with trimethylsilylazide in refluxing carbon tetrachloride according to Equation 4.9.



The infrared spectrum reveals two very strong bands at 1090cm⁻¹ and 1075 cm⁻¹ assignable to the ν(W-N) vibration²⁴, and characteristic W-Cl stretches below 400 cm⁻¹. (2) is less soluble than (1), consistent with the reported polymeric asymmetric bridged nitrogen structure³³.

4.3.3 Syntheses of $\text{Mo}(\text{N})\text{Cl}_3\text{L}_2$ ($\text{L} = \text{CH}_3\text{CN}$ (3), THF (4)).

In order to gain a convenient access to the alternative base adduct starting materials, analogous to those used in $\text{Nb}(\text{O})\text{Cl}_3(\text{PMe}_3)_3$ preparations, reactions of reduced metal halide species with trimethylsilylazide have been investigated. Thus, the reaction of molybdenum tetrachloridebis(acetonitrile) with trimethylsilylazide yields a red solution from which previously uncharacterised molybdenum nitridotrichloridebis(acetonitrile) (3) can be isolated as a red-brown microcrystalline solid. Characterisation was provided by elemental analysis and infra-red spectroscopy. In particular, analytical data showed that two acetonitrile ligands are coordinated to the metal centre, implying a six coordinate and therefore most likely mononuclear species (Figure 4.3) analogous to the niobium oxo derivative $\text{Nb}(\text{O})\text{Cl}_3(\text{CH}_3\text{CN})_2$ ³⁴. The infrared spectrum gives a very strong absorption at 1042 cm^{-1} assignable to the $\nu(\text{Mo}-\text{N})$ stretching vibration of a molybdenum-nitrogen triple bond²³. Bands for coordinated acetonitrile are observed at 2305 cm^{-1} and 938 cm^{-1} , corresponding to $\nu(\text{N}-\text{C})$ stretch and bend respectively.

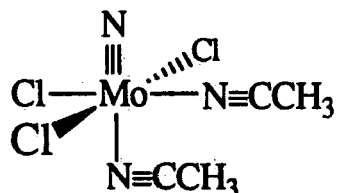
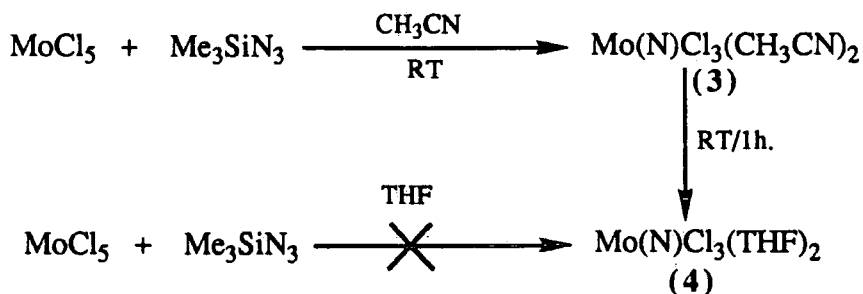


Figure 4.3, *Proposed molecular structure of $\text{Mo}(\text{N})\text{Cl}_3(\text{CH}_3\text{CN})_2$ (3).*

Analogous treatment of $\text{MoCl}_4(\text{THF})_2$ with trimethylsilylazide in THF solvent did not afford $\text{Mo}(\text{N})\text{Cl}_3(\text{THF})_2$ (4), but a red-orange intractable oil³⁰ possibly resulting from non-innocent participation of THF. However, (4) can be obtained as a brown solid in 83% yield, by the dissolution of (3) in THF. Characterisation of (4) is again provided by elemental analysis and infrared spectroscopy, which suggests that (3) and

(4) are isostructural. A strong band at 1035 cm^{-1} is attributable to the $\nu(\text{M-N})$ stretch and an absorption at 387 cm^{-1} is indicative of a Mo-Cl stretch³⁵

The preparations of (3) and (4) are summarised in Scheme 4.1.

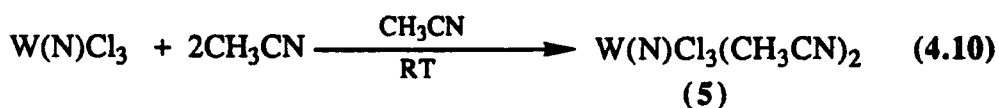


Scheme 4.1, Syntheses of (3) and (4).

4.3.4 Synthesis of $\text{W(N)Cl}_3(\text{CH}_3\text{CN})_2$ (5).

The reaction of $\text{WCl}_4(\text{CH}_3\text{CN})_2$ with trimethylsilylazide does not afford the tungsten nitrido species analogue of (3) cleanly. Although the infrared spectrum of the solid obtained from this reaction clearly indicates the presence of a nitrido species with a strong absorption observed at 1090 cm^{-1} , an additional strong band at *ca.* 2100 cm^{-1} and a broad band at 1240 cm^{-1} are indicative of $\nu_{\text{as}}(\text{N}_3)$ and $\nu_{\text{s}}(\text{N}_3)$ vibrations of an azido ligand³⁵.

Dissolution of $[\text{W(N)Cl}_3]_n$ in acetonitrile at elevated temperatures affords an orange solution, from which $\text{W(N)Cl}_3(\text{CH}_3\text{CN})_2$ (5) can be isolated as a brown solid in 63% yield (Equation 4.10).



Experimental evidence suggests that (5) is isostructural to (3) and (4).

The infrared spectrum shows bands consistent with coordinated acetonitrile and a very

strong absorption at 1090 cm⁻¹ corresponding to the W-N triple bond. W-Cl absorptions are found in the range 410-289 cm⁻¹ 35.

4.4 The Reaction of Molybdenum Nitrido Compounds with Trimethylphosphine:

The Preparation, Structure and Reactivity of a Molybdenum Phosphiniminato Complex.

4.4.1 The Preparation of [Mo(NPMe₃)Cl₂(PMe₃)₃]Cl ·CH₂Cl₂ (6).

Treatment of a dichloromethane suspension of [Mo(N)Cl₃]₄ with four equivalents of trimethylphosphine did not form the desired Mo(N)Cl₃(PMe₃)₃ species, but rather the pale green d² complex [Mo(NPMe₃)Cl₂(PMe₃)₃]⁺Cl⁻ (6), which was isolated in 82% yield (Equation 4.11).



Compound (6) is soluble in chlorocarbons and sparingly soluble in aromatic solvents. Elemental analysis confirms the stoichiometry C₁₃H₃₈NCl₅P₄Mo, implying incorporation of a CH₂Cl₂ molecule within the crystal lattice. The infra-red spectrum displays absorptions typical of coordinated PMe₃ at 950cm⁻¹ [δ(CH₃)] and 725cm⁻¹ [ρ(CH₃)]³⁶. A strong band at 1130cm⁻¹ is indicative of a phosphiniminato ligand, which typically occur in the range 1100-1150cm⁻¹ and has been assigned to the ν(P-N) vibration³⁷. Compound (6) is diamagnetic: the ¹H NMR spectrum shows trimethylphosphine in three different environments (Figure 4.4). A triplet at δ 1.64, corresponds to two metal bound PMe₃ groups disposed *trans* to each other on the metal centre, and doublets at δ 1.79 and 2.08, are assigned to the unique metal bound PMe₃

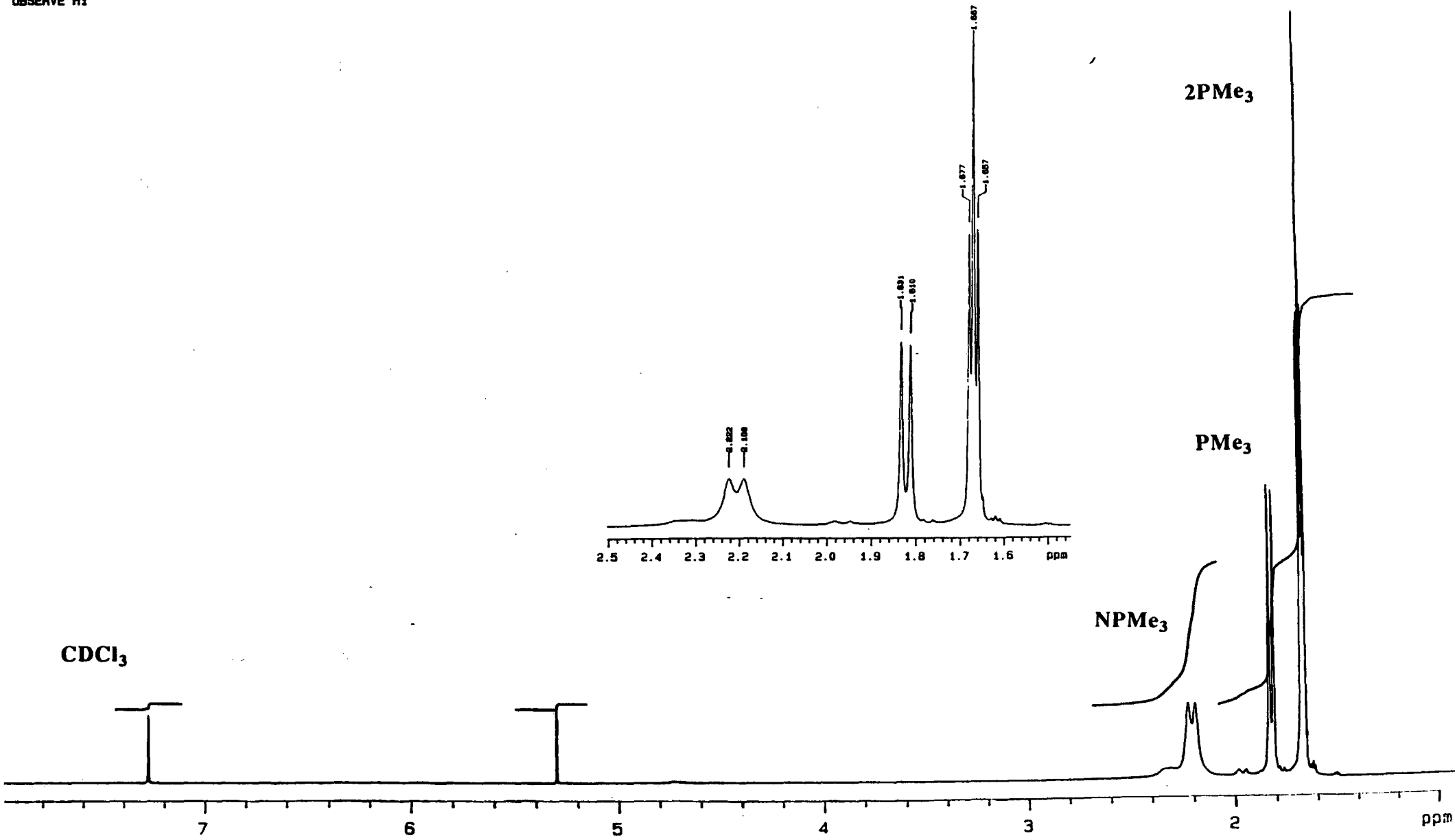


Figure 4.4, The 400MHz ¹H NMR spectrum of [Mo(NPMe₃)Cl₂(PMe₃)₃]Cl·CH₂Cl₂ (6).

and the PMe_3 of the phosphiniminato ligand respectively. The latter is slightly broadened, possible due to the presence of the quadrupolar nitrogen atom.

The ^{31}P (^1H) NMR spectrum (CDCl_3) reveals three resonances: a triplet at δ -2.0, a doublet at δ 2.0 (ratio 2:1) for the phosphorus of the three metal bound PMe_3 groups, and a singlet at δ 60.0 for the phosphorus of phosphiniminato ligand.

The chloride infrared stretching region of (6) displays Mo-Cl stretches at 355cm^{-1} , and 270cm^{-1} suggesting a *cis*-dichloro arrangement of the halide ligands³⁸. This, coupled with the requirement for *trans* PMe_3 ligands suggests a meridional arrangement of PMe_3 groups, a structure which was subsequently confirmed by X-ray crystallography³⁹ (following section).

4.4.2 Molecular Structure of $[\text{Mo}(\text{NPMe}_3)\text{Cl}_2(\text{PMe}_3)_3]\text{Cl}\cdot\text{CH}_2\text{Cl}_2$ (6).

An excellent crop of green needles may be obtained by allowing a CH_2Cl_2 solution of (6), layered with an equal volume of toluene, to stand at room temperature for 24 h. A suitable crystal was picked for single crystal X-ray analysis and sealed in a 0.5mm Lindemann capillary tube. The data were collected and analysed by Dr W. Clegg of the University of Newcastle-upon-Tyne³⁹. The molecular structure of the cation of (6) is illustrated in Figure 4.5, and bond lengths and angles collected in Table 4.2.

The X-ray analysis confirms an octahedral coordination geometry with meridional PMe_3 's and a *cis*-dichloro ligand arrangement. The Mo-N-P angle of $167.6(3)^\circ$ and Mo-N distance of $1.775(4)\text{\AA}$ are consistent with lone pair donation from the nitrogen to molybdenum³⁷, while the N-P distance of $1.636(4)\text{\AA}$ lies within the range expected for a nitrogen-phosphorus double bond ($\text{P}=\text{N} \cong 1.56\text{\AA}$, $\text{P}-\text{N} \cong 1.77\text{\AA}$ ⁴⁰).

X-ray structures have been reported for eight other phosphiniminato complexes; important bond lengths and angles are collected in Table 4.3 for comparison.

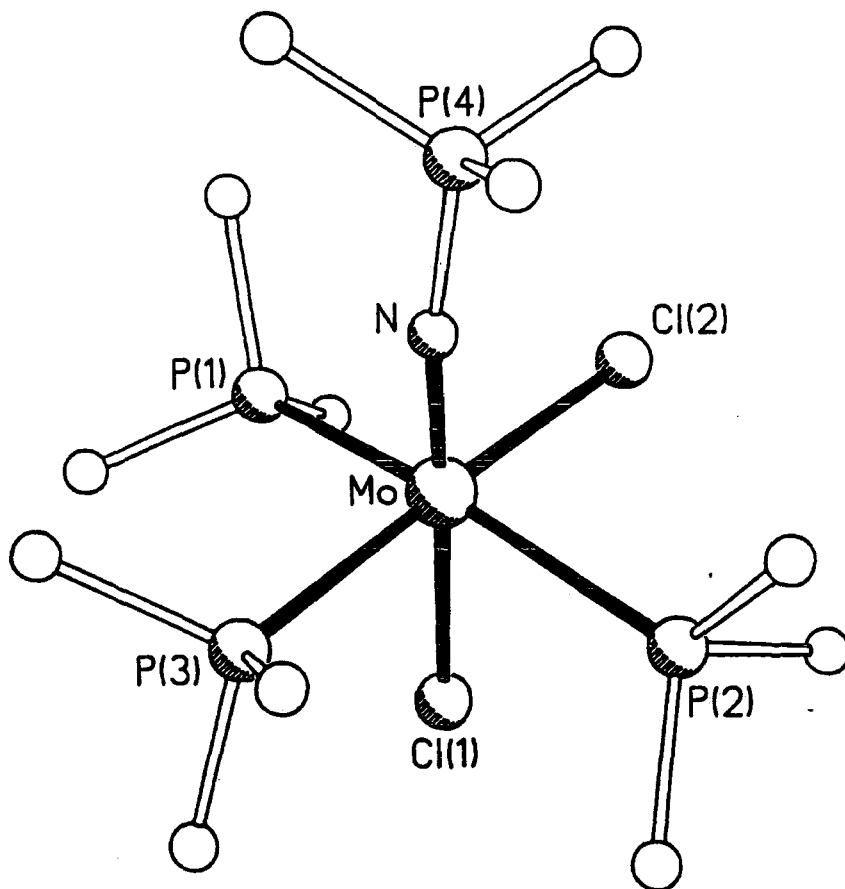


Figure 4.5, *The molecular structure of $[Mo(NPMe_3)Cl_2(PMe_3)_3]^+(6)$.*

| | | | |
|----------------------|-----------|----------------------|-----------|
| Mo - Cl(1) | 2.482(2) | Mo - Cl(2) | 2.522(2) |
| Mo - P(1) | 2.530(2) | Mo - P(2) | 2.516(1) |
| Mo - P(3) | 2.489(2) | Mo - N | 1.775(4) |
| P(1) - C(11) | 1.781(12) | P(1) - C(12) | 1.836(12) |
| P(1) - C(13) | 1.812(8) | P(2) - C(21) | 1.829(9) |
| P(2) - C(22) | 1.822(12) | P(2) - P(23) | 1.776(13) |
| P(3) - C(31) | 1.815(8) | P(3) - P(32) | 1.829(8) |
| P(3) - C(33) | 1.806(7) | N - P(4) | 1.636(4) |
| P(4) - C(41) | 1.786(8) | P(4)-C(42) | 1.768(8) |
| P(4) - C(43) | 1.781(9) | | |
| Cl(1) - Mo - Cl(2) | 89.1(1) | Cl(1) - Mo - P(1) | 80.8(1) |
| Cl(2) - Mo - P(1) | 83.1(1) | Cl(1) - Mo - P(2) | 80.5(1) |
| Cl(2) - Mo - P(2) | 86.1(1) | P(1) - Mo - P(2) | 158.5(1) |
| Cl(1) - Mo - P(3) | 87.7(1) | Cl(2) - Mo - P(3) | 176.8(1) |
| P(1) - Mo - P(3) | 96.3(1) | P(2) - Mo - P(3) | 93.4(1) |
| Cl(1) - Mo - N | 177.1(1) | Cl(2) - Mo - N | 93.8(1) |
| P(1) - Mo - N | 99.9(1) | P(2) - Mo - N | 99.4(1) |
| P(3) - Mo - N | 89.4(1) | Mo - P(1) - C(11) | 122.2(5) |
| Mo - P(1) - C(12) | 111.7(4) | C(11) - P(1) - C(12) | 104.8(6) |
| Mo - P(1) - C(13) | 113.4(3) | C(11) - P(1) - C(13) | 98.8(6) |
| C(12) - P(1) - C(13) | 103.7(6) | Mo - P(2) - C(21) | 112.9(3) |
| Mo - P(2) - C(22) | 119.6(3) | C(21) - P(2) - C(22) | 102.5(6) |
| Mo - P(2) - C(23) | 114.2(3) | C(21) - P(2) - C(23) | 101.9(5) |
| C(22) - P(2) - C(23) | 103.7(6) | Mo - P(3) - C(31) | 114.9(3) |
| Mo - P(3) - C(32) | 116.8(3) | C(31) - P(3) - C(32) | 97.0(4) |
| Mo - P(3) - C(33) | 116.9(3) | C(31) - P(3) - C(33) | 105.7(4) |
| C(32) - P(3) - C(33) | 103.0(6) | Mo - N - P(4) | 167.6(3) |
| N - P(4) - C(41) | 111.7(3) | N-P(4) - C(42) | 110.7(3) |
| C(41) - P(4) - C(43) | 109.5(5) | C(42) - P(4) - C(43) | 107.2(3) |
| C(41) - P(4) - C(43) | 109.5(5) | C(42) - P(4) - C(43) | 111.2(5) |

Table 4.2, Bond distances (Å) and angles (°) for [Mo(NPMe₃)Cl₂Mo(PMe₃)₃]Cl (6).

| Complex | M-N (Å) | N-P (Å) | M-N-P (°) | Ref. |
|--|----------|----------|-----------|------|
| [NbCl ₄ (NPPH ₃) ₂] | 1.776(8) | 1.637(9) | 171.1°(6) | 41 |
| [TaCl ₄ (NPPH ₃) ₂] | 1.801(8) | 1.593(9) | 176.8(7) | 42 |
| [TaCl ₄ (NPPH ₃) ₂] ^{-a} | 1.97 | 1.56 | 162 | 41 |
| Mo(NO)(NPMe ₂ Ph)(dttt) ^b | 1.904(6) | 1.606(6) | 129.7(4) | 43 |
| [Mo(NPMe ₃)Cl ₂ (PMe ₃)]Cl | 1.775(4) | 1.636(4) | 167.6(3) | 39 |
| WF ₄ (NPPH ₃) ₂ | 1.825(6) | 1.594(6) | 157.2(4) | 44 |
| W(NPMe ₃)Cl ₅ ^c | 1.750 | 1.661 | 163.1 | 45 |
| Re(NPPH ₃)(SPh) ₄ | 1.743(7) | 1.634(9) | 163.1(6) | 46 |
| ReCl ₃ (NO)(NPPH ₃)(OPPh ₃) | 1.855(8) | 1.630(8) | 138.5(5) | 47 |
| RuCl ₃ (NPEt ₂ Ph)(PEt ₂ Ph) ₂ | 1.841(3) | 1.586(3) | 174.9(3) | 48 |

^a Only partial details published. ^b dttt = 2,3; 8,9-dibenzo-1,4,7,10-tetrathiadecane (2-)

^c Full details not yet available.

Table 4.3

The bonding of the phosphiniminato ligand may be envisaged to occur mainly through the canonical forms ((I)-(III)) shown in Figure 4.6.

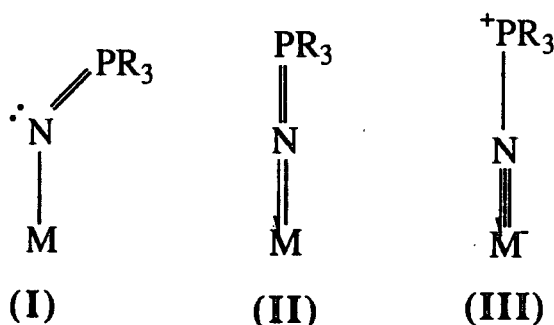


Figure 4.6, Canonical forms for the bonding of phosphiniminato ligands.

Clearly, if form (I) dominates the bonding, a substantial bending at nitrogen would be expected, while forms (II) and (III) require an essentially linear M-N-P arrangement. Analysis of the metal-nitrogen and nitrogen-phosphorus bond distances for the range of compounds collected in Table 4.3, suggest that the most common geometry is close to that of (II), with a M-N-P angle of 163°-177°. There is structural

evidence for a contribution from the bent form (I) in the two bis(phosphiniminato) structures, which show significant bending at nitrogen ($M-N-P = 157^\circ - 162^\circ$) and somewhat longer M-N bond lengths. Here, competitive π -donation to the metal by two phosphiniminato ligands may be a contributing factor. In $ReCl_3(NO)(NPPh_3)(OPPh_3)$ and $Mo(NO)(NPhMe_2)(dtd)$ the nitrogen is even closer to sp^2 hybridisation with angles of $138.5(5)^\circ$ and $129.7(4)^\circ$ respectively; this has been attributed to favourable overlap of the nitrogen with the vacant $d_{x^2-y^2}$ orbital of phosphorus in the first case⁴⁷ and steric hindrance of the aromatic rings of dtd and [NPhMe₂] ligand in the second case (Figure 4.7)⁴³.

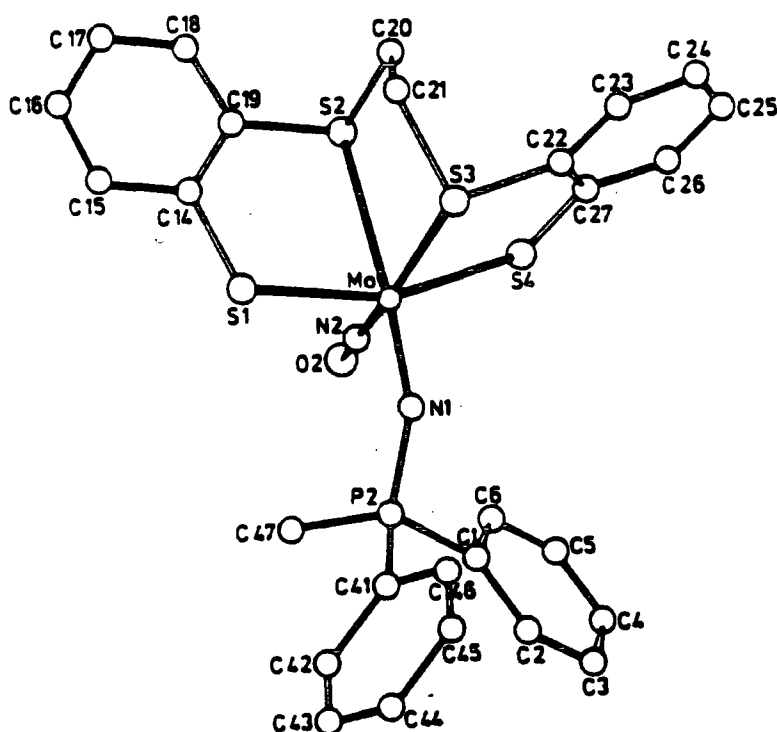


Figure 4.7. *The molecular structure of $Mo(NO)(NPhMe_2)(dtd)$.*

It is of some interest to note the isoelectronic relationship of cationic (6) to the neutral d^2 molybdenum oxo complex $\text{Mo}(\text{O})\text{Cl}_2(\text{PMe}_2\text{Ph})_3$ for which bond stretch isomers occur. There is no evidence for two forms of (6) by infrared spectroscopy, although the complexity of the spectra in the M-N and M-P region and the additional complication of coupling of these vibrations make identifying additional species difficult.

4.4.3 A Molecular Orbital Study of NPR_3 Bonding in $[\text{Mo}(\text{NPMe}_3)\text{Cl}_2(\text{PMe}_3)_3]^+$.

The phosphiniminato complex (6), has been subjected to quantum chemical Fenske-Hall MO calculations⁴⁹ in order to learn more about the metal-phosphiniminato interaction. The frontier orbitals of metal fragment $[\text{MoCl}_2(\text{PMe}_3)_3]^{2+}$ and phosphiniminato ligand $[\text{NPMe}_3]^-$ were constructed and then these orbitals were interacted to give a final bonding picture. The axial framework used for this calculation is illustrated in Figure 4.8

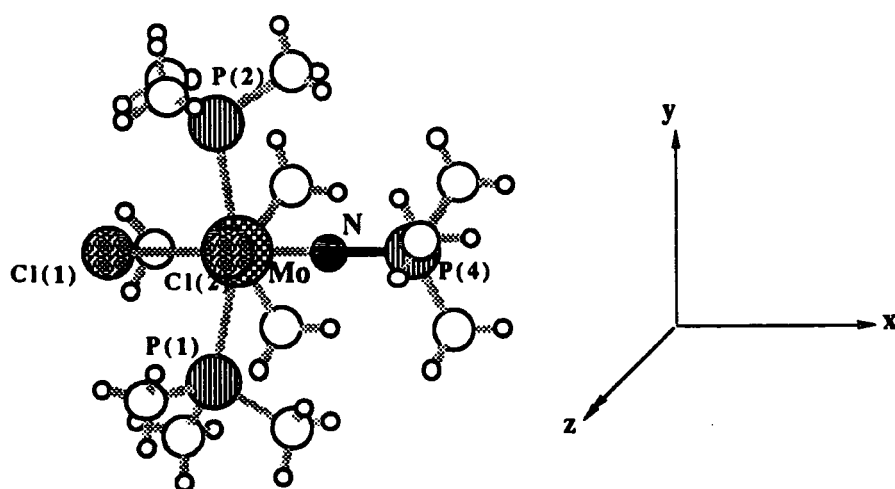


Figure 4.8, Coordinate axes adopted for FHMO calculation on $[\text{Mo}(\text{NPMe}_3)\text{Cl}_2(\text{PMe}_3)]^+$.

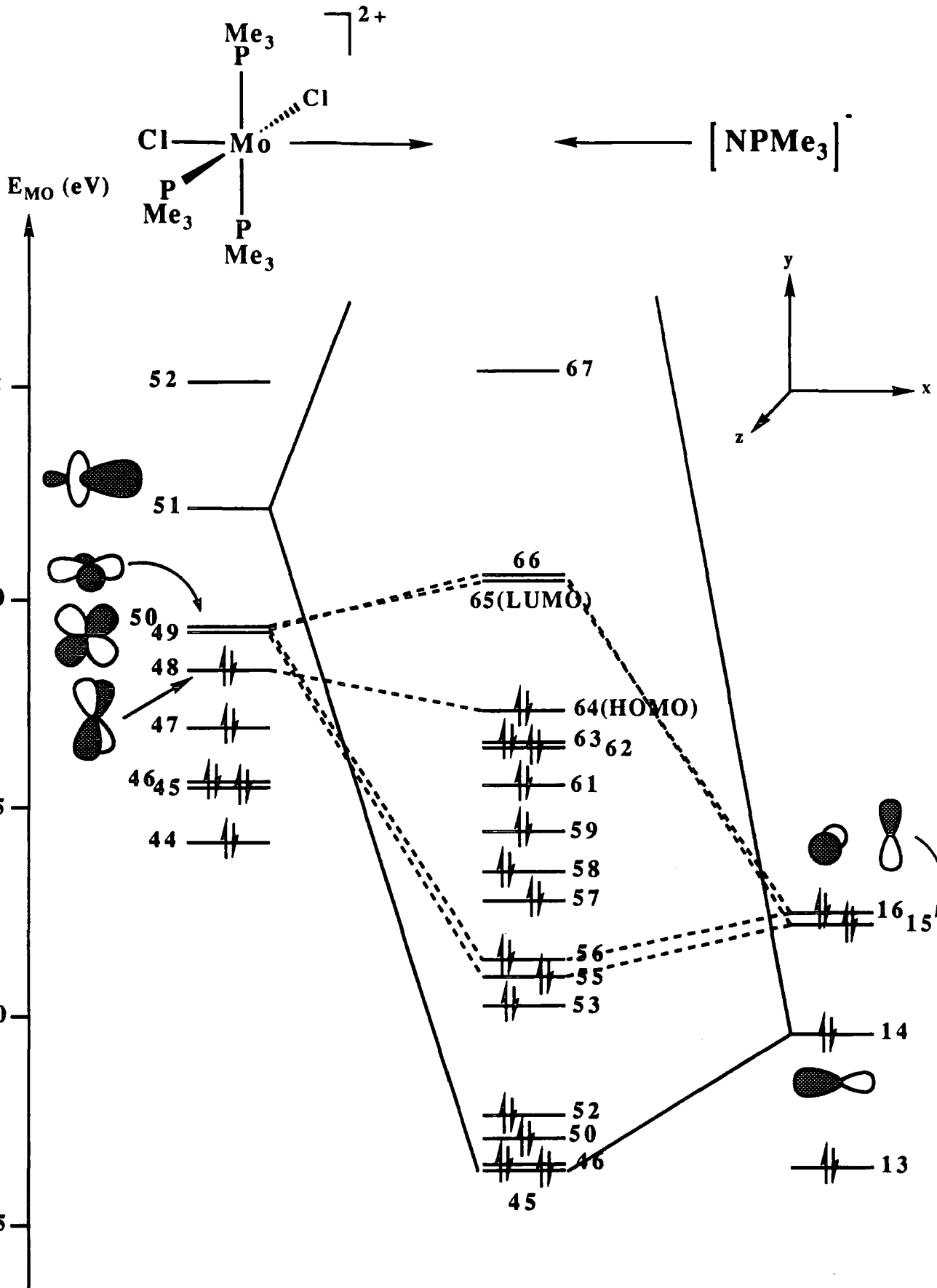


Figure 4.9, Molecular orbital correlation diagram, showing the interactions of the fragments $[Mo(PMe_3)_3Cl_2]^{2+}$ and $[N(PMe_3)]^-$. Representations of the fragment MO's show the most important orbital contributions only.

a). The $[\text{MoCl}_2(\text{PMe}_3)_3]^{2+}$ Fragment.

The percentage compositions of the frontier orbitals (MO 48-52) of $[\text{MoCl}_2(\text{PMe}_3)_3]^{2+}$ are collected in Table 4.4.

| Orbital | Composition, % | |
|----------|----------------------------|--|
| | Ligands Cl, PMe_3 | Metal |
| 48(HOMO) | 33 | 67 d_{yz} |
| 49(LUMO) | 19 | 68 d_{xy} , 10 d_{xz} , 3 p_y |
| 50 | 19 | 67 d_{xz} , 10 d_{xy} , 4 p_z |
| 51 | 15 | 33 $d_{x^2-y^2}$, 15 d_{z^2} , 10 s, 17 p_x |
| 52 | 96 | 2 $d_{x^2-y^2}$, 2 d_{xz} |

Table 4.4

The HOMO consists mainly of d_{yz} character with the LUMO and SLUMO being mainly of π -symmetry, with a high contribution from d_{xy} and d_{xz} respectively. MO 51 is mainly of σ -type symmetry directed along the x-axis. An illustration of these frontier orbitals can be seen in the left-hand side of Figure 4.9

b). The $[\text{NPMe}_3]^-$ Fragment.

The frontier orbitals of the $[\text{NPMe}_3]^-$ fragment are illustrated on the right-hand side of Figure 4.9. From Table 4.5 it can be seen that these orbitals consist of one N sp -type MO directed along the x-axis, and two essentially degenerate MO's which are mostly p_y and p_z in character.

| Composition, % | | |
|----------------|---|---|
| Orbital | Nitrogen | Phosphorus |
| 14 | 69 p _x , 9 s, 3 p _z | 5 p _x , 3 d _{x²-y²} |
| 15(HOMO) | 75 p _y , 2 p _z | 12 d _{x²-y²} |
| 16 | 74 p _z , 3 p _x , 2 p _y | 7 d _{xz} , 5 d _{z²} |
| 17 | ----- | 39 d _{z²} , 27 s, 14 p _z , 11 d _{xz} , 3 p _y |

Table 4.5

c). The Interaction of $[\text{MoCl}_2(\text{PMe}_3)_3]^{2+}$ with $[\text{NPMe}_3]^-$.

The correlation diagram for $[\text{Mo}(\text{NPMe}_3)\text{Cl}_2(\text{PMe}_3)_3]^+$ arising by interaction of the frontier orbitals of $[\text{MoCl}_2(\text{PMe}_3)_3]^{2+}$ and $[\text{NPMe}_3]^-$ is shown in Figure 4.9. The strongest interaction is between filled $[\text{NPMe}_3]^-$ fragment MO 14 and empty metal fragment MO 51, which both have a significant component along the x-axis. This σ -type dative interaction leads to formation of complex MO 45. Interaction of essentially degenerate metal fragment LUMO(49) and SLUMO(50) with $[\text{NPMe}_3]^-$ fragment filled MO's 15 and 16 respectively, leads to the formation of two weak π -dative bonds found in complex MO's 55 and 56 respectively. The strength of these bonding interactions, in terms of percentage Mulliken overlap population, is compared in Table 4.6

| Metal Fragment MO | $[\text{NPMe}_3]^-$ Fragment MO | % of Total Mull.Ov. Pop. |
|-------------------|---------------------------------|--------------------------|
| 49 | 15 | 20.0 |
| 49 | 16 | 6.2 |
| 50 | 15 | 6.4 |
| 50 | 16 | 16.1 |
| 51 | 14 | 45.0 |

Table 4.6

Inspection of the final Mulliken population, indicates a total charge transfer from the $[\text{NPMe}_3]^-$ fragment to the metal fragment of *ca.* $1.1e^-$.

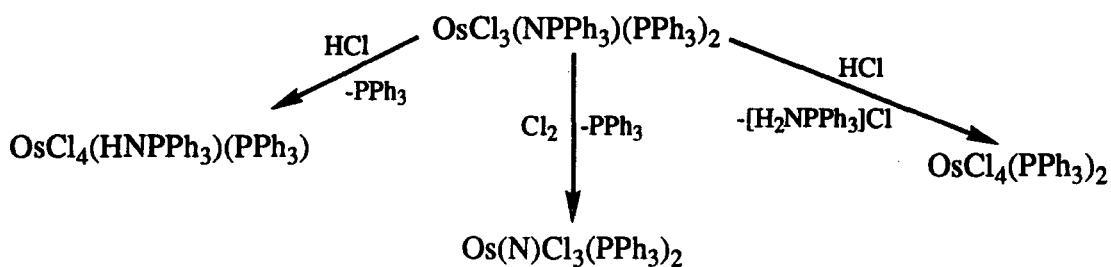
The metal fragment HOMO remains essentially non-bonding in the complex and accommodates the d electron pair. The considerable complex HOMO-LUMO energy gap of 2.44eV is consistent with the observed diamagnetism of this species.

These calculations suggest that the nitrogen of the NPMe_3 ligand in $\text{Mo}(\text{NPMe}_3)\text{Cl}_2(\text{PMe}_3)_3$ is sp hybridised, with the molybdenum-nitrogen interaction consisting of a strong σ -dative bond and two weaker, but significant, π -type dative bonds. This is reminiscent of the metal oxygen bonding in $\text{Mo}(\text{O})\text{Cl}_2(\text{PR}_3)_3^2$ and suggests that the bonding of the NPMe_3 ligand lies somewhere between canonical forms (II) and (III). (Section 4.4.2)

4.4.4 Conversion of (6) into an Anionic Nitrido-bridged Dimer:

Preparation of $\{[\text{MoCl}_3(\text{PMe}_3)_2]_2\text{N}\}[\text{Me}_3\text{PNPMe}_3]$ (7).

There are few reported reactions or transformations of NPR_3 complexes. It is known that the phosphiniminato ligand can be protonated to form the phosphinimine ligand which can be further protonated and thence removed from the metal. Complexes of the type $\text{MX}_3(\text{NPR}_3)(\text{PR}_3)_2$ react with chlorine to generate nitrido complexes in good yields (Scheme 4.2)⁵⁰, and there is some evidence that $-\text{NPR}_3$ ligands can suffer hydrolytic cleavage to form amido complexes (Equation 4.12).



Scheme 4.2, Reactivity of $\text{OsCl}_3(\text{NPPh}_3)(\text{PPh}_3)_2$.

4.4.4.1 The Molecular Structure of



Large orange prisms readily form at the interface of a layered methylene chloride/toluene (50:50) solution. A crystal of dimensions 0.08 x 0.19 x 0.23 mm was sealed in a Lindemann capillary tube and a single crystal X-ray structure determination carried out by Dr W. Clegg of the University of Newcastle-upon-Tyne³⁹. The molecular structure of (3) is illustrated in Figure 4.10 and bond lengths and angles are shown in Table 4.7.

The X-ray structure of (3) reveals eclipsed ligand axes for the dimolybdenum anion with staggered *trans*-orientated PMe_3 groups and a meridional arrangement of chloro ligands resulting in overall D_{2d} symmetry. The M-N distances, averaging 1.86 Å, are equivalent within experimental error, and correspond to double bonds. The bonds to the chloro ligands lying *trans* to the nitrido group are considerably elongated, 2.535(3) Å and 2.571(3) Å respectively, compared with the *cis*-Mo-Cl distances (av. 2.411(2) Å). A similar lengthening of the halide ligands *trans* to a bridging nitride have been noted in the related anions $[\text{W}_2\text{NCl}_{10}]^-$ and $[\text{Ta}_2\text{NBr}_{10}]^-$, and have been ascribed to the considerable *trans* influence of the nitrido ligand^{51, 52}.

4.4.4.2 The Metal-Nitrogen Bonding in



The metal-nitrogen bonding in symmetrically bridged nitrido species related to (7) has been discussed by Wheeler, Hoffmann and Strähle²³. They have shown that the bonding may be interpreted as two M-N double bonds with two σ and two perpendicular π -orbitals forming two degenerate $d\pi$ - $p\pi$ - $d\pi$ three centred π -molecular orbitals (Figure 4.11). In a d^0 example such as $[(\text{TaBr}_5)_2\mu\text{-N}]^{3-}$ non-bonding orbitals remain unoccupied, but in the d^2 complex (7) each of the non-bonding orbitals will

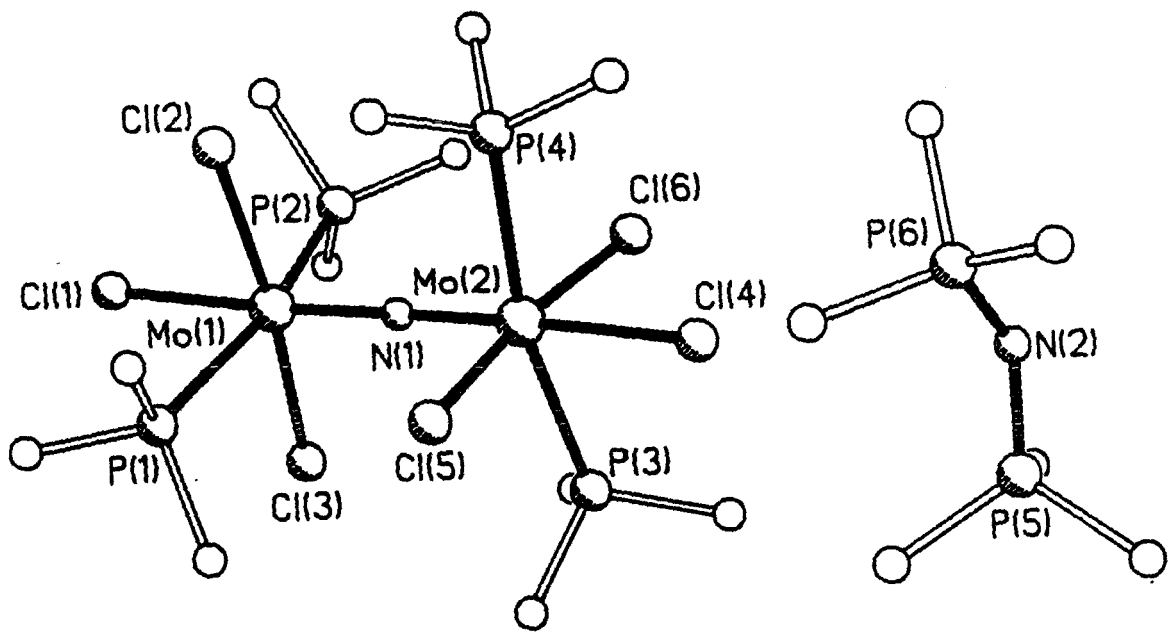


Figure 4.10, The molecular structure of $[(PMe_3)_2Cl_3MoNMoCl_3(PMe_3)_2][Me_3PNPMe_3]$ (7)

| | | | |
|---------------|-----------|---------------|-----------|
| Mo(1) - N(1) | 1.873(8) | Mo(1) - Cl(1) | 2.535(3) |
| Mo(1) - Cl(2) | 2.411(2) | Mo(1) - Cl(3) | 2.419(2) |
| Mo(1) - P(1) | 2.578(3) | Mo(1) - P(2) | 2.557(3) |
| Mo(2) - N(1) | 1.851(8) | Mo(2) - Cl(4) | 2.571(3) |
| Mo(2) - Cl(5) | 2.418(2) | Mo(2) - Cl(6) | 2.396(3) |
| Mo(2) - P(3) | 2.552(2) | Mo(2) - P(4) | 2.569(2) |
| P(1) - C(11) | 1.804(9) | P(1) - C(12) | 1.804(14) |
| P(1) - C(13) | 1.832(9) | P(2) - C(21) | 1.821(13) |
| P(2) - C(22) | 1.772(13) | P(2) - C(23) | 1.766(19) |
| P(3) - C(31) | 1.785(10) | P(3) - C(32) | 1.769(14) |
| P(3) - C(33) | 1.771(16) | P(4) - C(41) | 1.812(13) |
| P(4) - C(42) | 1.815(9) | P(4) - C(43) | 1.806(9) |
| N(2) - P(5) | 1.564(6) | N(2) - P(6) | 1.560(6) |
| P(5) - C(51) | 1.773(12) | P(5) - C(52) | 1.786(12) |
| P(5) - C(53) | 1.776(9) | P(6) - C(61) | 1.779(12) |
| P(6) - C(62) | 1.758(13) | P(6) - C(63) | 1.760(10) |

| | | | |
|-----------------------|-----------|-----------------------|----------|
| N(1) - Mo(1) - Cl(1) | 176.8(2) | N(1) - Mo(1) - Cl(2) | 92.3(2) |
| Cl(1) - Mo(1) - Cl(2) | 85.2(1) | N(1) - Mo(1) - Cl(3) | 94.4(2) |
| Cl(1) - Mo(1) - Cl(3) | 88.2(1) | Cl(2) - Mo(1) - Cl(3) | 173.2(1) |
| N(1) - Mo(1) - P(1) | 96.4(2) | Cl(1) - Mo(1) - P(1) | 85.6(1) |
| Cl(2) - Mo(1) - P(1) | 91.5(1) | Cl(3) - Mo(1) - P(1) | 86.9(1) |
| N(1) - Mo(1) - P(2) | 97.9(2) | Cl(1) - Mo(1) - P(2) | 80.2(1) |
| Cl(2) - Mo(1) - P(2) | 89.4(1) | Cl(3) - Mo(1) - P(2) | 90.6(1) |
| P(1) - Mo(1) - P(2) | 165.6(1) | N(1) - Mo(2) - Cl(4) | 175.9(2) |
| N(1) - Mo(2) - Cl(5) | 92.9(2) | Cl(4) - Mo(2) - Cl(5) | 83.0(1) |
| N(1) - Mo(2) - Cl(6) | 97.2(2) | Cl(4) - Mo(2) - Cl(6) | 86.9(1) |
| Cl(5) - Mo(2) - Cl(6) | 169.9(1) | N(1) - Mo(2) - P(3) | 96.1(2) |
| Cl(4) - Mo(2) - P(3) | 84.0(1) | Cl(5) - Mo(2) - P(3) | 93.5(1) |
| Cl(6) - Mo(2) - P(3) | 85.3(1) | N(1) - Mo(2) - P(4) | 94.9(2) |
| Cl(4) - Mo(2) - P(4) | 85.4(1) | Cl(5) - Mo(2) - P(4) | 92.1(1) |
| Cl(6) - Mo(2) - P(4) | 87.2(1) | P(3) - Mo(2) - P(4) | 167.4(1) |
| Mo(1) - N(1) - Mo(2) | 175.3(4) | Mo(1) - P(1) - C(11) | 115.7(3) |
| Mo(1) - P(1) - C(12) | 115.7(4) | C(11) - P(1) - C(12) | 102.0(5) |
| Mo(1) - P(1) - C(13) | 114.9(4) | C(11) - P(1) - C(13) | 104.3(5) |
| C(12) - P(1) - C(13) | 102.4(5) | Mo(1) - P(2) - C(21) | 113.1(4) |
| Mo(1) - P(2) - C(22) | 114.5(4) | C(21) - P(2) - C(22) | 101.8(8) |
| Mo(1) - P(2) - C(23) | 118.8(6) | C(21) - P(2) - C(23) | 99.6(7) |
| C(22) - P(2) - C(23) | 106.8(8) | Mo(2) - P(3) - C(31) | 115.0(3) |
| Mo(2) - P(3) - C(32) | 114.5(4) | C(31) - P(3) - C(32) | 104.7(7) |
| Mo(2) - P(3) - C(33) | 114.8(5) | C(31) - P(3) - C(33) | 102.9(6) |
| C(32) - P(3) - C(33) | 103.6(10) | Mo(2) - P(4) - C(41) | 116.1(3) |
| Mo(2) - P(4) - C(42) | 115.8(3) | C(41) - P(4) - C(42) | 103.1(5) |
| Mo(2) - P(4) - C(43) | 112.7(3) | C(41) - P(4) - C(43) | 102.5(5) |
| C(42) - P(4) - C(43) | 105.1(4) | P(5) - N(2) - P(6) | 141.7(5) |
| N(2) - P(5) - C(51) | 112.6(5) | N(2) - P(5) - C(52) | 114.6(4) |
| C(51) - P(5) - C(52) | 106.9(5) | N(2) - P(5) - C(53) | 109.4(4) |
| C(51) - P(5) - C(53) | 105.6(5) | C(52) - P(5) - C(53) | 107.3(5) |
| N(2) - P(6) - C(61) | 114.5(4) | N(2) - P(6) - C(62) | 112.9(5) |
| C(61) - P(6) - C(62) | 106.8(5) | N(2) - P(6) - C(63) | 109.0(4) |
| C(61) - P(6) - C(63) | 106.8(5) | C(62) - P(6) - C(63) | 106.5(6) |

Table 4.7. Bond distances (Å) and angles (°) for $[(PMe_3)_2Cl_3MoNMoCl_3(PMe_3)_2][Me_3PNPMe_3]$ (7).

become singly occupied (Figure 4.11), accounting for the paramagnetism observed in (7).

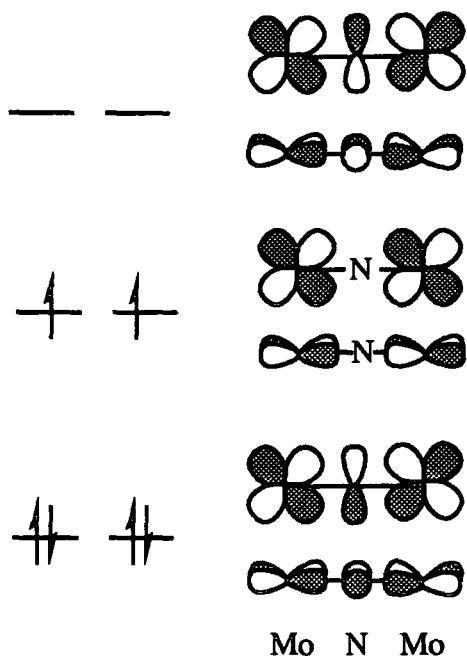


Figure 4.11, *The frontier orbitals of $[(PMe_3)_2Cl_3Mo=N=MoCl_3(PMe_3)_2]^-$.*

4.4.5 UV/Visible Studies on the Conversion of Complex (6) to (7).

The UV/visible spectrum for (6) in methylene chloride gives an absorption maximum at 795 nm ($\epsilon = 17 \times 10^3 \text{ mol}^{-1}\text{cm}^2$), i.e towards the red end of the visible spectrum; binuclear species (7) absorbs at 403 nm ($\epsilon = 1260 \times 10^3 \text{ mol}^{-1}\text{cm}^2$) (Figure 4.12).

Since the paramagnetism of (7) necessarily ruled out the use of NMR to follow the conversion of (6) to (7), UV/visible spectroscopy thus offered a method of monitoring the transformation.

From experiments monitoring the loss of (6) and formation of (7) over a range of concentrations in dichloromethane, the following conclusions were reached:

- (1) the formation of (7) from (6) does not follow first or second order kinetics, implying that the reaction mechanism is complex.

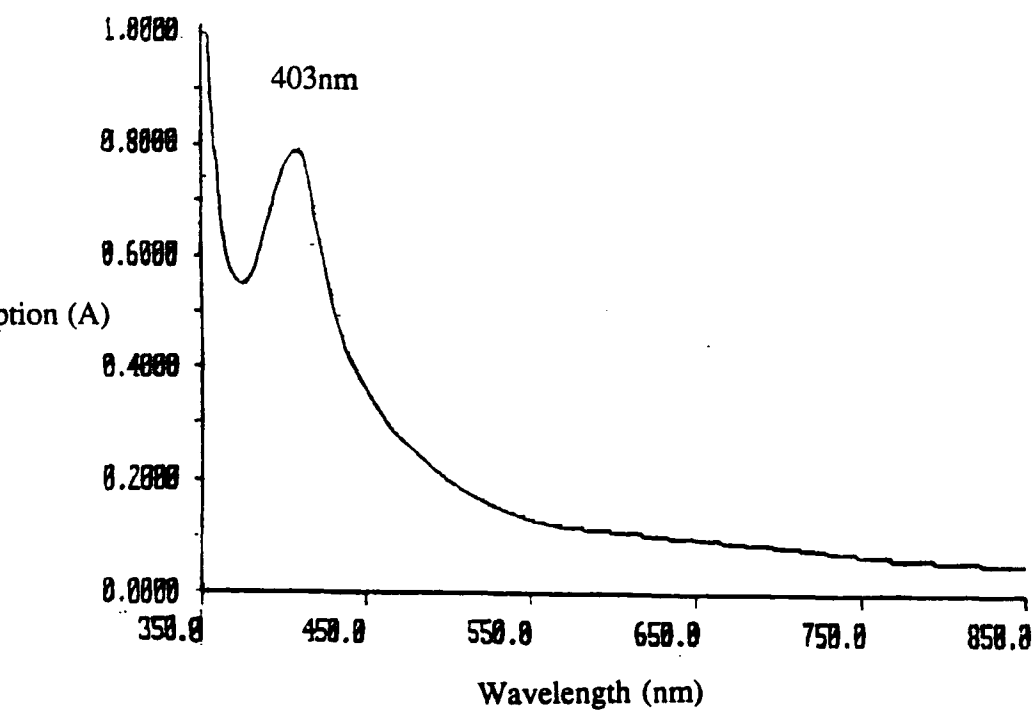
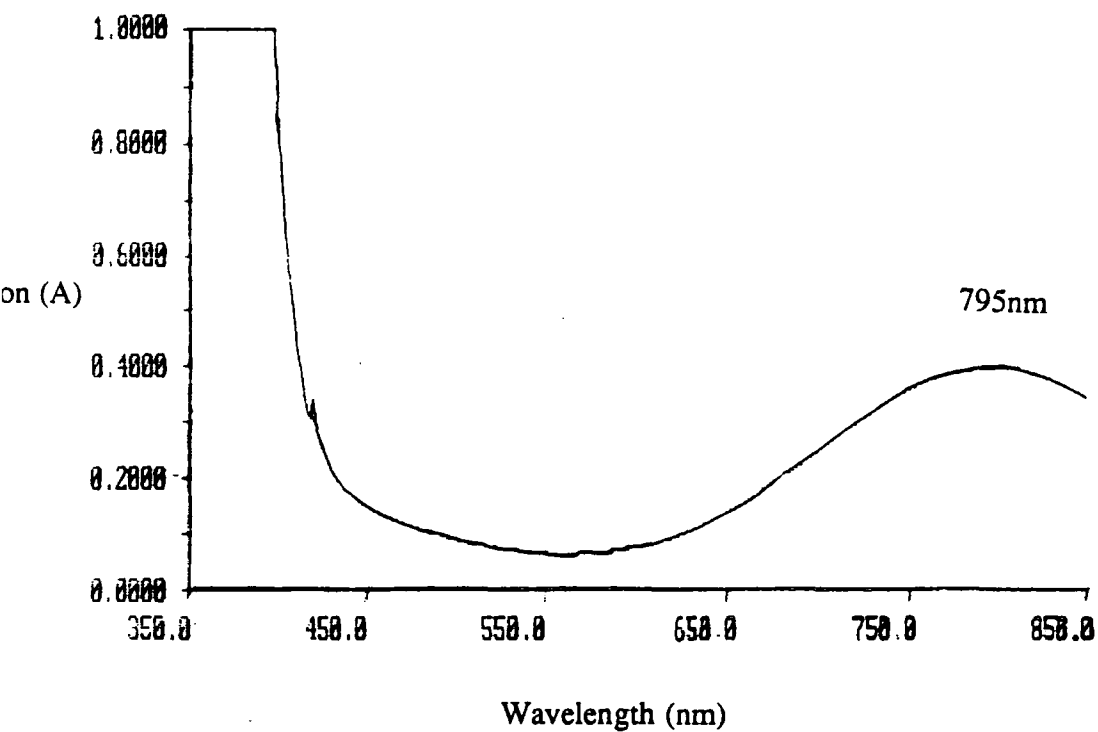


Figure 4.12, The UV/visible spectra of (A) $[Mo(NPMe_3)Cl_2(PMe_3)_3]Cl$ (6) and (B) $[(PMe_3)_2Cl_3MoNMoCl_3(PMe_3)_2][Me_3PNPMe_3]$ (7)

- (2) addition of excess phosphine or chloride ion to methylene chloride solutions of (6) have no effect on the rate of loss of starting material or formation of product, suggesting that the loss of phosphine or coordination of chloride ion are not rate determining steps in the reaction mechanism.
- (3) Addition of excess bromide ion to a solution of (6) in methylene chloride does lead to incorporation of bromine into the product, evident as a small shoulder at *ca.* 470 nm, in the UV/visible spectrum of the final solution.

Further insight into the reaction mechanism would require the observation or trapping of intermediates for which, unfortunately, there is presently no evidence.

4.4.6 Further Attempts to Prepare $\text{Mo(N)Cl}_3(\text{PMe}_3)_3$.

4.4.6.1 The Reaction of Mo(N)Cl_3 with Neat PMe_3 .

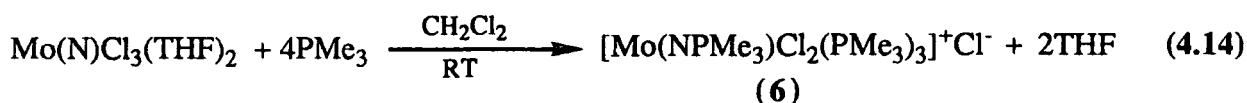
Bond-stretch isomers in the niobium oxo system have also been obtained from the reaction of Nb(O)Cl_3 with neat PMe_3 ⁵⁴. The reaction of Mo(N)Cl_3 with PMe_3 was repeated in the absence of dichloromethane in an attempt to isolate $\text{Mo(N)Cl}_3(\text{PMe}_3)_3$ rather than phosphiniminato species (6). Over a period of several days, a stirred suspension of Mo(N)Cl_3 was consumed to form a red-orange solution. Removal of solvent led to the formation of a red-brown oil, which was extracted with dichloromethane and cooled to -20°C to afford (6) in low yield. The red species may possibly be due to an unstable nitrido species which reacts subsequently in dichloromethane to form the phosphiniminato species (6). Unfortunately, it has not proved possible to isolate this species.

Similar red solutions are observed in the reaction of Mo(N)Cl_3 with trimethylphosphine in dichloromethane at -20°C , but again the only isolable product is phosphiniminato species (6).

4.4.6.2 The Reaction of Mo(N)Cl₃L₂ with PMe₃ (L = CH₃CN, THF).

The reaction of Nb(O)Cl₃(CH₃CN)₂ with trimethylphosphine allows preferential isolation of one bond-stretch isomer of Nb(O)Cl₃(PMe₃)₃¹⁹, namely the bond-lengthened (β) form. This is presumably due to the nature of the monomeric starting material.

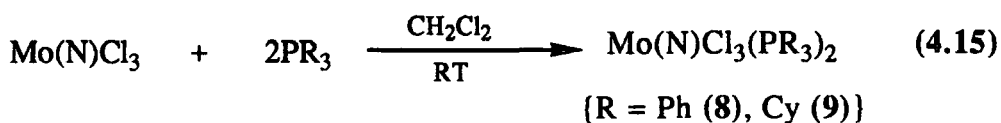
Therefore, reactions of base-coordinated molybdenum nitrido species (3) and (4) with trimethylphosphine were carried out to see if a different product would result to that generated from the tetrameric base free nitrido (1). In both cases an orange-brown solution is formed, from which low yields of compound (6) can be isolated. The reaction of Mo(N)Cl₃(THF)₂ with PMe₃ is cleaner giving a 55% yield of (6) (Equation 4.14).



4.5 The Reaction of Mo(N)Cl₃ with Other Tertiary Phosphines:

Preparation of Mo(N)Cl₃(PR₃)₂ (R = Ph (8), Cy (9)).

The reaction of Mo(N)Cl₃ (1) with dimethylphenylphosphine in dichloromethane leads to the formation of an intractable brown oil, while the reaction (1) with triphenylphosphine and tricyclohexylphosphine yield moisture sensitive *bis* phosphine adducts of the type Mo(N)Cl₃(PR₃)₂ according to Equation 4.15.



The products are isolated as moisture sensitive, pale brown solids upon removal of solvent and washing with light petroleum ether. The infrared spectrum shows

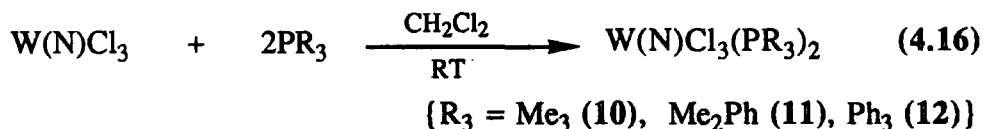
absorptions at 1130 cm⁻¹ (8) and 1120 cm⁻¹ (9), consistent with the presence of a terminal nitride ligand, and bands between 310-380 cm⁻¹ assignable to (Mo-Cl) stretching vibrations³⁵. Compounds (8) and (9) are surprisingly insoluble in aromatic and aliphatic hydrocarbons, and show only sparing solubility in chlorocarbons. This insolubility may suggest that these compounds are not simple monomeric pseudo octahedral monomers, as found in analogous Nb(O)Cl₃(PR₃)₂ (R₃ = Ph₃, Ph₂Me, Et₃), but may be halogen bridged dimeric structures, similar to that for the analogous Nb(O)Cl₃(PMe₃)₂ complex⁵⁴. However the mass spectra of (8) and (9) show no fragment ions attributable to binuclear species.

4.6 The Reaction of W(N)Cl₃ with Tertiary Phosphines:

Preparation of W(N)Cl₃(PR₃)₂

(R₃ = Me₃ (10), Me₂Ph (11), PPh₃ (12)).

Compounds of the type W(N)Cl₃(PR₃)₂ have been prepared as shown in Equation 4.16. Characterisation of these species is provided by elemental analysis, infrared and NMR spectroscopies and mass spectrometry (details are given in Chapter 6, section 6.4).



The products (10)-(12) are isolated as moisture sensitive, pale green crystalline products upon layering a dichloromethane solution of the crude reaction product with toluene.

Compound (10) and (11) readily absorb moisture and decompose upon exposure (*ca.* 30-40 s) to moist air, whereas (12) is not very hygroscopic, possibly reflecting the reduced lability of the triphenylphosphine ligand.

The infrared spectra of (10)-(12) were recorded over the range 4000-250 cm^{-1} . Apart from absorptions attributable to the tertiary phosphine ligands, the spectra show bands assignable to metal-nitrogen and metal-chlorine stretching modes. In particular, strong absorptions at 1165 cm^{-1} (10) 1135 cm^{-1} (11) and 1138 cm^{-1} (12) are tentatively assigned to the terminal nitrido ligand. Although these values are higher than previous recorded values for transition metal terminal nitrido stretches, they are not inconsistent with the relatively high stretching frequency seen in the $[\text{W}(\text{N})\text{Cl}_3]_n$ (2) starting material ($\nu(\text{W}-\text{N}) = 1090 \text{ cm}^{-1}$). Bands observed between 330-300 cm^{-1} are assigned to (W-Cl) stretching vibrations³⁵.

Compounds (10)-(12), are insoluble in aromatic and aliphatic hydrocarbons, and are only slightly soluble in chlorocarbons. Consistent with the solubilising nature of the phosphine ligands, (10) is the most soluble and (12) the least. Again, general insolubility may be the result of a dimeric halogen bridging structure in the solid state (Figure 4.13), although there is no evidence for a dimeric formulation in the mass spectra of (10)-(12).

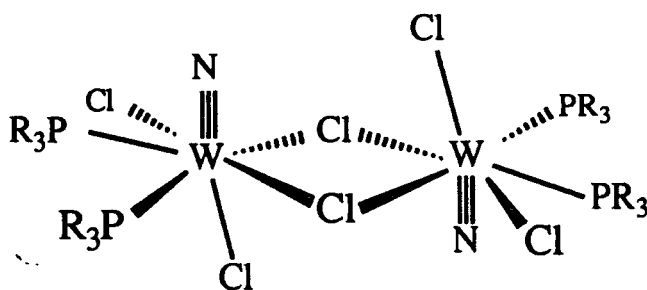


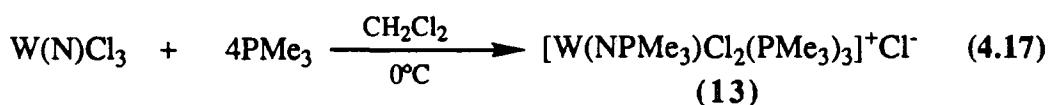
Figure 4.13, *Proposed molecular structure of species of the type $\text{W}(\text{N})\text{Cl}_3(\text{PR}_3)_2$.*

The 250 MHz ^1H NMR spectra (d^2 -dichloromethane) of (10)-(12) consist of broadened resonances for the phenyl and methyl hydrogens suggesting the occurrence of ligand exchange on the NMR timescale. Similar observations are seen in the analogous $\text{Nb}(\text{O})\text{Cl}_3(\text{PR}_3)_2$ ($\text{R}_3 = \text{Ph}_3$ and Ph_2Me)⁵⁴ and have been reported for

$\text{Nb(O)Cl}_3(\text{HMPA})_2$ ⁵⁵. The low solubility of these complexes precluded ³¹P NMR and low temperature studies.

4.7 The Preparation of $[\text{W}(\text{NPMe}_3)\text{Cl}_2(\text{PMe}_3)_3]^+\text{Cl}^-$ (13).

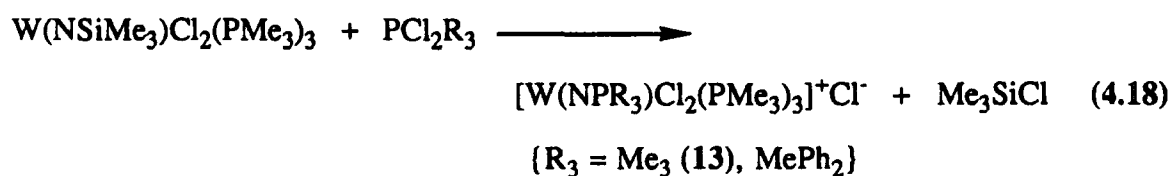
When W(N)Cl_3 is reacted with excess PMe_3 at low temperature, a small quantity (ca. 3%) of the compound $[\text{W}(\text{NPMe}_3)\text{Cl}_2(\text{PMe}_3)_3]\text{Cl}$ (13), analogous to (6), can be isolated from an oily reaction product as bottle green crystals. (Equation 4.17)



Elemental analysis confirms the stoichiometry of $\text{C}_{12}\text{H}_{36}\text{NCl}_3\text{P}_4\text{W}$ and the infrared spectrum reveals an absorption at 1180 cm^{-1} which is tentatively assigned to the $\nu(\text{P-N})$ stretch. This band is higher than previously reported for phosphiniminato species, possibly reflecting particularly strong P-N, and conversely weak W-N interactions.

The reaction of $\text{W(N)Cl}_3(\text{PMe}_3)_2$ (10) with PMe_3 fails to yield (13), even at elevated temperature.

The structure of this compound has been confirmed by Doherty and co-workers, who have very recently isolated and characterised $[\text{W}(\text{NPR}_3)\text{Cl}_2(\text{PMe}_3)_3]^+\text{Cl}^-$ ($\text{R}_3 = \text{PMePh}_2$ and PMe_3 (13)) from the reaction of $\text{W}(\text{NSiMe}_3)\text{Cl}_2(\text{PMe}_3)_3$ with PCl_2R_3 (Equation 4.18)⁴⁵.



4.8 Attempts to Prepare Rhenium Nitrido Bond-Stretch Isomers.

Rhenium complexes of the type $\text{Re}(\text{N})\text{Cl}_2(\text{PR}_3)_3$ ($\text{R}_3 = \text{Et}_2\text{Ph}$, $^n\text{Pr}_3$, Et_3) were first isolated by Chatt and co-workers in 1964⁵⁶. Structural studies on $\text{Re}(\text{N})\text{Cl}_3(\text{PEt}_2\text{Ph})_3$ revealed an unusually long Re-N bond length of 1.778 Å²¹. By a similar procedure, Forsellini et al. have prepared and characterised $\text{Re}(\text{N})\text{Cl}_2(\text{PMe}_2\text{Ph})_3$ by X-ray crystallography; the Re-N bond length in this species is 1.660 Å²². Interestingly, in both cases the Re-Cl bond of the chlorine *trans* to the oxygen is long; 2.563 Å and 2.633 Å respectively. These substantial structural differences seem unlikely to be entirely the result of steric compression, as suggested by Ibers and Doedens²¹, and are typical of structural differences seen in the d^2 Mo bond-stretch isomers. This system, therefore, seemed worthy of further investigation.

An attempt to prepare rhenium nitrido halide starting materials was unsuccessful. The synthetic route developed to species of the type $\text{M}(\text{N})\text{Cl}_3$ and $\text{M}(\text{N})\text{Cl}_3\text{L}_2$ ($\text{M} = \text{Mo}$, $\text{L} = \text{CH}_3\text{CN}$, THF; $\text{M} = \text{W}$, $\text{L} = \text{CH}_3\text{CN}$), failed to give analogous rhenium nitrido starting materials. The reaction of $\text{ReCl}_4(\text{CH}_3\text{CN})_2$ with trimethylsilyl azide in acetonitrile or methylene chloride led to recovery of starting material and an unidentified compound showing absorptions characteristic of metal azide vibrational stretches in the infrared spectrum.

Therefore, we resorted to the previously established synthetic entry into these species, involving the reduction of potassium per-rhenate with hydrazine dihydrochloride in the presence of phosphines.

4.8.1 The Reaction of KReO_4 with $\text{H}_2\text{NNH}_2 \cdot 2\text{HCl}$ and PMe_3 .

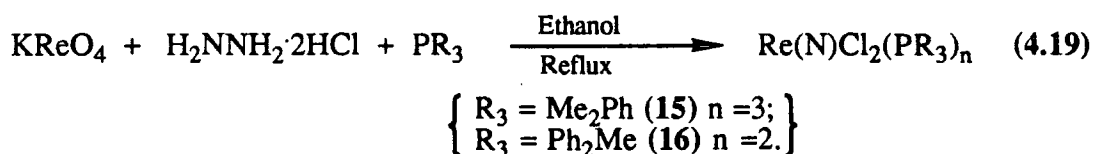
The reaction of potassium per-rhenate with hydrazine dihydrochloride and trimethylphosphine in ethanol at elevated temperatures (80°C) affords a yellow solution. Removal of solvent and recrystallisation from ethanol yields yellow rhombic crystals of an unknown species (14), which is air stable, insoluble in aromatic and aliphatic hydrocarbons, but soluble in chlorocarbons. Elemental analysis suggests a stoichiometry of $\text{C}_6\text{H}_{18}\text{NOCl}_2\text{P}_2\text{Re}$. Strong, sharp absorptions at 1050 cm^{-1} and 1043 cm^{-1} in the infrared spectrum suggest the presence of at least one Re-N triple bond, and a very strong band at 900 cm^{-1} is tentatively assigned to a terminal Re-O stretching vibration³⁵. Further bands in the infrared spectrum at 946 cm^{-1} and in the range $340\text{--}320\text{ cm}^{-1}$, are indicative of the C-P stretching vibration in coordinated PMe_3 , and $\nu(\text{Re-Cl})$ stretching vibrations. The 400 MHz ^1H NMR spectrum reveals three distinct resonances in the region δ 1.94-2.03, indicating the presence of coordinated PMe_3 in at least three environments.

A partial structure determination, hampered by severe disorder problems, suggests that (14) exists as an ion pair with the anion and cation both containing rhenium. This product was not investigated further.

4.8.2 The Reduction of KReO_4 with $\text{H}_2\text{NNH}_2 \cdot 2\text{HCl}$ in the Presence of PR_3 ($\text{PR}_3 = \text{PMe}_2\text{Ph}$, PPh_2Me):

Preparation of $\text{Re}(\text{N})\text{Cl}_2(\text{PMe}_2\text{Ph})_3$ (15) and $\text{Re}(\text{N})\text{Cl}_2(\text{PMePh}_2)_2$ (16).

The reduction of potassium per-rhenate with hydrazine dihydrochloride in the presence of certain phosphines, proceeds smoothly in refluxing ethanol, as shown in Equation 4.19.



Products (15) and (16) were isolated as air stable, yellow, crystalline solids on removal of the volatile components and washing with a small quantity of cold ethanol. Compound (15) was first prepared by Chatt and co-workers and characterised by infrared spectroscopy and elemental analysis⁵⁶. Subsequently, a single crystal X-ray study has shown (15) to possess pseudo octahedral geometry, with meridional PMe_2Ph groups, *cis* halogen atoms, and nitrogen *trans* to chlorine (Figure 4.14)²².

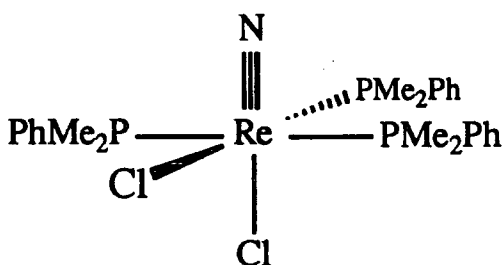


Figure 4.14, Molecular structure of $\text{Re}(\text{N})\text{Cl}_2(\text{PMe}_2\text{Ph})_3$.

NMR data have previously not been reported for (15). The ^1H NMR spectrum reveals two triplets at δ 1.73 and δ 2.01 (ratio 1:1) due to diastereotopic methyl groups of the *trans* orientated PMe_2Ph ligands, and a doublet at δ 1.30, which is assigned to the protons of the unique PMe_2Ph group *trans* to the chlorine. Confirmation of this

structure also comes from the 101 MHz ^{31}P (^1H) NMR spectrum, which shows the two different phosphine environments as triplet and doublet resonances at δ -28.3 and δ -16.3 respectively.

There is no experimental evidence for the existence of two bond-stretch isomers of $\text{Re}(\text{N})\text{Cl}_2(\text{PMe}_2\text{Ph})_3$ (**15**). The infrared spectrum shows the presence of only one Re-N triple bond, at 1058 cm^{-1} , unlike $\text{Nb}(\text{O})\text{Cl}_3(\text{PMe}_3)_3$ which shows a Nb-O stretching vibration for each isomer. Recrystallisation of (**15**) from methylene chloride did not lead to the formation of a second isomer.

Compound (**16**) was characterised by elemental analysis, mass spectrometry and infrared, ^{31}P NMR and ^1H NMR spectroscopies. A sharp band at 998 cm^{-1} is assigned to a terminal nitride ligand, and an absorption at 290 cm^{-1} is indicative of a Re-Cl stretching vibration. The ^1H and ^{31}P (^1H) NMR spectra both show the presence of equivalent phosphine ligands; a doublet resonance at δ 1.76 in the ^1H spectrum is assigned to PMePh_2 methyl protons and a singlet resonance occurs at δ -16.3 in the ^{31}P spectrum.

The structure of (**16**) is likely to be similar to that of the structurally characterised analogue $\text{Re}(\text{N})\text{Cl}_2(\text{PPh}_3)_2$, which is best described as a distorted square-based pyramid, with the nitrogen at the apex and the P atoms moved out of the basal plane of the Cl atoms toward the Re (Figure 4.15)⁵⁷.

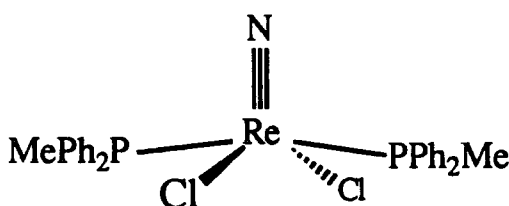


Figure 4.17, Proposed molecular structure of $\text{Re}(\text{N})\text{Cl}_2(\text{PMePh}_2)_3$.

The differing structures of (**15**) and (**16**) may be a consequence of the steric demands of the phosphine ligands. However, repeated washing of the generally more oily extracts generated in the formation of (**16**), could also lead to the loss of

phosphine. It is of interest to note that Chatt and co-workers have reported the preparation of $\text{Re}(\text{N})\text{Cl}_2(\text{PMePh}_2)_3$ by a procedure related to that used in the isolation of (16)⁵⁸. It is therefore likely that both species can be isolated, and that PMePh_2 is weakly bound and therefore readily lost from the *tris* phosphine complex, by repeated washing or prolonged exposure to a dynamic vacuum.

There is no evidence for the existence of bond-stretch isomers of (15) or (16), although a rhenium nitrido halide route may still be worthy of investigation.

4.8 Summary and Conclusions:

The availability of both base-free and base-stabilised Group 6 nitrido halide species, the latter by a new synthetic procedure, allowed their reactions with tertiary phosphines to be investigated, in an attempt to form bond-stretch isomer species analogous to $\text{Nb}(\text{E})\text{X}_3(\text{PMe}_3)_3$ (E = O, S). Seven coordinate d^0 nitrido species of the type $\text{M}(\text{N})\text{Cl}_3(\text{PMe}_3)_3$, although possibly formed initially could not be isolated; rather initial red solutions reacted further to give green phosphiniminato compounds. These may possibly result from decomposition of initially formed $\text{M}(\text{N})\text{Cl}_3(\text{PMe}_3)_3$, since $\text{Nb}(\text{E})\text{Cl}_3(\text{PMe}_3)_3$ are known to decompose over a period of 24h in solution to give $\text{E}=\text{PMe}_3$ and a paramagnetic species⁵⁴.

There appears to be no spectroscopic evidence for bond-stretch isomerism in nitrido rhenium compounds or any of the other metal-nitrogen species investigated here.

4.10 References

1. J. Chatt, L. Manojlovic-Muir and K.W. Muir, *J. Chem. Soc. Chem. Commun.*, 1971, 655.
2. (a) Y. Jean, A. Lledos, J.K. Burdett and R. Hoffmann, *J. Chem. Soc. Chem. Commun.*, 1988, 140.
(b) Y. Jean, A. Lledos, J.K. Burdett and R. Hoffmann, *J. Chem. Am. Chem. Soc.*, 1988, **110**, 4506.
3. K. Wieghardt, G. Backes-Dahmann, B. Nuber and J. Weiss, *Angew. Chem. Int. Ed. Engl.*, 1985, **24**, 777.
4. L. Manojlovic-Muir, *J. Chem. Soc. (A)*, 1971, 2796.
5. B.L. Haymore W.A. Goddard III and J.C. Allison, *Proc. Int. Conf. Coord. Chem. 23rd.*, 1984, 535.
6. L. Manojlovic-Muir and K.W. Muir, *J. Chem. Soc., Dalton Trans.*, 1972, 686.
7. K. Wieghardt, G. Backes-Dahmann, W. Holzbach, W. Swiridoff and J. Weiss, *Z. Anorg. Allg. Chem.*, 1983, **499**, 44.
8. S. Lincoln and S.A. Koch, *Inorg. Chem.*, 1986, **25**, 1594.
9. M.R. Churchill and F.J. Rotella, *Inorg. Chem.*, 1978, **17**, 668.
10. M.W. Bishop, J. Chatt and J.R. Dilworth, *J. Chem. Soc. Dalton Trans.*, 1979, 1603.
11. F. Weller and K. Dehnicke, *Z. Anorg. Allg. Chem.*, 1982, **495**, 135.
12. C.D. Garner, L.H. Hill, F.E. Mabbs and D.L. McFadden, *J. Chem. Soc. Dalton Trans.*, 1977, 853.
13. K. Wieghardt, B. Nuber and J. Weiss, *Angew. Chem. Int. Ed. Engl.*, 1985, **24**, 790.
14. L. Saussine, H. Mimoun, A. Mitschler and J. Fischer, *Nouv. J. Chim.*, 1980, **4**, 235.
15. C.M. Che, Y.K. Wang and T.C.W. Mak, *J. Chem. Soc. Chem. Commun.*, 1985, 988.

16. K. Aoyagi, Y. Yukawa, K. Shimuzu and M. Mukaida, *Bull. Chem. Soc. Jpn.*, 1986, **59**, 1493.
17. U. Muller and I. Lorenz, *Z. Anorg. Allg. Chem.*, 1980, **463**, 110.
18. Y. Gorbunov, V.I. Pakhomov and E.S. Kovaleva, *Zh. Strukh. Khim.*, 1972, **13**, 165.
19. A. Shaw, *Thesis*, 1989, A. Bashall, V.C. Gibson, T.P. Kee, M. McPartlin and A. Shaw, *In Press*.
20. V.C. Gibson, T.P. Kee, R.M. Sorrell, A.P. Bashall and M. McPartlin, *Polyhedron*, 1988, **7**, 2221
21. P.W.R. Corfield, R.J. Doedens and J.A. Ibers, *Inorg. Chem.*, 1967, **6**, 197.
22. E. Forsellini and U. Casellato, *Acta Cryst.*, 1982, **B 38**, 3081.
23. K. Dehnicke and J. Strähle, *Angew. Chem., Int. Ed. Engl.*, 1981, **20**, 413.
24. K. Dehnicke and J. Strähle, *Z. Anorg. Allg. Chem.*, 1965, **339**, 171.
25. J. Strähle, *Z. Anorg. Allg. Chem.*, 1974, **405**, 139.
26. K. Dehnicke, W. Liese and P. Köhler, *Z. Naturforsch.*, 1977, **B32**, 1487.
27. K. Dehnicke and W. Liebelt, *Z. Anorg. Allg. Chem.*, 1979, **453**, 9.
28. U. Künzel, *Dissertation, Universität Tübingen*, 1980.
29. K. Seyforth and R. Taube, *J. Organomet. Chem.*, 1982, **229**, C19.
30. J. Chatt and J.R. Dilworth, *J. Chem. Soc., Chem. Commun.*, 1974, 517; *J. Indian Chem. Soc.*, 1974, **54**, 13.
31. W.P. Griffith, *Coord. Chem. Rev.*, 1970, **5**, 459.
32. J. Strähle, *Angew. Chem., Int. Ed. Engl.*, 1969, **8**, 925.
33. 20. W.P. Griffith, *Coord. Chem. Rev.*, 1972, **8**, 369.
34. C. Chavant, J.C. Daran, Y. Jeannin, G. Constant and R. Morancho, *Acta Cryst.*, 1975, **B31**, 1828.
35. D.M. Adams, *'Metal -Ligand and Related Vibrations'*, Edward Arnold, London, 1967.
36. J. Nieman, J.H. Huffman and K.G. Caulton, *J. Organomet. Chem.*, 1983, **255**, 193.

37. 'Miscellaneous Nitrogen-containing Ligands,' B. F. G. Johnson, B. L. Haymore and J.R. Dilworth, '*Comprehensive Coordination Chemistry*,' ed. G. Wilkinson Pergamon Press, Oxford, 1987, vol 2, pp. 122-125.
38. R.J. Burt, G.J. Leigh and D.L. Leigh and D.L. Hughes, *J. Chem. Soc., Dalton Trans.*, 1981, 793.
39. V.C. Gibson, D.N. Williams and W. Clegg, *J. Chem. Soc., Chem. Commun.*, 1989, 1863.
40. H.R. Allcock '*Phosphorus-nitrogen Compounds*', 1972, Academic Press, N.Y.
41. H. Bezler and J. Strähle, *Z. Naturforsch., Teil B*, 1979, **34**, 1199.
42. H. Bezler and J. Strähle, *Z. Naturforsch., Teil B*, 1982, **38**, 317.
43. D. Sellmann, J. Keller, M. Moll, C.F. Campana and M. Haase, *Inorg. Chim. Acta*, 1988, **121**, 243.
44. H.W. Roesky, U. Seseke, M. Noltemeyer, P.G. Jones and G.M. Sheldrick, *J. Chem. Soc., Dalton Trans.*, 1986, 1309.
45. N.M. Doherty, '*199th ACS National Meeting, Boston*', 22nd-27th April, 1990.
46. J.R. Dilworth, B.D. Neaves, J.P. Hutchinson and J.A. Zubieta, *Inorg. Chim. Acta*, 1982, **65**, L223.
47. N. Mronga, F. Weller and K. Dehnicke, *Z. Anorg. Allg. Chem.*, 1983, **502**, 35.
48. F.L. Phillips and A.C. Skapski, *J. Chem. Soc., Chem. Commun.*, 1974, 49; *J. Chem. Soc., Dalton Trans.*, 1976, 1448.
49. R.F. Fenske and M.B. Hall, *Inorg Chem.*, 1972, **11**, 768.
50. D. Pawson and W.P. Griffith, *J. Chem. Soc., Dalton Trans.*, 1975, 417.
51. T. Godemeyer, A. Berg, H.D. Gross, U. Müller and K. Dehnicke, *Z. Naturforsch.*, 1985, **B 40**, 999.
52. T. Godemeyer, K. Dehnicke and D. Fenske, *Z. Naturforsch.*, 1985, **B40**, 1005.
53. R.A. Wheeler, R. Hoffmann and J. Strähle, *J. Am. Chem. Soc.*, 1986, **108**, 5381.
54. T.P. Kee, *Thesis*, 1988; *Unpublished Observations*, 1989.
55. L. G. Hubert-Pfalzgraf and A.A. Pinkerton, *Inorg. Chem.*, 1977, **16**, 1895.

56. J. Chatt, J.D. Garforth, N.P. Johnson and G.A. Rowe, *J. Chem. Soc.(A)*, 1964, 1012.
57. R.J Doedens and J.A. Ibers, *Inorg. Chem.*, 1967, 6, 204.
58. J. Chatt, C.D. Falk, G.J. Leigh and R.J. Paske, *J. Chem. Soc. (A)*, 1969, 2288.

CHAPTER FIVE

**A Quantum Chemical Analysis of the
Bonding in the Seven Coordinate Bond-Stretch Isomers of
Nb(O)Cl₃(PMe₃)₃ and the Closely
Related Hypothetical Nitride Mo(N)Cl₃(PMe₃)₃.**

5.1 Introduction.

In the previous chapter attempts have been described to prepare Mo and W nitrido species of the type $M(N)Cl_3(PMe_3)_3$, by procedures analogous to those used in the formation of the oxo and thiohalide bond-stretch isomers $M(E)X_3(PMe_3)_3$ ($M = Nb$, $E = O, S$, $X = Cl, Br$ and $M=Ta$; $E=S$; $X=Cl$)^{1,2}. It was anticipated that should a compound of this type prove accessible, it too would be expected to exhibit this phenomenon. However, in the event, seven coordinate nitrido species proved elusive.

This chapter describes the results of calculations on the oxo isomers, in an attempt to identify any important differences in their bonding which might offer an insight into the origin of the phenomenon, and then to establish whether or not similar bonding differences prevail in the related hypothetical nitride $Mo(N)Cl_3(PMe_3)_3$.

5.2 Molecular Orbital Calculations on Bond-stretch Isomer Systems.

5.2.1 Extended Hückel M.O. Calculations.

Hoffmann, Burdett, Jean and Lledos⁴ have analysed the bonding in model compounds for the d^2 and d^1 systems $Mo(O)Cl_2(PMe_2Ph)_3$ ⁵ and $[W(O)Cl_2(MeNCH_2CH_2)_3]^+$ ⁶. In these Extended Hückel Molecular Orbital (EHMO) calculations, they found that bond-stretch isomerism of the latter appears to arise by a crossing of filled and empty metal orbitals (a first order Jahn-Teller effect). This is shown schematically in Figure 5.1. If the states A and B resulting from configurations (a)¹ and (b)¹ are of the same symmetry, configuration interaction will mix them and an energy surface such as 4 will result. But, if A and B are of different spatial geometry two minima are likely to survive, with a large energy barrier between them (energy surface 3).

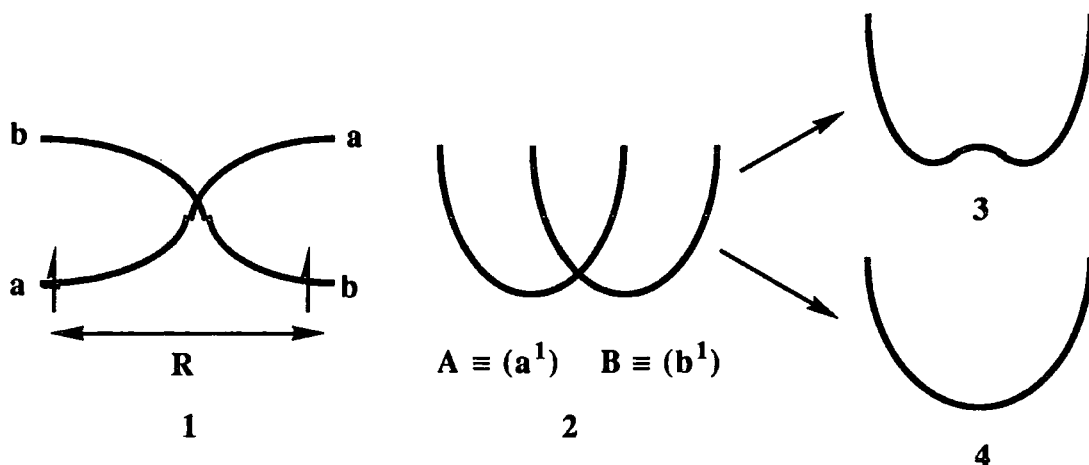


Figure 5.1, Orbital crossing of states A and B.

This phenomenon is related to the presence of different potential energy curves for the different electronic states of molecules e.g. ground and excited states, and is more likely to be found in odd rather than even electron systems if the levels a and b are of different geometry. In general, Hoffmann and co-workers found that π -donor ligands *cis* to the oxygen favour orbital crossing in the d-block, while π -donor ligands *trans* to the oxygen work against this crossing. Conversely, the orbital crossing upon M-O bond lengthening is favoured by π -acceptor ligands *trans* to the oxygen, while π -acceptor ligands *cis* are unfavourable. This could also account for bond-stretch isomerism in d^2 rhenium complexes of the type $\text{Re}(\text{N})\text{Cl}_2(\text{PR}_3)_3$.

Orbital crossing cannot explain bond-stretch isomerism in the Chatt system, for which the model compound $\text{Mo}(\text{O})\text{Cl}_2(\text{PR}_3)_3$ has been examined. Here, Hoffmann suggests that the effect is a consequence of Second Order Jahn-Teller (SOJT)⁷ distortions, i.e. essentially a competition between the σ and π -bonding components of the metal-oxygen and metal-chlorine bonds, resolved through potential energy surfaces of separate E_σ and E_π components. E_π involves all the MO's in which the chlorine lone pairs orthogonal to metal-chlorine bonds participate, the second E_σ component is made up of the remaining MO's. Although there is no orbital crossing in the d-block along the distortion D_{4h} to C_{4v} (lengthening of M-O bond), there is mixing which leads to a stabilisation of filled MO's and destabilisation of empty ones, typical of a SOJT effect⁷.

$\text{Nb}(\text{O})\text{Cl}_3(\text{PMe}_3)_3$ reveals O-M-Cl angles of *ca.* 120° and a *zero* d electron count suggesting that orbital crossings within the d manifold are unlikely to hold any significance here.

5.2.2 Fenske-Hall M.O. Calculations.

Fenske-Hall quantum chemical MO calculations⁸ have not previously been reported on these types of systems. The following sections describe the results of FHMO calculations on the bond-stretch isomers of the general formula $\text{Nb}(\text{E})\text{Cl}_3(\text{PMe}_3)_3$ (E=O,S), and the hypothetical nitrido complex $\text{Mo}(\text{N})\text{Cl}_3(\text{PMe}_3)_3$. From these studies, we hoped that firstly any significant electronic differences between the two isomers would be apparent, and secondly, by monitoring the changes over a range of Nb-E distances, an understanding of the origin of such a large energy barrier between the two isomers may result.

Initial calculations on $\text{Nb}(\text{E})\text{Cl}_3(\text{PMe}_3)_3$ involved its fragmentation into the metal fragment $[\text{NbCl}_3(\text{PMe}_3)_3]$ and ligand E. The compositions of the frontier orbitals of these fragments were determined, and subsequently interacted to construct a correlation diagram. From the two fragment analysis, the nature of the Nb-E bonding was probed. Further fragmentation into the metal fragment $[\text{Nb}(\text{PMe}_3)]^{3+}$ and E and 3Cl^- ligands, allows an analysis of chlorine-metal interactions and their competition with Nb-E interactions. These calculations were carried out over a range of Nb-E values extending beyond the experimentally determined short (α) and long (β) Nb-E distances. Also, although the coordinates of the isomers show only minor differences, the calculations were run using the coordinates of both isomers to see if these differences could have a significant effect on the results of the calculations.

5.3 Fenske-Hall MO Calculations on α and β -Nb(O)Cl₃(PMe₃)₃.

The coordinates used for the calculations on α - and β -Nb(O)Cl₃(PMe₃)₃ are those obtained from single crystal X-ray structures on the two isomers of Nb(O)Cl₃(PMe₃)₃¹ (Chapter 6, section 6.5). The α and β -isomers differ essentially in two respects, i.e the Nb-O and Nb-Cl bond distances. These are summarised in Table 5.1

| Bond | Bond Length (Å) | |
|--------------------|---|--|
| | α -Nb(O)Cl ₃ (PMe ₃) ₃ | β -Nb(O)Cl ₃ (PMe ₃) ₃ |
| Nb-O | 1.781(6) | 1.929(6) |
| Nb-Cl ₁ | 2.516(3) | 2.487(2) |
| Nb-Cl ₂ | 2.533(3) | 2.509(2) |
| Nb-Cl ₃ | 2.505(3) | 2.492(2) |

Table 5.1

It can be seen that while the Nb-O distances differ by 0.148 Å, the three Nb-Cl distances change by *ca.* 0.025 Å (average).

For convenience, all calculations were carried out using the same reference axes, Nb-O being placed along the x-axis and niobium atom at the axial origin (Figure 5.2).

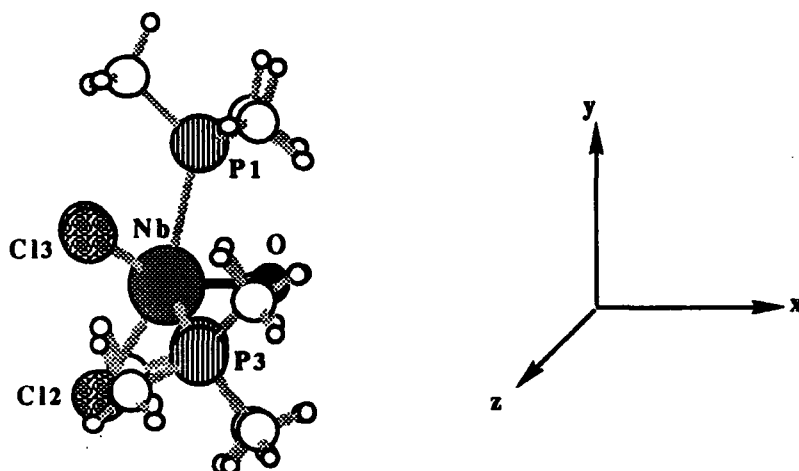


Figure 5.2, Coordinate axes adopted for FHMO calculation on Nb(O)Cl₃(PMe₃)₃.

5.3.1 Two Fragment Analysis

a) The $[\text{NbCl}_3(\text{PMe}_3)_3]$ Fragment.

The frontier orbitals of the α - and β - $[\text{NbCl}_3(\text{PMe}_3)_3]$ fragments were determined in terms of percentage contribution of atomic orbitals. The fragments were found to have very similar orbital contributions, differing in only small % character (Table 5.2).

| MO | α -Composition | | β -Composition | |
|----------|-----------------------|--|----------------------|--|
| | Ligands | Metal | Ligands | Metal |
| 49 | 97 | 3 p_x | 98 | 3 p_x |
| 50 | 94 | 4 p_z , 2 d_{xz} | 94 | 4 p_z , 2 d_{xz} |
| 51 | 91 | 5 p_x , 2 d_{z^2} , 2 $d_{x^2-y^2}$ | 93 | 5 p_x , 2 d_{z^2} |
| 52(HOMO) | 31 | 35 d_{xz} , 25 d_{yz} , 5 $d_{x^2-y^2}$, 4 d_{z^2} | 33 | 34 d_{xz} , 33 d_{yz} |
| 53(LUMO) | 30 | 41 d_{xy} , 11 $d_{x^2-y^2}$, 10 d_{z^2} , 8 d_{yz} | 29 | 41 d_{xy} , 22 $d_{x^2-y^2}$, 8 d_{z^2} |
| 54 | 27 | 39 $d_{x^2-y^2}$, 24 d_{z^2} , 6 s, 4 p_x | 30 | 31 $d_{x^2-y^2}$, 28 d_{z^2} , 6 s, 5 p_x |
| 55 | 100 | 0 | 100 | 0 |

Table 5.2

The orbitals of greatest significance, HOMO, LUMO and SLUMO, are depicted schematically in Figure 5.3.

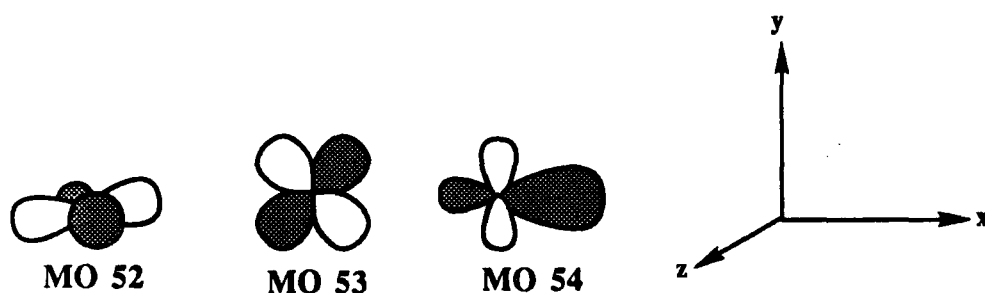


Figure 5.3, The frontier orbitals of the $[\text{NbCl}_3(\text{PMe}_3)_3]$ fragment.

b) Interaction of $[\text{NbCl}_3(\text{PMe}_3)_3]$ with $[\text{O}]$.

Correlation diagrams for the interaction of α - and β - $[\text{NbCl}_3(\text{PMe}_3)_3]$ fragments with neutral oxygen to form α - and β - $\text{Nb}(\text{O})\text{Cl}_3(\text{PMe}_3)_3$ species are shown in Figures 5.4 and 5.5 respectively. MO's 52 and 53 (HOMO and LUMO) are essentially degenerate, hence both orbitals are singly occupied; the oxygen was considered as the neutral six electron atom with electron configuration $2s^2 2p_x^2 2p_y^1 2p_z^1$. It should be noted that the choice of electron distribution is arbitrary and has no effect on the final MO correlation diagram.

In terms of inter-fragment Mulliken overlap populations, the most important interactions, in both isomers, are those between metal fragment MO's 53(LUMO) and O $2p_y$; 52(HOMO) and O $2p_z$ and 54(SLUMO) and O $2p_x$. Correlation diagrams of α and β isomers are both dominated by a strong σ -type interaction of the oxygen $2p_x$ occupied orbital with empty $d_{x^2-y^2}$ niobium orbital 54 (SLUMO). This interaction can be thought to give rise to a strong σ dative covalent bond, leading to the formation of complex MO 44 in the α case and divided between complex MO's 45,46,48 and 49 in the β isomer. The calculations show that in terms of overall σ Mulliken overlap population the Nb-O bonding in the α isomer is stronger (α , 0.195; β , 0.186), comprising of more s-character and less p-character than for the β isomer (See Table 5.4).

The π -interactions, between oxygen $2p_y$ and $2p_z$ and niobium d-orbitals, are significantly different in the α and β isomers. In the α isomer, π -bonding molecular orbitals arise from the interaction of approximately degenerate HOMO and LUMO of the $[\text{NbCl}_3(\text{PMe}_3)_3]$ fragment (52(HOMO), 35% d_{xz} ; 53(LUMO) 41% d_{xy}) with the singly occupied $2p_z$ and $2p_y$ oxygen orbitals respectively. These interactions give rise to π bonding complex MO's 45, 46 and 47,48, and π^* filled antibonding complex MO's 53 and 54(SHOMO). Complex MO's 53 and 54 also contain a significant contribution from $[\text{NbCl}_3(\text{PMe}_3)_3]$ fragment MO's 49 and 50, which possess a large percentage of chlorine 3p character. The effect of chlorine 3p involvement will be probed further through five fragment analyses to be described in a later section.

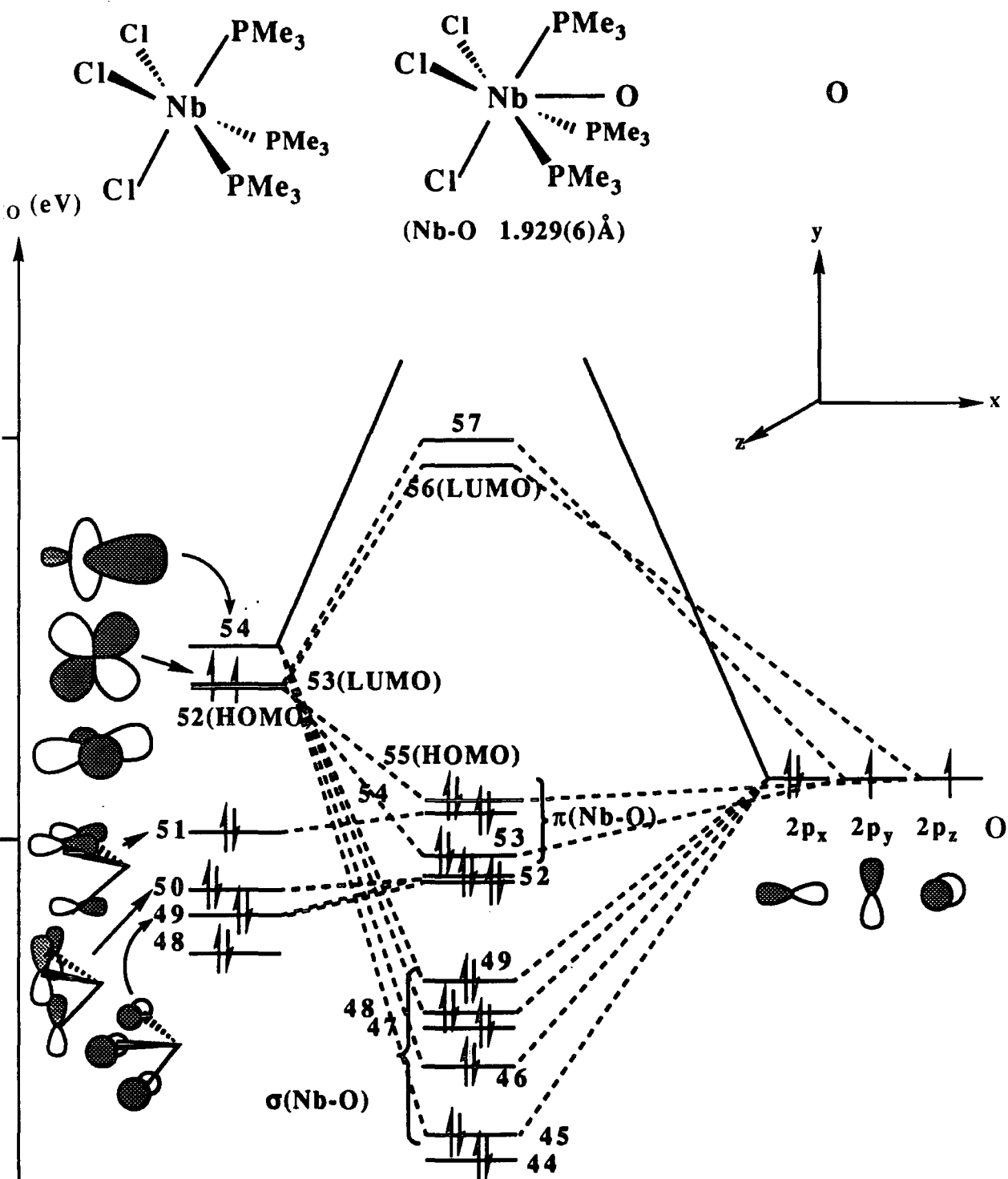


Figure 5.5, Orbital correlation diagram showing the interaction of metal fragment $[NbCl_3(PMe_3)_3]$ with O, at the β Nb-O bond distance. Representations of the fragment orbitals show most important contributions only.

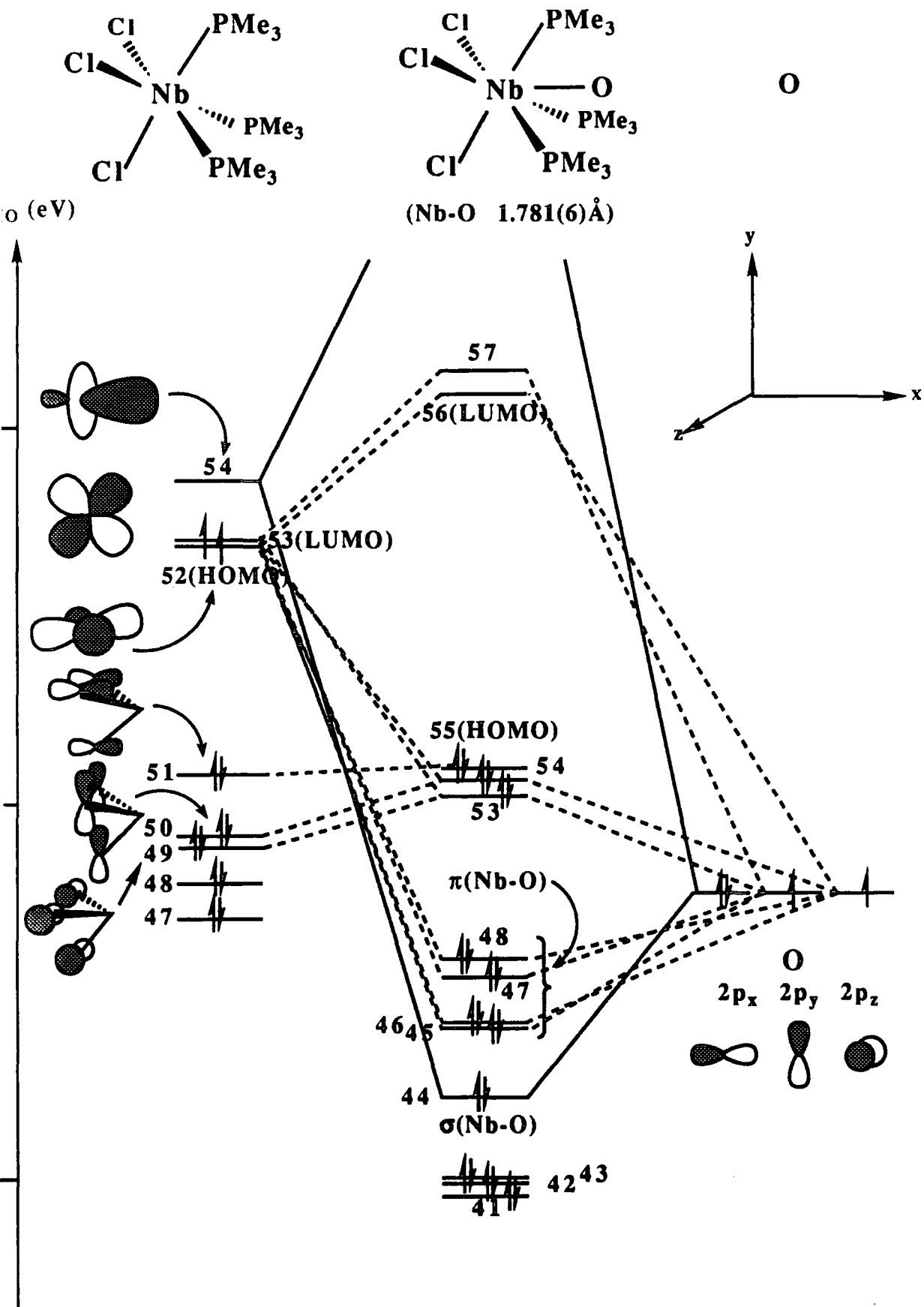


Figure 5.4, Orbital correlation diagram showing the interaction of metal fragment $[NbCl_3(PMe_3)_3]$ with O, at the α Nb-O bond distance. Representations of the fragment orbitals show most important contributions only.

Compositions of $\text{NbCl}_3(\text{PMe}_3)_3$ fragment MO's 49, 50 and 51 complex MO's 53, 54 and 55 are shown in Table 5.3.

| [$\text{NbCl}_3(\text{PMe}_3)_3$] ^a MO | Composition (%) | |
|---|--|--------------------|
| | Chlorine | Metal |
| 49 | 30 3p _y Cl1, 16 3p _y Cl2, 28 3p _y Cl3 | 3 |
| 50 | 13 3p _z Cl1, 42 3p _z Cl2, 20 3p _z Cl3 | 5 |
| 51 | 22 3p _x Cl1, 21 3p _x Cl2, 23 3p _x Cl3 | 9 |
| $\alpha\text{-Nb(O)Cl}_3(\text{PMe}_3)_3$ MO | Metal Fragment | Oxygen |
| 53 | 72 MO 49, 7 MO 53 | 11 2p _y |
| 54 | 73 MO 50, 8 MO 52 | 12 2p _z |
| 55 | 98 MO 51 | ----- |
| $\beta\text{-Nb(O)Cl}_3(\text{PMe}_3)_3$ MO | Metal Fragment | Oxygen |
| 53 | 35 MO 49, 13 MO 53 | 39 2p _y |
| 54 | 85 MO 51 | 3 2p _z |
| 55 | 40 MO 50, 12 MO 51, 12 MO 52 | 32 2p _z |

^a Fragment coordinates taken from $\alpha\text{-Nb(O)Cl}_3(\text{PMe}_3)_3$ X-ray structure.

Table 5.3, Composition of metal fragment MO's 49, 50, & 51 and α & β complex MO's 53, 54 & 55.

However, using the Mulliken overlap matrix, it is possible to assess whether the individual interactions of $\text{NbCl}_3(\text{PMe}_3)_3$ fragment MO's 49 and 50 (essentially Cl 3p) with the oxygen orbitals are bonding or antibonding. At the α Nb-O bond distance, these orbitals are found to be net antibonding with respect to the oxygen.

In the $\beta\text{-Nb(O)Cl}_3(\text{PMe}_3)_3$ case, weak π -bonding is observed as a result of the interaction of singly occupied 2p_z and 2p_y AO's of the oxygen, and the $\text{NbCl}_3(\text{PMe}_3)_3$ HOMO and LUMO respectively. These interactions give rise to essentially non-bonding complex MO's 53 and 55(HOMO). At the β Nb-O bond length there is much reduced mixing of the frontier orbitals with the metal fragment 3p chlorine MO's. Table 5.3, shows the percentage composition of complex MO's 53, 54 and 55. The net

interaction of metal fragment MO's 49 and 50 with the oxygen is found to be weakly bonding at greater bond distances.

The Mulliken overlap population shows larger π -overlap in the α bond-stretch isomer, as shown in Table 5.4.

| Metal frag. MO | Ligand frag. MO | α -Nb(O)Cl ₃ (PMe ₃) ₃ | β -Nb(O)Cl ₃ (PMe ₃) ₃ |
|----------------|-----------------|---|--|
| 54 | 2s | 0.068 | 0.040 |
| 54 | 2p _x | 0.127 | 0.145 |
| 53(LUMO) | 2p _y | 0.112 | 0.091 |
| 52(HOMO) | 2p _z | 0.107 | 0.091 |

Table 5.4

The final Mulliken population, i.e. at self-consistency, gives an indication of the charge transferred to and from the NbCl₃(PMe₃)₃ fragment molecular orbitals and oxygen atomic orbitals after interaction. In both α and β cases, after interaction the oxygen 2p_y and 2p_z AO's gain electron density, and the metal fragment HOMO and LUMO lose electron density. The 2p_x oxygen orbital loses, while the empty [NbCl₃(PMe₃)₃] fragment MO 54 gains electron density. The important complex Mulliken populations of α and β isomers is shown in Table 5.5. In the β isomer, more electron density is transferred to the empty metal fragment MO 54, and more electron density gained by the 2p_y and 2p_z oxygen AO's. The overall effective charge on the oxygen of the two species is equivalent within calculational error (α , -0.79; β , -0.77). It is interesting to note that at the α bond distance a small quantity of electron density is lost from the NbCl₃(PMe₃)₃ fragment MO's 49 and 50, these orbitals being high in Cl_{1,2,3} 3p character (see Table 5.3).

| Orbital | Start pop. | α -Nb(O)Cl ₃ (PMe ₃) ₃ | β -Nb(O)Cl ₃ (PMe ₃) ₃ |
|-------------------|------------|---|--|
| | | End pop. | End pop. |
| MO 49 | 2 | 1.985 | 1.993 |
| MO 50 | 2 | 1.976 | 1.985 |
| MO 51 | 2 | 1.994 | 1.991 |
| MO 52 | 1 | 0.422 | 0.379 |
| MO 53 | 1 | 0.423 | 0.403 |
| MO 54 | 0 | 0.451 | 0.456 |
| O 2p _s | 2 | 1.846 | 1.894 |
| O 2p _x | 2 | 1.671 | 1.605 |
| O 2p _y | 1 | 1.604 | 1.629 |
| O 2p _z | 1 | 1.610 | 1.637 |

Table 5.5

It is clear that the metal fragment MO's high in Cl 3p character are involved in the frontier orbitals of α and β -Nb(O)Cl₃(PMe₃)₃. It is therefore feasible that these π -orbital bonding and anti-bonding interactions are important in the bond-stretch isomerism effect observed in this system. As mentioned earlier, Hoffmann et al. have suggested that the competition between σ and π -bonding of ancillary ligands may be important in bond-stretch isomerism for certain species⁴.

5.3.2 Five Fragment Analysis.

a) The [Nb(PMe₃)₃]³⁺ Fragment.

In order to determine the involvement of the Cl 3p orbitals and probe their competition with oxygen AO's, the interaction of the frontier orbitals of [Nb(PMe₃)₃]³⁺ with the three chloride (Cl⁻) ligands and a neutral oxygen atom at the crystallographically determined Nb-O bond distances of 1.781(6)Å (α -isomer) and

1.929(6)Å (β -isomer) were studied. Table 5.6 summarises the composition of the important fragment MO's.

| Complex MO | Composition of $[\text{Nb}(\text{PMe}_3)_3]^{3+}$ Fragment ^a (%) | |
|------------|---|---|
| | Metal | Phosphorus |
| 37 | 17 s, 12 $d_{x^2-y^2}$, 3 d_{z^2} | P1 15 p_y ; P2 5 p_y , 9 p_z ; P3 9 p_z |
| 38 | 19 d_{z^2} , 8 d_{yz} , 6 $d_{x^2-y^2}$, 5 d_{xy} , 4 p_y | P1 18 p_y ; P2 4 p_y , 7 p_z |
| 39 | 23 d_{yz} , 6 d_{z^2} , 4 p_z | P2 4 p_y , 7 p_z ; P3 18 p_z |
| 40(HOMO) | 73 d_{xz} , 13 d_{yz} , 2 d_{z^2} | -- |
| 41(LUMO) | 77 d_{xy} , 7 d_{z^2} , 3 $d_{x^2-y^2}$ | -- |
| 42 | 55 $d_{x^2-y^2}$, 19 d_{z^2} , 18 s | -- |

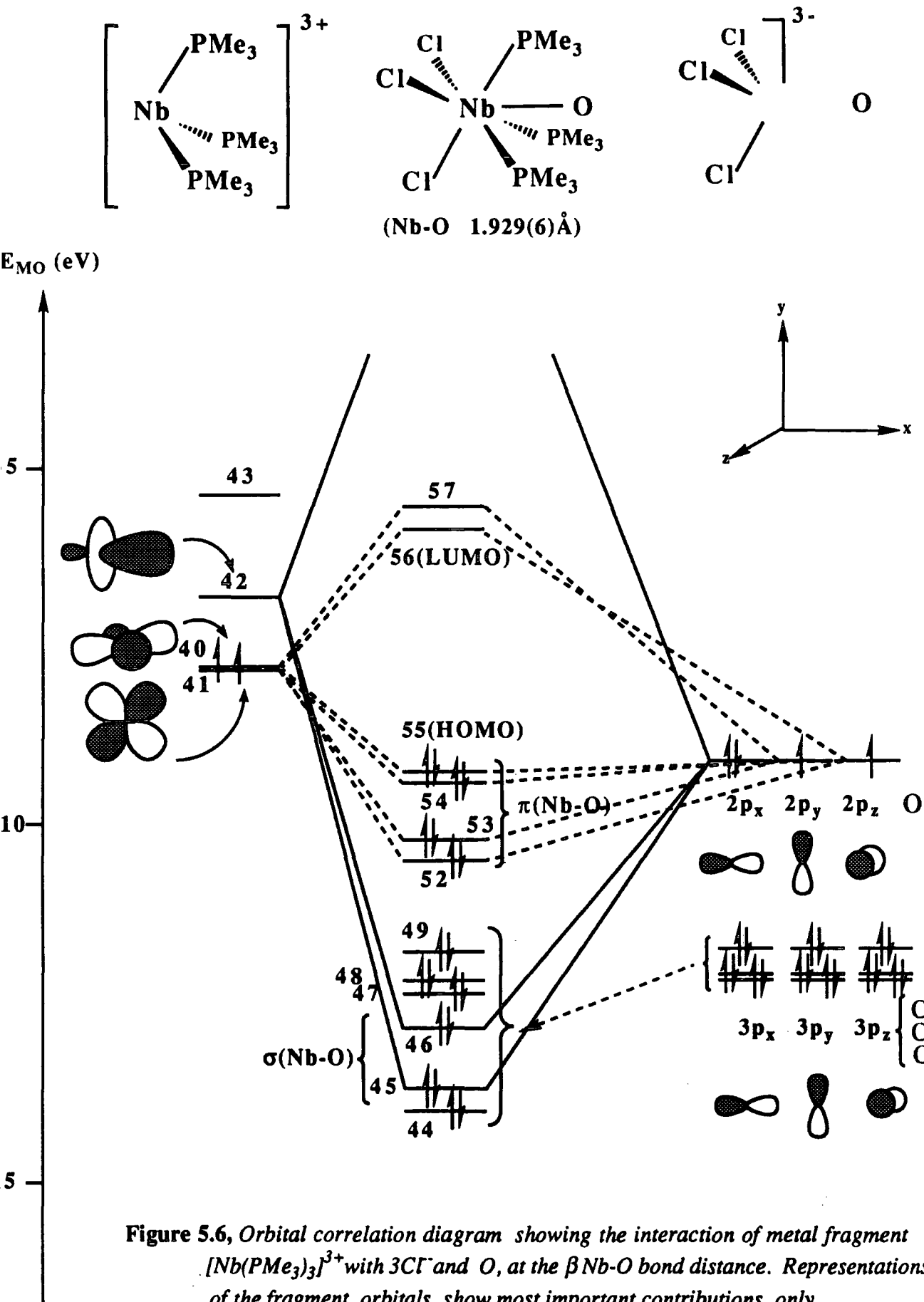
^a Fragment coordinates taken from α - $\text{Nb}(\text{O})\text{Cl}_3(\text{PMe}_3)_3$ X-ray structure.

Table 5.6

Since the bonding picture is more straight forward for the β isomer, the bonding in this species is discussed first.

b) β - $\text{Nb}(\text{O})\text{Cl}_3(\text{PMe}_3)_3$ Bonding Description.

The left-hand side of Figure 5.6 shows the frontier orbitals of the $[\text{Nb}(\text{PMe}_3)_3]^{3+}$ fragment. Fragment molecular orbitals (MO's) 40 and 41, the highest occupied and lowest unoccupied molecular orbitals (HOMO and LUMO) respectively, are π -symmetry orbitals (d_{xz} and d_{xy}) suitable for overlap with oxygen atomic orbitals (AO's) $2p_z$ and $2p_y$. 40 and 41 are close in energy and may be considered as singly occupied. This description would be consistent with the paramagnetism observed for the $\text{MX}_3(\text{PR}_3)_3$ species⁹, assuming the geometry of this fragment is close to that found for $[\text{NbCl}_3(\text{PMe}_3)_3]$ in $\text{Nb}(\text{O})\text{Cl}_3(\text{PMe}_3)_3$. MO 42 is an empty σ -symmetry orbital (55% $d_{x^2-y^2}$) which overlaps strongly with oxygen AO $2p_x$ to give the σ bond found mainly in complex MO's 45 and 46. The transfer of electron density from the oxygen $2p_x$



orbital (approximately) suggest that the σ interaction may be described as an O \rightarrow Nb dative covalent bond.

Π -interactions between Nb and O arise by the overlap of singly occupied $2p_z$ and $2p_y$ oxygen AO's with the essentially degenerate HOMO(40) and LUMO(41) of $[\text{Nb}(\text{PMe}_3)_3]^{3+}$. These interactions give rise to the complex molecular orbitals 53 and 55(HOMO), which are weakly π -bonding.

Weak chlorine-niobium $p\pi$ - $d\pi$ bonding interactions, found in complex MO's 44-49, arise from the interactions of Cl_{1,2,3} 3p AO's and metal fragment MO's.

Of particular note for the β isomer is the lack of mixing of the chlorine 3p AO's with oxygen containing complex MO's. This is not the case in the α isomer and appears to provide the key to the instability of the α isomer versus the β form.

c) α -Nb(O)Cl₃(PMe₃)₃ Bonding Description.

The interaction diagram for the α isomer is shown in Figure 5.7. The bonding is still dominated by a strong σ interaction between the oxygen $2p_x$ AO and the empty metal fragment MO 42(55% $d_{x^2-y^2}$), but with increased overlap between 2s and $2p_x$ AO's of oxygen with the $d_{x^2-y^2}$ niobium orbital; this is consistent with the shorter Nb-O bond distance. For comparison, the Mulliken overlap population ($2s + 2p_z$ of the O atom) is 0.199 for the α isomer compared with 0.177 for the β isomer. The π -interactions in the α -isomer are similar in nature to those found in the β isomer, but stronger. Thus, oxygen $2p_z$ and $2p_y$ AO's interact with fragment MO's 40 and 41, giving rise to π -bonding MO's 45, 46, 47 and 48. The corresponding Mulliken overlap population is 0.234 compared to 0.147 for the analogous β -isomer. However, a significant difference in the α -isomer is the presence of filled π^* antibonding molecular orbitals arising from the interaction of the oxygen AO's $2p_z$ and $2p_y$ with metal fragment orbitals 38 and 39 (Table 5.5) respectively. These antibonding interactions give rise to the formation of the complex frontier orbitals 53 and

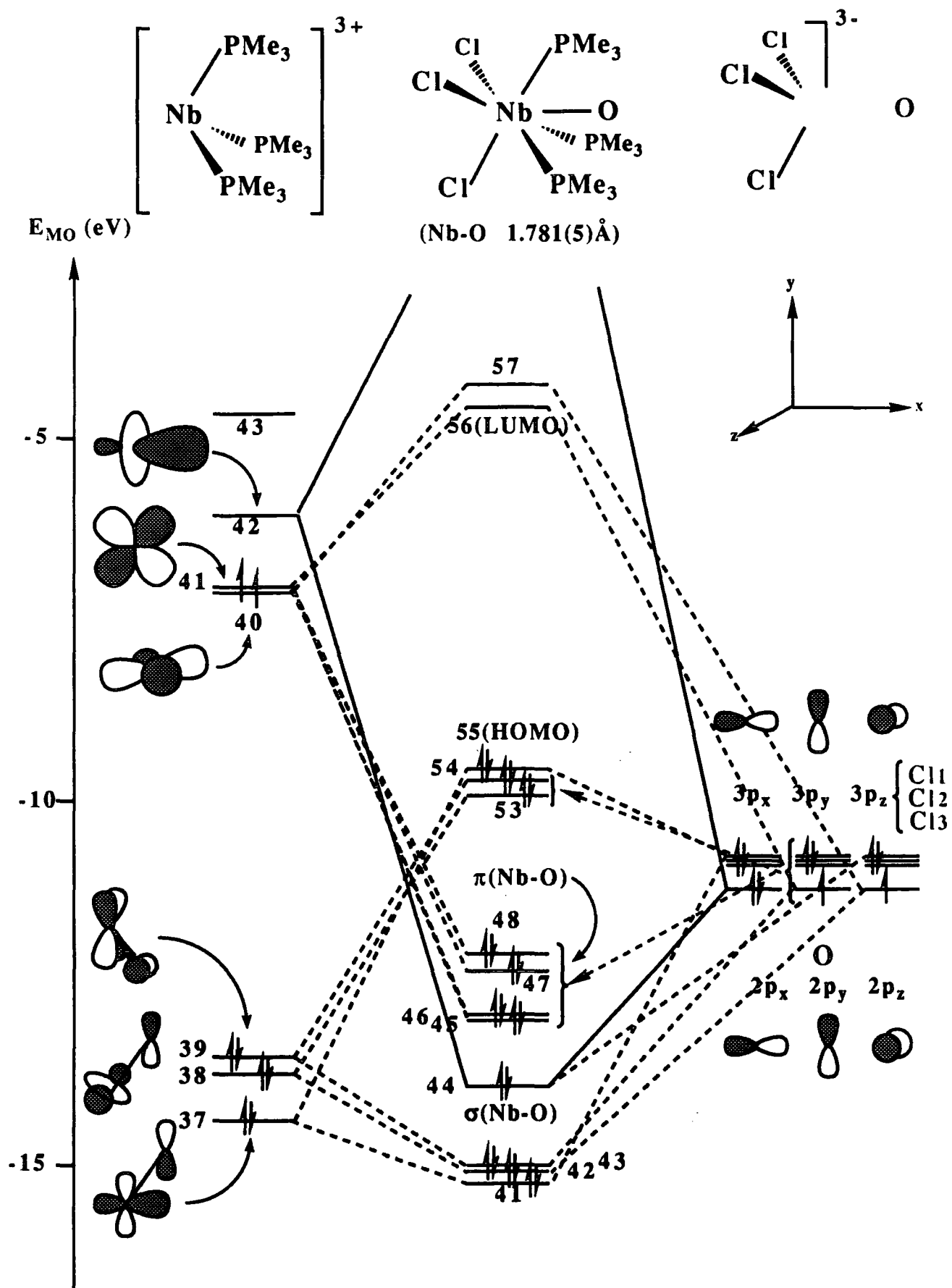


Figure 5.7, Orbital correlation diagram showing the interaction of metal fragment $[\text{Nb}(\text{PMe}_3)_3]^{3+}$ with 3Cl^- and O , at the α Nb-O bond distance. Representation of the fragment orbitals show most important contributions only.

54(SHOMO). The bonding counterparts to these interactions are found in complex MO's 42 and 43.

Further contributions to π^* antibonding character in these complex MO's is also arise from the interactions of the Cl1 $3p_y$ and Cl2 $3p_z$ with metal fragment MO's 38 and 39 respectively. Together, these antibonding interactions reflect the competition between filled oxygen and chlorine π -symmetry orbitals for $d\pi$ orbitals on the niobium atom and result in exceptionally long Nb-Cl bonds¹⁰. Further destabilisation of the α -Nb(O)Cl₃(PMe₃)₃ complex results from σ^* antibonding between Cl1 $3p_x$ and metal fragment orbital 37 giving rise to complex HOMO(55); the weak σ -bonding interaction between Cl1 $3p_x$ and metal fragment MO 37 is found in complex MO 41.

The composition of complex MO's of α and β -Nb(O)Cl₃(PMe₃)₃ are compared in Table 5.7.

d) Mulliken Population Analysis.

The final Mulliken populations of the α and β isomers give an indication of the charge (no. of electrons) on the separate fragments after interaction. The oxygen $2p_x$ and $2p_y$ orbitals gain electrons (assuming a neutral oxygen prior to the interaction), in both α and β isomers. The metal fragment HOMO and LUMO lose electrons, assuming that these MO's are degenerate, hence singly occupied. In both α and β isomers the oxygen $2p_z$ AO loses electrons to the metal d_{z^2} MO, this is consistent with a dative σ -dative covalent bond. The oxo ligand of the α isomer gains 0.73 electrons, (i.e. net atomic charge, -0.73), whereas the β isomer gains 0.77 electrons (net atomic charge -0.77). The chlorines remain essentially eight electron species i.e. Cl⁻ (α av. 7.55e⁻, β av. 7.50e⁻). Table 5.8 summarises the important changes in electron distribution of the fragment orbitals.

| MO | Composition of α -Nb(O)Cl ₃ (PMe ₃) ₃ (%) | | | Composition of β -Nb(O)Cl ₃ (PMe ₃) ₃ (%) | | |
|----------|--|---|--------------------|---|--|---|
| | Metal | Chlorine | Oxygen | Metal | Chlorine | Oxygen |
| 44 | 11 MO 37, 12 MO 42 | 12 3p | 64 2p _x | 3 MO 39, 12 MO 40, 11 MO 43 | 23 3p _x , 26 3p _y , 21 3p _z | 1 2p _z |
| 45 | 9 MO 38, 12 MO 41 | 3 3p _x , 22 3p _y , 23 3p _z | 16 2p _y | 8 MO 41, 9 MO 42, 4 MO 44 | 6 3p _x , 5 3p _y , 48 3p _z | 16 2p _x |
| 46 | 9 MO 39, 20 MO 40 | 9 3p _x , 21 3p _y , 20 3p _z | 12 2p _z | 8 MO 41, 9 MO 42, 3 MO 44 | 5 3p _x , 36 3p _y | 34 2p _x |
| 47 | 4 MO 41, 12 MO 44 | 21 3p _x , 17 3p _y , 2 3p _z | 25 2p _y | 7 MO 40, 4 MO 43 | 55 3p _x , 15 3p _y , 6 3p _z | 8 2p |
| 48 | 5 MO 40, 11 MO 43 | 41 3p _x , 14 3p _z | 25 2p _z | 2 MO 40, 2 MO 41 4 MO 44 | 34 3p _x , 10 3p _y , 26 3p _z | 12 2p _x , 3 2p _y , 3 2p _z |
| 53 | 18 MO 38, 1 MO 41 | 58 3p _y , 10 3p _z | 11 2p _y | 14 MO 38, 4 MO 41 | 4 3p _x , 27 3p _y , 9 3p _z | 39 2p _y |
| 54 | 20 MO 39, 1 MO 40 | 12 3p _y , 52 3p _z | 12 2p _z | 20 MO 37, 4 MO 45 | 55 3p _x , 2 3p _y , 2 3p _z | 4 2p |
| 55(HOMO) | 20 MO 37, 4 MO 45 | 68 3p _x , 3 3p _y | ----- | 16 MO 39, 3 MO 40 | 7 3p _x , 7 3p _y , 32 3p _z | 32 2p _z |

Table 5.7, Composition of the the frontier orbitals of α and β -Nb(O)Cl₃(PMe₃)₃ in terms of % metal fragment MO's and chloride and oxygen ligand AO's.

| Orbital | Start pop. | α -Nb(O)Cl ₃ (PMe ₃) ₃ | β -Nb(O)Cl ₃ (PMe ₃) ₃ |
|-------------------|------------|---|--|
| | | End pop. | End pop. |
| MO 37 | 2 | 1.956 | 1.954 |
| MO 38 | 2 | 1.962 | 1.964 |
| MO 39 | 2 | 1.960 | 1.968 |
| MO 40 | 1 | 0.587 | 0.590 |
| MO 41 | 1 | 0.586 | 0.588 |
| MO 42 | 0 | 0.501 | 0.536 |
| O 2ps | 2 | 1.846 | 1.895 |
| O 2p _x | 2 | 1.671 | 1.605 |
| O 2p _y | 1 | 1.604 | 1.629 |
| O 2p _z | 1 | 1.610 | 1.639 |
| Cl 3p | 2 | 1.86 ^a | 1.84 ^a |

^a Average value taken from Cl1,2 and 3 3p orbitals

Table 5.8

5.3.3 Fenske-Hall MO Calculations on Nb(O)Cl₃(PH₃)₃.

The principal differences in the electronic structure of the two isomers appear to arise as a result of interaction of fragment MO's 37 38 and 39 in the case of the α -isomer with oxygen 2p and chlorine 3p orbitals. The energies of these fragment MO's is noticeably decreased on moving from the α to β Nb-O bond length (α , *ca.* -15eV; β , *ca.* -18 eV) The compositions of MO's 37-39 also indicate significant contributions from phosphorous 3p orbitals (Table 5.7), which suggests that the energies of the p-orbitals on phosphorus may play a significant part in bond-stretch isomerism. Of course, the p-orbitals energies will be most dramatically affected by the phosphine substituents. The more electron releasing substituents e.g. PMe₃ will lead to relatively higher phosphorus orbital energies, possibly allowing better overlap with Nb d-orbitals.

In order to determine whether the electronic nature of the R group in $\text{Nb}(\text{O})\text{Cl}_3(\text{PR}_3)_3$ could have an effect on the composition and energy of the frontier orbitals, the calculations were carried out on the model species $\text{Nb}(\text{O})\text{Cl}_3(\text{PH}_3)_3$ at several Nb-O bond lengths (1.692-2.087 Å). Determination of the composition of $[\text{Nb}(\text{PH}_3)_3]^{3+}$ reveals the same trend as seen in $\text{Nb}(\text{O})\text{Cl}_3(\text{PMe}_3)$, the HOMO (13) and LUMO (14) consisting mainly of Nb d_{xz} (73%) and d_{xy} (76%) respectively, and the lower lying orbitals containing a substantial P 3p character (MO's 10-12).

On interaction of the metal fragment with 3 chloride ligands (Cl^-) and oxygen (O) a similar bonding picture to that seen in $\text{Nb}(\text{O})\text{Cl}_3(\text{PMe}_3)_3$ is obtained. At long Nb-O bond lengths there is still no significant interaction of metal fragment MO's 10-12 with O and Cl^- to form π^* antibonding interactions, but at shorter bond lengths π^* antibonding becomes apparent.

The only significant difference on replacing PMe_3 ligands with PH_3 ligands, is in the energies of the frontier orbitals 10-12, which appear to remain at a similar relative energy to the HOMO 13 at all Nb-O bond lengths. This result suggests that the reduced involvement of the three metal fragment equivalent MO's (37-39) at longer Nb-O distances, may be more a consequence of the oxygen A.O energies than donating ability of the phosphine.

5.3.4 Variation of the Nb-O Bond Length in $\text{Nb}(\text{O})\text{Cl}_3(\text{PMe}_3)_3$.

Having used Fenske-Hall MO calculations to construct correlation diagrams for the interaction of metal fragment $[\text{NbCl}_3(\text{PMe}_3)_3]$ and neutral oxygen, calculations were run at differing Nb-O bond lengths in order to monitor the effect of bond lengthening on key orbital interactions, and possibly identify energy minima corresponding to differing bond lengths. The calculations were first performed using the coordinates of the α -isomer and then using the coordinates of the β -isomer. Eighteen Nb-O bond lengths were selected in the range 1.692-2.177 Å. The energies,

Mulliken overlap populations, final Mulliken populations and composition of the frontier orbitals of the final complex were monitored at each Nb-O bond length.

a) The MO Energies.

The overall energy of the $\text{Nb(O)Cl}_3(\text{PMe}_3)_3$ complex is found to increase slightly on extending the Nb-O bond length. (Figure 5.8).

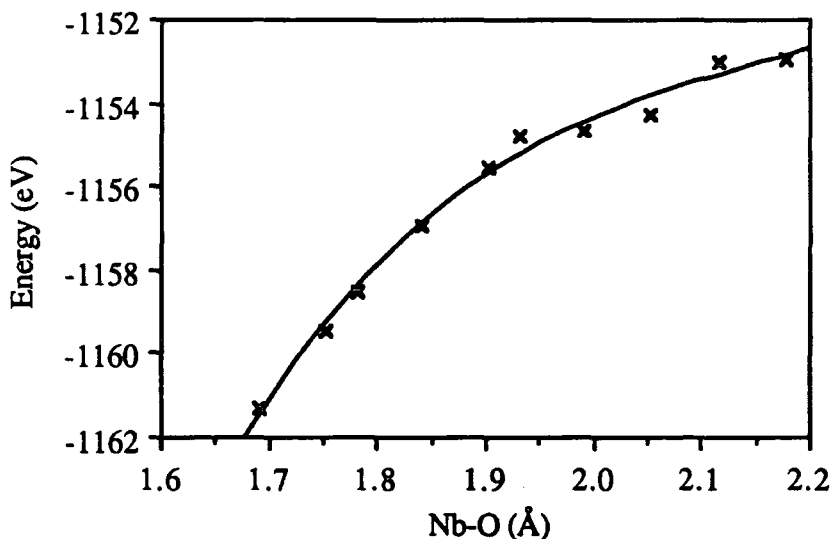


Figure 5.8, The total energy of the occupied MO's of $\text{Nb(O)Cl}_3(\text{PMe}_3)_3$ on variation of the Nb-O bond length.

This trend appears at variance with the experimental observation that the β isomer is thermodynamically more stable, but caution is required in the interpretation of this result, as it may be an anomaly arising from the Fenske-Hall method.

Selected orbitals have also been monitored. A summation of the energy of occupied $\text{Nb(O)Cl}_3(\text{PMe}_3)_3$ complex MO's 49-55(HOMO) does show an energies minimum on variation of Nb-O bond length. This minimum arises in the range 1.85-1.91 Å, significantly closer to the β than the α Nb-O bond length (Figure 5.9)

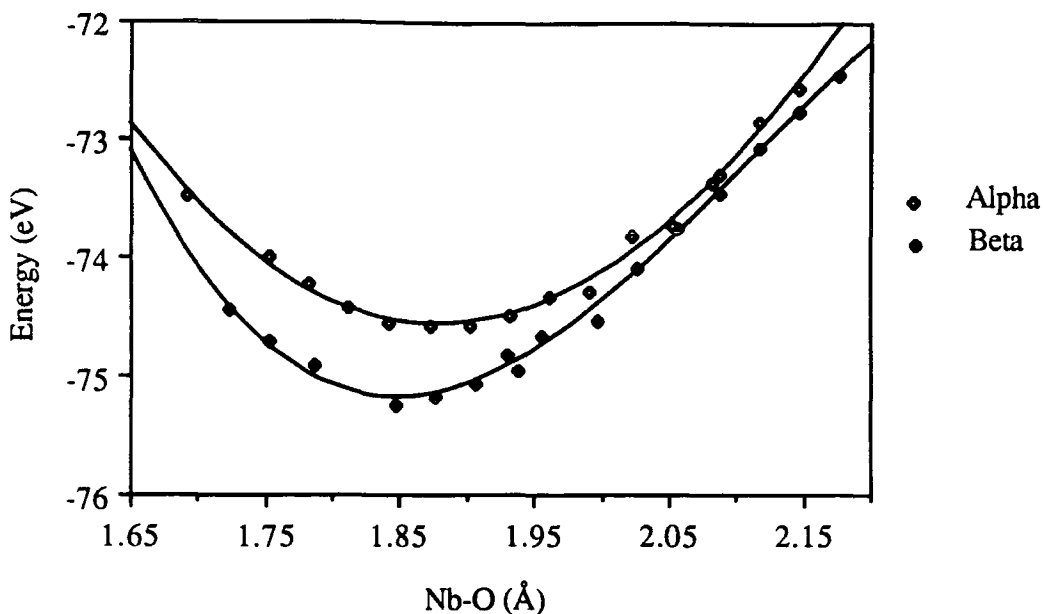


Figure 5.9, *The variation of the summed energies of frontier MO's 49-55 of $Nb(O)Cl_3(PMe_3)_3$ with Nb-O bond length.*

The energies of the individual frontier orbitals MO's 54 and 55, appear to drop to an energy minimum at a Nb-O bond length of *ca.* 1.90Å, close to the bond length found in β - $Nb(O)Cl_3(PMe_3)_3$ (1.929Å)(Figure 5.10). An energy minimum for complex MO 53 is found at a slightly shorter Nb-O bond distance of *ca.* 1.85Å .

b) The MO Compositon.

The compositions of frontier MO's 51 to 55(HOMO) were also monitored against the change in Nb-O bond distance. From the two fragment interaction calculations discussed earlier, it can be seen that there is a 'crossing' of MO's 54 and 55 on moving from α to β Nb-O bond lengths, i.e. when fragment MO 52 and oxygen $2p_z$ AO character is no longer found in complex MO 54 but in MO 55(HOMO) (see table 5.3). This cross-over position coincides with the point at which the Cl 3p dominated metal fragment MO's 49 and 50 become less involved in complex frontier MO's 53 and 54, and are found in lower lying complex MO's 51 and 52 respectively. From Figure

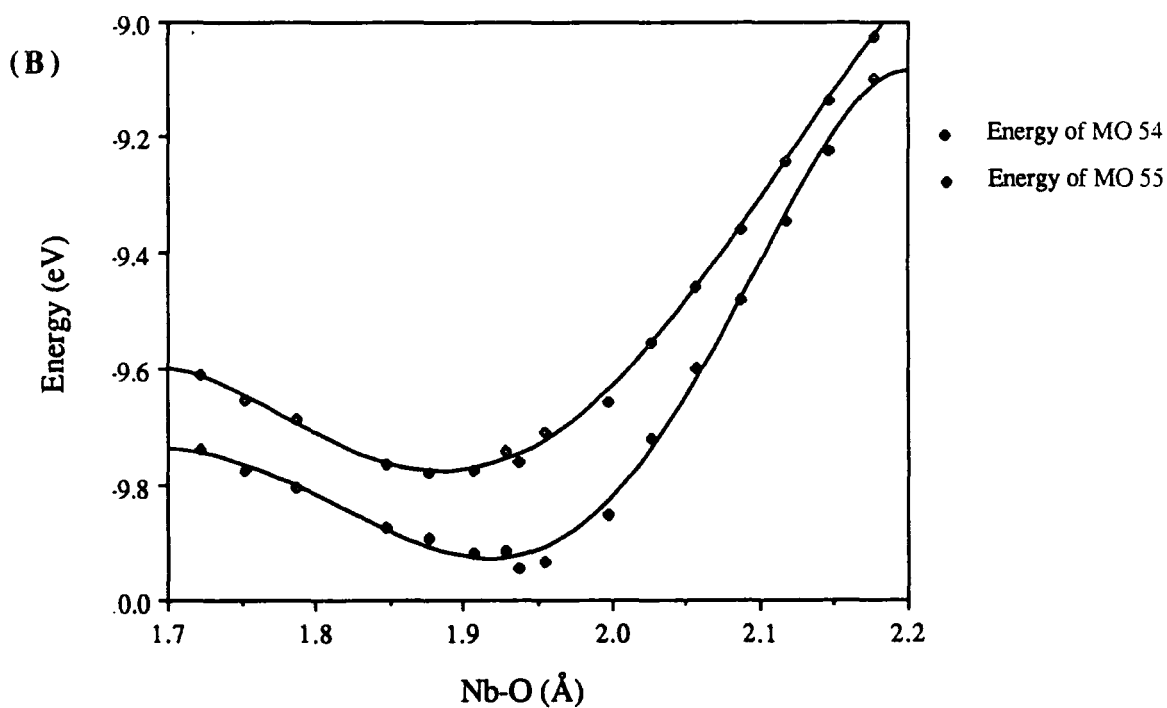
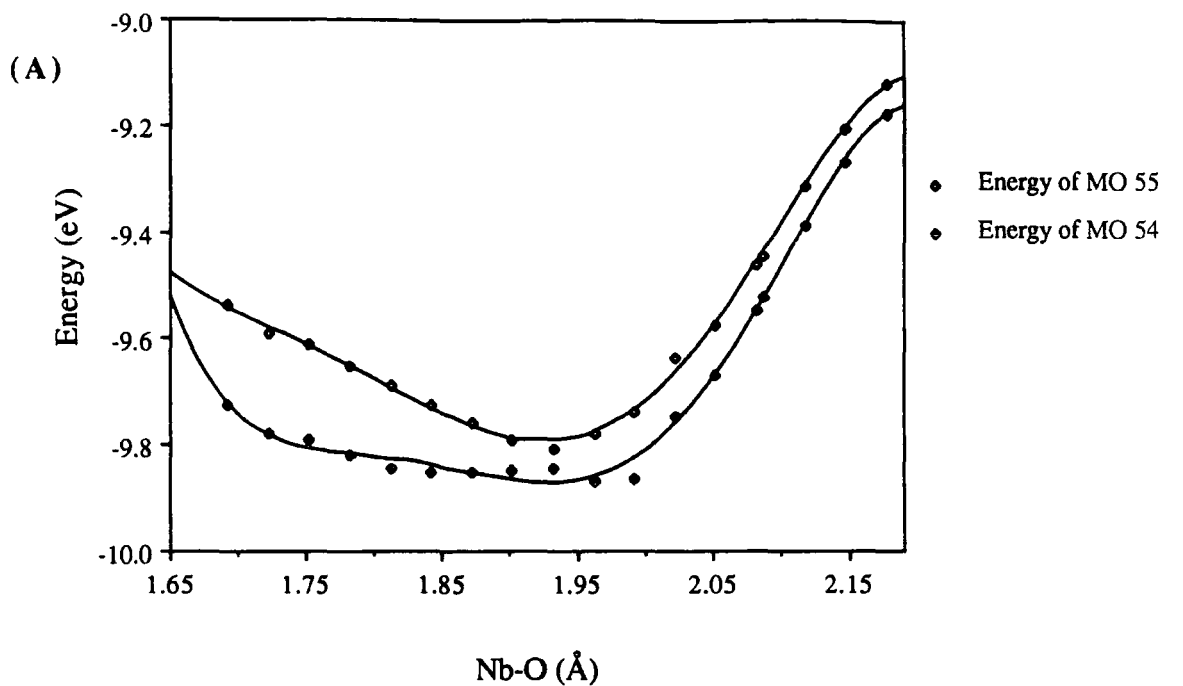


Figure 5.10, The energy of MO's 54 and 55 of complex $Nb(O)Cl_3(PMe_3)_3$ on variation of Nb-O bond lengths:

(A) Using α - $NbCl_3(PMe_3)_3$ coordinates,

(B) Using β - $NbCl_3(PMe_3)_3$ coordinates.

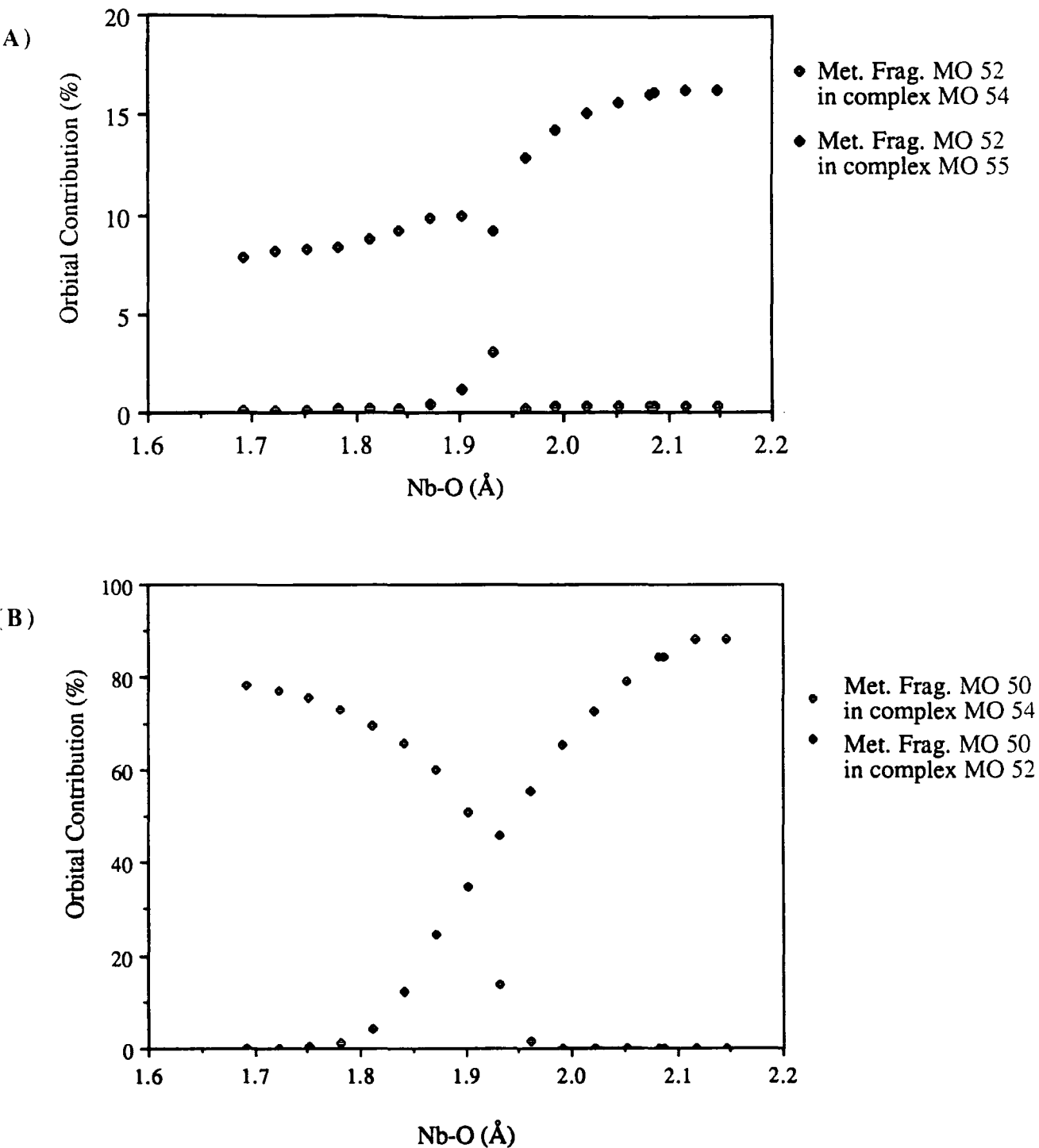


Figure 5.11, Composition of $Nb(O)Cl_3(PMe_3)_3$ complex MO's, on variation of Nb-O bond length:
 (A) % of metal fragment MO 52 in complex MO's 54 & 55
 (B) % of metal fragment MO 50 in complex MO's 54 & 52

5.11, it can be seen that the change over is quite abrupt and that the Nb-O bond length at this cross-over point is i.e. 1.92-1.95 Å, in the region of the Nb-O β bond length.

Another frontier orbital crossing is found at a slightly longer Nb-O bond length of *ca* 1.98 Å, when complex MO 53 becomes MO 54, containing contributions from fragment MO 53 and oxygen 2p_y (Figure 5.12).

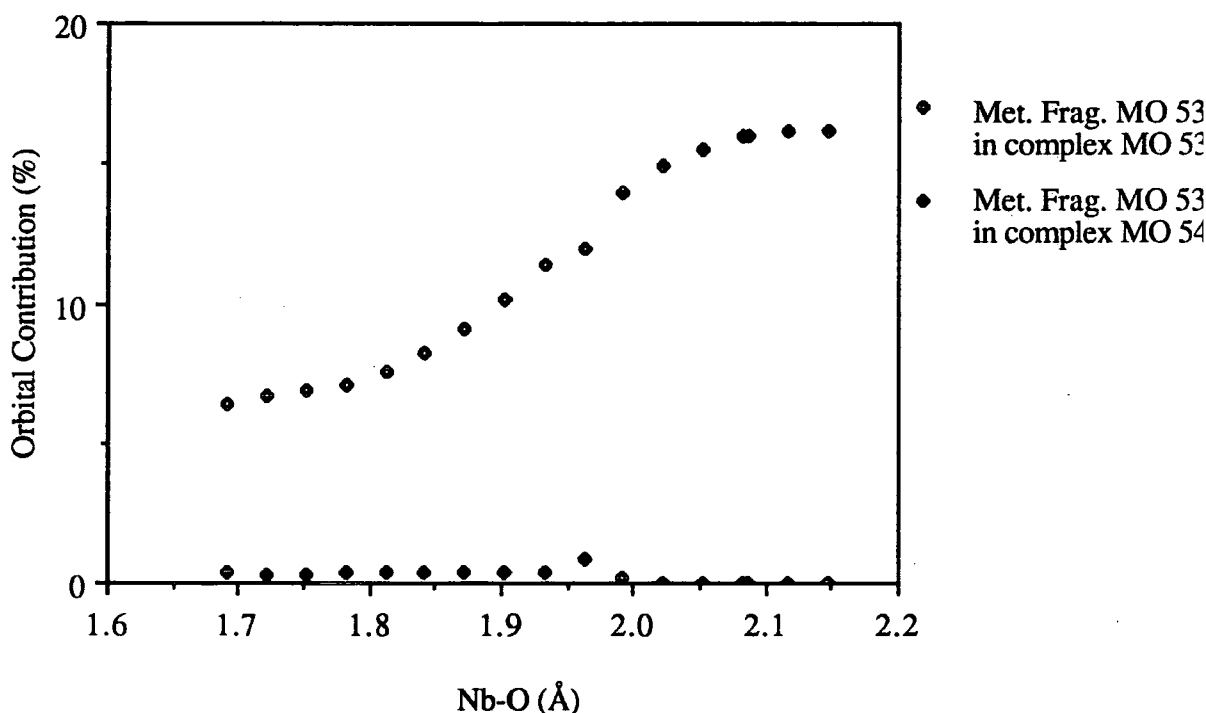


Figure 5.12, % of metal fragment MO 53 in $Nb(O)Cl_3(PMe_3)_3$ complex MO's 53 & 54, on variation of Nb-O bond length.

These orbital cross-overs may be regarded as a consequence of the second-order Jahn-Teller effect, leading to stabilisation of certain filled levels, and distinct therefore from the cross-overs identified in d^1 complexes.

c) The Mulliken Overlap Population and Final Mulliken Population.

From Figure 5.13 it can be seen that an increase of Nb-O bond length in complex $Nb(O)Cl_3(PMe_3)_3$ causes a decrease in Mulliken overlap population of oxygen π -symmetry orbitals, 2p_y and 2p_z with metal fragment π -symmetry orbitals 53 and 52

respectively, i.e. a weakening of Nb-O π -bonding. The σ -bonding, taken as a combination of oxygen 2s and 2p_x overlap with metal fragment MO 54, shows a very small decrease on lengthening the Nb-O distance. However, it is interesting to note that a 'cross-over' in the σ and π -bonding occurs between the bond lengths established for the two isomers.

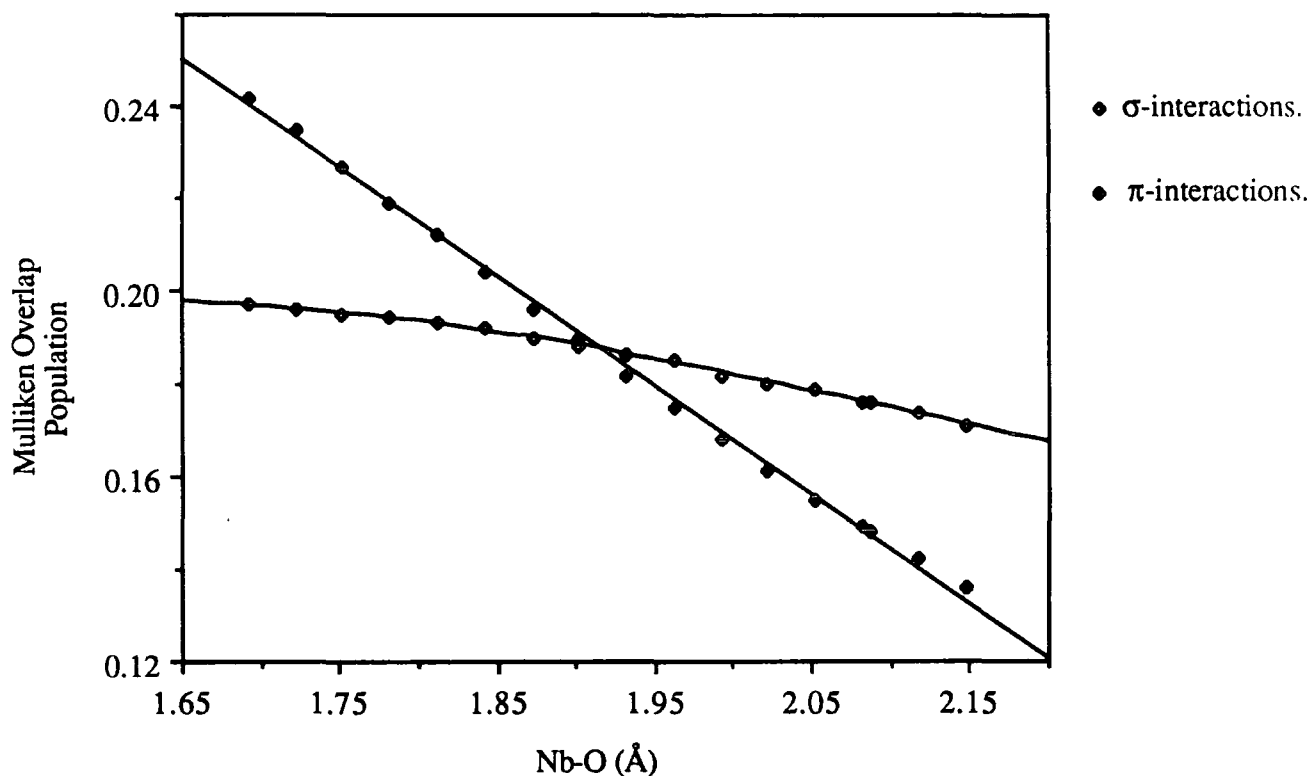


Figure 5.13, σ and π interfragment Mulliken Overlap population, on variation of the Nb-O bond length.

The final Mulliken population is best seen in terms of total charge loss from the metal fragment and gain on the oxygen atom. As expected an increased Nb-O bond length leads to a greater charge on the oxygen atom (Figure 5.14)

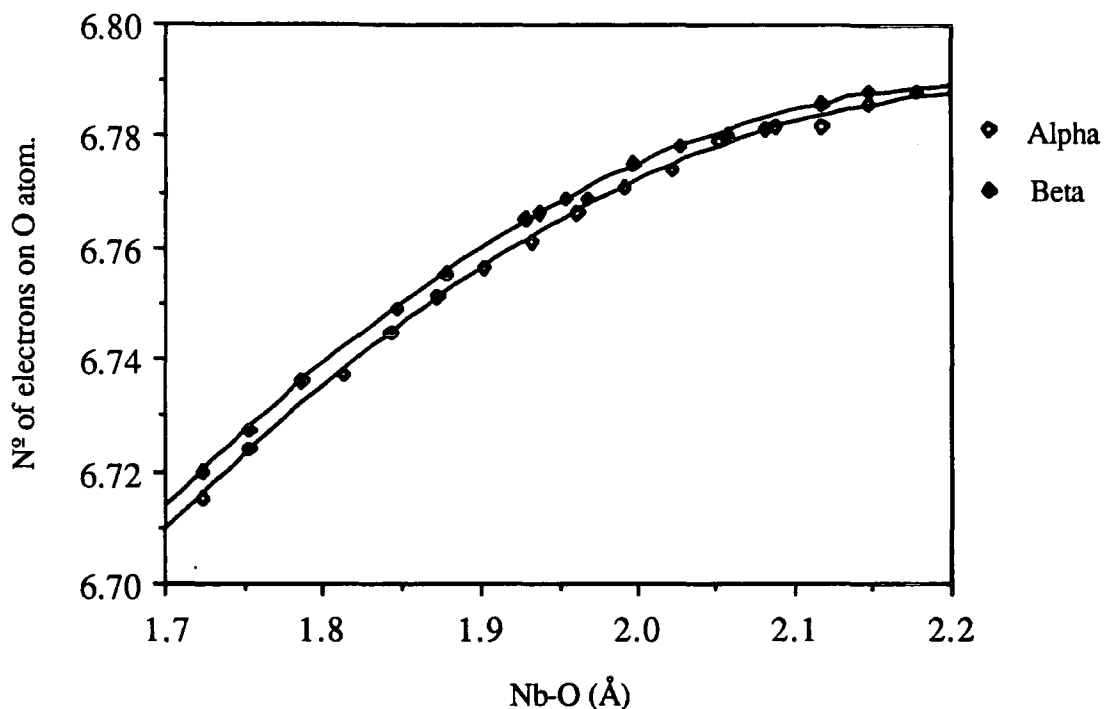


Figure 5.14, *Final Mulliken population on oxygen after interaction with α - and β - $\text{NbCl}_3(\text{PMe}_3)_3$ metal fragment, on variation of Nb-O bond length.*

d) Oxygen-Hydrogen Interatomic distances.

The possibility of a steric effect accounting for the stabilisation of two bond-stretch isomers in these relatively crowded seven coordinate molecules was also considered. Therefore, the interatomic distances between oxygen and the closest hydrogens of the PMe_3 ligands (Figure 5.15) were monitored against the Nb-O bond length.

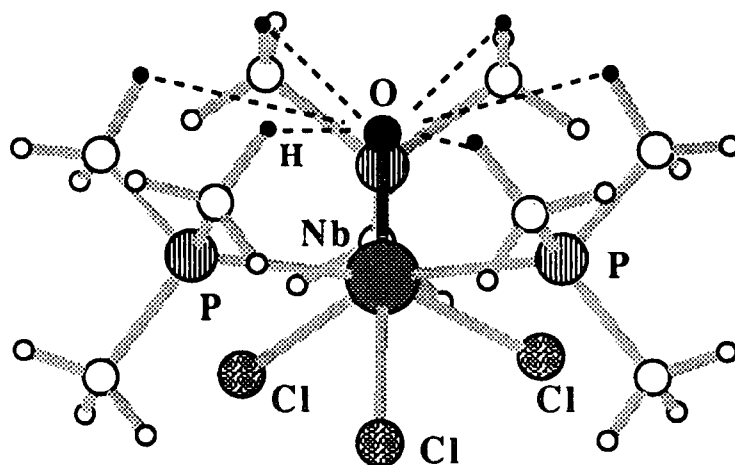


Figure 5.15, Diagram to show the six H's closest to the oxygen in $Nb(O)Cl_3(PMe_3)_3$. Dotted lines illustrate possible O...H hydrogen bonding.

Figure 5.16 shows the average distance of the six hydrogens (H(11B), H(13A), H(21A), H(23B), H(31C) and H(32A)) from the oxygen on variation of the Nb-O bond length. The closest H...O distance is between H(13A) and O (2.70 Å), and the largest between H(11B) and O (2.99 Å). It should be noted, that all distances are below 3 Å and lie just within hydrogen bonding range¹¹.

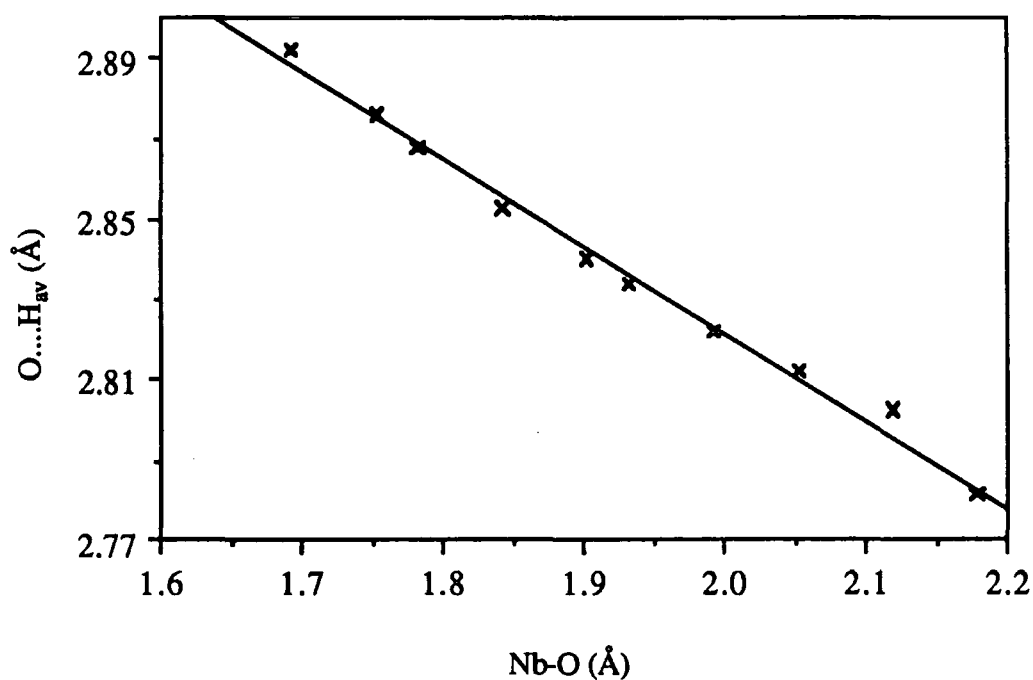
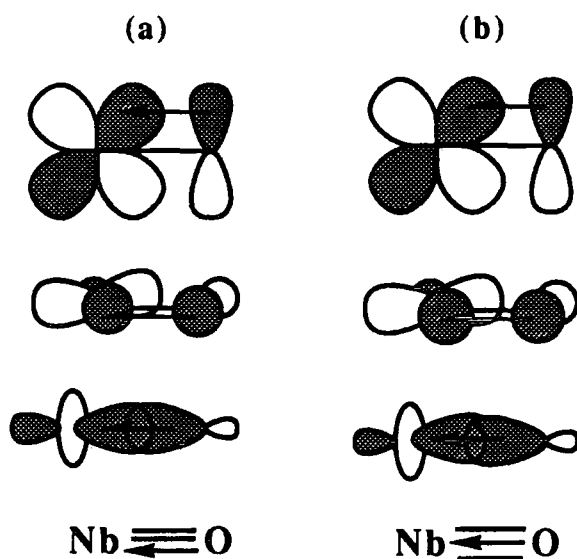


Figure 5.16, Average interatomic distance between the six hydrogens and closest to the oxygen atom in $Nb(O)Cl_3(PMe_3)_3$, on variation of Nb-O bond length.

A linear decrease in the average O...H distance on increasing the Nb-O bond length appears to preclude a steric explanation for bond-stretch isomerism, although an unusual electronic effect due to multiple hydrogen bonding cannot, at this stage, be ruled out.

5.3.5 Overall Bonding Description

The overall bonding description in both α and β isomers appears to consist of a σ -dative covalent interaction and two π -covalent bonds. This bonding picture is similar to the bonding picture described by Rappé and Goddard for $\text{Cr}(\text{O})\text{Cl}_4$ ¹², Figure 5.17(a), rather than the traditional description involving $\sigma + \pi$ covalent bonds with additional $p\pi-d\pi$ lone pair donations (Figure 5.17(b))¹⁸. However, some caution in the interpretation of these MO calculations in favour of a particular bonding picture is required. Confirmation must await supporting *ab initio* calculations.



5.17, A comparison of Nb-O bonding:
 (a) Traditional bonding picture.
 (b) Goddard & Rappé bonding picture.

5.4 Fenske-Hall MO Calculations on $\text{Nb}(\text{S})\text{Cl}_3(\text{PMe}_3)_3$.

As discussed earlier, two isomeric forms of $\text{Nb}(\text{S})\text{Cl}_3(\text{PMe}_3)_3$, which are isostructural and isomorphous with their oxo analogues, have been isolated in this laboratory. (Figure 5.18).

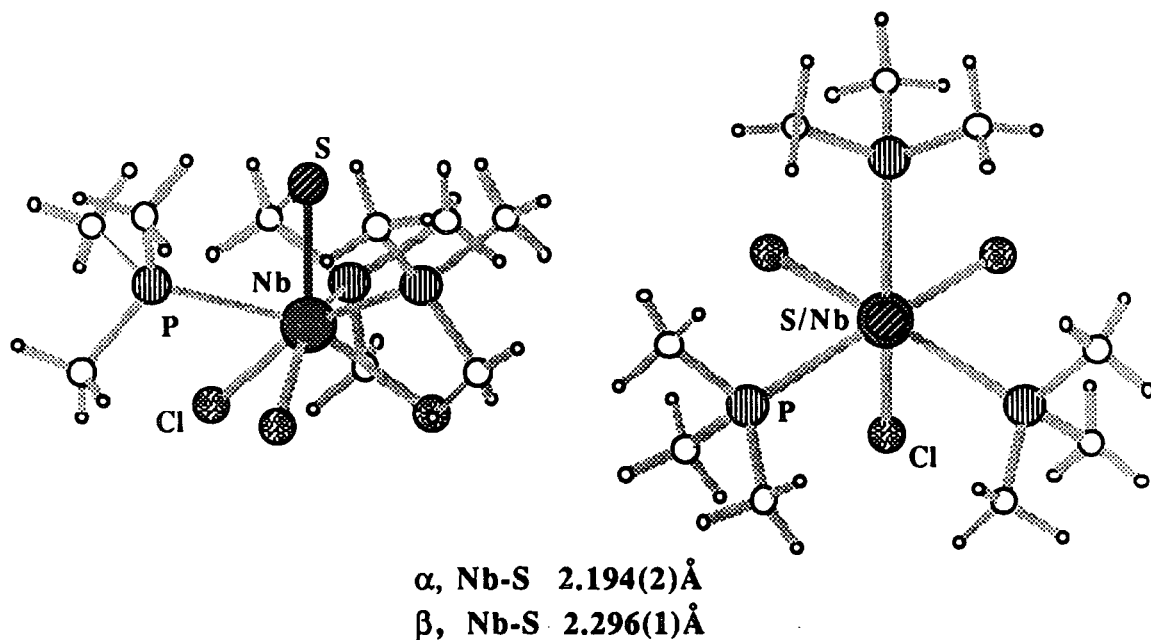


Figure 5.18, The molecular structure of α and β - $\text{Nb}(\text{O})\text{Cl}_3(\text{PMe}_3)_3$.

The two yellow and green isomers differ mainly in Nb-S bond length with minor changes in Nb-Cl bond lengths. These differences are shown in Table 5.9.

| Bond | Bond Length (Å) | |
|--------|---|--|
| | α - $\text{Nb}(\text{S})\text{Cl}_3(\text{PMe}_3)_3$ | β - $\text{Nb}(\text{S})\text{Cl}_3(\text{PMe}_3)_3$ |
| Nb-S | 2.194(2) | 2.296(1) |
| Nb-Cl1 | 2.490(2) | 2.475(1) |
| Nb-Cl2 | 2.516(2) | 2.501(1) |
| Nb-Cl3 | 2.491(2) | 2.482(2) |

Table 5.9

Clearly, the differences in Nb-E and Nb-Cl bond lengths are not as pronounced as for Nb(O)Cl₃(PMe₃)₃, but are still significant. The Nb-S bond length difference between isomers is 0.102 Å and the Nb-Cl bond length difference is *ca.* 0.013 Å (average).

Quantum mechanical Fenske-Hall MO calculations, analogous to those described for Nb(O)Cl₃(PMe₃)₃, have been carried out on Nb(S)Cl₃(PMe₃)₃ by T.K. Wells¹³.

In the five fragment analysis, the composition of fragment frontier orbital and differences in the frontier orbitals of the α and β isomers were found to be very similar to their oxo analogues. In α -Nb(S)Cl₃(PMe₃)₃, interaction of sulphur and chlorine 3p_y and 3p_z AO's with filled metal fragment orbitals lead to π^* antibonding found in the highest filled complex MO's. As in Nb(O)Cl₃(PMe₃)₃, these unfavourable interactions are removed on elongation of the Nb-S bond to form β -Nb(S)Cl₃(PMe₃)₃.

Interestingly, as for the oxygen analogue, the Nb-S bonding appears to consist of a σ -dative covalent interaction and two π -covalent bonds. Also, a greater Mulliken overlap population is found between the metal fragment and the sulphur in α and β -Nb(S)Cl₃(PMe₃)₃ than their oxo counterparts. This is reflected in the final Mulliken population which indicates less electron density is retained on the sulphur atom (α , net atomic charge -0.63; β net atomic charge -0.67) compared with the oxygen atom. This is not entirely surprising as sulphur has more diffuse AO's, which are closer in energy to the niobium d-orbitals.

5.5 Fenske-Hall MO Calculations on Mo(N)Cl₃(PMe₃)₃

As discussed in chapter 4, the reaction of M(N)Cl₃ with PMe₃ failed to yield the desired M(N)Cl₃(PMe₃)₃ (M = W, Mo) complexes. Instead, phosphiniminato derivatives were isolated and found to subsequently convert to binuclear μ_2 -nitrido species. It was shown by A. Shaw that the niobium oxo and sulphido bond-stretch isomers decompose to give O=PMe₃ and S=PMe₃ respectively, presumably via migration of PMe₃ to the metal bound oxo and sulphido ligand². The phosphiniminato

ligand must arise by attack of PMe_3 on the metal-bound nitride ligand, suggesting that the phosphiniminato species may arise by an analogous decomposition of a first-formed terminal nitrido species, possibly $\text{Mo}(\text{N})\text{Cl}_3(\text{PMe}_3)_3$.

5.5.1 Mo-N Bonding in $\text{Mo}(\text{N})\text{Cl}_3(\text{PMe}_3)_3$.

The geometry of $\text{Mo}(\text{N})\text{Cl}_3(\text{PMe}_3)_3$ used in these MO calculations was based on the monocapped octahedral $\text{Nb}(\text{O})\text{Cl}_3(\text{PMe}_3)_3$ species, with facial arrangements of the chloro and trimethylphosphine ligands (Figure 5.19).

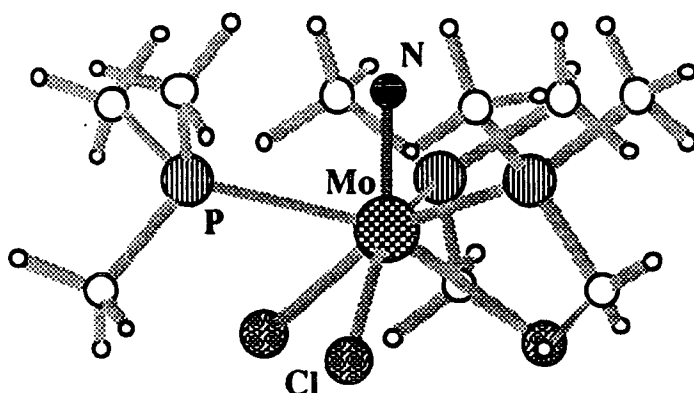


Figure 5.19, The structure used for calculations on the hypothetical molecule $\text{Mo}(\text{N})\text{Cl}_3(\text{PMe}_3)_3$.

Using Fenske-Hall quantum mechanical calculations the frontier orbitals of $[\text{Mo}(\text{PMe}_3)_3]^{4+}$ were constructed, and subsequently interacted with three chloride (3Cl^-) ligands and an N^- ligand (these ligand charges were chosen to allow direct comparison with the niobium oxo analogues) at three Mo-N distances, 1.60Å (a), 1.70Å (b) and 1.80Å (c), which span the range of known transition metal-nitride bond lengths¹⁴. A correlation diagram for this interaction at Mo-N bond length (b) is shown in Figure 5.20.

The overall bonding picture at Mo-N lengths (a), (b) and (c), indicates the formation of a σ -type dative bond between N sp_x and metal $\text{d}_{x^2-y^2}$, and two weaker π -type covalent bonds formed by the interaction of N $2p_y$ and $2p_z$ with metal d_{xy} and d_{xz}

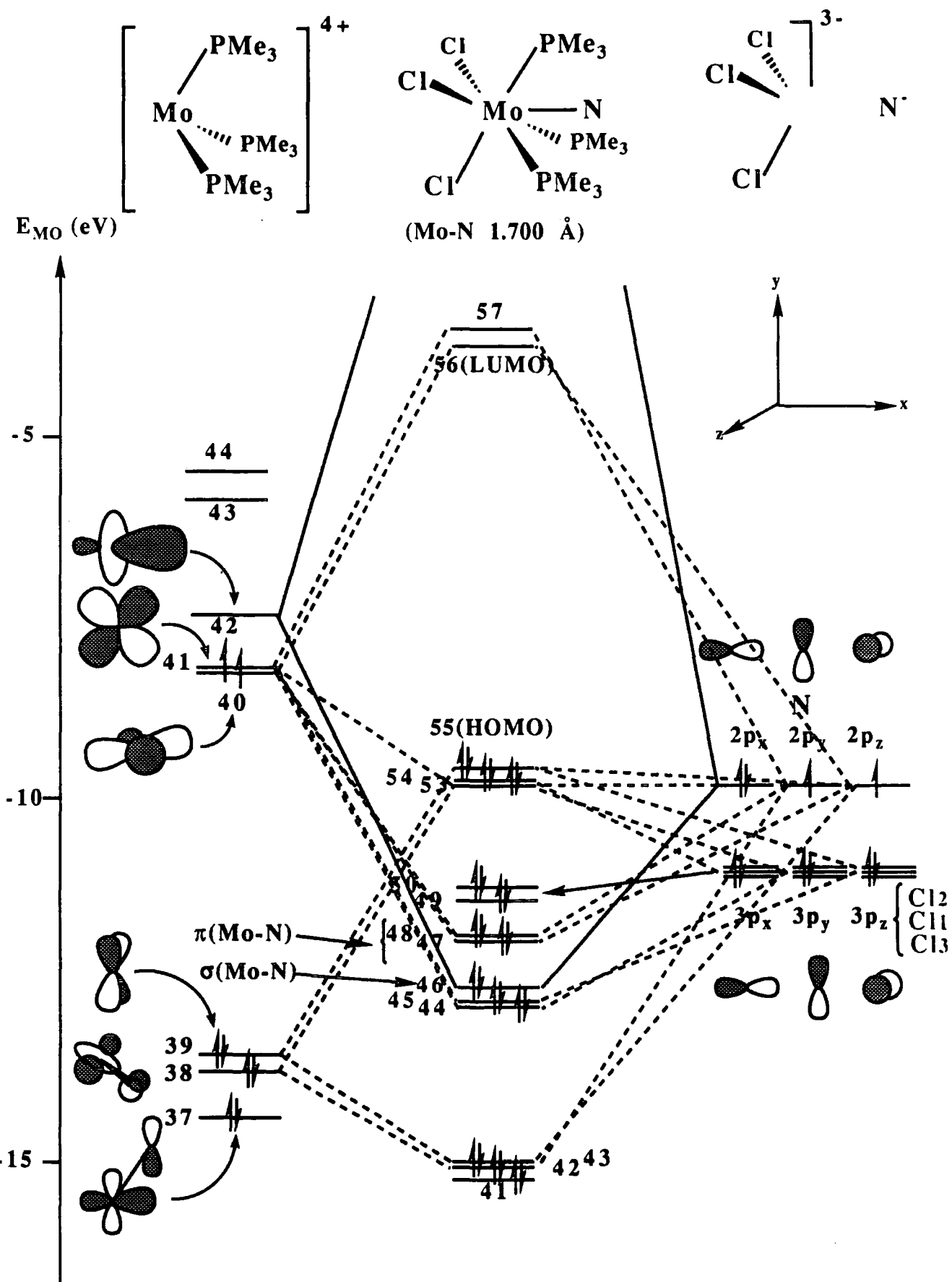


Figure 5.20, *Orbital correlation diagram showing the interaction of hypothetical metal fragment $[\text{Mo}(\text{PMe}_3)_3]^{4+}$ with 3Cl^- and N^- . Representations of the fragment orbitals show most important contributions only.*

respectively. (Figure 5.20). Although the same Mo-N bonding interactions are seen at all three Mo-N distances, in terms of Mulliken overlap population, the overall bond strength understandably decreases on lengthening the Mo-N bond (Table 5.10).

| | | Mo(N)Cl ₃ (PMe ₃) ₃ | | |
|-----------------------------------|-----------------|---|--------------|--------------|
| Metal frag. MO | Nitrogen AO | Mo-N, 1.60 Å | Mo-N, 1.70 Å | Mo-N, 1.80 Å |
| 42 | 2s | 0.112 | 0.093 | 0.075 |
| 42 | 2p _x | 0.139 | 0.154 | 0.165 |
| 41(LUMO) | 2p _y | 0.181 | 0.161 | 0.142 |
| 40(HOMO) | 2p _z | 0.178 | 0.158 | 0.139 |
| Total Mulliken Overlap Population | | 0.610 | 0.566 | 0.521 |

Table 5.10, *The Mulliken overlap population of the A.O's of N⁻ with those of the [Mo(PMe₃)₃]⁴⁺ fragment on variation of the Mo-N bond length.*

Compared with the Nb-E bonding in Nb(E)Cl₃(PMe₃)₃ (E = O, S), the nitrogen bonding is significantly stronger in terms of Mulliken overlap population, which is consistent with greater electron charge density on the metal fragment. For example, at the Mo-N length in (b), the final Mulliken population indicates a net atomic charge on the nitrogen of -0.78, i.e. a charge transfer of 2.22e⁻ to the metal centre from a nitride (N³⁻) ligand. c.f. a charge transfer of 1.27e⁻ to the metal centre from O²⁻ in α-Nb(O)Cl₃(PMe₃)₃.

In the α and β isomers of Nb(E)Cl₃(PMe₃)₃, lengthening of the M-E (E=O,S) bond removes unfavourable π* and σ* antibonding interactions arising from Cl 3p and E p interactions. In Mo(N)Cl₃(PMe₃)₃, although a small amount of Cl π* antibonding is found, variation of the Mo-N bond length from (a) to (c) makes little difference to its magnitude. The only significant difference found on variation of Mo-N bond length, is a MO crossing of the Cl 3p_x dominated SHOMO with the third highest occupied Mo-N π-bonding MO, on increasing bond length from (a) to (b). This is similar to the crossing of MO 53 with MO 54 in Nb(O)Cl₃(PMe₃)₃.

If Cl and E π^* antibonding interactions are important for destabilising one isomer in favour of a second M-E bond-lengthened form, these calculations suggest that bond-stretch isomers of the hypothetical species $\text{Mo}(\text{N})\text{Cl}_3(\text{PMe}_3)_3$ are unlikely to exist, at least over reasonable Mo-N distances. However, this conclusion may also reflect how little is still understood about the origin of the effect in this system and the phenomenon in general.

5.6 Summary and Conclusions.

The calculations presented in this chapter reveal striking electronic differences between isomers of $\text{Nb}(\text{E})\text{Cl}_3(\text{PMe}_3)_3$ upon elongation of the multiply-bonded main group atom. The antibonding interactions at short Nb-E distances account for the instability of this species with respect to conversion to a bond-lengthened (β) form and also explain why relatively long Nb-Cl distances are observed in the α -isomer. Monitoring the frontier orbital energies over a range of Nb-O distances shows that a rather abrupt change occurs in the region 1.85 -1.95 Å with a 'crossing over' of frontier levels, although the significance of this in creating two energy minima could not be established using the calculations employed here.

Examination of related phosphine species did not provide convincing evidence that the donor ability of the phosphine is crucial to the effect, which is therefore more likely to be overridden by the oxygen AO energies.

No evidence could be obtained for the likely existence of bond-stretch isomers in closely related nitrido complexes.

5.7 References.

1. V.C. Gibson, T.P. Kee, R.M. Sorrell, A.P. Bashall and M. McPartlin, *Polyhedron*, 1988, **7**, 2221
2. A. Shaw, *Thesis*, 1989; A. Bashall, V.C. Gibson, T.P. Kee, M. McPartlin and A. Shaw, *In Press*.
3. O. Robinson and D.N. Williams, *Unpublished O¹⁸ labelling studies*.
4. (a) Y. Jean, A. Lledos, J.K. Burdett and R. Hoffmann, *J. Chem. Soc. Chem. Commun.*, 1988, 140.
(b) Y. Jean, A. Lledos, J.K. Burdett and R. Hoffmann, *J. Chem. Am. Chem. Soc.*, 1988, **110**, 4506.
5. J. Chatt, L. Manojlovic-Muir and K.W. Muir, *J. Chem. Soc. Chem. Commun.*, 1971, 655.
6. K. Wieghardt, G. Backes-Dahmann, B. Nuber and J. Weiss, *Angew. Chem. Int. Ed. Engl.*, 1985, **24**, 777.
7. J.K. Burdett, *"Molecular Shapes"*, 1980, Wiley, New York.
8. R.F. Fenske and M.B. Hall, *Inorg Chem.*, 1972, **11**, 768.
9. M.E. Clay and M.T. Brown, *Inorg. Chim. Acta.*, 1982, **58**, 1; S.M. Rocklage, H.W. Turner, J.D. Fellmann and R.R. Schrock, *Organometallics*, 1982, **1**, 703.
10. A.G Orpen L. Brammer, F.H. Allen, O. Kennard, D.G. Watson and R. Taylor, *J. Chem. Soc., Dalton Trans.*, 1989, **12**, S1.
11. F. Cotton and G. Wilkinson, *"Advanced Inorganic Chemistry 4th Ed."*, 1980, Wiley, New York.
12. A.K. Rappé and W.A. Goddard, III, *J. Am. Chem. Soc.*, 1982, **104**, 3287; *ibid.*, 1982, **104**, 448.
13. T.K. Wells, *Unpublished Results*, Durham University, 1990.
14. W.P. Griffith, *Coord. Chem. Rev.*, 1972, **8**, 369.

CHAPTER SIX

Experimental Details.

6.1 General.

6.1.1 Experimental Techniques.

All manipulations of air and/or moisture sensitive materials were performed on a conventional vacuum/inert atmosphere (nitrogen or argon) line using standard Schlenk and cannular techniques, or in an inert atmosphere (nitrogen or argon) filled glove box.

Elemental analyses were performed by the microanalytical services of this department.

Infra red spectra were recorded on Perkin-Elmer 577 and 457 grating spectrophotometers using either KBr or CsI windows. Absorptions abbreviated as: vs (very strong), s (strong), m (medium), w (weak), br (broad), sp (sharp), sh (shoulder).

Mass spectra were recorded on a VG 7070E Organic Mass Spectrometer.

UV/visible spectra were recorded on the Perkin-Elmer Lambda 2/Epson PC AX2.

NMR spectra were recorded on the following instruments, at the frequencies listed, unless stated otherwise: Varian 400MHz ^1H (399.952 MHz), ^{13}C (100.577 MHz); Bruker AC 250, ^1H (250.13 MHz), ^{13}C (62.90 MHz), ^{31}P (101.26 MHz); Varian EM 360L, ^1H (60 MHz); Hitachi Perkin Elmer R-24(B), ^1H (60 MHz). The following abbreviations have been used for band multiplicities: s (singlet), d (doublet), t (triplet), q (quartet), qnt (quintet), sxt (sextet), spt (septet), m (multiplet). Chemical shifts are quoted as δ in ppm with respect to the following references, unless stated otherwise: ^{31}P (dilute aq. H_3PO_4 , 0 ppm); ^{13}C (C_6D_6 , 128.0 ppm); ^1H (C_6D_6 , 7.15 ppm, CDCl_3 , 7.24 ppm, CD_2Cl_2).

6.1.2 Solvents and Reagents

The following NMR solvents were dried by vacuum distillation from a suitable drying agent (in parentheses) and stored over activated 4Å molecular sieves:

d⁶-benzene (phosphorus (V) oxide), d⁸-toluene (phosphorus (V) oxide) and d-chloroform (phosphorus (V) oxide), d²-dichloromethane (phosphorus (V) oxide).

The following solvents were dried by prolonged reflux over a suitable drying agent, being freshly distilled and deoxygenated before use (drying agent in parentheses): toluene (sodium metal), petroleum ether (40-60°C and 100-120°C, lithium aluminium hydride), pentane (lithium aluminium hydride), octane (lithium aluminium hydride), tetrahydrofuran (sodium benzophenone ketyl), acetonitrile (calcium hydride), dichloromethane (calcium hydride), 1,2-dichloroethane (calcium hydride), carbon tetrachloride (calcium hydride) and diethylether (lithium aluminium hydride).

The following chemicals were prepared by previously published procedures: LiOAr¹ (Ar = 2,6-ⁱPr₂C₆H₃, 2,6-Me₂C₆H₃, 2,6-Ph₂C₆H₃), LiO^tBu¹, PMe₃², CpNbCl₄³, CpTaCl₄³, Cp*TaCl₄⁴, Cp*TaCl₂(PMe₃)₂⁵, MoCl₄(CH₃CN)₂⁶, MoCl₄(THF)₂⁶, WCl₄(CH₃CN)₂⁷, ReCl₄(CH₃CN)₂⁸, NHR(SiMe₃)⁹, LiNHR⁹ (R = ^tBu, 2,6-ⁱPr₂C₆H₃), NCN(SiMe₃)₂¹⁰, W(O)Cl₄¹¹, Me₃CCH₂MgCl¹².

The following chemicals were obtained commercially and used as received unless stated otherwise: molybdenum pentachloride (Aldrich), tungsten hexachloride (Aldrich), tantalum pentachloride (Aldrich), niobium pentachloride (Aldrich), rhenium pentachloride (Aldrich), potassium perrhenate (Aldrich) hydrazine dihydrochloride (Aldrich), triphenylphosphine (BDH), tricyclohexylphosphine (BDH), dimethylphenylphosphine (Aldrich), methylphenylphosphine (Aldrich), chloromethylsilane (Aldrich), heptamethyldisazane (Aldrich, dried and stored over 4Å molecular sieves), 2,6-dimethylphenol (Aldrich), 2,6-diisopropylphenol (Aldrich), tertiarybutanol (Aldrich), hexamethyldisilathiane (Fluka, distilled, dried and stored over 4Å molecular sieves), trimethylsilylazide (Fluka, dried and stored over 4Å molecular sieves), n-butyl lithium (Aldrich), phosphorus pentachloride (Aldrich), triethylamine (Aldrich), methylmagnesium chloride 3.0M in THF (Aldrich).

6.1.3 Computational Methods.

The Fenske-Hall calculations were carried out using the MEDIEVAL (II) program. (A modified version of the the original program¹³), courtesy of Dr. C. E. Housecroft, University of Cambridge. The calculations were run on the Cambridge University Phoenix IBM mainframe, accessed from Durham MTS mainframe via JANET network.

Manipulations of molecular coordinates were carried out on the Apple Macintosh SE 20, using the "Molecular Editor" software, available from Drexel University, Philadelphia.

6.1.4 Basis Functions for FHMO Calculations.

The Fenske-Hall calculations employed single ζ Slater functions for the 1s, 2s and 3s functions of N, O, C, S, P and Cl. The exponents were obtained by curve fitting the double ζ function of Clementi¹⁴ while maintaining orthogonal functions; the double ζ functions were used directly for the 2p and 3p orbitals. For P, an expanded atomic orbital basis set used an exponent for the 3d functions of 1.80. An exponent of 1.20 was used for hydrogen corresponding to the minimum energy exponent for methane¹⁵. The niobium, molybdenum and zirconium functions, chosen for the +1 oxidation state, were based on the results of Richardson¹⁶, and augmented by 5s and 5p functions with an exponent of 2.20 (Table 6.1). It has been recognised that at least two Slater-type-orbitals (STO's) are required to represent valence-shell 4d orbitals¹⁷, these are shown in Table 6.2. In the case of molybdenum two STO's were also used for 3d orbitals.

| Orbital | Zirconium | | Niobium | | Molybdenum | |
|---------|-----------|----------|---------|----------|------------|----------|
| | ζ | C | ζ | C | ζ | C |
| 1s | 39.163 | 0.03360 | 40.152 | 0.03174 | 41.127 | 0.03004 |
| 2s | 15.295 | -0.11756 | 15.713 | -0.11108 | 15.426 | -0.11322 |
| 2p | 17.576 | -0.07870 | 18.061 | -0.07450 | 18.973 | -0.06743 |
| 3s | 7.964 | 0.27025 | 8.230 | 0.25419 | 8.670 | 0.24052 |
| 3p | 7.916 | 0.23979 | 8.198 | 0.22502 | 8.552 | 0.20559 |
| 4s | 3.779 | -0.69408 | 3.970 | -0.62158 | 4.146 | -0.55880 |
| 4p | 3.432 | -0.82878 | 3.625 | -0.73011 | 3.805 | -0.64974 |
| 5s | 2.200 | 1.18430 | 2.200 | 1.14818 | 2.200 | 1.12108 |
| 5p | 2.200 | 1.27049 | 2.200 | 1.21299 | 2.200 | 1.17129 |

Table 6.1, The s and p-orbital exponents and coefficients used in Fenske-Hall MO calculations.

| Orbital | Zirconium | | Niobium | | Molybdenum ^a | | |
|---------|-----------|----------|---------|----------|-------------------------|----------|----------|
| | ζ | C | ζ | C | ζ | C 3d | C 4d |
| 3d | 7.836 | -0.17008 | 8.183 | -0.18847 | 13.825 | 0.27666 | -0.07761 |
| 3d' | - | - | - | - | 7.550 | 0.76450 | -0.18639 |
| 4d | 3.506 | 0.40500 | 3.684 | 0.44952 | 3.870 | 0.04188 | 0.48953 |
| 4d' | 1.660 | 0.73643 | 1.794 | 0.69351 | 1.923 | -0.00862 | 0.65715 |

^a The Molybdenum calculations incorporate two STO's for both 3d and 4d orbitals.

Table 6.2, The 3d and 4d orbital exponents and coefficients used in Fenske-Hall MO calculations.

6.2 Experimental Details to Chapter 2.

6.2.1 Reaction of Cp*TaCl₂(PMe₃)₂ with Me₃SiN₃:

*Preparation of Cp*Ta(NSiMe₃)Cl₂ (1).*

Trimethylsilylazide (0.11 g, 0.93 mmol.) in toluene (10 cm³) was added to a stirred solution of Cp*TaCl₂(PMe₃)₂ (0.50 g, 0.93 mmol) in toluene (20 cm³). The mixture was allowed to stir for 10h. during which time the solution changed colour from red through orange to yellow with the evolution of gas, which was vented. The solvent was removed under reduced pressure and the resultant oil washed with cold light petroleum ether (5cm³, b.p 40-60°C) to afford a yellow solid, which was dried *in vacuo*. Yield, 0.12g, (28%).

Elemental analysis for C₁₃H₂₄NCl₂Ta Found (Required): %C, 23.18 (23.71); %H, 3.28 (3.46); %N, 3.32 (3.46); %Cl, 17.12 (17.53); %Ta 43.14 (44.68).

Infrared data (Nujol, CsI, cm⁻¹): 1240(s), 1130(vs), 1030(w), 940(w), 845(vs), 787(m), 755(s), 690(m), 635(w), 460(w).

Mass spectral data (CI, isobutane carrier gas, m/z, ³⁵Cl, ¹⁸¹Ta): 473 [M]⁺, 458 [M-Me]⁺ 400 [M-SiMe₃]⁺, 386 [M-NSiMe₃]⁺.

¹H NMR data (250Mz, d⁶-benzene, 298K): 0.21 (s, 9, SiMe₃) 1.97 (s, 15, C₅Me₅).

6.2.2 Reaction of CpNbCl₄ with (Me₃Si)₂NMe:

Preparation of CpNb(NMe)Cl₂ (2) .

(Me₃Si)₂NMe (2.93g, 16.7 mmol.) in acetonitrile (30 cm³) was added dropwise at room temperature to a stirred suspension of CpNbCl₄ (5.0g, 16.7 mmol.) in acetonitrile (100 cm³). The red suspension was consumed over a period of 2h. to give an orange-yellow solution, which was stirred for a further 6h. Removal of the volatile components, followed by washing with light petroleum ether (2 x 25 cm³, 40-60°C) and drying *in vacuo* gave a yellow powder, which was recrystallised from toluene. Yield, 3.74g, (87%)

Elemental analysis for C₆H₈NCl₂Nb Found (Required): %C, 27.93 (27.94); %H, 3.28 (3.13); %N, 5.14 (5.43); %Cl, 27.84 (27.49); %Nb 35.51 (36.02).

Infrared data (Nujol, CsI, cm⁻¹): 3045(w), 1446(sh), 1427(m), 1250(m), 1007(s), 928(w), 852(s), 840(m), 820(vs), 720(w), 593(w), 428(m), 381(vs), 343(m), 289(w).

Mass spectral data (CI, isobutane carrier gas, m/z ³⁵Cl): 257 [M]⁺, 242 [M-Me]⁺, 228 [M-NMe]⁺.

¹H NMR data (250MHz, d⁶-benzene, 298K): 3.21 (s, 3, Me), 5.72 (s, 5, C₅H₅)

¹³C NMR data (100MHz, d⁶-benzene, 298K): 54.31 (q, J_{CH} = 119 Hz, Me), 112.90 (d, J_{CH} = 178 Hz, C₅H₅).

6.2.3 Reaction of Cp*TaCl₄ with (SiMe₃)₂NMe

*Preparation of [Cp*TaCl₃]₂(μ-NMe) (3).*

An acetonitrile solution of (Me₃Si)₂NMe (0.38g, 2.18 mmol. in 10 cm³) was added dropwise to a stirred suspension of Cp*TaCl₄ (1.0g, 2.18 mmol.) in acetonitrile (20 cm³) over a period of 5min. The mixture was stirred at room temperature for 24h. to yield an orange solution and a pale orange solid. The solid was removed from the supernatant solution by filtration, washed with light petroleum ether (2 x 5 cm³, 40-60°C) and dried *in vacuo*. Yield 0.68g (71%).

Elemental analysis for C₂₁H₃₃NCl₆Ta₂ Found (Required): %C, 28.81 (28.86); %H, 3.61 (3.81); %N, 1.67 (1.60), %Cl, 23.22 (24.37); %Ta 41.92 (41.40).

Infrared data (Nujol, CsI, cm⁻¹): 1375(s), 1115(w), 1030(w), 670(vs), 387(s), 309(s), 292(m,sh), 278(m).

Mass spectral data (CI, isobutane carrier gas, m/z ³⁵Cl, ¹⁸¹Ta): 421 [Cp*TaCl₃]⁺, 416 [Cp*Ta(NMe)Cl₂]⁺, 402 [Cp*Ta(N)Cl₂]⁺.

6.2.4 Reaction of CpTaCl₄ with (Me₃Si)₂NCN

Preparation of [CpTa(NCN)Cl₂(CH₃CN)]_n (6).

An acetonitrile solution of (Me₃Si)₂NCN (0.48g, 2.58 mmol. in 10 cm³) was added dropwise to a stirred suspension of CpTaCl₄ (1.0g, 2.58 mmol.) in acetonitrile (20 cm³) over a period of 5min. The mixture was stirred at room temperature for 12h. to yield an orange solution and a red-orange solid. The supernatant solution was filtered from the microcrystalline solid, which was collected, washed with light petroleum ether (2 x 5 cm³, 40-60°C) and dried *in vacuo*. Yield 0.64g (63%).

Elemental analysis for $C_8H_8N_3Cl_2Ta$ Found (Required): %C, 24.53 (24.12); %H, 2.24 (2.03); %N, 10.72 (10.56); %Cl, 17.79 (17.81); %Ta 46.37 (45.46).

Infrared data (Nujol, CsI, cm^{-1}): 3100(w), 2000(vs, br), 1420(m, sh), 1255(w), 1025(w), 851(s), 783(w, br), 690(w), 450(m, br), 280(m).

Mass spectral data (CI, isobutane carrier gas, m/z, ^{35}Cl , ^{181}Ta): 316 $[CpTaCl_2]^+$.

6.2.5 Reaction of $CpNbCl_4$ with Me_3SiNH^tBu :

Preparation of $CpNb(N^tBu)Cl_2$ (7).

A dichloromethane solution of Me_3SiNH^tBu (9.69g, 66.70 mmol. in 50 cm^3) was added dropwise at room temperature to a stirred suspension of $CpNbCl_4$ (10.0g, 33.35 mmol.) in dichloromethane (150 cm^3). The red suspension was consumed over a period of 12h. to give an orange-red solution. Removal of the volatile components, followed by washing with cold light petroleum ether (15 cm^3 b.p 40-60°C) to remove amine, and drying *in vacuo* gave a brown solid. Extraction of the brown solid with diethylether (2 x 100 cm^3) gave a yellow solution, which on concentration and cooling to -78°C afforded yellow moisture sensitive crystals. Yield, 7.77g (78%).

Elemental analysis for $C_9H_{14}NCl_2Nb$ Found (Required): %C, 36.19 (36.03); %H, 4.88 (4.70); %N, 4.81 (4.67); %Cl, 23.33 (23.63); %Nb, 30.80 (30.97).

Infrared data (Nujol, CsI, cm^{-1}): 3040(w), 1378(m), 1242(s), 1218(s), 1150(m), 1020(m), 1010(m), 844(m), 812(s), 805(s), 720(w), 576(w), 550(m), 535(m), 395(vs), 378(s), 343(s), 305(m).

Mass spectral data (CI, isobutane carrier gas, m/z ^{35}Cl): 299 $[M]^+$, 284 $[M-Me]^+$, 269 $[M-2Me]^+$, 228 $[M-N^tBu]^+$, 207 $[M-^tBu-Cl]^+$.

$^1\text{H NMR data}$ (250MHz, d^6 -benzene, 298K): 1.02 (s, 9, CMe_3), 5.88 (s, 5, C_5H_5).

$^{13}\text{C NMR data}$ (100MHz, d^6 -benzene, 298K): 30.40 (q, $J_{\text{CH}} = 127$ Hz, CMe_3), 69.98 (s, CMe_3), 112.41 (d, $J_{\text{CH}} = 178$ Hz, C_5H_5).

6.2.6 Reaction of CpNbCl_4 with $\text{Me}_3\text{SiNH}(2,6\text{-iPr}_2\text{C}_6\text{H}_3)$:

(A) Preparation of $[\text{CpNb}(\text{NAr})\text{Cl}_3]\text{-}[\text{Me}_3\text{SiNH}_2\text{Ar}]^+$ (8).

A toluene solution of $\text{Me}_3\text{SiNH}(2,6\text{-iPr}_2\text{C}_6\text{H}_3)$ (0.83g, 3.34 mmol. in 15 cm^3) was added dropwise at room temperature to a stirred suspension of CpNbCl_4 (1.0g, 3.34 mmol.) in toluene (20 cm^3). The mixture was stirred for 12h. to give an orange-red solution and a microcrystalline precipitate. The solid was removed from the supernatant solution by filtration, washed with light petroleum ether ($2 \times 10\text{ cm}^3$, b.p. $40\text{-}60^\circ\text{C}$) and dried *in vacuo* to afford a microcrystalline yellow-orange solid. Yield, 0.41g (40 %).

Elemental analysis for $\text{C}_{32}\text{H}_{50}\text{N}_2\text{Cl}_3\text{SiNb}$ Found (Required): %C, 55.15 (55.69); %H, 5.40 (5.49); %N, 3.22 (3.47); %Cl, 14.87 (15.41); %Nb 12.12 (13.46).

Infrared data (Nujol, CsI , cm^{-1}): 3052(w), 3029(w), 1622(w), 1588(w), 1425(w), 1350(w), 1310(w,sh), 1332(m), 1285(m), 1114(w), 1024(w), 986(w), 934(w), 856(m), 819(s), 798(s), 758(vs), 843(w), 831(w), 457(w), 402(m), 382(m), 321(w).

Mass spectral data (CI, isobutane carrier gas, m/z ^{35}Cl): 263 $[\text{CpNbCl}_3]^+$, 228 $[\text{CpNbCl}_2]^+$.

(B) Preparation of CpNb(NAr)Cl₂ (9) (Ar = 2,6-ⁱPr₂C₆H₃).

A dichloromethane solution of Me₃SiNH(-2,6-ⁱPr₂C₆H₃) (3.33g, 26.68 mmol. in 30 cm³) was added dropwise at room temperature to a stirred suspension of CpNbCl₄ (4 g, 13.34 mmol.) in dichloromethane (40 cm³). The red suspension was consumed over a period of 12h. to give a red solution. Removal of the volatile components under reduced pressure, followed by washing with cold light petroleum ether (1 x 15cm³, b.p 40-60°C) to remove amine, and drying overnight *in vacuo* gave a red solid. Extraction of the pale red solid with pentane (2 x 50cm³) gave a red solution which on removal of solvent, followed by concentration and cooling to -78°C, afforded red moisture sensitive crystals. Yield, 4.26g (79%).

Elemental analysis for C₁₇H₂₂NCl₂Nb Found (Required): %C, 50.12 (50.52); %H, 5.32 (5.49); %N, 3.13 (3.47); %Cl, 17.79 (17.54); %Nb 22.03 (22.99).

Infrared data (Nujol, CsI, cm⁻¹): 3052(w), 3029(w), 1622(w), 1588(w), 1425(w), 1350(w), 1310(w,sh), 1332(m), 1285(m), 1114(w), 1024(w), 986(w), 934(w), 856(m), 843(w), 831(w), 819(s), 798(s), 758(vs), 457(w), 402(m), 382(m), 321(w).

Mass spectral data (CI, isobutane carrier gas, m/z ³⁵Cl): 403 [M]⁺, 388 [M-Me]⁺, 368 [M-Cl]⁺, 228 [M-NAr]⁺.

¹H NMR data (250MHz, d⁶-benzene, 298K): 1.24 (d, 12, ³J_{HH} = 6.8 Hz), (CHMe₂), 3.72 (sept., 2, ³J_{HH} = 6.9 Hz, CHMe₂), 5.82 (s, 5, C₅H₅), 6.88 (t, 1, ³J_{HH} = 6.6 Hz, H_p), 6.98 (d, 2, ³J_{HH} = 7.5 Hz, H_m).

¹³C NMR data (100MHz, d⁶-benzene, 298K): 24.07 (q, J_{CH} = 126 Hz, CHMe₂), 28.52 (d, J_{CH} = 128 Hz, CHMe₂), 113.52 (d, J_{CH} = 178 Hz, C₅H₅), 122.82 (d, J_{CH} = 158 Hz, ring C), 126.65 (d, J_{CH} = 159 Hz, ring C), 145.49(s, ring C), 152.01(s, ring C).

6.2.7 Reaction of CpTaCl₄ with LiN^tBuSiMe₃:

Preparation of CpTa(N^tBu)Cl₂ (10).

1,2 dichloroethane (40 cm³) was added, *via* cannula, to a weighed mixture of LiN^tBuSiMe₃ (0.78g, 5.16 mmol.) and CpTaCl₄ (2.00g, 5.16 mmol.). The yellow suspension was heated to 80°C and stirred for 24h. to yield a pale solid and red-orange solution. The reaction mixture was cooled and the resultant suspension was removed from the supernatant solution by filtration. The volatile components were then removed under reduced pressure to afford a yellow-brown solid. The solid was extracted with hot octane (2 x 50 cm³) to give a yellow solution, which on removal of solvent *in vacuo* gave a waxy yellow solid. Yield, 0.18g (9%)

Elemental analysis for C₉H₁₄NCl₂Ta Found (Required): %C, 26.13 (27.86); %H, 3.23 (3.64); %N, 2.85 (3.61); %Cl, 17.77 (18.27); %Ta, 44.37 (46.63).

Mass spectral data (CI, isobutane carrier gas, m/z ³⁵Cl): 387 [M]⁺, 372 [M-Me]⁺.

Infrared data (Nujol, CsI, cm⁻¹): 3050(w), 1410(m), 1362(sh), 1298(s), 1222(m), 1025(w), 850(s), 818(vs), 805(s, sh), 783(m, sh), 730(m), 550(w), 445(w), 352(m), 302(vs), 285(s, sh).

¹H NMR data (250MHz, d⁶-benzene, 298K): 1.11 (s, 9, CMe₃), 5.81 (s, 5, C₅H₅).

6.2.8 Reaction of CpTaCl₄ with LiN(2,6-*i*Pr₂C₆H₃)(SiMe₃):

*Preparation of CpTa(N-2,6-*i*Pr₂C₆H₃)Cl₂ (11).*

1,2 dichloroethane (30 cm³) was added, *via* cannula, to a weighed mixture of LiN(2,6-*i*Pr₂C₆H₃)(SiMe₃) (0.66g, 2.58mmol.) and CpTaCl₄ (1g, 2.58 mmol.) . The yellow suspension was heated to 80°C and stirred for 24h. to yield a pale solid and a red-orange solution. The mixture was allowed to cool to room temperature and the solid was filtered from the supernatant solution. The volatile components were then removed under reduced pressure to afford a yellow-brown solid. Extraction of the solid with hot octane (2 x 50 cm³) gave a yellow solution, which on removal of solvent *in vacuo* gave a waxy yellow solid. Yield, 0.08g (7%)

Elemental analysis for C₁₇H₂₂NCl₂Ta Found (Required): %C, 40.51 (41.48); %H, 4.10 (4.50), %N 2.13 (2.85); %Cl, 15.77 (14.41); %Ta, 33.14 (36.76).

Mass spectral data (CI, isobutane carrier gas, m/z ³⁵Cl): 491 [M]⁺, 476 [M-Me]⁺, 316 [M-NAr].

¹H NMR data (250MHz, d⁶-benzene, 298K): 1.20 (d, 12, J_{HH} = 6.7Hz, (CHMe₂), 3.72 (sept., 2, ³J_{HH} = 6.9 Hz, CHMe₂), 6.32 (s, 5, C₅H₅), 6.83 (t, 1, ³J_{HH} = 7 Hz, H_p), 7.02 (d, 2, ³J_{HH} = 8 Hz, H_m).

6.2.9 Reaction of Cp*TaCl₄ with Me₃SiNH^tBu:

*Preparation of Cp*Ta(N^tBu)Cl₂ (12).*

A 1,2 dichloroethane solution of Me₃SiNH^tBu (0.33g, 2.18 mmol. in 15 cm³) was added dropwise at room temperature to a stirred suspension of Cp*TaCl₄ (1.00g, 2.18 mmol.) in 1,2 dichloroethane (20 cm³). The orange-yellow suspension was heated to 80°C and stirred for 24h. to yield an orange solution. The solution was

cooled to room temperature and the volatile components were removed under reduced pressure to afford a yellow-brown solid. Extraction of the solid with hot octane (2 x 50 cm³) gave a yellow solution, which on removal of solvent *in vacuo* gave a waxy orange-yellow solid. Yield, 0.11g (11%)

Elemental analysis for C₁₄H₂₄NCl₂Ta Found (Required): %C, 26.13 (27.86); %H, 3.23 (3.64); %N, 2.85 (3.61); %Cl, 17.77 (18.27).

Infrared data (Nujol, CsI, cm⁻¹): 1480(m, sh), 1470(s, sh), 1429(w), 1295(m), 1270(s), 1020(m), 840(w, sh), 805(w), 730(m), 660(w), 420(w), 360(w), 342(m), 300(vs).

¹H NMR data (250MHz, d⁶-benzene, 298K): 1.23 (s, 9, CMe₃), 1.94 (s, 15, C₅Me₅).

6.2.10 Reaction of CpNb(NMe)Cl₂ with PMe₃:

Preparation of CpNb(NMe)Cl₂(PMe₃) (14).

Trimethylphosphine (1.18g, 15.51 mmol.) was condensed onto a frozen solution of CpNb(NMe)Cl₂ (2g, 7.75 mmol.) in toluene (40 cm³). On warming the mixture to room temperature an immediate reaction ensued leading to the formation of a pale precipitate and yellow solution. After stirring for a further 12h., the supernatant solution was filtered from the off-white solid, which was collected, washed with light petroleum ether (2 x 10 cm³) and dried *in vacuo*. Recrystallisation of the solid from hot toluene afforded pale yellow needles. Yield, 2.209g (85%).

Elemental analysis for C₉H₁₇NCl₂PNb Found (Required): %C, 32.19 (32.36); %H, 5.22 (5.13); %N, 3.98 (4.19); %Cl, 21.00 (21.23); %Nb 28.12 (27.81).

Infrared data (Nujol, CsI, cm^{-1}): 3040(w), 1445(m, sh), 1419(m), 1289(w), 1278(w), 1240(s), 960(s), 945(m, sh), 814(vs), 807(vs), 734(w), 741(w), 577(w), 394(m), 282(m).

^1H NMR data (250MHz, d-chloroform, 298K): 1.58 (d, 9, $^2J_{\text{PH}} = 9.2$ Hz, PMe_3), 3.85 (s, 3, NMe), 6.16 (s, 5, C_5H_5).

^{13}C NMR data (100MHz, d-chloroform, 298K): 14.68 (q/d, $J_{\text{CH}} = 130$ Hz, $J_{\text{CP}} = 26$ Hz, PMe_3), 54.86 (q, $J_{\text{CH}} = 137$ Hz, NMe), 109.90 (d, $J_{\text{CH}} = 177$ Hz, C_5H_5).

6.2.11 Reaction of $\text{CpNb}(\text{NMe})\text{Cl}_2$ with $\text{LiO}-2,6\text{-Me}_2\text{C}_6\text{H}_3$:

Preparation of $\text{CpNb}(\text{NMe})(\text{O}-2,6\text{-Me}_2\text{C}_6\text{H}_3)_2$ (15).

Toluene (40 cm^3) chilled to *ca.* -78°C was added to a weighed mixture of $\text{CpNb}(\text{NMe})\text{Cl}_2$ (0.5g, 1.94 mmol.) and $\text{LiO}-2,6\text{-Me}_2\text{C}_6\text{H}_3$ (0.50g, 3.88 mmol.). The solution was allowed to warm to room temperature and stirred for 12h. during which time a pale yellow solution and pale gelatinous precipitate were formed. Filtration of supernatant solution from the solid, followed by concentration to half volume and cooling to *ca.* -78°C afforded pale yellow crystals. The crystals were collected, washed with cold light petroleum ether (2 x 5 cm^3 , b.p. $40\text{-}60^\circ\text{C}$) and dried *in vacuo*. Yield, 0.62g (74%).

Elemental analysis for $\text{C}_{22}\text{H}_{26}\text{NO}_2\text{Nb}$ Found (Required): %C, 61.19 (61.54); %H, 6.10 (6.10); %N, 2.98 (3.26); %Nb 21.32 (21.64).

Infrared data (Nujol, CsI, cm^{-1}): 3024(w,sh), 1589(m), 1276(vs), 1225(vs, sh), 1215(vs), 1088(s), 1062(w), 1020(m), 1010(m), 890(s), 866(s), 819(s), 811(s), 798(vs), 761(vs), 752(vs), 738(s), 730(s), 599(w), 572(m), 561(m), 400(m), 380(s), 266(w).

Mass spectral data (CI, isobutane carrier gas, m/z): 429 [CpNb(NMe)(OAr)₂]⁺, 308 [CpNb(NMe)(OAr)]⁺, 122[ArOH]⁺.

¹H NMR data (250MHz, d-chloroform, 298K): 2.50 (s, 12, C₆H₃Me₂), 3.30 (s, 3, NMe), 6.16 (s, 5, C₅H₅), 7.02 (t, 2, ³J_{CH} = 6.6 Hz, H_p), 7.23 (d, 4, ³J_{CH} = 7.4, H_m).

¹³C NMR data (100MHz, d-chloroform, 298K): 17.36 (d, J_{CH} = 128 Hz, C₆H₃Me₂), 111.36 (d, J_{CH} = 174 Hz, C₅H₅), 119.98 (d, J_{CH} = 155 Hz, ring C), 126.00 (d, J_{CH} = 156 Hz, ring C), 128.27 (s, ring C), 162.70 (s, ring C).

6.2.12 Reaction of CpNb(NMe)Cl₂ with LiO^tBu:

Preparation of CpNb(NMe)(O-^tBu)₂ (16).

Diethylether (40 cm³) at -78°C was added, *via* cannula, to a weighed mixture of CpNb(NMe)Cl₂ (0.5g, 1.94 mmol.) and LiO^tBu (0.31g, 3.88 mmol.). The solution was allowed to warm to room temperature and stirred for 12h. during which time a pale yellow solution and pale gelatinous precipitate were formed. The suspension was filtered from the supernatant solution, from which the solvent was removed and the residue dried *in vacuo* overnight. The resultant brown oily solid was washed with cold pentane (10cm³) to yield crude product. Yield, 0.6g (95%) Sublimation at 50°C (5 x 10⁻⁴ Torr) afforded the product as a white crystalline solid.

Elemental analysis for C₁₄H₂₆NO₂Nb Found (Required): %C, 50.11 (50.46); %H, 7.28 (7.86); %N, 4.01 (4.20); %Nb 20.98 (21.64).

Infrared data (CsI, cm⁻¹): 3042(w), 2960(vs), 2920(vs,sh), 2765(w, sp), 1420(m, sh), 1458(m), 1385(m), 1361(vs), 1272(vs), 1232(s), 1186(vs), 1010(s, sh), 975(vs, br), 800(s), 780(vs), 595(m), 552(s), 480(m), 391(m), 377(m), 360(m).

Mass spectral data (CI, isobutane carrier gas, m/z): 269 [M-64]⁺, 267 [M-66], 177 [M-156].

¹H NMR data (400MHz, d⁶-benzene, 298K): 1.31 (s, 18, CMe₃), 3.43 (s, 3, Me), 6.08 (s, 5, C₅H₅).

¹³C NMR data (100MHz, d⁶-benzene, 298K): 32.19 (q, J_{CH} = 125 Hz, CMe₃), 50.8 (s, br, NMe), 77.30 (s, CMe₃), 109.37 (d, J_{CH} = 173Hz, C₅H₅).

6.2.13 Reaction of CpNb(N^tBu)Cl₂ with PMe₃:

Preparation of CpNb(N^tBu)Cl₂(PMe₃) (17).

Trimethylphosphine (0.25g, 3.33 mmol.) was condensed onto a frozen solution of CpNb(N^tBu)Cl₂ (0.5g, 1.67 mmol.) in toluene (30 cm³). The mixture was warmed to room temperature and stirred for 12h to afford a yellow solution and a pale precipitate. The supernatant solution was filtered from the solid, which was collected, washed with light petroleum ether (15cm³) and dried *in vacuo*, to give a white powder (0.46g). Concentration of the yellow supernatant solution to half volume and cooling to -78°C afforded pale yellow needles (0.10g). Combined yield, 0.56g (89%).

Elemental analysis for C₁₂H₂₃NCl₂PNb Found (Required): %C, 38.00 (38.32); %H, 6.11 (6.12); %N, 4.00 (3.72); %Cl, 18.87 (18.85); %Nb 24.45 (24.70).

Infrared data (Nujol, CsI, cm⁻¹): 3043(w), 1430(m), 1380(m), 1295(m), 1289(m), 1238(s), 1219(m), 1125(w), 1029(m), 1015(w), 965(s), 950(m, sh), 928(w), 843(s), 836(s), 805(vs), 742(m), 630(w), 580(w), 549(w), 532(w), 332(w), 323(w), 289(m).

¹H NMR data (250Mz, d-chloroform, 298K): 1.26 (s, 9, CMe₃), 1.63 (d, 9, J_{PH} = 9.1 Hz, PMe₃), 6.20 (s, 5, C₅H₅).

¹³C NMR data (100MHz, d-chloroform, 298K): 16.23 (q/d, J_{CH} = 130 Hz, J_{CP} = 26 Hz, PMe₃), 30.82 (q, J_{CH} = 127 Hz, CMe₃), 71.41 (s, CMe₃), 109.72 (d, J_{CH} = 177 Hz, C₅H₅).

6.2.14 a). Reaction of CpNb(N^tBu)Cl₂ with LiO-2,6-ⁱPr₂C₆H₃:

Preparation of CpNb(N^tBu)(O-2,6-ⁱPr₂C₆H₃)₂ (18).

Diethylether (40 cm³) chilled to *ca.* -78°C was added to a weighed mixture of CpNb(N^tBu)Cl₂ (0.5g, 1.67 mmol.) and LiO-2,6-ⁱPr₂C₆H₃ (0.61g, 3.33 mmol.). The solution was allowed to warm to room temperature and stirred for 12h. during which time a pale yellow solution and pale gelatinous precipitate were formed. The mixture was filtered and the solvent removed from the supernatant solution under reduced pressure. The resultant oily solid was washed with cold light petroleum ether (2 x 5 cm³, b.p. 40-60°C) and dried *in vacuo* to afford a cream crystalline solid. Yield, 0.74g (76%). Crystals of the product were grown by cooling a saturated pentane solution to *ca.* -20°C.

Elemental analysis for C₃₃H₄₈NO₂Nb Found (Required): %C, 67.80 (67.90); %H, 8.57 (8.31); %N, 2.17 (2.40); %Nb 15.95 (15.92).

Infrared data (Nujol, CsI, cm⁻¹): 3039(w, sh), 3028(w), 1590(m), 1435(vs), 1362(s), 1332(vs), 1326(vs), 1265(vs), 1250(vs), 1239(vs), 1206(vs), 1190(vs), 1162(w), 1137(w), 1110(m), 1096(m), 1042(m), 1012(m), 937(w), 892(s), 871(s), 855(s), 815(s), 798(vs), 756(vs), 700(s), 593(m), 524(w), 420(w), 392(m), 380(m), 369, 338(w).

Mass spectral data (CI, isobutane carrier gas, m/z): 583 [M]⁺, 568 [M-Me]⁺, 526 [M-^tBu]⁺, 407 [M-Ar-Me]⁺, 178 [ArOH]⁺.

¹H NMR data (250MHz, d⁶-benzene, 298K): 0.87 (s, 9, CMe₃), 1.28 (d, ³J_{HH} = 6.8 Hz, CHMe₂), 3.60 (sept., 4, ³J_{HH} = 6.8 Hz, CHMe₂), 6.28 (s, 5, C₅H₅), 6.99 (t, 2, ³J_{HH} = 7.0 Hz, H_p), 7.13 (d, 4, ³J_{HH} = 7.2 Hz, H_m).

¹³C NMR data (100MHz, d-chloroform, 298K): 23.58 (q, J_{CH} = 125 Hz, CHMe₂), 26.01 (d, J_{CH} = 130 Hz, CHMe₂), 31.20 (q, J_{CH} = 127 Hz, CMe₃), 60.03 (s, CMe₃), 110.34 (d, J_{CH} = 175 Hz), 120.36 (d, J_{CH} = 160 Hz, ring C), 122.75 (d, J_{CH} = 149 Hz, ring C), 136.23 (s, ring C), 161.27 (s, ring C).

6.2.14 b) Reaction of CpNb(N^tBu)Cl₂ with LiO-2,6-Ph₂C₆H₃:

Preparation of CpNb(N^tBu)(O-2,6-Ph₂C₆H₃)₂ (19).

Diethylether (40 cm³) chilled to *ca.* -78°C was added, *via* cannula, to a weighed mixture of CpNb(N^tBu)Cl₂ (0.3g, 1.00 mmol.) and LiO-2,6-Ph₂C₆H₃ (0.50g, 2.00 mmol.). The solution was allowed to warm to room temperature and stirred for 12h. during which time a pale yellow solution and pale gelatinous precipitate were formed. The suspension was filtered and the resultant yellow supernatant solution cooled to *ca.* -78°C to afford pale yellow crystals. The crystals were collected, washed with cold light petroleum ether (2 x 5 cm³, b.p. 40-60°C) and dried *in vacuo*. Yield, 0.72g (87%).

Elemental analysis for C₄₅H₄₀NO₂Nb Found (Required): %C, 75.21 (75.01); %H, 5.55 (5.60); %N, 1.83 (1.95); %Nb, 12.52 (12.91).

Infrared data (Nujol, CsI, cm^{-1}): 3030(w, sh), 1602(w), 1583(w), 1495(w), 1412(vs), 1358(w, sh), 1311(w), 1230(s), 1085(w), 1071(w), 1029(w), 877(w), 859(m,sp), 811(w), 800(m), 762(s, sp), 758(s, sp), 708(s, sh), 802(vs, sp), 632(w), 612(w), 599(w), 585(w), 391(w).

Mass spectral data (CI, isobutane carrier gas, m/z): 264 $[\text{M}-2\text{Ar}]^+$, 247 $[\text{ArOH}]^+$, 227 $[\text{ArH}]^+$, 215 $[\text{M}-505]^+$, 202 $[\text{M}-518]$.

^1H NMR data (400MHz, d^6 -benzene, 298K): 0.64 (s, 9, CMe_3), 5.13 (s, 5, C_5H_5), 6.88 (t, 2, $J_{\text{HH}} = 7.6$ Hz, NC_6H_3 , H_p), 7.10 (t, 4, $J_{\text{HH}} = 7.2$ Hz, C_6H_5 , H_p), 7.25 (d, 4, $J_{\text{HH}} = 7.6$ Hz, C_6H_3 , H_m), 7.27 (t, 8, $J_{\text{HH}} = 7.6$ Hz, C_6H_5 , H_m), 7.54 (d, 8, $J_{\text{HH}} = 8.4$ Hz, C_6H_5 , H_o).

^{13}C NMR data (100MHz, d^6 -benzene, 298K): 31.31 (q, $J_{\text{CH}} = 126$ Hz, CMe_3), 67.90 (s, CMe_3), 110.19 (d, $J_{\text{CH}} = 174$ Hz, C_5H_5), 120.96 (d, $J_{\text{CH}} = 160$ Hz, ring C), 126.78 (d, $J_{\text{CH}} = 162$ Hz, ring C), 128.51 (d, $J_{\text{CH}} = 186$ Hz, ring C), 130.64 (d, $J_{\text{CH}} = 158$ Hz, ring C), 130.71 (d, $J_{\text{CH}} = 159$ Hz, ring C), 132.42 (s, ring C), 140.67 (s, ring C), 162.70 (s, ring C).

6.2.15 Reaction of $\text{CpNb}(\text{N}^t\text{Bu})\text{Cl}_2$ with LiO^tBu :

Preparation of $\text{CpNb}(\text{N}^t\text{Bu})(\text{O}^t\text{Bu})_2$ (20).

Diethylether (40 cm^3) at -78°C was added to a weighed mixture of $\text{CpNb}(\text{N}^t\text{Bu})\text{Cl}_2$ (0.5g, 1.67 mmol.) and LiO^tBu (0.27g, 3.34 mmol.). The solution was allowed to warm to room temperature and stirred for 12h. during which time a yellow-brown solution and pale gelatinous precipitate were formed. The suspension was filtered and the solvent removed from the supernatant solution under reduced pressure to yield a pale brown oil. Sublimation failed to yield a solid product.

Infrared data (CsI, cm^{-1}): 3042(w), 2960(vs), 2767(sp), 1460(m), 1420(m), 1385(m), 1360(vs), 1260(vs), 1230(s), 1186(vs), 990(vs, br), 810(s, br), 780(vs), 560(s), 480(m), 391(m), 377(m), 360(m).

^1H NMR data (400MHz, d^6 -benzene, 298K): 1.19 (s, 18, OCMe_3), 1.30 (s, 9, CMe_3), 6.16 (s, 5, C_5H_5).

^{13}C NMR data (100MHz, d^6 -benzene, 298K): 32.13 (q, $J_{\text{CH}} = 125$ Hz, CMe_3), 32.62 (q, $J_{\text{CH}} = 126$ Hz OCMe_3), 65.41 (s, OCMe_3), 76.14 (s, NCMe_3), 109.23 (d, $J_{\text{CH}} = 172$ Hz, C_5H_5).

6.2.16 Reaction of $\text{CpNb}(\text{N}^t\text{Bu})\text{Cl}_2$ with MeMgCl :

Preparation of $\text{CpNb}(\text{N}^t\text{Bu})\text{Cl}(\text{Me})$ (21).

A THF solution of MeMgCl (4.45 cm^3 , 3.0M in THF, 13.34mmol.) was added dropwise to stirred solution of $\text{CpNb}(\text{N}^t\text{Bu})\text{Cl}_2$ (4g, 13.34 mmol.) in cold diethylether (50 cm^3 at *ca* -78°C). On allowing the mixture to warm room temperature, an immediate reaction ensued, resulting in the formation of a brown-orange solution and a pale precipitate. After stirring for a further 6h., the solid was filtered from the supernatant solution. The volatile components were then removed under reduced pressure to afford a brown-red oil. The oil was dissolved in pentane (20 cm^3) and cooled *ca* -78°C to afford orange crystals, which were collected and dried *in vacuo*. Yield, 2.72g (73%). Melting point $54\text{-}55^\circ\text{C}$.

Elemental analysis for $\text{C}_6\text{H}_8\text{NCINb}$ Found (Required): %C, 42.76 (42.96); %H, 6.00 (6.13); %N, 4.75 (5.01); %Cl 12.45 (12.68); %Nb, 33.00 (33.23).

Infrared data (Nujol, CsI, cm^{-1}): 3052(w), 1402(w), 1360(s), 1248(vs), 1219(s), 1137(m), 1020(s), 1015(s, sh), 840(m, sh), 828(vs), 801(vs), 575(w), 543(m), 471(s), 387(s), 362(m), 342(s), 303(m).

Mass spectral data (CI, isobutane carrier gas, m/z ^{35}Cl): 279 $[\text{M}]^+$, 264 $[\text{M}-\text{Me}]^+$, 249 $[\text{M}-2\text{Me}]^+$, 223 $[\text{M}-t\text{Bu}]^+$.

^1H NMR data (250MHz, d^6 -benzene, 298K): 1.13 (s, 9, CMe_3), 1.15 (s, 3, NMe), 5.69 (s, 5, C_5H_5).

^{13}C NMR data (100MHz d^6 -benzene, 298K): 31.25 (q, $J_{\text{CH}} = 127$ Hz, CMe_3), 65.06 (s, CMe_3), 66.74 (s, br, Me), 108.55 (d, $J_{\text{CH}} = 176$ Hz, C_5H_5).

6.2.17 Reaction of $\text{CpNb}(\text{N}^t\text{Bu})\text{Cl}(\text{Me})$ with PMe_3 :

Preparation of $\text{CpNb}(\text{N}^t\text{Bu})\text{Cl}(\text{Me})(\text{PMe}_3)$ (22).

Trimethylphosphine (0.08g, 2.00 mmol.) was condensed onto a frozen solution of $\text{CpNb}(\text{N}^t\text{Bu})\text{Cl}(\text{Me})$ (0.3g, 1.00 mmol.) in toluene (20 cm^3). The mixture was allowed to warm to room temperature and stirred for 12h. to afford a yellow solution and pale precipitate. The supernatant solution was filtered from the solid, which was collected, washed with light petroleum ether (15 cm^3) and dried *in vacuo* to afford a pale yellow powder (0.10g). Yield, 0.22g (62%).

Elemental analysis for $\text{C}_{13}\text{H}_{26}\text{NCIPNb}$ Found (Required): %C, 44.10 (43.90); %H, 7.68 (7.37); %N, 3.87 (3.94); %Cl, 9.51 (9.97); %Nb 25.67 (26.12).

Infrared data (Nujol, CsI, cm^{-1}): 3052(w), 1423(m), 1358(s), 1308(w), 1289(m), 1242(s), 1215(m), 1125(w), 1019(m), 1013(m), 960(s), 94(s), 918(w), 821(vs), 801(vs), 739(m), 671(w), 577(w), 548(w), 532(w), 463(m), 330(w).

Mass spectral data (CI, isobutane carrier gas, m/z ^{35}Cl): 279 [M-PMe₃]⁺, 264 [M-PMe₃-Me]⁺, 249 [M-PMe₃-2Me]⁺, 223 [M-PMe₃-3Me-H]⁺ 208 [M-PMe₃-N^tBu]⁺, 76 [PMe₃]⁺.

¹H NMR data (250MHz, d-chloroform, 298K): 0.67 (s, 3 Me), 1.19 (s, 9, CMe₃), 1.42 (d, 9, J_{PH} = 8 Hz, PMe₃), 5.87 (s, 5, C₅H₅).

¹³C NMR data (400MHz, d-chloroform, 298K): 16.23 (q d, J_{CH} = 130 Hz, J_{CP} = 26 Hz, PMe₃), 30.82 (q, J_{CH} = 127 Hz, CMe₃), 71.41 (s, CMe₃), 109.72 (d, J_{CH} = 177 Hz, C₅H₅).

6.2.18 a). Reaction of CpNb(N^tBu)Cl₂ with Me₃CCH₂MgCl:

Preparation of CpNb(N^tBu)(CH₂CMe₃)₂ (23).

A diethylether solution of Me₃CCH₂MgCl (2.22 cm³, 1.54 M, 3.42 mmol.) was added to a stirred solution of CpNb(N^tBu)Cl₂ (0.5g, 1.67 mmol.) in diethylether (30cm³) at *ca* -78°C. On allowing the mixture to warm to room temperature an immediate reaction ensued leading to the formation of a brown solution and a pale precipitate, which were stirred for a further 6h. The supernatant solution was filtered from the solid and the volatile components removed under reduced pressure to afford a brown-red oil. The oil was dissolved pentane (10cm³) and cooled to *ca* -78°C to yield pale yellow crystals, which were collected and dried *in vacuo*. Yield, 0.45g (73%). Melting point 31-32°C.

Elemental analysis for C₁₉H₃₆NNb Found (Required): %C, 61.10 (61.44); %H, 9.60 (9.77); %N, 3.41 (3.77); %Nb, 24.68 (25.01).

Infrared data (CsI, cm^{-1}): 3010(w, sh), 2700(w), 1460(m), 1445(m, sh), 1375(w, sh), 1358(s), 1242(vs), 1232(vs), 1129(w), 1018(m), 810(vs), 799(vs), 754(w), 580(w), 532(w), 520(w), 368(w).

Mass spectral data (CI, isobutane carrier gas, m/z): 446 [M+C₅H₁₂] 414 [M+C₃H₈]⁺.

¹H NMR data (400MHz, d⁶-benzene, 298K): -0.20 (d, 2, ³J_{HH} = 11.3 Hz, CH₂), 1.22 (s, 18, CH₂CMe₃), 1.32 (s, 9, N-CMe₃), 2.31 (d, 2, ³J_{HH} = 11.3 Hz, CH₂), 5.68 (s, 5, C₅H₅).

¹³C NMR data (100MHz, d⁶-benzene, 298K): 32.81 (q, J_{CH} = 126 Hz, N-CMe₃), 34.47 (q, J_{CH} = 124 Hz, CH₂CMe₃), 34.83 (t, J_{CH} = 123 Hz, CH₂CMe₃), 65.64 (s, N-CMe₃), 81.23 (s, br, CH₂CMe₃), 106.36 (d, J_{CH} = 173, C₅H₅).

6.2.18 b) Reaction of CpNb(N^tBu)Cl₂ with Me₃CCHDMgBr:

Preparation of CpNb(N^tBu)(CHDCMe₃)₂ (24).

A diethylether solution of Me₃CCHDMgBr (1.67 mmol.) was added to solution of CpNb(N^tBu)Cl₂ (0.5g, 1.67 mmol.) in cold diethylether (20cm³ at ca -78°C). On allowing the mixture to warm to room temperature an immediate reaction ensued leading to the formation of a brown solution and a pale precipitate, which were stirred for a further 6h. The supernatant solution was filtered from the solid and the volatile components removed under reduced pressure to afford a brown-red oil. The oil was dissolved pentane (10cm³) and cooled to ca -78°C to yield pale yellow crystals, which were collected and dried *in vacuo*. 0.10g (32%).

Infrared data (Nujol, CsI, cm^{-1}): 3050(w, sh), 2697(w), 2585(w), 2496(w), 1607(w), 1507(w), 1461(s), 1301(w), 1245(vs), 1232(vs), 1129(w), 1025(s), 810(vs), 800(vs), 730(m), 650(m, br), 580(w, sh), 540(w), 455(w), 355(w).

¹H NMR data (400MHz, d⁶-benzene, 298K): -0.30 (s, 0.5, CH), -0.25 (s, 0.5 CH), 1.21(s, 18, CH₂CMe₃), 1.32 (s, 9, N-CMe₃), 2.21 (s, 0.5 CH), 2.25 (s, 0.5, CH), 5.68 (s, 5, C₅H₅).

¹³C NMR data (100MHz, d⁶-benzene, 298K): 32.81 (q, J_{CH} = 126, N-CMe₃), 34.47 (q, J_{CH} = 124, CH₂CMe₃), 34.83 (t, J_{CH} = 123, CH₂CMe₃), 65.64 (s, N-CMe₃), 81.23 (s, br, CH₂CMe₃), 106.36 (d, J_{CH} = 173, C₅H₅).

6.2.19 Reaction of CpNb(N^tBu)Cl₂ with LiNH^tBu:

Preparation of CpNb(N^tBu)(NH^tBu)Cl (25).

Diethylether (40 cm³) at -78°C was added, *via* cannula, to a weighed mixture of CpNb(N^tBu)Cl₂ (0.5g, 1.67 mmol.) and LiNH^tBu (0.13g, 1.67 mmol.). The solution was allowed to warm to room temperature and stirred for 12h. during which time a yellow-brown solution and pale precipitate were formed. The suspension was filtered from the supernatant solution from which the solvent was removed under reduced pressure to yield a pale brown oil. The oil was dissolved in pentane (10 cm³) and cooled to *ca* -78°C to yield a pale brown powder, which was collected and dried *in vacuo*. Yield, 0.26g (46%).

Elemental analysis for C₁₃H₂₄NCINb Found (Required): %C, 46.85 (46.37); %H, 7.42 (7.18); %N, 8.04 (8.32); %Cl 10.21 (10.53); %Nb, 27.05 (27.59).

Infrared data (CsI, cm⁻¹): 3092(w), 3052(w), 1587(w), 1400(w), 1360(s), 1250(vs), 1218(s), 1038(m, sp), 1015(s, sp), 1007(m, sh), 826(vs), 799(vs), 720(w), 577(w), 541(m), 394(s), 360(m), 342(s), 305(w).

Mass spectral data (CI, isobutane carrier gas, m/z ^{35}Cl): 336 $[\text{M}]^+$, 306 $[\text{M}-2\text{Me}]^+$, 265 $[\text{M}-t\text{Bu}]^+$, 207 $[\text{CpNbCl}(\text{N})]^+$

^1H NMR data (400MHz, d^6 -benzene, 298K): 1.18 (s, 9, CMe_3), 1.25 (s, 9, CMe_3), 5.89 (s, 5, C_5H_5), 7.6 (s, 1, br, NH).

^{13}C NMR data (100MHz, d^6 -benzene, 298K): 31.72 (q, $J_{\text{CH}} = 127$ Hz, CMe_3), 33.49 (q, $J_{\text{CH}} = 125$ Hz CMe_3), 57.00 (s, CMe_3), 67.36 (s, NCMe_3), 108.48 (d, $J_{\text{CH}} = 174$ Hz, C_5H_5).

6.2.20 a). Reaction of $\text{CpNb}(\text{N}^t\text{Bu})\text{Cl}(\text{Me})$ with LiNH^tBu :

Preparation of $\text{CpNb}(\text{N}^t\text{Bu})(\text{NH}^t\text{Bu})(\text{Me})$ (26).

A diethylether solution of $\text{CpNb}(\text{N}^t\text{Bu})\text{Cl}(\text{Me})$ (0.5g, 1.79 mmol. in 15cm^3) at *ca.* -78°C was added to a stirred suspension of LiNH^tBu (0.27g, 1.79 mmol) in diethylether (15cm^3). On warming the solution to room temperature, an immediate reaction led to the formation of a pale brown solution and pale precipitate. After stirring for 12h., the suspension was filtered from the supernatant solution, from which the solvent removed under reduced pressure to yield a pale brown oil. The oil was dissolved in pentane (10cm^3) and cooled to *ca.* -78°C to afford pale orange crystals, which were collected and dried at 0°C *in vacuo*. Yield, 0.31g (55%). Melting point $21-22^\circ\text{C}$.

Elemental analysis for $\text{C}_{14}\text{H}_{27}\text{NNb}$ Found (Required): %C, 53.09 (53.16); %H, 9.02 (8.60); %N, 7.91 (8.86); %Nb, 30.33 (29.37).

Infrared data (CsI , cm^{-1}): 3300(w), 3050(w), 1435(m, sh), 1425(m), 1358(m, sp), 1288(m, sh), 1243(vs), 1215(m), 1122(w), 1019(m, sh), 1012(m), 943(m), 916(w), 830(vs, sp), 803(vs, sp), 567(w), 545(m), 470(s), 370(m).

¹H NMR data (400MHz, d⁶-benzene, 298K): 0.58 (s, 3, Me), 1.29 (s, 9, CMe₃), 1.25 (s, 9, CMe₃), 5.71 (s, 5, C₅H₅), 6.72 (s, br, 1, NH).

¹³C NMR data (100MHz, d⁶-benzene, 298K): 32.93 (q, J_{CH} = 125 Hz, CMe₃), 33.25 (q, J_{CH} = 125 Hz CMe₃), 59.22 (s, CMe₃), 65.52 (s, NCMe₃), 108.32 (d, J_{CH} = 174 Hz, C₅H₅).

6.2.20 b). Reaction of CpNb(N^tBu)Cl(Me) with LiNHAr:

Preparation of CpNb(N^tBu)(NHAr)(Me)

(Ar = -2,6-*i*Pr₂C₆H₃) (27) .

A diethylether solution of CpNb(N^tBu)Cl(Me) (0.5g, 1.79 mmol. in 15 cm³) at *ca.* -78°C was added to a stirred suspension of LiNH^tAr (0.44g, 1.79 mmol.) in diethylether (15 cm³). On warming the solution to room temperature an immediate reaction led to the formation of a yellow solution and pale precipitate. After stirring for a further 12h., the suspension was filtered from the supernatant solution, which was concentrated to half volume and cooled to *ca.* -78°C to afford yellow crystals. The crystals were collected, washed with cold pentane (10 cm³,) and dried *in vacuo*. Yield, 0.58g (78%). Melting point 154-155°C

Elemental analysis for C₂₂H₃₅NNb Found (Required): %C, 62.44 (62.85); %H, 8.29 (8.39); %N, 6.29 (6.66); %Nb, 21.60 (22.01).

Infrared data (CsI, cm⁻¹): 3288(w), 3045(w), 2800(w, sh), 1618(w), 1587(w), 1429(s), 1360(m), 1337(vs), 1288(s), 1256(m), 1204(m), 1102(w), 1018(m, sp), 1012(m, sp), 978(m), 966(s), 806(vs), 797(s, sh), 782(s), 756(vs, sp), 625(w), 542(w), 492(w), 448(w), 370(w).

Mass spectral data (CI, isobutane carrier gas, m/z): 420 [M]⁺, 402 [M-CH₆]⁺, 389 [M-C₂H₇]⁺, 387 [M-C₂H₉]⁺, 347 [M-C₅H₁₃]⁺, 330, [M-C₆H₁₈]⁺, 327 [M-C₆H₂₁]⁺, 314 [M-C₇H₂₂]⁺, 312 [M-C₇H₂₄]⁺, [M-NC₇H₂₂]⁺.

¹H NMR data (400MHz, d⁶-benzene, 298K): 0.75 (s, 3, Me), 1.16 (s, 9, CMe₃), 1.33(d, ³J_{HH} = 6.8 Hz, 12, CHCMe₂), 4.10 (sept, 2, ³J_{HH} = 7.0 Hz, CHMe₂), 5.71 (s, 5, C₅H₅), 6.96 (t, ³J_{HH} = 7.6 Hz, H_p), 7.10 (d, ³J_{HH} = 7.7 Hz, H_m).

¹³C NMR data (100MHz, d⁶-benzene, 298K): 28.02 (d, J_{CH} = 129, CHCMe₂), 33.38 (q, J_{CH} = 125 Hz, CMe₃), 57.58 (s, CMe₃), 65.34 (q, br, Me), 107.45 (d, J_{CH} = 173 Hz, C₅H₅), 122.71 (d, J_{CH} = 155 Hz, H_o), 123.38, (d, J_{CH} = 159 Hz, H_p), 144.01 (s, H_m), 152.04 (s, H_i).

6.3 Experimental Details to Chapter 3.

6.3.1 Geometry and Coordinates for FHMO Calculations.

The coordinates used in the Fenske-Hall quantum chemical MO calculations on compounds, CpNb(NMe)Cl₂¹⁸, CpNb(NMe)Cl₂(PMe₃)¹⁸ and Cp₂ZrCl₂¹⁹, were taken from the fractional coordinates of the single crystal X-ray data, and converted to the cartesian coordinates shown in Tables 6.3, 6.4 and 6.5 respectively.

For Cp₂ZrH₂, the coordinates were taken from the Cp₂ZrCl₂ single crystal X-ray structure¹⁹, with Zr-H bond lengths of 1.78Å, taken from the X-ray structure of [(η⁵-C₅H₄CH₃)₂ZrH(μH)]₂²⁰. The calculations on the model species CpNb(NMe)H₂ were carried out using the coordinates of crystallographically characterised CpNb(NMe)Cl₂¹⁸, with Nb-H lengths taken from the the X-ray structure of Cp₂NbH₃ at 1.78Å²¹.

Calculations on the model system CpNb(η²-CHPMe₂)Cl₂ and CpNb(η²-PMe₂CH)H₂ were carried out using the geometry of the crystallographically

| Atomic Label | X Coordinate | Y Coordinate | Z Coordinate |
|--------------|--------------|--------------|--------------|
| Nb | 0.000 | 0.000 | 0.000 |
| Cl(1) | -0.542 | -1.333 | 1.863 |
| Cl(1') | -0.542 | -1.333 | -1.863 |
| N | 1.752 | 0.000 | 0.000 |
| C(1) | 3.124 | 0.408 | 0.000 |
| H(1) | 3.173 | 1.367 | 0.000 |
| H(2) | 3.560 | 0.066 | 0.783 |
| H(2') | 3.560 | 0.066 | -0.783 |
| C(2) | 0.113 | 2.337 | 0.000 |
| H(2R) | 0.980 | 2.789 | 0.000 |
| C(3) | -0.620 | 2.089 | 1.129 |
| H(3R) | -0.334 | 2.121 | 2.040 |
| C(3') | 0.620 | 2.089 | -1.129 |
| H(3R') | 0.334 | 2.121 | -2.040 |
| C(4) | -1.864 | 1.512 | 0.694 |
| H(4R) | -2.581 | 1.216 | 1.259 |
| C(4) | 1.864 | 1.512 | -0.694 |
| H(4R) | 2.581 | 1.216 | -1.259 |

Table 6.3, Coordinates used in the FHMO calculations on CpNb(NMe)Cl₂.

| Atomic Label | X Coordinate | Y Coordinate | Z Coordinate |
|--------------|--------------|--------------|--------------|
| Nb(1) | 0.000 | 0.000 | 0.000 |
| Cl(1) | -1.221 | -2.125 | 0.478 |
| Cl(2) | -0.121 | -0.952 | -2.301 |
| P(1) | 0.331 | -0.375 | 2.553 |
| C(11) | 1.352 | 0.884 | 3.370 |
| C(12) | 1.246 | -1.898 | 2.864 |
| C(13) | -1.112 | -0.510 | 3.622 |
| H(11A) | 0.920 | 1.739 | 3.425 |
| H(11B) | 2.122 | 0.949 | 2.803 |
| H(11C) | 1.620 | 0.604 | 4.249 |
| H(12A) | 0.820 | -2.695 | 2.537 |
| H(12B) | 1.369 | -1.968 | 3.814 |
| H(12C) | 2.098 | -1.793 | 2.437 |
| H(13A) | -1.700 | -1.140 | 3.199 |
| H(13B) | -1.548 | 0.340 | 3.687 |
| H(13C) | -0.890 | -0.822 | 4.502 |
| C(14) | -1.010 | 1.917 | 1.113 |
| C(15) | -2.052 | 1.394 | 0.333 |
| C(16) | -1.693 | 1.511 | -0.970 |
| C(17) | -0.430 | 2.119 | -1.032 |
| C(18) | -0.028 | 2.380 | 0.261 |
| H(14) | -0.985 | 1.950 | 2.072 |
| H(15) | -2.868 | 1.016 | 0.661 |
| H(16) | -2.217 | 1.229 | -1.723 |
| H(17) | 0.064 | 2.316 | -1.830 |
| H(18) | 0.788 | 2.808 | 0.523 |
| N(1) | 1.771 | 0.000 | 0.000 |
| C(19) | 3.145 | 0.295 | 0.006 |
| H(9A) | 3.261 | 1.248 | 0.044 |
| H(9B) | 3.518 | -0.039 | -0.809 |
| H(9C) | 3.589 | -0.111 | 0.752 |

Table 6.4. *Coordinates used in the FHMO calculations on CpNb(NMe)Cl₂(PMe₃).*

| Atomic Label | X Coordinate | Y Coordinate | Z Coordinate |
|--------------|--------------|--------------|--------------|
| Zr | 0.000 | 0.000 | 0.000 |
| Cl(1) | 1.617 | 0.000 | 1.833 |
| Cl(2) | 1.612 | 0.000 | -1.823 |
| C(1) | 0.068 | 2.505 | 0.308 |
| C(2) | -0.913 | 2.021 | 1.175 |
| C(3) | -1.925 | 1.491 | 0.434 |
| C(4) | -1.576 | 1.633 | -0.955 |
| C(5) | -0.375 | 2.257 | -0.991 |
| C(6) | -0.404 | -2.270 | 0.972 |
| C(7) | 0.115 | -2.489 | -0.294 |
| C(8) | -0.873 | -2.009 | -1.200 |
| C(9) | -1.938 | -1.632 | 0.937 |
| C(10) | -1.614 | -1.632 | 0.937 |
| H(1) | 0.932 | 3.091 | 0.586 |
| H(2) | -0.931 | 2.168 | 2.244 |
| H(3) | -2.888 | 1.181 | 0.813 |
| H(4) | -2.233 | 1.467 | -1.797 |
| H(5) | 0.101 | 2.624 | -1.887 |
| H(6) | 0.058 | -2.623 | 1.879 |
| H(7) | 0.991 | -3.071 | -0.540 |
| H(8) | -0.887 | -2.158 | -2.269 |
| H(9) | -2.898 | -1.179 | -0.787 |
| H(10) | -2.274 | -1.468 | 1.775 |

Table 6.5, Cartesian coordinates used in FHMO calculations on Cp_2ZrCl_2 .

characterised complex $\text{Cp}^*\text{Ta}(\eta^2\text{-CHPMe}_2)\text{H}_2(\text{PMe}_3)^{5,22}$. Bond distances used in this calculation were: Nb-Cl = 2.56Å, Nb-H 1.78Å, Nb-C(Cp) = 2.42Å, Nb-C(η^2 -CHPMe₂) = 2.00Å, Nb-P = 2.66Å, P-C = 1.84Å, C-H(Cp) = 0.96Å. The geometry was idealised to C_s symmetry, Cl-Nb-Cl bond angle = 108.4 °.

6.4 Experimental Details to Chapter 4.

6.4.1 Synthesis of Mo(N)Cl₃ (1).

A carbon tetrachloride solution of Me₃SiN₃ (2.11g, 18.30 mmol. in 20cm³) was added dropwise to a stirred suspension of MoCl₅ (5g, 18.30 mmol.) in carbon tetrachloride (30cm³), over a period of 10min. An immediate reaction ensued, with effervescence and formation of a red-orange solution. The mixture was refluxed for 12h. resulting in the formation of a brown amorphous solid and a pale brown solution. After cooling to room temperature, the solid was isolated by cannula filtration, washed with petroleum ether (2 x 10cm³, b.p. 40-60°C) and dried *in vacuo*. Yield 3.17g (80%).

Elemental analysis for NCl₃Mo, Found (Required): N, 6.03 (6.48); %Cl, 48.02 (49.17); %Mo, 43.88 (44.35).

Infrared data (Nujol, CsI, cm⁻¹): 1045(s), 720(w), 424(m, sh), 412(s), 364(m, 317(m), 272(s).

6.4.2 Synthesis of W(N)Cl₃ (2).

A carbon tetrachloride solution of Me₃SiN₃ (1.45g, 12.61 mmol. in 20cm³) was added dropwise to a stirred suspension of WCl₆ (5g, 12.61 mmol.) in carbon tetrachloride (30cm³), over a period of 10min. An immediate reaction ensued, with

effervescence and formation of a red-orange solution. The mixture was refluxed for 12h. resulting in the formation of an orange amorphous solid and a pale orange solution. After cooling to room temperature, the supernatant liquid was filtered from the solid, which was collected, washed with petroleum ether (2 x 10cm³, b.p. 40-60°C) and dried *in vacuo*. Yield, 3.00g (78%)

Elemental analysis for NCl₃W, Found (Required): %N, 4.11 (4.60); %Cl, 35.54 (34.96); %W, 59.83 (60.43).

Infrared data (Nujol, CsI, cm⁻¹): 1090(vs), 1075(s), 786(w), 392(m), 363(m), 337(m).

6.4.3 Synthesis of Mo(N)Cl₃(CH₃CN)₂ (3).

An acetonitrile solution of Me₃SiN₃ (1.73g, 15.0 mmol in 15 cm³) was added dropwise to a stirred suspension of MoCl₄(CH₃CN)₂ (4.80g, 15.0 mmol.) in acetonitrile (40cm³) at room temperature, over a period of 15 minutes. An immediate reaction ensued, a gas was evolved, and a dark red solution formed. After stirring for 24h., the solvent was removed under reduced pressure, and the oily dark red solid was washed with petroleum ether (2 x 10 cm³, b.p. 40-60°C) and dried *in vacuo*. Yield 3.98g (89%).

Elemental analysis for C₄H₆N₃Cl₃Mo, Found (Required): %C, 15.71 (16.01); %H, 1.97 (2.03); %N, 13.06 (14.08); %Cl, 35.44 (35.64); %Mo 31.90 (32.15).

Infrared data (nujol, KBr, cm⁻¹): 2305(s), 2292 (s) 1395(m), 1361(m), 1195(w), 1042(s), 988(w, sh), 932(m, sp), 420(m), 387(s).

6.4.4 Synthesis of $\text{Mo}(\text{N})\text{Cl}_3(\text{THF})_2$ (4).

Tetrahydrofuran (30cm^3) was added to $\text{Mo}(\text{N})\text{Cl}_3(\text{CH}_3\text{CN})_2$ (1g, 3.35mmol.). The resultant dark brown solution was stirred at room temperature for 1h. The solvent was then removed under reduced pressure to give an oily solid. Washing with petroleum ether ($2 \times 10\text{cm}^3$, b.p. $40\text{-}60^\circ\text{C}$), afforded a dark brown solid. Yield 1.00g (83%).

Elemental analysis for $\text{C}_8\text{H}_{16}\text{NO}_2\text{Cl}_3\text{Mo}$, Found (Required): %C, 26.13 (26.65); %H, 4.20 (4.47); %N, 3.19 (3.89); %Cl, 28.98 (29.65); %Mo, 25.31 (26.61).

Infrared data (nujol, KBr, cm^{-1}): 1650(w), 1362(m), 1340(w), 1033(s), 918(w), 860(s), 725(w), 667(w), 387(m, sh).

6.4.5 Synthesis of $\text{W}(\text{N})\text{Cl}_3(\text{CH}_3\text{CN})_2$ (5).

An acetonitrile solution of Me_3SiN_3 (0.85g, 7.36 mmol, in 15cm^3) was added dropwise to a stirred maroon suspension of $\text{WCl}_4(\text{CH}_3\text{CN})_2$ (3g, 7.36 mmol.) in acetonitrile (40cm^3) at room temperature over a period of 10 minutes. An immediate reaction ensued, a gas was evolved, and a dark red solution formed. After stirring for 48h., the solvent was removed under reduced pressure and the oily dark red solid was washed with petroleum ether ($2 \times 10\text{cm}^3$, b.p. $40\text{-}60^\circ\text{C}$) and dried *in vacuo*. Yield, 1.79g (63%).

Elemental analysis for $\text{C}_4\text{H}_6\text{N}_3\text{Cl}_3\text{W}$, Found (Required): %C, 12.33 (12.44); %H, 1.43 (1.57); %N, 9.23 (10.88); %Cl, 28.22 (27.53); %W 46.17 (47.57).

Infrared data (nujol, KBr, cm^{-1}): 2309(s, sp), 2295(s, sp), 1405(m), 1366(m, sp), 1090(vs), 1030(w), 942(s, sp), 410(m), 369(s), 338(s).

6.4.6 Reaction of Mo(N)Cl₃ with PMe₃:

Preparation of [Mo(NPMe₃)Cl₂(PMe₃)₃]⁺Cl⁻ (6).

(A) in Dichloromethane.

Trimethylphosphine (1.41g, 18.49 mmol.) was condensed onto a frozen solution of Mo(N)Cl₃ (1.00g, 4.62 mmol.) in dichloromethane (40 cm³). On allowing the mixture to warm to room temperature an immediate reaction ensued and a red-brown solution was formed. On stirring for 12h. pale green crystals precipitated from the solution which were collected, washed with toluene (2 x 5 cm³) and dried *in vacuo*. Removal of the volatile components from the supernatant liquid yielded a pale green powder, which was washed with cold toluene (3 x 10 cm³). Extraction of the solid in dichloromethane (15 cm³) followed by layering with an equivalent volume of toluene afforded pale green needle crystals. Combined yield, 2.30g (82%).

Elemental analysis for C₁₃H₃₈NCl₅P₄Mo, Found (Required): %C 25.58 (25.79); H 6.11 (6.32); N, 2.15 (2.31); %Cl, 29.53 (29.27); %Mo, 15.22 (15.84).

Infrared data (Nujol, KBr, cm⁻¹): 3090(m), 1601(w), 1433(m), 1415(s), 1298(vs), 1287(s), 1280(s), 1259(w), 1130(vs), 950(vs), 882(w), 877(w), 853(m), 795(w), 771(w), 725(vs), 690(m), 670(m), 476(w), 415(w), 382(m), 355, 270.

Mass spectral data (CI, isobutane carrier gas, m/z ³⁵Cl): 603 [M]⁺, 575 [M-C₂H₄]⁺, 547 [C₄H₈]⁺, 520, [M-PMe₃]⁺.

¹H NMR data (400MHz, d⁶-benzene, 298K): 1.67 (t, ²J_{PH} = 4Hz, 18, 2PMe₃), 1.82 (d, ²J_{PH} = 14Hz, 9, *cis* PMe₃), 2.20 (d, ²J_{PH} = 14Hz, 9, NPMe₃)

³¹P NMR data (101MHz, d-chloroform, 298K): -1.97 (t, ²J_{PP} = 14Hz, 2PMe₃), 2.02 (d, ²J_{PP} = 14Hz, PMe₃), 60.02 (br,s, NPMe₃).

(B) in neat Trimethylphosphine.

Trimethylphosphine (15 cm³) was condensed onto Mo(N)Cl₃ (0.5g, 2.23 mmol.). The mixture was allowed to warm to room temperature and stirred for 72h, to afford a red solution. Removal of trimethylphosphine under reduced pressure yielded a red-orange oily solid. The solid was dissolved in dichloromethane to give an orange solution, which was concentrated to half volume and cooled to -20°C to afford pale green crystals of (6). Yield, 0.43g (30%).

6.4.7 Reaction of Mo(N)Cl₃(THF)₂ with PMe₃.

Trimethylphosphine (1.69g, 22.19 mmol.) was condensed onto a frozen solution of Mo(N)Cl₃(THF)₂ (2.00g, 5.55 mmol.) in dichloromethane (40 cm³). The mixture was allowed to warm to room temperature and stirred for 24h, to afford a red-brown solution. Removal of volatiles under reduced pressure afforded an oily brown solid, from which the pale green-brown amorphous powder was obtained by washing with cold toluene (3 x 10 cm³). The crude product solid was dissolved in dichloromethane (15 cm³) and layered with toluene (15 cm³). The mixture was allowed to stand at room temperature for 48h. to afford pale green needles of (6). Yield, 1.85g (55%).

6.4.8 Conversion of [Mo(NPMe₃)Cl₂(PMe₃)₃]⁺Cl⁻ (6) to [(MoCl₃(PMe₃)₂)₂N]⁻[PMe₃NPMe₃]⁺ (7).

A pale green solution [Mo(NPMe₃)Cl₂(PMe₃)₃]⁺Cl⁻ (1.00g, 1.65 mmol.), in dichloromethane (30 cm³) was heated to 50°C. After 2h., the now orange solution was allowed to cool and the volatile components were removed under reduced pressure to yield an oily orange solid. After washing with toluene (2 x 10 cm³), the orange solid was dissolved in dichloromethane (15 cm³) and layered with toluene (15 cm³). On

standing for 48 h., large orange prisms formed at the dichloromethane/toluene interface. Combined yield, 0.71g (88%).

Elemental analysis for $C_{19}H_{56}NCl_3P_6Mo_2$, Found (Required): %C 23.37 (23.43); H 5.78 (5.79); N, 2.47 (2.88); %Cl, 29.44 (29.12); %Mo, 19.40 (19.70).

Infrared data (Nujol, KBr, cm^{-1}): 1430(w, sh), 1421(m), 1426(w), 1338(s), 1302(s), 1285(vs), 1235(m), 963(vs), 884(m, sp), 873(m), 855(w), 757(m, sp), 747(s, sh), 731(m, sp), 700(w), 679(w), 402(m), 370(m).

Mass spectral data (CI, isobutane carrier gas, m/z ^{35}Cl): 886 [M]⁺, 810 [M-PMe₃] 318 [MoCl₂(PMe₃)₂]⁺, 242 [MoCl₂(PMe₃)]⁺.

6.4.9 Reaction of Mo(N)Cl₃ with PPh₃:

Preparation of Mo(N)Cl₃(PPh₃)₂ (8).

Dichloromethane (30cm³), was added to a mixture of Mo(N)Cl₃ (0.5g, 2.31mmol) and PPh₃ (2.42g, 9.24mmol). The resultant suspension was stirred at room temperature for 24h, to give a brown solution and a beige solid. The supernatant solution was filtered from the solid, which was collected, washed with light petroleum ether (2 x 10cm³) and dried *in vacuo*. Yield, 1.25g (74%)

Elemental analysis for $C_{36}H_{30}NCl_3P_2Mo$ Found (Required): %C, 58.12 (58.36); %H, 3.79 (4.08); %N, 2.03 (1.89); %Cl 14.50 (14.36); %Mo, 12.80 (12.95).

Infrared data (nujol, KBr, cm^{-1}): 1585(w), 1482(s), 1435(vs, sp), 1185(w), 1130(s, sp), 1087(m), 1045(w), 1029(w), 997(w), 754(vs), 748(vs), 732(m), 696(vs), 534(s), 508(m), 493(m), 365(s).

Mass spectral data (CI, isobutane carrier gas, m/z ^{96}Mo): 358 $[\text{Mo-PPh}_3]^+$, 263 $[\text{PPh}_3\text{H}]^+$, 96 $[\text{Mo}]^+$.

^1H NMR data (250MHz, d^2 -dichloromethane, 298K): 7.4 (s, br, 12, H_o), 7.5(s, br, 18, $\text{H}_\text{m/p}$).

6.4.10 Reaction of $\text{Mo}(\text{N})\text{Cl}_3$ with PCy_3 :

Preparation of $\text{Mo}(\text{N})\text{Cl}_3(\text{PCy}_3)_2$ (9).

Dichloromethane (30cm^3), was added to a mixture of $\text{Mo}(\text{N})\text{Cl}_3$ (0.5g, 2.31mmol) and PCy_3 (9.24mmol). The resultant suspension was consumed during stirring at room temperature for 24h to form a red-brown solution. The solvent was removed under reduced pressure to afford an oily brown solid, which on washing with petroleum ether ($2 \times 10\text{cm}^3$, b.p $40\text{-}60^\circ\text{C}$) yielded a pale brown solid. Yield, 0.54g (30%).

Elemental analysis for $\text{C}_{36}\text{H}_{66}\text{NCl}_3\text{P}_2\text{Mo}$ Found (Required): %C, 55.22 (55.64); %H, 8.70 (8.56); %N, 1.99 (1.80); %Cl 13.50 (13.69).

Infrared data (nujol, CsI, cm^{-1}): 1278(w), 1220(m), 1120(s), 1080(vs, br), 1040(s), 1005(s), 968(s), 895(s), 850(s), 820(w), 760(w), 720(w), 563(m), 547(s), 535(s), 448(w), 400(w), 325(vs).

6.4.11 Reaction of $\text{W}(\text{N})\text{Cl}_3$ with PMe_3 :

(A) Preparation of $\text{W}(\text{N})\text{Cl}_3(\text{PMe}_3)_2$ (10).

Trimethylphosphine (1.00g, 13.15 mmol.) was condensed onto a frozen mixture of $\text{W}(\text{N})\text{Cl}_3$ (1g, 3.29 mmol.) and dichloromethane (40 cm^3). The mixture was allowed to warm to room temperature and stirred for 12h during which time dissolution

of the orange suspension led to the formation of a red-brown solution. Removal of solvent under reduced pressure yielded a red-brown oil, which was washed with petroleum ether (2 x 10cm³, b.p. 40-60°C) and dried *in vacuo* to afford an amorphous brown solid. The solid was redissolved in dichloromethane (10cm³) and layered with toluene (20cm³). After 24h., an olive green powder was obtained. This was filtered and washed the resultant solid with toluene/dichloromethane (2 x 10cm³, 2:1). Yield, 0.53g (35%).

Elemental analysis for C₆H₁₈NCl₃P₂W Found (Required): %C, 14.98 (15.79); %H, 3.90 (3.98); %N, 2.70 (3.07); %Cl 22.87 (23.31); %W, 38.99 (40.29).

Infrared data (nujol, CsI, cm⁻¹): 1429(m), 1302(m, sp), 1288(m, sp), 1165(vs), 980(vs, sh), 965(vs), 891(w), 884(m), 855(w), 774(m, sp), 752(m), 721(w), 685(w), 430(w), 330(m), 317(vs), 275(m).

Mass spectral data (CI, isobutane carrier gas, m/z ¹⁸³W): 343 [M-PMe₃-Cl]⁺, 259 [WPMe₃]⁺, 77 [PMe₃+H]⁺.

¹H NMR data (250MHz, d²-dichloromethane, 298K): 1.18 (s, br).

(B) Preparation of [W(NPMe₃)Cl₂(PMe₃)₃]⁺Cl⁻ (13).

The reaction was repeated as described above, but after the addition of trimethylphosphine the mixture was allowed to warm to 0°C. After 4h, filtration yielded a brown powder, which analysed as W(N)Cl₃, and a green-brown solution. The solution was concentrated to half volume, layered with toluene (10 cm³) and cooled to -20°C. After several days bottle green needles were formed at the solvent interface, which were isolated and washed with a toluene/dichloromethane mixture (3:1, 2 x 5 cm³) and dried *in vacuo*. Yield, 0.12g (6%).

Elemental analysis for $C_{12}H_{36}NCl_3P_4W$ Found (Required): %C, 23.55 (23.69); %H, 5.49 (5.96); %N, 2.29 (2.30); %Cl 17.98 (17.48); %W, 32.10 (30.21).

Infrared data (nujol, CsI, cm^{-1}): 1430(m), 1410(m), 1290(s), 1284(m), 1180(vs), 960(vs), 882(w), 795(w), 771(w), 727(vs), 690(m), 415(w), 380(m), 320(m), 290(w).

6.4.12 Reaction of $W(N)Cl_3$ with PMe_2Ph :

Preparation of $W(N)Cl_3(PMe_2Ph)_2$ (11).

Dimethylphenylphosphine (0.91g, 6.57 mmol.) was added, *via* syringe, to $W(N)Cl_3$ (0.5g, 1.64 mmol.) in dichloromethane (30 cm^3). The mixture was stirred at room temperature for 24h. during which time the orange suspension was consumed to give a red-brown solution. Removal of solvent under reduced pressure yielded a red-brown oil, which was washed with petroleum ether (2 x 10 cm^3 , b.p. 40-60°C) and dried *in vacuo* to afford a pale brown solid. A dichloromethane solution of the solid (10 cm^3) was layered with toluene (10 cm^3) and cooled to 0°C. After 48h., pale green crystals formed, which were collected, washed with a toluene/dichloromethane mixture (3:2, 10 cm^3) and dried *in vacuo*. Yield, 0.34g (36%).

From the supernatant liquid red crystals were isolated in low yield analysing as $WCl_4(PMe_3)_3$.

Elemental analysis for $C_{16}H_{22}NCl_3P_2W$ Found (Required): %C, 33.54 (33.10); %H, 4.01 (3.82); %N, 2.10 (2.41); %Cl 19.07 (18.32); %W, 31.03 (31.67).

Infrared data (nujol, CsI, cm^{-1}): 3035(w, sh), 1592(w), 1440(s), 1415(m), 1306(m), 1295(m), 1200(m), 1145(vs), 1100(s, sh), 1090(s), 1070(m), 947(m), 918(vs), 870(s), 738(s), 690(m), 488(m), 442(m), 412(w), 310(s, sh), 296(vs).

Mass spectral data (CI, isobutane carrier gas, m/z ^{183}W): 303 $[\text{W}(\text{NH})\text{Cl}_3]^+$, 139 $[\text{PMe}_2\text{Ph}+\text{H}]^+$.

^1H NMR data (400MHz, d^2 -dichloromethane, 298K): 2.34(s, br, 12), 7.16 (t, 2, $^3\text{J}_{\text{HH}} = 7\text{Hz}$, H_p), 7.17 (d,4, $^3\text{J}_{\text{HH}} = 7\text{Hz}$, H_m), 7.23 (d,4, $^3\text{J}_{\text{HH}} = 7\text{Hz}$, H_o).

6.4.13 Reaction of $\text{W}(\text{N})\text{Cl}_3$ with PPh_3 :

Preparation of $\text{W}(\text{N})\text{Cl}_3(\text{PPh}_3)_2$ (12).

Dichloromethane (50 cm^3) was added to weighed mixture of triphenylphosphine (1.72g, 6.57 mmol) and $\text{W}(\text{N})\text{Cl}_3$ (0.5g, 1.64 mmol.) . The mixture was stirred for 24h. to afford a pale solid and a red-brown solution. The solution was isolated by cannula filtration and the solvent removed under reduced pressure to afford an oily green solid, which was washed with petroleum ether ($2 \times 10\text{cm}^3$, b.p. $40\text{-}60^\circ\text{C}$) and dried *in vacuo* to afford an amorphous green solid. A saturated dichloromethane solution of the solid (10cm^3) was layered with toluene (20cm^3), and cooled to 0°C . After 48h., pale green-yellow crystals were formed, which were isolated and washed with cold dichloromethane. Overall yield, 0.77g (57%).

Elemental analysis for $\text{C}_{36}\text{H}_{30}\text{NCl}_3\text{P}_2\text{W}$ Found (Required): %C, 51.58 (52.17); %H, 3.68 (3.65); %N, 1.46 (1.69); %Cl 12.26 (12.83); %W, 21.00 (22.18).

Infrared data (nujol, CsI , cm^{-1}): 3020(w, sh), 1587(w), 1436(s), 1216(m), 1195(w), 1177(m), 1138(vs), 1085(s), 1027(w), 998(w), 748(m), 725(vs), 685(s), 569(w), 535(vs), 522(m, sh), 495(w), 325(m), 301(s).

Mass spectral data (CI, isobutane carrier gas, m/z ^{183}W): 445 $[\text{WPPh}_3]^+$, 370 $[\text{WPPh}_2+2\text{H}]^+$, 263 $[\text{PPh}_3+\text{H}]^+$.

¹H NMR data (250MHz, d²-dichloromethane, 298K): 7.4 (s, br, 12, H_{m/p}), 7.7 (s, br, 8, H_o).

6.4.14 Reaction of KReO₄ with H₂NNH₂·2HCl and PMe₃.

Trimethylphosphine (3.61g, 47.50 mmol.) was condensed on to a frozen mixture of KReO₄ (2g, 6.91 mmol.) and H₂NNH₂·2HCl (1g, 9.53 mmol.) in ethanol (50 cm³). The mixture was allowed to warm to room temperature and heated to reflux with stirring for 72h. The resultant yellow solution was cooled, filtered and the volatile components removed under reduced pressure to afford a pale yellow crystalline solid. The solid was washed with cold ethanol (2 x 5 cm³ at -78°C) and recrystallised from ethanol to give yellow rhombic crystals. Yield for C₆H₁₈NOCIP₂Re, 1.26g (45%)

Elemental analysis for C₆H₁₈NOCIP₂Re Found (Required): %C, 17.71 (17.85); %H, 4.62 (4.49); %N, 3.50 (3.47); %Cl 9.60 (8.78); %W, 45.19 (46.11).

Infrared data (nujol, CsI, cm⁻¹): 1420(m), 1315(m), 1290(s), 1050(s, sp), 1043(m, sp), 946(vs), 900(vs), 860(m), 742(m), 726(s), 672(m), 368(w), 338(s), 328(s, sh), 319(m).

¹H NMR data (400MHz, d-chloroform, 298K): 1.85(t, 18, J_{CP} = 4.4 Hz, PMe₃), 1.94 (d, 9, J_{CP} = 9.6 Hz, PMe₃), 2.03 (t, 9, J_{CP} = 3.2 Hz, PMe₃).

³¹P NMR data (101MHz, decoupled, d-chloroform, 298K): -17.3 (PMe₃), -26.2 (PMe₃), -31.71 (PMe₃).

6.4.15 Reaction of KReO_4 with $\text{H}_2\text{NNH}_2 \cdot 2\text{HCl}$ and PMe_2Ph :

Preparation of $\text{Re}(\text{N})\text{Cl}_2(\text{PMe}_2\text{Ph})_3$ (15).

Dimethylphenylphosphine (3.78g, 23.75 mmol.) was added to a mixture of KReO_4 (1g, 3.46 mmol.) and $\text{H}_2\text{NNH}_2 \cdot 2\text{HCl}$ (0.5g, 4.76 mmol.) in ethanol (40 cm^3). The mixture was heated to reflux and stirred for 72 h to form a yellow solution and pale solid. The supernatant solution was removed from the solid by filtration and the volatile components removed under reduced pressure to yield a waxy yellow crystalline solid, which was washed with cold ethanol (2 x 5 cm^3 at ca. -78°C). Prolonged cooling of a saturated ethanol solution of (14) to -20°C afforded yellow rhombic crystals. Yield, 1.44g (61%)

Elemental analysis for $\text{C}_{24}\text{H}_{33}\text{NCl}_2\text{P}_3\text{Re}$ Found (Required): %C, 42.27 (42.05); %H, 4.88 (4.85); %N, 1.96 (2.04); %Cl 10.21 (10.34); %Re, 26.55 (27.16).

Infrared data (nujol, CsI, cm^{-1}): 3030(w), 1602(w), 1500(w, sh), 1490(m, sh), 1445(s), 1429(m), 1335(w), 1316(m), 1301(s, sp), 1290(m), 1207(m), 1185(vs), 1170(m), 1130(s), 1112(m), 1089(w), 1058(vs, sp), 1037(w), 1008(w), 945(vs), 918(vs), 878(s), 857(m), 750(vs), 733(s), 725(s), 716(s), 704(vs), 687(m), 498(vs), 446(vs), 379(w), 366(m), 298(m).

Mass spectral data (CI, isobutane carrier gas, m/z ^{185}Re): 261 [$\text{ReN}(\text{PMe}_2)+\text{H}$] $^+$, 140[$\text{PMe}_2\text{Ph}+2\text{H}$] $^+$, 123[$\text{PMePh}+2\text{H}$].

^1H NMR data (400MHz, d-chloroform, 298K): 1.30 (d, 6, $^2\text{J}_{\text{HP}} = 9.6$ Hz, PMe_2Ph), 1.73 (t, 6, $\text{J}_{\text{HP}} = 4.2$ Hz, *trans*- PMe_2Ph), 2.01 (t, 6, $\text{J}_{\text{CP}} = 4.2$ Hz, *trans*- PMe_2Ph), 6.91 (t, 2, $^3\text{J}_{\text{HH}} = 6.4$ Hz, H_p), 7.03 (m, 4, ring H), 7.05 (t, 1, $^3\text{J}_{\text{HH}} = 7.2$ Hz, H_p), 7.24 (m, 4, $^3\text{J}_{\text{HH}} = 5.2$ Hz, ring H), 7.49 (m, 4, $^3\text{J}_{\text{HH}} = 5.2$ Hz, ring H).

¹³C NMR data (100MHz, ¹H decoupled, d-chloroform, 298K): 10.71 (t, J_{CP} = 17 Hz PMe₂Ph), 17.69 (t, J_{CP} = 17 Hz, PMe₂Ph), 18.80 (d, J_{CP} = 37 Hz, PMe₂Ph), 127.92 (s, ring C), 128.02 (s, ring C), 128.56 (t, J_{CP} = 4 Hz, ring C), 129.71 (s, ring C), 129.82 (s, ring C), 129.90 (s, ring C), 130.32 (t, J_{CP} = 4 Hz, ring C).

³¹P NMR data (101MHz, d-chloroform, 298K): -28.25 (t, ²J_{PP} = 15 Hz, PMe₂Ph), -16.28 (d, ²J_{PP} = 15 Hz, 2PMe₂Ph).

6.4.16 Reaction of KReO₄ with H₂NNH₂·2HCl and PMePh₂:

Preparation of Re(N)Cl₂(PMePh₂)₂ (16).

Methyldiphenylphosphine (4.75g, 23.75 mmol.) was added to a mixture of KReO₄ (1g, 3.46 mmol.) and H₂NNH₂·2HCl (0.5g, 4.76 mmol.) in ethanol (40 cm³). The mixture was heated to reflux and stirred for 72 h to form a yellow solution and pale solid. After cooling, the supernatant solution was filtered from the solid and the volatile components were removed under reduced pressure to give a yellow oil, which was washed with cold ethanol (3 x 10 cm³ ca -78°C) and dried *in vacuo* overnight. Prolonged cooling of a saturated ethanol/chloroform solution of the product to -20°C afforded yellow rhombic crystals. Yield, 1.11g (48%)

Elemental analysis for C₂₆H₃₃NCl₂P₂Re Found (Required): %C, 47.39 (46.05); %H, 4.22 (3.90); %N, 1.77 (2.09); %Cl 9.60 (10.34).

Infrared data (nujol, CsI, cm⁻¹): 3028(w), 1595(w), 1488(m), 1445(vs), 1435(m), 1342(m), 1323(m), 1308(m), 1175(vs), 1125(s), 1111(s), 1110(s, sh), 1072(m), 1055(m), 1030(w), 998(s, sp), 887(vs), 860(w), 773(s), 753(vs), 740(vs), 714(s, sp), 693 (vs), 510(vs), 450(w), 413(m), 383 (w, sh), 308(w), 290(w).

¹H NMR data (400MHz, d-chloroform, 298K): 1.76 (d, 6, J_{CP} = 16.5 Hz, PMePh₂), 7.2-7.3(m, 12, H_{p/m}), 7.5-7.6 (m, 8, H_o).

³¹P NMR data (101MHz, decoupled, d-chloroform, 298K): -16.33 (s, br, PMePh₂).

6.4.17 Coordinates Used in FHMO Calculations on



The coordinates used in the Fenske-Hall quantum mechanical MO calculations on $[\text{Mo}(\text{NPMe}_3)\text{Cl}_2(\text{PMe}_3)_3]^+$, were taken from the fractional coordinates of the single crystal X-ray data²³ and converted to the cartesian coordinates shown in Table 6.7.

6.5 Experimental Details to Chapter 5.

6.5.1 Geometry and Coordinates Used in FHMO Calculations.

The coordinates used in the Fenske-Hall quantum mechanical MO calculations on compounds $\alpha\text{-Nb}(\text{O})\text{Cl}_3(\text{PMe}_3)_3$ ²⁴, $\beta\text{-Nb}(\text{O})\text{Cl}_3(\text{PMe}_3)_3$ ²⁵ were taken from the fractional coordinates of the single crystal X-ray data and converted to the cartesian coordinates shown in Table 6.8, and 6.9 respectively.

The calculations on model species $\text{Nb}(\text{O})\text{Cl}_3(\text{PH}_3)_3$ and $\text{Mo}(\text{N})\text{Cl}_3(\text{PMe}_3)_3$ were carried out using modified coordinates of crystallographically characterised $\alpha\text{-Nb}(\text{O})\text{Cl}_3(\text{PMe}_3)_3$ ²⁴ Bond distances used in these calculations were: P-H = Å, Mo-Cl = Mo-N = 1.60-1.80Å²⁶.

| Atomic Label | X Coordinate | Y Coordinate | Z Coordinate |
|--------------|--------------|--------------|--------------|
| Mo | 0.000 | 0.000 | 0.000 |
| Cl(1) | -2.478 | 0.014 | -0.127 |
| Cl(2) | -0.165 | 0.016 | 2.515 |
| P(1) | -0.432 | -2.476 | 0.291 |
| C(11) | -1.025 | -3.498 | -1.041 |
| C(12) | 1.043 | -3.352 | 0.958 |
| C(13) | -1.722 | -2.838 | 1.512 |
| P(2) | -0.408 | 2.478 | 0.124 |
| C(21) | -1.333 | 2.972 | 1.624 |
| C(22) | -1.342 | 3.305 | -1.203 |
| C(23) | 1.067 | 3.454 | 0.270 |
| P(3) | 1.050 | 1.271 | -3.252 |
| C(31) | 0.832 | -1.447 | -3.296 |
| C(32) | -1.573 | 0.068 | -3.325 |
| C(33) | -1.573 | 0.068 | -3.325 |
| N | 1.775 | 0.000 | 0.000 |
| P(4) | 3.373 | 0.015 | 0.353 |
| C(41) | 4.223 | 1.341 | -0.489 |
| C(42) | 3.523 | 0.234 | 2.113 |
| H(11A) | -0.448 | -3.396 | -1.801 |
| H(11B) | -1.917 | -3.236 | -1.279 |
| H(11C) | -1.024 | -4.417 | -0.762 |
| H(12A) | 1.781 | -3.225 | 0.336 |
| H(12B) | 0.852 | -4.289 | 1.016 |
| H(12C) | 1.268 | -2.998 | 1.801 |
| H(13A) | -1.562 | -2.326 | 2.307 |
| H(13B) | -1.699 | -3.775 | 1.727 |
| H(13C) | -2.582 | -2.612 | 1.151 |
| H(21A) | -2.164 | 2.490 | 1.654 |
| H(21B) | -1.510 | 3.914 | 1.599 |
| H(21C) | -0.814 | 2.763 | 2.404 |
| H(22A) | -2.170 | 2.840 | -1.345 |
| H(22B) | -0.828 | 3.299 | -2.013 |
| H(22C) | -1.526 | 4.214 | -0.949 |
| H(23A) | 1.621 | 3.092 | 0.965 |

| | | | |
|--------|--------|--------|--------|
| H(23B) | 0.829 | 4.358 | 0.488 |
| H(23C) | 1.549 | 3.443 | -0.560 |
| H(31A) | 0.778 | 2.130 | -2.923 |
| H(31B) | 0.942 | 1.244 | -4.206 |
| H(31C) | 1.972 | 1.120 | -3.052 |
| H(32A) | 0.418 | -2.259 | -2.995 |
| H(32B) | 1.766 | -1.463 | -3.071 |
| H(32C) | 0.735 | -1.372 | -4.249 |
| H(33A) | -2.088 | 0.788 | -2.954 |
| H(33B) | -2.043 | -0.758 | -3.203 |
| H(33C) | -1.435 | 0.225 | -4.262 |
| H(41A) | 5.155 | 1.319 | -0.262 |
| H(41B) | 3.847 | 2.182 | -0.221 |
| H(41C) | 4.123 | 1.233 | -1.438 |
| H(42A) | 5.077 | -1.465 | 0.044 |
| H(42B) | 4.032 | -1.592 | -1.118 |
| H(42C) | 3.729 | -2.229 | 0.281 |
| H(43A) | 4.452 | 0.246 | 2.358 |
| H(43B) | 3.084 | -0.491 | 2.561 |
| H(43C) | 3.113 | 1.064 | 2.371 |

Table 6.6, Cartesian coordinates used in the FHMO calculations on $[Mo(NPMe_3)Cl_2(PMe_3)_3]^+$.

| Atomic Label | X Coordinate | Y Coordinate | Z Coordinate |
|--------------|--------------|--------------|--------------|
| Nb | 0.000 | 0.000 | 0.000 |
| O | 1.781 | 0.000 | 0.000 |
| Cl(1) | -1.539 | 0.777 | -1.830 |
| Cl(2) | -1.308 | -2.153 | 0.244 |
| Cl(3) | -1.471 | 1.201 | 1.630 |
| P(1) | 0.600 | 2.550 | -0.340 |
| P(2) | 0.621 | -1.478 | -2.088 |
| P(3) | 0.627 | -0.967 | 2.379 |
| C(11) | 1.546 | 2.826 | -1.844 |
| C(12) | -0.713 | 3.794 | -0.433 |
| C(13) | 1.703 | 3.137 | 0.979 |
| C(21) | 1.656 | -0.615 | -3.258 |
| C(22) | -0.672 | -2.136 | -3.136 |
| C(23) | 1.598 | -2.913 | -1.591 |
| C(31) | 1.701 | -2.414 | 2.227 |
| C(32) | 1.628 | 0.199 | 3.328 |
| C(33) | -0.669 | -1.464 | 3.511 |
| H(11A) | 0.963 | 2.496 | -2.698 |
| H(11B) | 2.465 | 2.262 | -1.792 |
| H(11C) | 1.770 | 3.882 | -1.956 |
| H(12A) | -1.419 | 3.514 | -1.197 |
| H(12B) | -0.289 | 4.758 | -0.665 |
| H(12C) | -1.207 | 3.833 | 0.526 |
| H(13A) | 2.535 | 2.451 | 1.083 |
| H(13B) | 1.156 | 3.193 | 1.910 |
| H(13C) | 2.074 | 4.118 | 0.718 |
| H(21A) | 2.482 | -0.177 | -2.732 |
| H(21B) | 1.076 | 0.166 | -3.741 |
| H(21C) | 2.031 | -1.294 | -4.004 |
| H(22A) | -1.371 | -2.700 | -2.533 |
| H(22B) | -0.244 | -2.780 | -3.880 |
| H(22C) | -1.182 | -1.315 | -3.619 |
| H(23A) | 1.038 | -3.508 | -0.891 |
| H(23B) | 2.510 | -2.577 | -1.131 |
| H(23C) | 1.834 | -3.513 | -2.469 |

| | | | |
|--------|--------|--------|-------|
| H(31A) | 1.213 | -3.182 | 1.651 |
| H(31B) | 1.933 | -2.790 | 3.215 |
| H(31C) | 2.613 | -2.122 | 1.729 |
| H(32A) | 2.442 | 0.575 | 2.729 |
| H(32B) | 2.023 | -0.308 | 4.191 |
| H(32C) | 1.005 | 1.027 | 3.645 |
| H(33A) | -1.329 | -2.165 | 3.033 |
| H(33B) | -1.234 | -0.594 | 3.828 |
| H(33C) | -0.218 | -1.930 | 4.373 |

Table 6.7, Coordinates used for FHMO calculations on $\alpha\text{-Nb(O)Cl}_3(\text{PMe}_3)_3$.

| Atomic Label | X Coordinate | Y Coordinate | Z Coordinate |
|--------------|--------------|--------------|--------------|
| Nb | 0.000 | 0.000 | 0.000 |
| O | 1.955 | 0.000 | 0.000 |
| Cl(1) | -1.568 | 0.758 | -1.750 |
| Cl(2) | -1.280 | -2.170 | 0.176 |
| Cl(3) | -1.432 | 1.145 | 1.672 |
| P(1) | 0.635 | 2.558 | -0.269 |
| P(2) | 0.597 | -1.391 | -2.178 |
| P(3) | 0.639 | -0.963 | 2.364 |
| C(11) | 1.591 | 2.897 | -1.772 |
| C(12) | -0.657 | 3.773 | -0.322 |
| C(13) | 1.728 | 3.194 | 1.044 |
| C(21) | 1.648 | -0.478 | -3.343 |
| C(22) | -0.729 | -2.100 | -3.219 |
| C(23) | 1.551 | -2.825 | -1.806 |
| C(31) | 1.687 | -2.390 | 2.203 |
| C(32) | 1.638 | 0.199 | 3.401 |
| C(33) | -0.659 | -1.533 | 3.479 |
| H(11A) | 2.399 | 2.218 | -1.834 |
| H(11B) | 1.981 | 3.915 | -1.753 |
| H(11C) | 0.947 | 2.751 | -2.636 |
| H(12A) | -1.370 | 3.473 | -1.097 |
| H(12B) | -0.223 | 4.730 | -0.568 |
| H(12C) | -1.151 | 3.839 | 0.640 |
| H(13A) | 2.556 | 2.541 | 1.182 |
| H(13B) | 1.178 | 3.276 | 1.970 |
| H(13C) | 2.100 | 4.163 | 0.769 |
| H(21A) | 1.159 | 0.405 | -3.675 |
| H(21B) | 1.875 | -1.102 | -4.200 |
| H(21C) | 2.556 | -01.86 | -2.820 |
| H(22A) | -1.372 | -1.308 | -3.512 |
| H(22B) | -1.289 | -2.808 | -2.620 |
| H(22C) | -0.347 | 2.603 | -4.103 |
| H(23A) | 0.999 | -3.461 | -1.121 |
| H(23B) | 2.464 | 2.472 | -1.326 |
| H(23C) | 1.783 | -3.388 | -2.705 |

| | | | |
|--------|--------|--------|-------|
| H(31A) | 2.527 | -2.161 | 1.556 |
| H(31B) | 1.097 | -3.207 | 1.762 |
| H(31C) | 1.933 | -2.790 | 3.215 |
| H(32A) | 1.105 | 1.111 | 3.560 |
| H(32B) | 2.559 | 0.422 | 2.894 |
| H(32C) | 1.849 | -0.255 | 4.356 |
| H(33A) | -1.331 | -0.734 | 3.645 |
| H(33B) | -0.247 | -1.833 | 4.420 |
| H(33C) | -1.193 | -2.365 | 3.015 |

Table 6.8, *Coordinates used for FHMO calculations on β -Nb(O)Cl₃(PMe₃)₃.*

6.6 Further Experimental Details.

6.6.1 Reaction of W(Ntol)Cl₄ with LiO-2,6-Me₂C₆H₃:

Preparation of W(Ntol)(O-2,6-Me₂C₆H₃)₄.

Diethylether (40 cm³) at *ca.* -78°C was added to a weighed mixture of W(Ntol)Cl₄ (1g, 2.32 mmol.) and LiO-2,6-Me₂C₆H₃ (1.19g, 9.28mmol). On warming the mixture to room temperature an immediate reaction led to the formation of a red solution and flocculent pale precipitate. After stirring for a further 12h., the suspension was filtered from the supernatant solution. The solvent was then removed under reduced pressure to afford a red crystalline solid, which was washed with cold light petroleum ether (2 x 5 cm³ b.p 40-60°C) and dried *in vacuo*. Yield, 1.60g (89%). The product was recrystallised from cold pentane to yield large red prisms.

Elemental analysis for C₃₉H₄₃NO₄W Found (Required): %C, 60.43 (60.55), %H, 5.53 (5.60), %N, 1.87 (1.81), %Nb 24.11 (23.76).

Infrared data (Nujol, CsI, cm⁻¹): 3030(w, sh), 1592(w), 1500(m), 1423(s), 1370(s), 1270(vs), 1240(s), 1210(vs), 1165(w), 1300(m), 1022(w), 970(w), 918(m, sh), 901(s), 890(s), 818(m), 767(s), 732(m), 723(m), 571(w), 485(w).

Mass spectral data (CI, isobutane carrier gas, m/z ¹⁸⁴W): 652 [M-OAr]⁺, 562 [W(N)(OAr)₃+H]⁺, 123 [ArOH₂]⁺, 122 [ArOH]⁺.

¹H NMR data (250MHz, d-chloroform, 298K): 2.17 (s, 24, O-C₆H₃Me₂), 2.50 (s, 3, C₆H₄Me), 6.66 (t, 4, ³J_{HH} = 7 Hz, O-C₆H₃, H_p), 6.72 (d, 2, ³J_{HH} = 8 Hz, C₆H₄, H_m), 6.89 (d, 8, ³J_{HH} = 7 Hz Hz, O-C₆H₃, H_m), 7.17 (d, 2, ³J_{HH} = 8 Hz, C₆H₄, H_o).

¹³C NMR data (63MHz, d-chloroform, 298K): 16.9 (q, J_{CH} = 127 Hz, C₆H₃Me₂), 20.9 (q, J_{CH} = 128 Hz, C₆H₄Me), 121.9 (d, J_{CH} = 161 Hz, ring C), 123.3 (s, ring C), 126.3 (d, J_{CH} = 162 Hz, ring C), 127.0 (d, J_{CH} = 160 Hz, ring C), 128.0 (d, J_{CH} = 161 Hz, ring C), 128.6, 151.8 (s, ring C), 161.6 (s, ring C).

6.6.2 The Synthesis of Nb(S)Cl₃(CH₃CN)₂.

A chilled (*ca.* -30°C) acetonitrile solution of (Me₃Si)₂S (1.97g, 12.6 mmol in 15 cm³) was added dropwise to a stirred suspension of NbCl₅ (3.0g, 11.1 mmol.) in acetonitrile (20 cm³) at *ca.* -30°C. The mixture was warmed to room temperature with stirring to give a green solution which gradually turned yellow with stirring overnight. The volatiles were removed under reduced pressure and the residue was dried *in vacuo*. to afford a 95% of crude Nb(S)Cl₃(CH₃CN)₂. An analytically pure sample was obtained extraction with acetonitrile followed by filtration, concentration of the supernatant solution, and cooling to *ca.* -30°C to afford yellow crystals. Yield, 2.26g (65%).

Elemental analysis for C₄H₆N₂Cl₃SNb Found (Required): %C, 15.11 (15.35); %H, 2.03 (1.91); %Cl, 32.87 (33.86); %N, 8.13 (8.87); %S, 10.12 (10.23); %Nb 29.90 (29.68).

Infrared data (Nujol, CsI, cm⁻¹): 2310(s, sp), 2280(s, sp), 1368(m), 1358(m), 1030(m), 523(s, sp), 379(m, sh), 370(m, sh), 354(s, sp), 334(s), 316(s, sp), 280(m).

6.6 References.

1. T.V. Lubben, P.T. Wolczanski and G.D. Van Duyne, *Organometallics*, 1984, **3**, 982.
2. W. Wolfsberger and H. Schmidbaur, *Synth. React. Inorg. Metal.-Org. Chem.*, 1974, **4**, 149.
3. M.J. Bunker, A. De Cian, M.L.H. Green, J.J.E. Moreau and N. Siganporia, *J. Chem. Soc., Dalton Trans.*, 1980, 2155.
4. V.C. Gibson, J.E. Bercaw, W.J. Burton Jr. and R.D. Sanner, *Organometallics*, 1986, **5**, 976.
5. T.P. Kee, *Thesis*, Durham University 1989, Chapter 2.
6. J.R. Dilworth and R.L. Richrads, *Inorg. Syn.*, **20**, 120, Ed. D.H. Busch.
7. E.A. Allen, B.J. Brisdon and G.W.A. Fowles, *J. Chem. Soc. (A)*, 1964, 4531.
8. E.A. Allen, N.P. Johnson, D.T. Rosevear and W. Wilkinson, *J. Chem. Soc., (A)*, 1969, 788.
9. R.R. Schrock, J.S. Mrdzek, G. Bazan, M. DiMare, and M. O'Regan, *J. Am. Chem. Soc.*, 1990, **112**, 3875; R.R. Schrock, *Unpublished results*, 1990.
10. A.J. Banister, W. Clegg, I.B. Gorrell, Z.V. Hauptman and W.H. Small, *J. Chem. Soc., Chem. Commun.*, 1987, 1611.
11. V.C. Gibson, T.P. Kee and A. Shaw, *Polyhedron*, 1988, **7**, 2217.
12. R.R. Schrock, *J. Am. Chem. Soc.*, 1985, **107**, 5957.
13. R.F. Fenske and M.B. Hall, *Inorg Chem.*, 1972, **11**, 768; D.L. Lichtenberger and R.F. Fenske, *J. Chem. Phys.*, 1976, **64**, 4247.
14. E. Clementi, *J. Chem. Phys.*, 1964, **40**, 1944.
15. W.J. Hehre, R.F. Stewart and J.A. Pople, *J. Chem. Phys.*, 1969, **51**, 2657.
16. J.A. Richardson, M.J. Blackman and J.E. Ranochak, *J. Chem. Phys.*, 1973, **58**, 3010.
17. H. Basch and H.B. Gray, *Theor. Chim. Acta*, 1966, **4**, 367.

18. V.C. Gibson, D.N. Williams, W. Clegg and D.C.R. Hockless, *Polyhedron*, 1989, **8**, 1819.
19. K. Prout, T.S. Cameron, R.A. Forder, S.R. Critchley, B. Denton and G.V. Rees, *Acta Crystallor.*, 1974, **B30**, 2290.
20. S.B. Jones and J.L. Petersen, *Inorg. Chem.*, 1981, **20**, 2889.
21. R.D. Wilson, T.F. Koetzle, D.W. Hart, A. Kuick, D.L. Tipton and R. Bau, *J. Am. Chem. Soc.*, 1977, **99**, 1775.
22. T.P. Kee, V.C. Gibson and W. Clegg, *J. Organomet. Chem.*, 1987, **325**, C14.
23. V.C. Gibson, T.P. Kee, R.M. Sorrell, A.P. Bashall and M. McPartlin, *Polyhedron*, 1988, **7**, 2221.
24. A. Shaw, *Thesis*, 1989; A. Bashall, V.C. Gibson, T.P. Kee, M. McPartlin and A. Shaw, *In Press*.
25. W.P. Griffith, *Coord. Chem. Rev.*, 1972, **8**, 369.

Appendices.

Appendix 1A: Crystal Data for CpNb(NMe)Cl₂.

| | |
|--|---|
| C ₆ H ₈ NCl ₂ Nb: | 257.95 |
| Crystal System: | Monoclinic |
| Space Group: | P2 ₁ /m |
| Cell Dimensions: | a = 7.178(6) Å |
| | b = 9.897(10) Å |
| | c = 7.199(6) Å |
| | β = 118.04(6)° |
| | U = 451.4 Å ³ |
| | Z = 2 |
| | D _c = 1.897 g cm ⁻³ |
| Final R-value: | 0.016 (R _w = 0.016) |

Appendix 1B: Crystal Data for CpNb(N^tBu)Cl₂.

| | |
|---|---|
| C ₉ H ₁₄ NCl ₂ Nb: | 300.0 |
| Crystal System: | Monoclinic |
| Space Group: | P2 ₁ /c |
| Cell Dimensions: | a = 12.977(1) Å |
| | b = 16.530(2) Å |
| | c = 12.726 Å |
| | β = 111.82(6)° |
| | U = 2534.3 Å ³ |
| | Z = 8 |
| | D _c = 1.572 g cm ⁻³ |
| Final R-value: | 0.019 (R _w = 0.030) |

Appendix 1C: Crystal Data for CpNb(N-2,6-*i*Pr₂C₆H₃)Cl₂.

| | |
|--|----------------------------------|
| C ₁₇ H ₂₂ NCl ₂ Nb: | 404.18 |
| Crystal System: | Orthorhombic |
| Space Group: | Cmc2 ₁ |
| Cell Dimensions: | a = 8.601(3) |
| | b = 16.641(27) |
| | c = 12.873(9) |
| | U = 1942.5 Å ³ |
| | Z = 4 |
| | D _c = 1.457 |
| Final R-value: | 0.0106 (R _w = 0.0229) |

Appendix 1D: Crystal Data for CpNb(NMe)Cl₂(PMe₃).

| | |
|--|----------------------------------|
| C ₉ H ₁₇ NPCL ₂ Nb: | 334.03 |
| Crystal System: | Monoclinic |
| Space Group: | P2 ₁ /c |
| Cell Dimensions: | a = 12.852(5) Å |
| | b = 14.453(7) Å |
| | c = 15.349(6) Å |
| | β = 107.65(4)° |
| | U = 2738.16 Å ³ |
| | Z = 8 |
| | D _c = 1.620 |
| Final R-value: | 0.0257 (R _w = 0.0241) |

Appendix 1E: Crystal Data for CpNb(N^tBu)Cl(Me).

| | |
|--|---|
| C ₁₀ H ₁₇ NCINb: | 279.61 |
| Crystal System: | Monoclinic |
| Space Group: | P2 ₁ /n |
| Cell Dimensions: | a = 6.7361(5) Å |
| | b = 14.0546(15) Å |
| | c = 13.6760(20) Å |
| | β = 97.522(9)° |
| | U = 1283.63 Å ³ |
| | Z = 4 |
| | D _c = 1.447 g cm ⁻³ |
| Final R-value: | 0.0114 (R _w = 0.0374) |

Appendix 1F: Crystal Data for [Mo(NPMe₃)Cl₂(PMe₃)₃]Cl·CH₂Cl₂.

| | |
|--|---|
| C ₁₂ H ₃₆ NP ₄ Cl ₃ Mo·CH ₂ Cl ₂ : | 605.6 |
| Crystal System: | Orthorhombic |
| Space Group: | P2 ₁ 2 ₁ 2 ₁ |
| Cell Dimensions: | a = 11.183(2) Å |
| | b = 14.262(3) Å |
| | c = 17.752(4) Å |
| | U = 2831.3 Å ³ |
| | Z = 4 |
| | D _c = 1.420 g cm ⁻³ |
| Final R-value: | 0.050 (R _w = 0.037) |

Appendix 1G: Crystal Data for



$\text{C}_{18}\text{H}_{54}\text{N}_2\text{P}_6\text{Cl}_6\text{Mo}_2\cdot\text{CH}_2\text{Cl}_2$: 974.0

Crystal System: Triclinic

Space Group: $P\bar{1}$

Cell Dimensions: $a = 10.880(2) \text{ \AA}$

$b = 14.620(3) \text{ \AA}$

$c = 15.493(3) \text{ \AA}$

$\alpha = 64.03(1)^\circ$

$\beta = 80.48(1)^\circ$

$\gamma = 81.36(1)^\circ$

$U = 2176.6 \text{ \AA}^3$

$Z = 2$

$D_c = 1.486 \text{ g cm}^{-3}$

Final R-value: 0.052 ($R_w = 0.039$)

Appendix 2

First Year Induction Courses: October 1987

The course consists of a series of one hour lectures on the services available in the department.

1. Departmental Organisation
2. Safety Matters
3. Electrical appliances and infrared spectroscopy
4. Chromatography and Microanalysis
5. Atomic absorption and inorganic analysis
6. Library facilities
7. Mass spectroscopy
8. Nuclear Magnetic Resonance
9. Glass blowing techniques

Research Colloquia, Seminars and Lectures Organised By the Department of Chemistry.

* - Indicates Colloquia attended by the author

During the Period: 1987-1988

BIRCHALL, Prof. D. (I.C.I. Advanced Materials) 25th April 1988
Environmental Chemistry of Aluminium

*BORER, Dr. K.(U.D.I.R.L.) 18th February 1988
The Brighton Bomb- A Forensic Science View

BOSSONS, L. (Durham Chemistry Teacher's Centre) 16th March 1988
GCSE Practical Assessment

* BUTLER, Dr. A.R. (University of St. Andrews) 5th November 1987
Chinese Alchemy

CAIRNS-SMITH, Dr. A. (Glasgow University) 28th January 1988
Clay Minerals and the Origin of Life

- * DAVIDSON, Dr. J. (Herriot-Watt University) November 1987
Metal Promoted Oligomerisation of Alkynes
- * GRADUATE CHEMISTS (N.E. Polytechnics and Universities) 19th April 1988
Graduate Symposium
- GRAHAM, Prof. W.A.G. (University of Alberta, Canada) 3rd March 1988
Rhodium and Iridium Complexes in the Activation of
Carbon-Hydrogen Bonds
- * GRAY, Prof. G.W. (University of Hull) 22nd October 1987
Liquid Crystals and their Applications
- HARTSHORN, Prof. M.P. (Canterbury Univ., New Zealand) 7th April 1988
Aspects of Ipso-Nitration
- * HOWARD, Dr. J. (I.C.I. Wilton) 3rd December 1987
Chemistry of Non-Equilibrium Processes
- * LUDMAN, Dr. C.J. (University of Durham) 10th December 1987
Explosives
- MCDONALD, Dr. W.A. (I.C.I. Wilton) 11th May 1988
Liquid Crystal Polymers
- MAJORAL, Prof. J.-P. (Universite' Paul Sabatier) 8th June 1988
Stabilisation by Complexation of Short-Lived
Phosphorus Species
- MAPLETOFT, Mrs. M. (Durham Chem. Teacher's Centre) 4th November 1987
Salter's Chemistry
- NIETO DE CASTRO, Prof. C.A. (University of Lisbon) 18th April 1988
Transport Properties of Non-Polar Fluids
- OLAH, Prof. G.A. (University of Southern California) 29th June 1988
New Aspects of Hydrocarbon Chemistry

- * PALMER, Dr. F. (University of Nottingham) 21st January 1988
Luminescence (Demonstration Lecture)
- PINES, Prof. A. (University of California, Berkeley, U.S.A.) 28th April 1988
Some Magnetic Moments
- RICHARDSON, Dr. R. (University of Bristol) 27th April 1988
X-Ray Diffraction from Spread Monolayers
- ROBERTS, Mrs. E. (SATRO Officer for Sunderland) 13th April 1988
Talk-Durham Chemistry Teacher's Centre - "Links
Between Industry and Schools"
- ROBINSON, Dr. J.A. (University of Southampton) 27th April 1988
Aspects of Antibiotic BioSynthesis
- * ROSE van Mrs. S. (Geological Museum) 29th October 1987
Chemistry of Volcanoes
- * SAMMES, Prof. P.G. (Smith, Kline and French) 19th December 1987
Chemical Aspects of Drug Development
- SEEBACH, Prof. D. (E.T.H. Zurich) 12th November 1987
From Synthetic Methods to Mechanistic Insight
- SODEAU, Dr. J. (University of East Anglia) 11th May 1988
Durham Chemistry Teacher's Centre Lecture: "Spray
Cans, Smog and Society"
- SWART, Mr. R. M. (I.C.I.) 16th December 1987
The Interaction of Chemicals with Lipid Bilayers
- * TURNER, Prof. J.J. (University of Nottingham) 11th February 1988
Catching Organometallic Intermediates
- UNDERHILL, Prof. A. (University of Bangor) 25th February 1988
Molecular Electronics

* WILLIAMS, Dr. D.H. (University of Cambridge) 26th November 1987
Molecular Recognition

* WINTER, Dr. M.J. (University of Sheffield) 15th October 1987
Pyrotechnics (Demonstration Lecture)

During the Period: 1988-1989

ASHMAN, Mr. A. (Durham Chemistry Teacher's Centre) 3rd May 1989
The Chemical Aspects of the National Curriculum

AVEYARD, Dr. R. (University of Hull) 15th March 1989
Surfactants at your Surface

AYLETT, Prof. B.J. (Queen Mary College, London) 16th February 1989
Silicon-Based Chips: - The Chemist's Contribution

* BALDWIN, Prof. J.E. (University of Oxford) 9th February 1989
Recent Advances in the Bioorganic Chemistry of Penicillin Biosynthesis

* BALDWIN & WALKER, Drs. R.R. & R.W. (Hull Univ.) 24th November 1988
Combustion: Some Burning Problems

BOLLEN, Mr. F. (Durham Chemistry Teacher's Centre) 18th October 1988
Lecture about the use of SATIS in the classroom

BUTLER, Dr. A.R. (St. Andrews University) 15th February 1989
Cancer in Linxiam: The Chemical Dimension

* CADOGAN, Prof. J.I.G. (British Petroleum) 10th November 1988
From Pure Science to Profit

CASEY, Dr. M. (University of Salford) 20th April 1989
Sulphoxides in Stereoselective Synthesis

- WATERS & CRESSEY, Mr. D. & T. (Durham Chemistry
Teacher's Centre) 1st February 1989
GCSE Chemistry 1988: "A Coroners Report"
- CRICH, Dr. D. (University College London) 27th April 1989
Some Novel Uses of Free Radicals in Organic Synthesis
- DINGWALL, Dr. J. (Ciba Geigy) 18th October 1988
Phosphorus-containing Amino Acids: Biologically
Active Natural and Unnatural Products
- * ERRINGTON, Dr. R.J. (University of Newcastle-upon-Tyne) 1st March 1989
Polymetalate Assembly in Organic Solvents
- FREY, Dr. J. (Southampton University) 11th May 1989
Spectroscopy of the Reaction Path: Photodissociation
Raman Spectra of NOCl
- * GRADUATE CHEMISTS, (Polytechs and Universities in
North East England) 12th April 1989
Symposium for presentation of papers by postgraduate students.
- * HALL, Prof. L.D. (Addenbrooke's Hospital Cambridge) 2nd February 1989
NMR - A Window to the Human Body
- HARDGROVE, Dr. G. (St. Olaf College U.S.A.) December 1988
Polymers in the Physical Chemistry Laboratory
- HARWOOD, Dr. L.(Oxford University) 25th January 1988
Synthetic Approaches to Phorbols Via Intramolecular
Furan Diels-Alder Reactions: Chemistry under Pressure
- JAGER, Dr. C. (Friedrich-Schiller University GDR) 9th December 1988
NMR Investigations of Fast Ion Conductors of the
NASICON Type
- JENNINGS, Prof. R.R. (Warwick University) 26th January 1989
Chemistry of the Masses

- * JOHNSON, Dr. B.F.G. (Cambridge University) 23rd February 1989
The Binary Carbonyls
- JONES, Dr. M.E. (Durham Chemistry Teacher's Centre) 14th June 1989
Discussion Session on the National Curriculum
- JONES, Dr. M.E. (Durham Chemistry Teacher's Centre) 28th June 1989
GCSE and A Level Chemistry 1989
- * LUDMAN, Dr. C.J. (Durham University) 18th October 1988
The Energetics of Explosives
- MACDOUGALL, Dr. G. (Edinburgh University) 22nd February 1989
Vibrational Spectroscopy of Model Catalytic Systems
- MARKO, Dr. I. (Sheffield University) 9th March 1989
Catalytic Asymmetric Osmylation of Olefins
- McLAUCHLAN, Dr. K.A. (University of Oxford) 16th November 1988
The Effect of Magnetic Fields on Chemical Reactions
- MOODY, Dr. C.J. (Imperial College) 17th May 1989
Reactive Intermediates in Heterocyclic Synthesis
- * MORTIMER, Dr. C. (Durham Chemistry Teacher's Centre) 14th December 1988
The Hindenberg Disaster - an Excuse for Some Experiments
- NICHOLLS, Dr. D. (Durham Chemistry Teacher's Centre) 11th July 1989
Demo. "Liquid Air"
- PAETZOLD, Prof. P. (Aachen) 23rd May 1989
Iminoboranes XB=NR: Inorganic Acetylenes
- PAGE, Dr. P.C.B. (University of Liverpool) 3rd May 1989
Stereocontrol of Organic Reactions Using 1,3-dithiane-1-oxides

- POLA, Prof. J. (Czechoslovak Academy of Science) 15th June 1989
Carbon Dioxide Laser Induced Chemical Reactions
New Pathways in Gas-Phase Chemistry
- REES, Prof. C.W. (Imperial College London) 27th October 1988
Some Very Heterocyclic Compounds
- REVELL, Mr. P. (Durham Chemistry Teacher's Centre) 14th March 1989
Implementing Broad and Balanced Science 11-16
- SCHMUTZLER, Prof. R. (Techn. Univ. Braunschweig) 6th October 1988
Fluorophosphines Revisited - New Contributions to an
Old Theme
- * SCHROCK, Prof. R.R. (M.I.T.) 13th February 1989
Recent Advances in Living Metathesis
- SINGH, Dr. G. (Teesside Polytechnic) 9th November 1988
Towards Third Generation Anti-Leukaemics
- * SNAITH, Dr. R. (Cambridge University) 1st December 1988
Egyptian Mummies: What, Where, Why and How
- STIBR, Dr. R. (Czechoslovak Academy of Sciences) 16th May 1989
Recent Developments in the Chemistry of Intermediate-
Sited Carboranes
- * VON RAGUE SCHLEYER, Prof. P. (Univ. Erlangen Nurnberg) 21st October 1988
The Fruitful Interplay Between Computational and
Experimental Chemistry
- * WELLS, Prof. P.B. (Hull University) 10th May 1989
Catalyst Characterisation and Reactivity

During the Period 1989-1990

- ASHMAN, Mr.A. (Durham Chemistry Teachers' Centre) 11th October, 1989

The National Curriculum - an update

- * BADYAL, Dr J.P.S. (Durham University) 1st November 1989
Breakthroughs in Heterogeneous Catalysis
- BECHER, Dr.J. (Odense University) 13th November 1989
Synthesis of New Macrocyclic Systems using
Heterocyclic Building Blocks.
- *BERCAW, Prof. J.E. (California Institute of Technology) 10th November 1989
Synthetic and Mechanistic Approaches to
Zieger-Natta Polymerisation of Olefins
- BLEASDALE, Dr. C. (Newcastle University) 21st February 1990
The Mode of Action of some anti-tumour Agents
- BOLLEN, Mr.F. (Formerly Science Advisor, Newcastle LEA) 27th March 1990
Whats New in Satis, 16-19.
- BOWMAN, Prof. J.M. (Emory University) 23rd March 1990
Fitting Experiment with Theory in Ar-OH
- * BUTLER, Dr. A. (St. Andrews University) 7th December 1989
The Discovery of Penicillin: Facts and Fancies
- CAMPBELL, Mr. W.A. (Durham Chemistry Teachers Centre) 12th September 1989
Industrial Catalysis- some ideas for the
National Curriculum.
- CHADWICK, Dr. P. (Dept. Physics, Durham University) 24th January 1990.
Recent Theories of the Universe (with reference
to National Curriculum Attainment Target 16)
- CHEETHAM, Dr.A.K. (Oxford University) 8th March 1990
Chemistry of Zeolite Cages

- CLARK, Prof. D.T. (ICI Wilton) 22nd February 1990
Spatially Resolved Chemistry (using Nature's Paradigm in the Advanced Materials Arena).
- * COLE-HAMILTON, Prof. D.J. (St. Andrews University) 29th November 1989
New Polymers from Homogeneous Catalysis
- CROMBIE, Prof. L. (Nottingham University) 15th February 1990
The Chemistry of Cannabis and Khat
- DYER, Dr. U. (Glaxo) 31st January 1990
Synthesis and Conformation of C-Glycosides
- * FLORIANI, Prof. C. (Lausanne Univ., Switzerland) 25th October 1989
Molecular Aggregates- A Bridge Between Homogeneous and Heterogeneous Systems
- GERMAN, Prof. L.S. (USSR Academy of Sciences, Moscow) 9th July 1990
New Syntheses in Fluoroaliphatic Chemistry:
Recent Advances in the Chemistry of Fluorinated Oxiranes.
- GRAHAM, Dr.D. (B.P. Research Centre) 4th December 1989
How Proteins Absorb to Interfaces
- * GREENWOOD, Prof. N.N. (University of Leeds) 9th November 1989
Novel Cluster Geometries in Metalloborane Chemistry
- HOLLOWAY, Prof. J.H. (University of Leicester) 1st February 1990
Noble Gas Chemistry
- HUGHES, Dr.M.N. (King's College, London) 30th November 1989
A Bug's Eye View of the Periodic Table

- HUISGEN, Prof. R. (Universität München) 15th December 1989
Recent Mechanistic Studies of [2+2] Additions
- IDDON, Dr.B. (University of Salford) 15th December 1989
Schools' Christmas Lecture-
The Magic of Chemistry
- JONES, Dr.M.E. (Durham University Teachers Centre) 3rd July 1990
The Chemistry A Level 1990
- JONES, Dr. M.E. (Durham University Teachers Centre) 21st November 1989
GCSE and Dual Award Science as a Starting Point
for A level Chemistry- How Suitable are They?
- JOHNSON, Dr. G.A.L. (Durham University Teachers Centre) 8th February 1990
Some Aspects of Local Geology in the National Science
Curriculum (Attainment Target 9)
- KLINOWSKI, Dr.J. (Cambridge University) 13th December 1989
Solid State NMR Studies of Zeolite Catalysts
- LANCASTER, Rev. R. (Kimbolton Fireworks) 8th February 1990
Fireworks - Principles and Practice.
- LUNAZZI, Prof. L. (University of Bologna) 12th February 1990
Application of Dynamic NMR to the Study of
Conformational Enantiomerism
- * PALMER, Dr. F. (Nottingham University) 17th October 1989
Thunder and Lightning
- PARKER, Dr. D. (Durham University) 16th November 1989
Macrocycles, Drugs and Rock'N'Roll
- * PERUTZ, Dr. R.N. (York University) 24th January 1990
Plotting the Course of C-H Activations with
Organometallics.

PLATONOV, Prof. V.E. (USSR Academy of Sciences, Novorsibirsk) 9th July 1990
Polyfluoroindanes: Synthesis and Transformation

POWELL, Dr.R.L. (ICI) 6th December 1989
The Development of CFC Replacements

POWIS, Dr. I. (Nottingham University) 21st March 1990
Spinning off in a Huff: Photodissociation
of Methyl Iodide

RICHARDS, Mr. C. (Health and Safety Exec., Newcastle) 28th February 1990
Safety in School Science Laboratories and COSHH

ROZHKOVA, Prof. I.N. (USSR Academy of Sciences, Moscow) 9th July 1990
Reactivity of Perfluoroalkyl Bromides

* STODDART, Dr.J.F. (Sheffield University) 1st March 1990
Molecular Lego

* SUTTON, Prof. D. (Simon Fraser Univ., Vancouver B.C.) 14th February 1990
Synthesis and Applications of Dinitrogen and Diazo
Compounds of Rhenium and Iridium.

THOMAS, Dr.R.K. (Oxford University) 28th February 1990
Neutron Reflectometry from Surfaces

THOMPSON, Dr. D.P. (Newcastle University) 7th February 1990
The Role of Nitrogen in Extending Silicate
Crystal Chemistry.

Conferences and Symposia Attended.

(*denotes paper presentation)

(#denotes poster presentation)

1. *"Twenty-third University of Strathclyde Inorganic Chemistry Conference"*, Glasgow, 27-28th June 1988.
2. *"Symposium in Honour of Professor Sir Geoffrey Wilkinson, FRS - Some Current Advances in Inorganic Chemistry"*, 19th July 1988.
3. *"International Conference on the Chemistry of the Early Transition Metals"*, The University of Sussex Brighton, 10-14th July 1989.
4. *"North East Graduate Symposium"*, University of Newcastle-upon-Tyne, 2nd April 1990.
5. *"199th ACS National Meeting - Boston, Mass"* , 22nd-27th April 1990.
6. *"Symposium in Honour of Professor Peter L. Pauson - Organometallic Chemistry of the Transition Metals"*, University of Strathclyde, Glasgow, 19th October 1990.

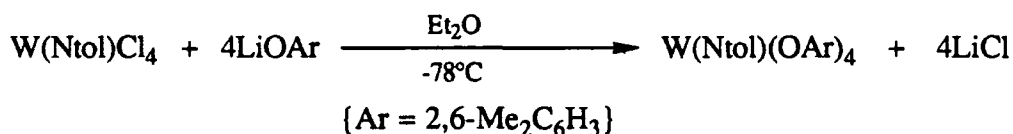
Publications

1. The Use of Hexamethyldisilthiane in the Synthesis of Transition Metal Sulphido-halides, Vernon C. Gibson, Alan Shaw and David N. Williams, *Polyhedron*, 1988, **8**, 549.
2. Facile Conversion of a Cationic Mo^{IV} Phosphinimato Complex into an Anionic Nitrido-bridged Dimer with a Bis(trimethylphosphine)iminium Counterion, Vernon C. Gibson, David N. Williams and William Clegg, *J Chem. Soc., Chem. Comm.*, 1989, 1863.
3. Synthesis, X-ray Structure and Reactivity of the Half-Sandwich Imido Complex (η -*C₅H₅)NbCl₂(NCH₃), Vernon C. Gibson, David N. Williams, William Clegg and David C.R. Hockless, *Polyhedron*, 1989, 1819.
4. Bond-Stretch Isomers of Nb(O)Cl₃(PMe₃)₃: a Bonding Analysis, Vernon C. Gibson, Catherine E. Housecroft and David N. Williams, *In Press*, 1990.

Appendix 3

Synthesis and Characterisation of W(Ntol)(O-2,6-Me₂C₆H₃)₄

Compounds of the type W(O)(OAr)₄ (Ar = 2,6-ⁱPr₂C₆H₃, 2,4,6-Me₃C₆H₂, 2,6-Me₂C₆H₃) have previously been prepared in this laboratory by Alan Shaw¹. For comparison, an analogous imido complex has been prepared by the reaction of W(Ntol)Cl₄ and LiO-2,6-Me₂C₆H₃ in ether. The reaction proceeds smoothly over 12h to afford a red solution from which W(Ntol)(O-2,6-Me₂C₆H₃)₄ can be isolated as a crystalline red solid in high yield (89%). The solid can be recrystallised from cold pentane to yield large red prisms. The reaction can be envisaged to occur as shown below:

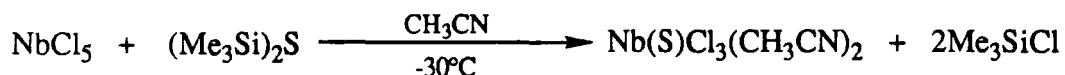


Characterisation is provided by elemental analysis, infrared, ¹H and ¹³C NMR spectroscopies and mass spectrometry (Chapter 6, section 6.6.1). In particular, elemental analysis confirms a stoichiometry of C₃₉H₄₃NO₄W, and ¹H NMR shows resonances attributable to the methyl protons of the tolyl and C₆H₃Me₂ groups at δ 2.17 and 2.50 respectively, and the expected signals in the aromatic region δ 6.6-7.2. The mass spectrum shows an envelope attributable to the [M-OAr]⁺ fragment ion.

W(Ntol)(O-2,6-Me₂C₆H₃)₄ is likely to possess a square pyramidal geometry with the imido ligand in the apical position, analogous to structurally characterised W(O)(O-2,6-ⁱPr₂C₆H₃)₄¹.

Synthesis and Characterisation of $\text{Nb(S)Cl}_3(\text{CH}_3\text{CN})_2$.

A synthesis of oxo and sulphido halides of the type Nb(E)Cl_3 and $\text{Nb(E)Cl}_3(\text{CH}_3\text{CN})_2$ ($M = \text{Ta, Nb}$; $E = \text{O, S}$) is essential for the preparation of bond-stretch isomers of the type $\text{Nb(E)Cl}_3(\text{PMe}_3)_3$. A convenient, high yield route to these species has been described, using commercially available reagents Me_3SiYR ($R = \text{alkyl, SiMe}_3$; $Y = \text{O, S}$)^{1,2}. Using the same synthetic strategy, NbCl_5 was reacted with $(\text{Me}_3\text{Si})_2\text{S}$ in acetonitrile to afford a yellow solution from which $\text{Nb(S)Cl}_3(\text{CH}_3\text{CN})_2$ can be isolated in a 89% yield³.



Characterisation of $\text{Nb(S)Cl}_3(\text{CH}_3\text{CN})_2$ is provided from elemental analysis and infrared spectroscopy (Chapter 6, section 6.6.2). In particular, the infrared spectrum shows two sharp absorption at 2310 cm^{-1} and 2330 cm^{-1} attributable to the $\nu(\text{C-N})$ stretches of coordinated acetonitrile, and a strong, sharp absorption at 523 cm^{-1} assigned to the $\nu(\text{Nb=S})$ stretching vibration.

$\text{Nb(S)Cl}_3(\text{CH}_3\text{CN})_2$ is likely to be monomeric and octahedral. Similarities in the infrared Nb-Cl stretching region $370\text{-}330 \text{ cm}^{-1}$ suggests that $\text{Nb(S)Cl}_3(\text{CH}_3\text{CN})_2$ possesses a *cis*-meridional arrangement of acetonitrile and chloro ligands analogous to that of structurally characterised $\text{Nb(O)Cl}_3(\text{CH}_3\text{CN})_2$ ⁴.

References:

1. A. Shaw, *Thesis*, Durham University, 1989.
2. V.C. Gibson, T.P. Kee, and A. Shaw, *Polyhedron*, 1988, **7**, 2217.
3. V.C. Gibson, A. Shaw and D. Williams, *Polyhedron*, 1988, **8**, 549.
4. C. Chavant, J.C. Daran, Y. Jeannin, G. Constant and R. Morancho, *Acta Cryst.*, 1975, **B31**, 1828.

